Armed Forces
Radiobiology Research Institute

Estimation of Radiation Risk Based on the Concept of Individual Variability of Radiosensitivity

Research Center of
Spacecraft Radiation Safety
Moscow, Russia

AFRRI Contract Report 96-1 Defense Nuclear Agency Contract DNA001-93-C-0152

Estimation of Radiation Risk Based on the Concept of Individual Variability of Radiosensitivity

Compiled by

Research Center of Spacecraft Radiation Safety Moscow, Russia

Principal Investigator
E. E. Kovalev

Senior Researcher
O. A. Smirnova

Published by

Armed Forces Radiobiology Research Institute Bethesda, Maryland, USA

Editor and NIS Initiatives Coordinator
Glen I. Reeves, M.D.

Scientific Director
E. John Ainsworth, Ph.D.

AFRRI Contract Report 96-1, June 1996 Defense Nuclear Agency Contract DNA001-93-C-0152

For information about this publication, write Armed Forces Radiobiology Research Institute, 8901 Wisconsin Avenue, Bethesda, MD 20889-5603, USA. Or call 011-301-295-0377. Or send electronic mail to reeves@vax.afrri.usuhs.mil.

Find more information about AFRRI on the Internet's World Wide Web at http://www.afrri.usuhs.mil.

This and other AFRRI publications are available to qualified users from the Defense Technical Information Center, Attention: OCP, 8725 John J. Kingman Road, Suite 0944, Fort Belvoir, VA 22060-6218; telephone (703) 767-8274. Others may contact the National Technical Information Service, 5285 Port Royal Road, Springfield, VA 22161; telephone (703) 487-4650. AFRRI publications are also available from university libraries and other libraries associated with the U.S. Government's Depository Library System.

DISCLAIMER NOTICE

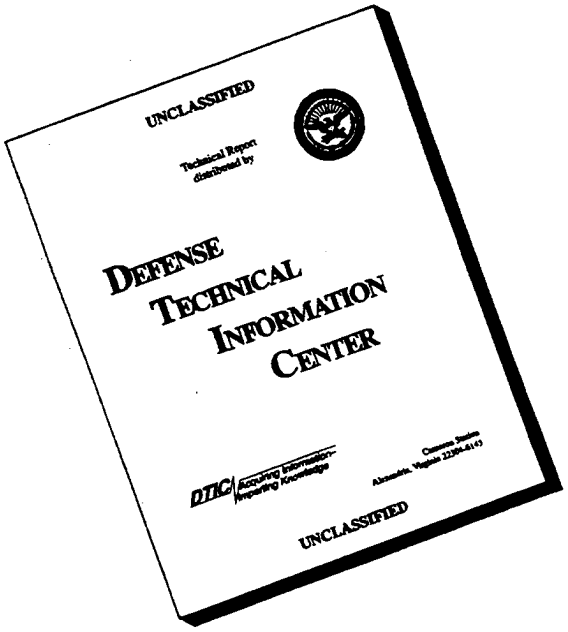

THIS DOCUMENT IS BEST QUALITY AVAILABLE. THE COPY FURNISHED TO DTIC CONTAINED A SIGNIFICANT NUMBER OF PAGES WHICH DO NOT REPRODUCE LEGIBLY.

FOREWORD

The problem of protection of cosmonauts and astronauts against the effects of chronic exposure to galactic cosmic radiation is an important and challenging one, particularly as we contemplate the exposures likely to be encountered on long-term missions, such as a voyage to Mars or a lunar colony. The accomplishments of our Russian colleagues in the area of long-term manned spaceflights are well known and need not be reviewed extensively here. One of the institutions furnishing the radiation biology support required for these long missions was the Research Center for Spacecraft Radiation Safety (RCSRS), whose researchers compiled this report.

The Armed Forces Radiobiology Research Institute (AFRRI) has had a long and fruitful relationship with the National Aeronautics and Space Administration (NASA) in the field of effects of space radiations on astronauts. AFRRI and NASA have a Memorandum of Understanding for research concerning radioprotectants and cancer research. Recently, AFRRI completed a study for NASA that outlines the requirements for further research on the biological effects of heavy charged particles.[1] The research achievements of a Russian collegial institute are therefore supplemental to our own in-house efforts. Our awareness of the achievements of the RCSRS was stimulated by a presentation given by the primary author at the World Space Congress.[2] This inspired us to support their efforts to provide documentation suitable for review by the scientific community.

The models presented in this report are based on experiments performed by researchers at the RCSRS at their own laboratories and those of the Joint Institute for Nuclear Research, Laboratory of Nuclear Problems, at Dubna, Russia. Collaborative research in the field has been going on between these institutions for several years. The relationships between the models presented here and other available data are discussed in the report.

Central to this report is the authors' hypothesis that the effects of chronic low-dose radiation on a large population is, as it were, skewed by the presence

[1]Design Study: Data Requirements Regarding Particle Carcinogenesis in the Space Radiation Environment. E. J. Ainsworth, Principal Investigator. Document submitted to NASA 31 March 1995 in fulfillment of contract T-1320S.

[2]Individual Doses of Cosmonauts Over the 30 Years of Soviet Space Flights. E. E. Kovalev and V. M. Petrov. Presentation given at the World Space Congress, Washington, D.C., 28 August-5 September 1992.

in the population of a number of individuals that are unusually susceptible to radiation effects; in other words, there exists a "hypersensitive" subpopulation, to use their term. This subpopulation, though small in number relative to the entire group, is large enough to affect the dose-response curve. Their hypothesis implies that this curve is pushed to the left, significantly more so than if this subpopulation were excluded from the analysis. We already know this is true for persons with ataxia telangiectasia, and there is concern about other genetically influenced repair deficiencies as well.

The authors conclude by discussing the applicability of their work to human populations. They stress the need for building a mathematical model for human radiation-induced mortality, and what its benefits would be. However, they are well aware of the problems involved in developing such a model, not the least of which are the heterogeneity of the human population and the marked shortage of data necessary for further model development and validation.

This document of course represents neither the final definitive word nor even the opinion of AFRRI or the Department of Defense on the issue of human radiation response. Nevertheless it is a thought-provoking and well-reasoned approach to the problem of radiation protection of both radiation workers and the general population. With the recent shift in radiation research away from focussing on prompt high-dose exposures to that of chronic low-dose exposures, this work represents a valuable contribution to our knowledge in this arena.

Glen I. Reeves, M.D.
NIS Initiatives Coordinator
Armed Forces Radiobiology Research Institute

CONTENTS

TASK II. Mathematical Models of Mortality Dynamics for Irradiated Mammalian Populations

TASK III. Analysis of Experimental and Clinical Data

INTRODUCTION

To evaluate the risk to a large group of people from continuous exposure to radiation the distributions of the radiation doses and the radiosensitivities within the group must be known. At the present time, there is no information on these distributions in the majority of cases. Therefore, the radiation risk is most often estimated as a product of the average radiation dose for a given population by the mean probability of a radiobiological effect (mortality, life shortening, etc.) for a unit of radiation dose. Radiosensitivity is generally obtained by extrapolating radiobiological data from high doses to low doses.

Experimental data and results of research carried out in regions that have been exposed to radiation—the Chernobyl catastrophe (Ukraine) or the nuclear weapon tests (Kazakhstan, the Altai Territory)—have been accumulated in the Research Center of Spacecraft Radiation Safety (RCSRS) and suggest that exposures to moderate and low radiation doses have more pronounced radiobiological effects than might be expected when extrapolating data from high to low doses.

This conclusion must not only be explained but must also be considered when estimating the risk of low radiation exposure.

Our hypothesis [1] is based on experimental studies suggesting that populations of various mammalian species, including humans, contain a small proportion (from 5% to 12%) of individuals that show so-called hyperradiosensitivity to both acute and continuous radiation. It is therefore reasonable to assume that this individual variability of radiosensitivity in the population of a mammalian species is responsible for the inadequate extrapolation of health effects from high radiation doses to moderate and low radiation doses. Indeed, at high doses and dose rates of acute and continuous radiation, hyperradiosensitive individuals have a negligible influence on the general pattern of radiation damage for the population as a whole—first, because of their small numbers in the population and, second, because they differ from the rest only by the delay in time of death.

Therefore, with high-dose radiation exposures the effect on health is determined by the contribution of individuals with average or low radiosensitivity. Moreover, in the range of very high doses and dose rates, where a single type of lethality prevails, the population may be considered homogeneous and may have a radiosensitivity index typical of most radioresistant individuals in the population.

By contrast, with low-dose radiation, health effects at both the level of the critical system and at the population level manifest themselves only in hyper-radiosensitive individuals, which markedly differ in radiosensitivity from the rest, especially from the most radioresistant group. Thus, information on the contribution of individual radiosensitivity to the dynamic and integral radiobiological effects for critical systems of the organism and for the population as a whole is of particular significance now.

In this research, we place a great emphasis on the use of methods of mathematical modeling. Mathematical models not only help analyze and generalize the experimental data, but they can also be successfully used to predict effects of radiation.

In our opinion, models that combine three levels of manifestation of adverse radiation effects—the population level, the organism level, and the body's critical system level—have the greatest promise. In contrast to models of the "black box" type [2], our models are capable of not only describing the experimental data but also predicting new correlations at the population level.

It is generally recognized that the immediate cause of death of irradiated mammals is failure of a vital system of the organism. This failure originates from disruption of cellular kinetics and reduction of the number of cells below the level required for survival [3]. Different ranges of dose and dose rate seem to affect particular critical organs whose radiation injury is crucial in the development of radiation-induced pathology and death of mammals [4]. Critical systems of the mammalian organism are bone marrow hematopoiesis, epithelium of the small intestine, and central nervous system. It should be noted that the death of mammals induced by the bone marrow syndrome, intestinal syndrome, or destruction of the central nervous system occurs at different time periods after irradiation. This enables one to use the mathematical model of one of the critical systems to model radiation-induced mortality of mammals. In the range of radiation doses that we are interested in, the critical systems are bone marrow hematopoiesis and the epithelium of the small intestine. In this report, mathematical models describing the dynamics of these critical systems in mammals exposed to acute and chronic radiation are proposed and investigated in detail. On this basis, mathematical models of radiation-induced mortality for homogeneous and nonhomogeneous (in radiosensitivity) mammalian populations are developed. The report also includes an analysis of experimental and clinical data in terms of the concepts forming the basis of our models.

The basis for the research involved in this particular report was laid by studies carried out over the last few years at RCSRS, the Institute of Biophysics, and the Institute of Biomedical Problems. These have been experimental and theoretical studies of individual hematopoietic lines (lymphopoiesis and granulocytopoiesis) in irradiated mammals. It was within this line of research that the first two-level model of bone marrow lymphopoiesis was constructed. The model described the dynamics of blood lymphocytes and their bone

marrow precursors in mammals exposed to acute radiation. This model of postirradiation lymphopoiesis dynamics was a system of four nonlinear differential equations. The coefficients included in the model were found in experiments performed by RCSRS researchers at the laboratory of Dr. N. Ryzhov in Dubna. Along with other radiobiological investigations there, we studied for some years the effects of gamma radiation and high energy protons on processes of bone marrow blood formation in rats [4]. A model of bone marrow lymphopoiesis based on experimental data [5] was reported in 1982 [6]; the two-level model was used as a component of the model of humoral immune response to the *T*-independent antigen in irradiated mammals [7]. Later, a three-level model of bone marrow lymphopoiesis and a four-level model of granulocytopoiesis under chronic irradiation were built. In addition to the lymphocyte concentration in the blood, we used concentrations of lymphocyte precursors in the bone marrow both capable and incapable of division as variables of lymphocytopoiesis. The variables of the granulocytopoiesis model included concentrations of cells of the granulocytic series (capable and incapable of division) in the bone marrow, concentration of granulocytes in the blood, and concentration of granulocytes in the tissues. As basic experimental material in modeling these hematopoietic lines we used the results of a chronic radiation experiment on rats conducted by Dr. T. Zukhbaya from RCSRS [8-11].

REFERENCES

1. Kovalev EE, Smirnova OA (1993) Estimation of radiation risk based on the concept of individual variability of radiosensitivity. COSPAR Colloquium No. 6: International Roundtable on Radiation Risk in Humans on Exploratory Missions in Space. Center of the German Physical Society "Physikzentrum", Bad Honnef, Germany

2. Arlett CF, Cole J, Green MHL (1989) Radiosensitive individuals in the population. In: Baverstock KF, Stather JW (eds) Low Dose Radiation: Biological Basis of Risk Assessment. London; New York; Philadelphia: Taylor and Francis, 240-252

3. Cox DR, Oakes D (1984) Analysis of survival data. London; New York: Chapman and Hall

4. Bond VP, Fliendner TM, Archambeau JO (1965) Mammalian radiation lethality: A disturbance in cellular kinetics. New York: Academic Press

5. Grigor'ev UG (ed.) (1967) Biological effects of the high energy protons. Moscow: Atomizdat

6. Smirnova OA, Govorun RD, Ryshov NI (1982) Mathematical model to study the postirradiation dynamics of lymphopoiesis. Radiobiologiya 22:468-473 (Russian)

7. Smirnova OA (1984) A mathematical model of radiation effect on the immune system. Immunology 2:38-42 (Russian)

8. Zukhbaya TN, Smirnova OA (1988) Mathematical model for the dynamics of granulocytopoiesis in mammals. Radiobiologiya 28:796-802 (Russian)

9. Zukhbaya TM, Smirnova OA (1989) The stimulating effect of prolonged radiation of small dose rates on mammalian lymphopoiesis. Kosmicheskaya Biologiya i Aviakosmicheskaya Meditsina 1:47-51 (Russian)

10. Smirnova OA, Zukhbaya TM (1991) The stimulating effect of prolonged irradiation with low dose rates on granulocytopoiesis. Kosmicheskaya Biologiya i Aviakosmicheskaya Meditsina 3:40-42 (Russian)

11. Zukhbaya TM, Smirnova OA (1991) An experimental and mathematical analysis of lymphopoiesis dynamics under continuous irradiation. Health Physics 61:87-95

Task I

Mathematical Models of Critical Systems in Irradiated Mammals

E. E. Kovalev, principal investigator
O. A. Smirnova, senior researcher

Abstract

A description and analysis of mathematical models developed for two critical systems, the hematopoietic and intestinal systems, are presented. The models, based on modern theories of regulation of the hematopoietic and intestinal epithelium systems, describe the dynamics of these systems in nonirradiated mammals and in mammals exposed to acute and chronic radiation. The first model uses the radiosensitivity indices of hematopoietic cells as its principal parameters. The key parameter of the second model is the radiosensitivity index of precursors of principal crypt cells. The variable parameters of the models are represented by the dose of acute radiation and the dose rate of chronic radiation. These models can be used for quantitative prediction of the effects of acute and chronic radiation on the hematopoietic and intestinal systems of mammals.

CHAPTER 1

Mathematical Model of the Blood-Forming System

1.1. Introduction

Mathematical modeling came into use in hematopoietic studies more than 30 years ago. Of the three principal research directions in this field, the direction of Lajtha et al. [1] concerned general problems of regulation of differentiation and self-maintenance of blood-forming stem cells. Models differed in basic assumptions and degree of detail for the processes studied [2]. Most of these models, however, yield qualitatively similar results, which makes a difficult final choice between the suggested regulatory mechanisms of stem cell differentiation and self-maintenance. Apparently, the solution of this problem requires that some essentially new experimental methods of analysis of the dynamics of pluripotent stem cells be developed.

The second direction of mathematical modeling was the study of separate lines of blood formation [2]. The most interesting data obtained in this direction of research can be found in references 3-10. The models were used to obtain various dynamic regimes characteristic of blood formation. In particular, the models described in references 3, 5-7, 9, and 10 made it possible to find solutions corresponding to the cyclic kinetics of hematopoiesis observed in some mammalian species. However, most of the above studies contain no analysis of the conditions of onset of stable oscillatory regimes. The models simulated the effects of several factors on the dynamics of bone marrow blood formation: hypoxia [3-5], blood transfusion [5, 8], hemorrhage [5, 8], weightlessness [4], drug treatment [8], and virus infection [3]. Modeling results were compared with corresponding experimental data at a quantitative level only in references 5 and 8.

At present, much attention is given to the third direction of hematopoietic research: the study of the effect of ionizing radiation on the blood formation process [2]. The dynamics of separate lines of blood formation in mammals following acute radiation exposure was modeled in references 5 and 11 to 13.

A disadvantage of most models is that they do not include an explicit form of the basic parameters: the dose of ionizing radiation and the characteristics of radiosensitivity of the blood-forming cells. This precludes the use of these models for predicting the response of lines of blood formation to various acute radiation doses. As regards model studies of the effect of a prolonged radiation exposure on hematopoiesis, we know of only a few such works [5, 14, 15]. In reference 14, the effect of chronic radiation on hematopoiesis was studied in the framework of a rather abstract model, therefore the results were largely qualitative. In reference 15, only the dynamics of the stem cells was described. In reference 5, models were proposed that described the dynamics of the bone marrow precursor cells of the granulocytopoietic and erythrocytopoietic systems exposed to prolonged radiation. These models are complicated, contain a large number of variables and coefficients, but do not include such basic parameters as the radiation dose rate and quantities characterizing the radiosensitivity of the blood-forming cells.

The purpose of our studies was to develop fairly simple models for all hematopoiesis lines; based on modern concepts, the models would describe the dynamics of both the functioning blood cells and their precursors in bone marrow. Our intention was to explicitly include in these models the parameters of the ionizing radiation and the basic hematological and radiobiological parameters. The models must also be able to reconstruct the principal dynamic regimes of hematopoiesis in nonirradiated mammals and to provide quantitative descriptions of formed elements of blood and their bone-marrow precursors during acute and chronic exposures to radiation. The results are presented in this chapter.

1.2. Generalized Model of the Dynamics of an Individual Hematopoietic Line in Nonirradiated and Irradiated Mammals

According to current concepts on the structure and mechanisms of operation of the hematopoietic system, the latter can be regarded as a complex of four subsystems: thrombocytopoiesis, lymphopoiesis, erythropoiesis, and granulocytopoiesis [16-18]. Each subsystem contains the entire set of cells, from stem cells (in the microenvironment predetermining their differentiation toward the respective hematopoietic line) to mature blood cells of this particular line.

Let us construct an elementary model of an individual hematopoietic line taking into account only the principal regulatory mechanisms of its function. For this purpose we divide all the cells of a particular hematopoietic line into three groups according to the degree of maturity and differentiation:

- Group X_1, bone marrow precursor cells (from stem cells in the respective microenvironment to morphologically identifiable dividing cells)

- Group X_2, nondividing maturing bone marrow cells
- Group X_3, mature blood cells

Bringing together all bone marrow precursor cells capable of dividing into a single group X_1 obviates the necessity to consider separately the complicated (and not yet well understood) processes of self-maintenance and predifferentiation of stem cells. In constructing the model, we assume that (1) the dynamics of X_1 cells is determined by the rate of their reproduction and passage to group X_2; (2) the dynamics of X_2 cells is determined by the arrival of cells from X_1 and passage to group X_3; and (3) the dynamics of X_3 cells is determined by the arrival of cells from group X_2 and their natural death. In accordance with the chalone theory of hematopoiesis regulation, we assume that the X_1 cell reproduction rate depends on the concentration of chalone, the specific inhibitor of cell division, which is the product of the vital activity and decay of cells and their progeny. As model variables, we take the concentrations of X_1, X_2, and X_3 cells and of the specific chalone (x_1, x_2, x_3, and I, respectively). By cell concentration, we mean the ratio of the total number of cells of a particular group to the total blood volume. Based on these assumptions, the dynamics of these concentrations is described by means of these differentiation equations:

$$\frac{dx_1}{dt} = Bx_1 - Cx_1, \tag{1.1}$$

$$\frac{dx_2}{dt} = Cx_1 - Fx_2, \tag{1.2}$$

$$\frac{dx_3}{dt} = Fx_2 - Ex_3, \tag{1.3}$$

$$\frac{dI}{dt} = G(x_1 + \theta_2 x_2 + \theta_3 x_3) - HI. \tag{1.4}$$

C and F are the specific rates of transfer of cells from group X_1 to group X_2 and from X_2 to X_3 (in simulating the dynamics of different lines of hematopoiesis, the parameters C and F can represent either constant coefficients or nonlinear functions of the concentrations of respective cells); E is the specific decay rate of cells; H is the chalone's specific decay rate; multipliers G, $G\theta_2$, and $G\theta_3$ in front of the variables x_1, x_2, and x_3 represent the dissimilar contributions of X_1, X_2, and X_3 cells to chalone production.

The influence of the chalone inhibitor on the reproduction rate of X_1 cells is described using the Ierusalimskii equation [19]

$$\beta = \alpha(1 + I/K)^{-1}, \tag{1.5}$$

where K is the inhibition constant, and α is the maximum specific rate of cell division. Experiments on isolation and uses of chalones have shown that they preserve their activity for several hours [16, 17]. Bearing in mind that the processes of differentiation and maturation of bone marrow cells last for several days, we consider equation 1.4 to be "rapid" in comparison with equations 1.1-1.3. Then, according to the Tikhonov theorem [19], equation 1.4 can be replaced by its stationary solution $I = (G/H)(x_1 + \theta_2 x_2 + \theta_3 x_3)$. We then have

$$\beta = \alpha[1 + \beta(x_1 + \theta_2 x_2 + \theta_3 x_3)]^{-1}, \quad \beta = G/(HK). \tag{1.6}$$

Thus, the model of the dynamics of a separate hematopoietic line for nonirradiated mammals is a system of three nonlinear differential equations 1.1-1.3.

When modeling the effect of ionizing radiation on hematopoiesis the following generally known hypotheses will be used. It is accepted as proven that radiation with sublethal doses does not practically affect the differentiation and life span of hematopoietic cells undamaged by radiation [20]. The effect of ionizing radiation is primarily manifested in the death of part of the radiosensitive cells of the blood-forming system. The cells most sensitive to radiation are the early precursors of blood cells (X_1 cells). A lower sensitivity (sometimes even radioresistance) is shown by nondividing maturing bone marrow X_2 cells and by mature X_3 cells of some lines [20-22]. Needless to say, radiosensitivity is a complicated function and depends on the age of cells and the stage of their life cycle at the time of radiation. However, to characterize the radiosensitivity of hematopoietic cells at each of the three stages of their development certain averaged values are used for simplicity. We also assume that all cells receive the same radiation dose. This assumption is equivalent to averaging the radiation dose over space.

The model equations 1.1-1.3 and 1.6 are used as a basis for an examination of the effect of ionizing radiation with a dose rate N on a separate line of hematopoiesis. We assume that cells of this particular line are radiosensitive at every stage of their development. As shown by experimental data, the radiosensitive cells can be tentatively divided into three groups according to their radiation response. The first group X_i includes undamaged cells, the second group X_{di} includes damaged cells that die within 1-2 days (mitotic death), and the third group X_{hdi} includes heavily damaged cells that die within the first 4-7 hours following irradiation (interphase death) [22]. As model variables, we take the concentrations of undamaged, damaged, and heavily damaged cells, x_i x_{di}, and x_{hdi}, respectively. Separation of cells into groups according to the extent of their damage and consideration for their dynamics are novel elements in modeling hematopoiesis in irradiated mammals. This approach makes it possible to collect more detailed information concerning the damage and recovery processes in radiosensitive cell populations as compared to other approaches. Of great importance is that this approach, as shown below, enables one to describe the contribution of radiation-damaged cells to the chalone control of hematopoiesis. According to the one-target-one-

hit model of cell damage [23], the specific damage rate is proportional to the radiation dose rate N. Therefore, the dynamics of hematopoietic cell concentration can be described by the system of nine differential equations:

$$\frac{dx_1}{dt} = B x_1 - Cx_1 - \frac{N}{D_1} x_1, \tag{1.7}$$

$$\frac{dx_2}{dt} = Cx_1 - Fx_2 - \frac{N}{D_2} x_2, \tag{1.8}$$

$$\frac{dx_3}{dt} = Fx_2 - Ex_3 - \frac{N}{D_3} x_3, \tag{1.9}$$

$$\frac{dx_{di}}{dt} = \frac{N}{D_i} \frac{1}{1 + \rho_i} x_i - v_1 x_{di}, \tag{1.10}$$

$$\frac{dx_{hdi}}{dt} = \frac{N}{D_i} \frac{\rho_i}{1 + \rho_i} x_i - v_2 x_{hdi}, \quad i = 1, 2, 3. \tag{1.11}$$

N/D_i are the specific rates of transition of cells X_i from the undamaged state to the damaged and heavily damaged states. The coefficients ρ_i represent the ratio of the number of heavily damaged X_{hdi} cells to the number of damaged X_{di} cells. Experimental data show that ρ_i depends on the dose rate N. The exact form of this dependence will be specified a bit later. The coefficients v_1 and v_2 represent the specific death rates of damaged and heavily damaged cells, respectively.

When modifying equation 1.6 that describes the X_1 cell reproduction rate, we take into account the contribution of X_{di} and X_{hdi} cells that died following irradiation to chalone production

$$B = \alpha \{1 + \beta [x_1 + \Phi x_{d1} + \Gamma x_{hd1} + \theta_2 (x_2 + \Phi x_{d2} + \Gamma x_{hd2}) + \theta_3 (x_3 + \Phi x_{d3} + \Gamma x_{hd3})]\}^{-1}. \tag{1.12}$$

The dimensionless multipliers Φ and Γ in front of the variables x_{di} and x_{hdi} represent the dissimilar contributions of damaged X_{di} and heavily damaged X_{hdi} cells to the production of the inhibitor I. The dissimilarity is due to differences in their specific death rates and $\Gamma/\Phi = v_2/v_1$.

In solving equations 1.7-1.11, initial conditions will differ for different problems. For example, in the case of irradiation of a healthy organism that has not been exposed to radiation earlier, the initial concentrations of undamaged X_i cells are equal to their stationary values, and the concentrations of damaged X_{di} and heavily damaged X_{hdi} cells are zero:

$$x_i(0) = \bar{x}_i, \quad x_{di}(0) = x_{hdi}(0) = 0, \quad i = 1, 2, 3. \tag{1.13}$$

When there is a group of radioresistant cells among the X_i cells in the model considered, we must let the parameter D_i tend to infinity, which will result in the absence of terms expressing the radiation effect.

The model can be substantially simplified if a radiation exposure of short duration (acute) is simulated: the characteristic times of equations 1.7-1.11 considerably exceed the time (T) of the irradiation. During irradiation, the cell dynamics is determined by the system of "rapid" equations

$$\begin{aligned} \frac{dx_i}{dt} &= -\frac{N}{D_i} x_i, \\ \frac{dx_{di}}{dt} &= \frac{N}{D_i} \frac{1}{1+\rho_i} x_i, \\ \frac{dx_{hdi}}{dt} &= \frac{N}{D_i} \frac{\rho_i}{1+\rho_i} x_i, \quad i = 1, 2, 3. \end{aligned} \tag{1.14}$$

As mentioned before, the initial conditions are described by relations 1.13.

With N = constant, equations 1.14 can be readily integrated:

$$\begin{aligned} x_i(T) &= \bar{x}_i \exp(-D/D_i), \\ x_{di}(T) &= \bar{x}_i (1+\rho_i)^{-1} [1 - \exp(D/D_i)], \\ x_{hdi}(T) &= \rho_i x_{di}(T), \quad (i = 1, 2, 3), \end{aligned} \tag{1.15}$$

where $D = N, T$ is the overall radiation dose. Relations 1.15 imply that D_i in equations 1.7-1.11 is equivalent to the conventional radiobiological dose D_0: after exposure to this dose, the number of X_i cells left undamaged is e (= 2.718...) times smaller than the initial number, i.e., constitutes 37% of their initial number (fig. 1.1*) [22]. Relationships 1.15 can serve as initial conditions of the model of postirradiation dynamics of damage and recovery of hematopoiesis. Then, in system 1.7 to 1.11, one should obviously put $N = 0$. When previously irradiated mammals are exposed to acute radiation doses, the initial concentrations of all the cells ($(x_i)_0$, $(x_{di})_0$, and $(x_{hdi})_0$) must be specified. Then, solutions to equations 1.14 and consequently, the initial conditions for system 1.7 to 1.11 will assume the form

$$\begin{aligned} x_i(T) &= (x_i)_0 \exp(-D/D_i), \\ x_{di}(T) &= (x_i)_0 (1+\rho_i)^{-1} [1 - \exp(-D/D_i)] + (x_{di})_0, \\ x_{hdi}(T) &= (x_i)_0 \rho_i (1+\rho_i)^{-1} [1 - \exp(-D/D_i)] + (x_{hdi})_0. \end{aligned} \tag{1.16}$$

*Figures begin on page 32.

Let us determine the dose dependence of the parameters ρ_i, which are the ratios of the heavily damaged to damaged cells. Based on experimental data, it has been shown that the fraction μ_i of X_i cells (which did not die in the interphase following acute irradiation with dose D) is an exponential function of D: $\mu_i = \exp(-D/D_{mi})$ [24]. The parameter D_{mi} is the dose after exposure to which the number of cells that have not died in the interphase is 37% of the initial number of cells (fig. 1.1) [22]. We set μ_i to be the combined fraction of undamaged X_i cells and damaged X_{di} cells. Accordingly, the fraction of heavily damaged X_{hdi} cells is

$$\omega_{hdi} = 1 - \mu_i = 1 - \exp(-D/D_{mi}). \tag{1.17}$$

The combined fraction of damaged X_{di} and heavily damaged X_{hdi} cells is defined by the expression $\omega_i = 1 - \exp(-D/D_i)$ (see equations 1.15). The fraction of damaged X_{di} cells is the difference between ω_i and ω_{hdi}:

$$\omega_{di} = \exp(-D/D_{mi}) - \exp(-D/D_i). \tag{1.18}$$

Then the parameter

$$\rho_i = \frac{\omega_{hdi}}{\omega_{di}} = \frac{1 - \exp(-D/D_{mi})}{\exp(-D/D_{mi}) - \exp(-D/D_i)}, \quad i = 1, 2, 3. \tag{1.19}$$

For $D \ll \min(D_{mi}, D_i)$, the coefficients ρ_i to a first approximation are

$$\rho_i = (D_{mi}/D_i - 1)^{-1}, \quad i = 1, 2, 3, \tag{1.20}$$

i.e., they are determined by the ratio of the parameters characterizing the radiosensitivity of X_i cells.

From physical considerations it is obvious that the simplified version (equation 1.20) of the expressions for the coefficients ρ_i can be used in differential equations 1.7 to 1.11 describing hematopoiesis dynamics in chronic radiation. The reason is that for any small interval of time dt, the condition of the applicability of formula 1.20, $D = N \cdot dt \ll (D_{mi}, D_i)$ will certainly be satisfied in the studied range of N variation.

Thus, we have shown how models of separate hematopoietic lines can be modified to describe the effects of chronic and acute radiation on the dynamics of hematopoiesis. Of great importance is that the model proposed contains in an explicit form the main characteristics of irradiation, namely dose D and dose rate N and also the conventional radiobiological parameters D_i and D_{mi} characterizing the radiosensitivity of the hematopoietic cells.

We examine below individual hematopoietic lines, each having its specific features of regulation and differing in cell radiosensitivity.

1.3. Thrombocytopoiesis

The generic cells of blood platelets (thrombocytes) are megakaryocytes, the giant cells of the bone marrow. The youngest morphologically identifiable cell of the megakaryocyte line is the dividing megakaryocytoblast. At the next differentiation stage (promegakaryocyte) the cells do not divide but grow in size by increasing their ploidy. A megakaryocyte can have 4, 8, 16, 32, or 64 nuclei. When the number of nuclei reaches 8, the megakaryocyte starts producing thrombocytes, which subsequently leave the bone marrow and pass into the blood. The number of thrombocytes produced by one megakaryocyte is proportional to the volume of its cytoplasm, which in turn is proportional to the number of nuclei of the mature megakaryocyte. On average, a megakaryocyte produces some 3,000-4,000 platelets and then dies. The blood platelets also undergo a natural process of dying. The control of the reproduction rate in the megakaryocytoblasts and their precursors is provided by a chalone—thrombocytopenin [16, 17].

X_1 denotes the bone marrow precursor cells (from stem cells in the respective microenvironment to megakaryocytoblasts), X_2 the nondividing cells (from promegakaryocytes to mature megakaryocytes), and X_3 the blood thrombocytes. Then, in accordance with equations 1.1 to 1.3 and relation 1.6, the dynamics of the respective concentrations x_1, x_2, x_3 are represented by the system of three differential equations

$$\frac{dx_1}{dt} = \frac{\alpha x_1}{1 + \beta (x_1 + \theta_2 x_2 + \theta_3 x_3)} - \gamma x_1, \tag{1.21}$$

$$\frac{dx_2}{dt} = f\gamma x_1 - \delta x_2, \tag{1.22}$$

$$\frac{dx_3}{dt} = \sigma \delta x_2 - \psi x_3. \tag{1.23}$$

The block-diagram of system 1.21 to 1.23 is given in figure 1.2. The coefficients α, β, θ_2, θ_3, $\gamma \equiv C$, $\delta \equiv F$, $\psi \equiv E$ in equations 1.21 to 1.23 have the same meaning as in equations 1.1 to 1.6.

The description of the complicated process of nucleus duplication in megakaryocytes, which eventually determines the megakaryocyte ploidy and the number of thrombocytes produced, is replaced in the model by a new integral quantity: coefficient of megakaryocyte ploidy f. It is known from experiments that in healthy mammals the platelet concentration in the blood, $\bar{x}_3$, the average ploidy of bone marrow megakaryocytes, $P(\bar{x}_3)$, and the thrombocyte yield per megakaryocyte, σ, are stable quantities. When the number of blood platelets is reduced ($x_3 < \bar{x}_3$), the average ploidy $P(x_3)$ increases: $P(x_3) > P(\bar{x}_3)$. The ratio of $P(x_3)$ to $P(\bar{x}_3)$ is the ploidy coefficient f. In accordance

with experimental data, the coefficient f is represented as decreasing function of thrombocyte concentration

$$f = P(x_3)/P(\bar{x}_3) = (h + \varphi x_3)^{-1}. \quad (1.24)$$

In formula 1.24, h and φ are certain constant parameters. Normally at $x_3 = \bar{x}_3$, $f = (h + \varphi \bar{x}_3)^{-1} = 1$, hence $\varphi \bar{x}_3 = 1 - h$. At $x_3 = 0$, $f = h^{-1}$, so the dimensionless parameter h must satisfy the condition

$$0 < h < 1. \quad (1.25)$$

When deriving equation 1.23, it was assumed that all X_2 cells have the same ploidy $P(\bar{x}_3)$ and produce the same number σ of thrombocytes after maturation. A change in the average ploidy is described in the model by an equivalent change of the concentration of X_2 cells. The concentration of X_1 cells that have just passed into phase X_2 is multiplied by coefficient f. This way of introducing coefficient f into equation 1.22 enables one to take into account in a dynamic form the delay effect between the control signal (deviation of thrombocyte concentration from the normal level) and the response (change of average megakaryocyte ploidy). Thus, the variable x_2 accounts for the dynamics of the total megakaryocyte mass in the bone marrow.

System 1.21 to 1.23 has two singular points. One singular point is trivial. The other is located in the positive octant ($\bar{x}_i > 0$) if $\alpha > \gamma$. In this case we identify the concentration $\bar{x}_i$ with the normal state of the thrombopoiesis system.

Data obtained by the methods of qualitative theory of differential equations and oscillation theory have shown that the trivial singular point is a stable node at $\alpha < \gamma$ and a saddle at $\alpha > \gamma$. The singular point in the positive octant can be either stable (node or focus) or unstable (saddle-focus). We derived algebraic equations determining in the space of the parameters the stability boundary for the second singular point. Analysis of these equations shows that loss of stability occurs (1) if the X_1 cell reproduction is mainly controlled by the inhibitor produced by X_3 cells, (2) if the time the cells stay in the X_2 and X_3 pools is sufficiently long, and (3) if the maximum specific reproduction rate of X_1 cells is within a certain range.

When the second singular point is unstable, then a stable limit cycle arises in the system 1.21 to 1.23. This cycle was obtained in solving equations 1.21 to 1.23 on a computer with the following values of the independent parameters: $\alpha = 4\ \text{day}^{-1}$, $\gamma = 2\ \text{day}^{-1}$, $\delta = 0.4\ \text{day}^{-1}$, $\psi = 0.5\ \text{day}^{-1}$, $\theta_2 = 0.4$, $\theta_3' = \sigma\theta_3 = 400$, $h = 0.9$. The parameters are chosen so that the values of the period T and the amplitude A of oscillations of the dimensionless concentration of X_3 cells ($\tilde{x}_3 = x_3/\bar{x}_3$), 14 days and 0.2, respectively (fig. 1.3A), correspond to the experimental data on grey collies, which showed in the norm stable oscillations of blood platelet concentration with a period T of 13 days and an amplitude A = 0.5 [25].

When the second singular point is a stable node or focus, the dynamics of the recovery processes is aperiodic or oscillatory. Experiments on rats in which platelets were removed from the blood [26] and, conversely, introduced into the blood [27] demonstrated damped oscillations of platelet concentration. These results were reproduced within the framework of system 1.21-1.23. The values of the parameters α, γ, δ, ψ were derived from experimental data [16, 20, 21] (table 1.1). The coefficient h varied from 0 to 1 in accordance with relationship 1.25. The parameters θ_2 and θ_3' varied over a wide range. Good agreement with experimental data [27] was obtained at $h = 0.5$, $\theta_2 = 0.1$, and $\theta_3' = 30$. Equations 1.21-1.23 describe both the recovery of the thrombocyte pool in the blood following its reduction by metabolic blood transfusion (fig. 1.4A) and the process of return of thrombocyte concentration to the normal level after injection of fresh thrombocytes into the blood (fig. 1.4B). In both cases the calculated dynamics of dimensionless platelet concentration has the form of damped oscillations. The χ^2-test was chosen for a quantitative comparison of the model and experimental results. The calculated values of $\chi^2 = 8.06$ and $\chi^2 = 8.8$ do not exceed their critical values of $\chi^2_{0,05} = 12.592$ (the number of degrees of freedom $n = 7 - 1 = 6$) and $\chi^2_{0,05} = 15.507$ ($n = 12 - 1 - 3 = 8$), i.e., there is a quantitative agreement.

As to the effect of ionizing radiation on thrombocytopoiesis, experiments [20, 21] have shown that platelets and all cells of the megakaryocyte line, beginning with promegakaryocytes, are radioresistant. The megakaryoblasts and their precursors are radiosensitive. Therefore, a model of thrombocytopoiesis dynamics in irradiated mammals must comprise five differential equations describing the concentrations of undamaged X_1, damaged X_{d1}, and heavily damaged X_{hd1} cells, and also the concentrations of radioresistant X_2 and X_3 cells (see section 1.2).

Our thrombocytopoiesis model was used in chronic irradiation simulation experiments on mice. It used the same values of the seven independent coefficients α, γ, δ, ψ, h, θ_2, $\theta_3' = \sigma\theta_3$ as did the model (equations 1.21-1.23) to describe thrombocytopoiesis dynamics in the absence of irradiation. The values of the coefficients ν_1 and ν_2 were taken from the literature [22]. The choice of the values of the parameters D_1, D_{m1}, and Φ was based on comparing the results of a numerical solution of the model equations with experimental data [28, 29] (table 1.1). Figure 1.5 demonstrates the computed dynamics of X_1, X_2, and X_3 cells for a moderate radiation dose rate. The figure also shows the results of experimental measurements of platelet concentration in the blood at different intervals of time after the onset of irradiation [28]. The model

Table 1.1. Parameters of the thrombocytopoiesis model.

Symbol	α	γ	δ	ψ	ν_1	ν_2	D_1	D_{m1}	Φ	θ_2	θ_3'	h
Value	2.4	1.4	0.35	0.35	0.5	6	2.4	4.8	209	0.1	30	0.5
Unit	day^{-1}	day^{-1}	day^{-1}	day^{-1}	day^{-1}	day^{-1}	Gy	Gy	-	-	-	-

describes the transition process in the form of damped oscillations. When the transition process is over, the dimensionless concentrations of X_1, X_2, and X_3 cells ($\tilde{x}_1 = x_1/\bar{x}_1$, $\tilde{x}_2 = x_2/\bar{x}_2$, and $\tilde{x}_3 = x_3/\bar{x}_3$, respectively) take on new, lower than normal stationary values, $\bar{\tilde{x}}_1$, $\bar{\tilde{x}}_2$, and $\bar{\tilde{x}}_3$. The large spread of experimental data [28] does not allow a detailed comparison with respect to transition process. Therefore, to check whether there is agreement between the model and the experimental results on the platelet concentration dynamics presented in figure 1.5, the χ^2-test was chosen as before. The calculated value of $\chi^2 = 4.195$ does not exceed the critical value $\chi^2_{0,05} = 12.592$ ($n = 6$), i.e., we do have quantitative agreement.

A rather similar thrombocytopoiesis dynamics was also obtained within the model for other (low and moderate) dose rates N of chronic irradiation. As in other experiments [28, 29], the new stationary level $\bar{\tilde{x}}_3$ lowered as the dose rate N increased. The same pattern was observed for the concentrations of X_1 and X_2 cells.

The relationship between the new stationary values of dimensionless concentrations of X_1, X_2, and X_3 cells and the radiation dose rate N is shown in figure 1.6. One can see that $\bar{\tilde{x}}_1$, $\bar{\tilde{x}}_2$, and $\bar{\tilde{x}}_3$ concentrations decrease with growing N and vanish when N becomes equal to or exceeds a certain critical level N_c. The latter is described in terms of the model parameters by the simple formula

$$N_c = D_1(\alpha - \gamma). \tag{1.26}$$

The meaning of equation 1.26 is as follows: The critical dose rate N_c is greater when the radiosensitivity of bone marrow cell precursors capable of dividing (X_1 cells) is smaller and the proliferation potential of these cells is higher.

Calculations have shown that with N values close to or exceeding $N_c = 2.4$ Gy/day, the dynamics of thrombocytopoiesis differs substantially from the one observed before. The kinetic curves showing the variation of X_1, X_2, and X_3 cell concentrations have an aperiodic shape. At $N \sim N_c$, the concentrations $\tilde{x}_1$, $\tilde{x}_2$, and $\tilde{x}_3$ reduce to low levels incompatible with life, and at $N \geq N_c$, they become equal to zero. These solutions can be regarded as corresponding to an irreversible depletion of the thrombocytopoietic system. Depletion of this kind was observed in mice during prolonged exposure to high radiation dose rates (fig. 1.7) [28, 30].

In turn, when a new stationary state sets up in the thrombocytopoietic system at low and moderate dose rates N, it can be regarded as system adaptation to chronic radiation and the stationary state itself as a new homeostasis. Note that adaptation to prolonged radiation exposures of cellular self-renewing systems, including that of thrombocytopoiesis, was observed in mammals by several authors [28, 29, 31].

It should be mentioned that all the parameters of the model were varied within reasonable ranges during a preliminary study on a computer. It was found that

minimal concentrations of X_1, X_2, and X_3 cells are largely determined by the parameter D_1, which specifies radiosensitivity of bone marrow thrombocyte precursors capable of dividing. The parameter D_1 as well as the coefficients θ_2, θ_3', and Φ exert a considerable effect on the new stationary concentrations of the X_1, X_2, and X_3 cells. All the quantities listed also depend on the variable parameter N—the dose rate of prolonged radiation.

The results obtained with this model are in qualitative agreement with patterns observed in studies of thrombocytopoiesis in various mammals exposed to chronic radiation [22, 32].

Next we simulated experiments with acute radiation of mice. The dynamics of thrombocytopoiesis for sublethal doses is shown in figure 1.8. Experimental data from reference 20 are represented by average values of platelet concentration in the peripheral blood of mice at different intervals of time following irradiation, and the model results are shown by three kinetic curves. The first curve represents the dynamics of the concentration for the entire X_1 pool, which includes undamaged, damaged, and heavily damaged cells. Starting from the time when concentrations of X_{d1} and X_{hd1} cells are at zero, this curve describes the concentration of undamaged X_1 cells. This representation of the computations allows reconstruction of not only the recovery process but also the dynamics of reduction of pool X_1 cell concentration as a result of death of some of these cells. The second and third kinetic curves in figure 1.8 describe the concentrations of radioresistant X_2 and X_3 cells, respectively. One can see that platelet concentration decreases both in the model and in the experiment within the first 8 days after irradiation. Then the recovery process sets up. By day 16 postirradiation the platelet concentration reaches a maximum and decreases once again. The recovery process, having the form of damped oscillations, is essentially completed in 50 days after irradiation.

We have also obtained a dependence on acute irradiation dose in the damage process of the thrombocytopoietic system similar to that observed in earlier experiments [20]. The initial decrease of platelet concentration in the blood of irradiated animals is greater the larger the radiation dose D. Similar dependencies on D are typical of minimal concentrations of X_1 and X_2 cells.

When varying the values of the parameters in the course of preliminary computer-aided study of the model, we found that the principal indices of postirradiation damage of the thrombocytopoietic system—namely the minimal levels of X_1, X_2, and X_3 cell concentrations—are largely determined by the parameter D_1, which specifies the radiosensitivity of bone marrow thrombocyte precursors (X_1 cells), and also by radiation dose D.

Dose dependencies of postirradiation dynamics of damage and recovery of the thrombocytopoietic system qualitatively agree with experimental data on other mammals [20].

1.4. Lymphopoiesis

The lymphocyte is a type of white blood cell (leukocyte). The first morphologically identifiable lymphocyte precursors in the bone marrow are lymphoblasts. These cells later reach the stage of nondividing maturing lymphocytes. Mature lymphocytes leave the bone marrow and pass into the blood. Lymphocytes are capable of passing from the blood flow to the lymph and back and also of residing in lymphatic organs (thymus, spleen, lymph nodes, etc.). Reproduction of bone-marrow lymphocyte precursors is controlled by the lymphocytic chalone [16, 17].

In describing bone marrow lymphopoiesis we restrict ourselves to examining the lymphocyte dynamics in the absence of any antigenic stimulation. We denote bone marrow precursor cells from stem cells in the respective microenvironment to lymphoblasts by X_1, nondividing maturing lymphoid cells of the bone marrow by X_2, and mature lymphocytes in the blood by X_3. By using equations 1.1 to 1.3 and relation 1.6, the pattern of variation of the concentrations x_1, x_2, and x_3 is described by the system of three differential equations:

$$\frac{dx_1}{dt} = \frac{\alpha x_1}{1 + \beta (x_1 + \theta_2 x_2 + \theta_3 x_3)} - \gamma x_1, \tag{1.27}$$

$$\frac{dx_2}{dt} = \gamma x_1 - \delta x_2, \tag{1.28}$$

$$\frac{dx_3}{dt} = \delta x_2 - \psi x_3. \tag{1.29}$$

The block diagram of system 1.27-1.29 is presented in fig. 1.2B. The meaning of the constants α, β, θ_2, θ_3, $\gamma \equiv C$, $\delta \equiv F$, $\psi \equiv E$ is the same as in equations 1.1-1.6 (see section 1.2).

System 1.27-1.29 has two singular points. The first singular point is trivial. The coordinates $\bar{x}_1, \bar{x}_2, \bar{x}_3$ of the second point are positive if $\alpha > \gamma$. In this case $\bar{x}_i$ is the normal lymphoid cell concentration. The trivial singular point is unstable (saddle) if $\alpha > \gamma$ and stable (node) if $\alpha < \gamma$. The second singular point can become unstable (saddle-focus). In this case the system has a particular solution: a stable limit cycle. Within model 1.27-1.29 we derived algebraic equations determining in the space of the parameters the bifurcation of generation of a stable limit cycle. The equations are similar to those obtained in the thrombocytopoiesis model and have the same physical meaning. The limit cycle was obtained in the model with the following values of the independent parameters: $\alpha = 2.4$ day^{-1}, $\gamma = 1.4$ day^{-1}, $\delta = 0.23$ day^{-1}, $\psi = 0.1$ day^{-1}, $\theta_2 = 0.5$, $\theta_3 = 10$ (fig. 1.3B). The parameters are chosen so that the period T and the amplitude A of oscillations of the X_3 cell dimensionless concentrations were about 50 days and $A = 1.2$, respectively. Note that a cyclic lymphopoiesis kinetics was observed in dogs and in humans [33, 34]. When

the second singular point is stable, it can be a node or a focus. The dynamics of the recovery processes is then either aperiodic or oscillatory, which is consistent with experimental observations.

It is well known that both mature lymphocytes and their precursors are radiosensitive [20-22]. The lymphopoiesis dynamics models for irradiated mammals include nine differential equations describing the concentrations of undamaged, damaged, and heavily damaged cells of the three groups: X_i, X_{di}, and X_{hdi} ($i = 1, 2, 3$) (see section 1.2).

The model was used to simulate lymphopoiesis dynamics during chronic irradiation of mice. The values of the coefficients θ_2, θ_3, Φ were chosen in the course of a computer-assisted numerical study of the model. The other 12 independent parameters were found on the basis of hematologic and radiobiological data [16, 20-22, 35] (table 1.2). Figure 1.9 shows the dynamics of X_1, X_2, and X_3 cell concentrations computed for chronic radiation at a low dose rate.The figure also gives the results of experiments [29] in which the lymphocyte concentration in the blood of *H* strain mice was measured at different time intervals after onset of radiation. There is good agreement between the model and experimental results on blood lymphocyte (X_3 cell) dynamics. The calculated value of $\chi^2 = 9.92$ does not exceed its critical value $\chi^2_{0,05} = 18.307$ (the number of degrees of freedom $n = 10$).

This model was used to study the lymphopoiesis dynamics for other low and moderate dose rates of chronic radiation. It has been found that when the transition process in the form of rapidly damped oscillations is over, the dimensionless concentrations of X_1, X_2, and X_3 cells take on new stationary values $\bar{\tilde{x}}_1$, $\bar{\tilde{x}}_2$, and $\bar{\tilde{x}}_3$. As in earlier experiments [28, 29], the stationary level of blood lymphocyte concentration $\bar{\tilde{x}}_3$ declines as N increases. The stationary concentrations $\bar{\tilde{x}}_1$ and $\bar{\tilde{x}}_2$ depend on the dose rate N in a more complicated way (fig. 1.10). Analysis of the model has shown that if the parameters satisfy the conditions $D_1/D_2 < \gamma/\delta$ and $\Phi < \mu/\psi$, the stationary concentrations $\bar{\tilde{x}}_1$ and $\bar{\tilde{x}}_2$ exceed the normal level at $0 < N < N_1$ and $0 < N < N_2$, respectively. This prediction of the model was confirmed experimentally [32, 36]. The effect of chronic radiation on lymphopoiesis is manifested in an enhanced mitotic activity of X_1 cells. This finding also agrees with an earlier experiment [37].

The elevated (compared to normal) concentration of lymphocyte precursors capable of dividing (X_1 cells) and of their nondividing progeny (X_2 cells) in the bone marrow of mammals can be regarded as a manifestation of stimulation of the lymphopoietic system adaptation to prolonged radiation at low dose

Table 1.2. Parameters of the lymphopoiesis model.

Symbol	α	γ	δ	ψ	ν_1	ν_2	D_1	D_{m1}	D_2	D_{m2}	D_3	D_{m3}	θ_2	θ_3	Φ
Value	2.4	1.4	0.2	0.1	0.5	6	1.4	13	1.4	13	1	6.5	0.1	0.16	1.01
Unit	day^{-1}	day^{-1}	day^{-1}	day^{-1}	day^{-1}	day^{-1}	Gy	Gy	Gy	Gy	Gy	Gy	-	-	-

rates. This phenomenon can be called radiation hormesis (opposite effects of low and high doses and dose rates of radiation on the biota), which has been the subject of intensive studies [38, 39]. Note that the curves in figure 1.10, which show the dependence of stationary concentrations of lymphoid cells in the bone marrow on the dose rate N of chronic radiation, have the same shape as a hypothetic generalized dose-effect curve illustrating the existence of radiation hormesis in continuous irradiation [39].

Figure 1.10 shows that for $N > N_1$ and $N > N_2$ the stationary concentrations of X_1 and X_2 cells decrease, respectively, as N increases. The stationary concentrations of X_1, X_2, and X_3 cells become equal to zero at $N \geq N_c$. The quantity N_c in the lymphopoiesis and thrombocytopoiesis models is defined by the same formula, 1.26, but is smaller for the lymphopoiesis system: $N_c = 1.4$ Gy/day.

In both the lymphopoiesis and thrombocytopoiesis models, the kinetic curves describing the concentrations of X_1, X_2, and X_3 cell pools at high dose rates N have an aperiodic character. The concentrations of lymphoid cells in the bone marrow and of lymphocytes in the blood drop to levels incompatible with life (at $N \sim N_c$) or to zero (at $N \geq N_c$). These model results agree with experimental data [30] and correspond to irreversible depletion of the lymphopoietic system in mammals, resulting in the death of irradiated animals (fig. 1.11).

During the preliminary computer study of the model all the parameters underwent variation. It was found that the minimal concentrations of X_1, X_2, and X_3 cells depend mainly on the parameters D_1, D_2, D_3 specifying the radiosensitivity of these cells. The parameters D_1, D_2, D_3 as well as the coefficients θ_2, θ_3, Φ have an appreciable influence on the new stationary levels of X_1, X_2, X_3 cell concentrations. The above quantities also depend on the variable parameter N—the dose rate of continuous irradiation.

The results obtained within the framework of the model are qualitatively consistent with the patterns observed in experiments on lymphopoiesis dynamics in various mammalian species during chronic irradiation [22, 32].

The dynamics of lymphopoiesis in acute irradiation at sublethal dose is shown in figure 1.12A. Hulse's experimental data [40] are represented by mean values of lymphoid cell concentrations in the bone marrow and lymphocyte concentrations in the blood of rats at various intervals after irradiation. Model data are indicated by three curves of cell concentrations for the three pools X_1, X_2, X_3, which include undamaged, damaged, and heavily damaged cells. Such a representation of the computations helps illustrate the dynamics of the damage and recovery of lymphopoiesis. A similar representation has already been used to describe the kinetics of radiosensitive X_1 cell concentration in the thrombocytopoiesis model (see section 1.3) and will be used to reproduce the postirradiation dynamics of radiosensitive cell concentrations in the erythropoietic and granulocytopoietic systems (see sections 1.5 and 1.6). Figure 1.12A shows that within the first postirradiation days the concentrations of lymphoid cells

in the bone marrow and blood decreased. The computations have shown that this decrease is larger the higher the radiation dose. Thereafter the recovery process sets up and is over within 50 days after irradiation. In comparison to experimental values, the overestimated theoretical values of lymphocyte concentration in the blood (pool X_3 cells) seem to be explained by an enhanced migration of lymphocytes from the blood to the lymph, which is not considered in our model.

In model simulation of the effect of acute irradiation on lymphopoiesis, all parameters were varied, too. It was found that the indices of radiation injury of the lymphopoietic system—minimal concentrations of cells of the X_1, X_2, X_3 pools—are largely determined by the coefficients D_1, D_2, and D_3 specifying the radiosensitivity of these cells and by the dose D.

Specific features of postirradiation lymphopoiesis dynamics obtained in the model qualitatively agree with results of experiments on the effects of acute irradiation on lymphopoiesis in various mammalian species [20].

Some interesting data were obtained in computer simulation of acute irradiation of animals that had been previously exposed to chronic irradiation at low dose rate N. The initial conditions were given by formula 1.16 (see section 1.2). Figure 1.12B shows the calculated dynamics of lymphopoiesis after acute irradiation of rats at the same dose as shown in figure 1.12A. Rats had been previously exposed to chronic irradiation with $N = 0.1$ Gy/day. One can see that prolonged preliminary radiation exposure at a low dose rate N stimulates the recovery processes in the lymphopoietic system: they become faster and more intense. Calculations have shown that as the preliminary irradiation dose rate N increases, the stimulating effect first grows and then diminishes. The maximum of the stimulating effect correlates well with the maximum stationary concentration of lymphocyte precursors capable of dividing in the bone marrow of mammals exposed to preliminary continuous irradiation (fig. 1.10). Thus, model solutions are consistent with the evidence demonstrating an enhancement of the ability for tissue self-repair in mammals (rats, mice, and humans) that have been exposed for a long time to elevated radiation levels [39, 41]. Modeling results indicate that to account for the stimulating effect there is no need to resort to any additional hypotheses on mechanisms of action of low dose rate radiation on lymphopoiesis. The stimulating effect can be described by the chalone theory of hematopoiesis regulation.

1.5. Erythropoiesis

Erythrocytes are red blood cells [16] that have a vital function: transporting oxygen in the blood. The first morphologically identifiable precursors of erythrocytes in the bone marrow are proerythroblasts. The reproducing cells of the erythrocytic series also include the basophilic erythroblast and early and

average polychromatophil normoblasts. The rate of reproduction of erythrocyte precursors is controlled by the erythrocytic chalones [16, 17]. Cell division ceases at the subsequent stages of differentiation and maturation (late polychromatophil normoblast, oxyphilic normoblast, pronormocyte, normocyte, reticulocyte, erythrocyte). Mature cells leave the bone marrow, circulate in the peripheral blood, then die. As before, we divide all the cells of the erythrocytic series into groups X_1, X_2, and X_3. In accordance with the above-stated concepts and model 1.1-1.3 and 1.6, the concentration dynamics in these groups can be described by differential equations 1.27-1.29. Therefore, all results of the analytic investigation of the lymphopoiesis model are valid for the erythropoiesis model. In particular, a stable limit cycle (fig. 1.3C) was found. The values of the independent parameters have been chosen so that the modeling results correspond to the cyclic kinetics of erythropoiesis in healthy dogs [42]; the values are $\alpha = 2.4$ day^{-1}, $\gamma = 1.4$ day^{-1}, $\delta = 0.3$ day^{-1}, $\psi = 0.033$ day^{-1}, $\theta_2 = 0.1$, and $\theta_3 = 2$.

As regards the effects of radiation on the erythropoiesis, experiments have shown that erythrocytes in the blood are radioresistant, whereas their precursor cells in bone marrow are sensitive to radiation [20-22]. Therefore, models of erythropoiesis dynamics for irradiated mammals comprise seven differential equations to describe the concentrations of undamaged, damaged, and heavily damaged X_i, Xd_i, and X_{hdi} cells, respectively, ($i = 1, 2$), and also the concentration of radioresistant X_3 cells (see section 1.2).

Our model was used to calculate erythropoiesis dynamics in mice exposed to chronic radiation. The values of the coefficients θ_2, θ_3, and Φ were chosen in the process of solving the equations numerically on a computer. The values of the other ten independent parameters were determined from hematologic and radiobiological experimental data [16, 20-22, 43] (table 1.3). The dynamics of X_1, X_2, and X_3 cell concentrations computed for chronic irradiation at a low dose rate are shown in figure 1.13. Also presented in the figure are the results of experiments [29] in which the erythrocyte concentration in the blood of mice of *H* strain was measured at various intervals of time from the onset of irradiation. The statistical χ^2-test was used to check the adequacy of the model and the experimental results. The computed value of $\chi^2 = 5.89$ did not exceed its critical value $\chi^2_{0,05} = 14.067$ (the number of degrees of freedom $n = 7$), which is indicative of agreement. Figure 1.13 demonstrates that upon completion of the transition process a new dynamic equilibrium state is established in the system. This equilibrium is analogous to a new homeostasis, and the process of its establishing is analogous to adaptation of the system to the effect of continuous irradiation. This model result is supported experimentally [28, 29, 31].

Table 1.3. Parameters of the erythropoiesis model.

Symbol	α	γ	δ	ψ	ν_1	ν_2	θ_2	θ_3	Φ	D_1	D_1	D_2	D_{m2}	D_i	D_c
Value	2.4	1.5	1.1	0.04	1	6	0.01	0.06	2.5	1.7	6	0.6	8	4	2
Unit	day^{-1}	day^{-1}	day^{-1}	day^{-1}	day^{-1}	day^{-1}	-	-	-	Gy	Gy	Gy	Gy	Gy	Gy

The transition process in the erythropoietic system has some peculiarities. Whereas the concentrations of X_1 and X_2 cells after irradiation drop to some minimal levels, then increase and assume new stationary values, the concentration of X_3 cells slowly reduces until it reaches a stationary level. This seems to be due to the "inertia" of the X_3 cell population resulting from the large life span of blood erythrocytes and their radioresistance. As in experiments [28, 29], the new stationary concentration of X_3 cells ($\bar{\bar{x}}_3$) decreases as N increases. The same relationship is valid for the stationary concentrations of X_1 and X_2 cells ($\bar{\bar{x}}_1$, $\bar{\bar{x}}_2$); (fig. 1.14). Figure 1.14 shows that $\bar{\bar{x}}_1$, $\bar{\bar{x}}_2$, $\bar{\bar{x}}_3$ are zero at $N \geq N_c$. Note that N_c is defined by the same formula 1.26 as in the lymphopoiesis and thrombocytopoiesis models and is close to the critical dose rate for the lymphopoietic system: $N_c = 1.53$ Gy/day.

At N values that are close to or exceed the critical dose rate, erythropoiesis dynamics is aperiodic as in models considered earlier. The concentrations of cells X_1, X_2, X_3 decrease to low values at $N \sim N_c$ and to zero at $N \geq N_c$. Comparison of the model dynamics of X_3 cells calculated for lethal dose rates with the corresponding experimental data on the kinetics of erythrocyte concentration in the blood of mice [30] demonstrates their qualitative and quantitative agreement for the first 10 days from onset of irradiation (fig. 1.15). The comparison could not be continued because of the death of the mice.

During a preliminary computer study of the model, all parameters were varied within reasonable ranges. It was found that minimal concentrations of X_1 and X_2 cells are mainly determined by the parameters D_1 and D_2 that specify the radiosensitivity of these cells. The same parameters, as well as the coefficients θ_2, θ_3, and Φ, govern to a considerable degree the new concentration levels for X_1, X_2 and X_3 cells. The values also depend on the variable parameter N—the dose rate of chronic irradiation.

The above results of numerical modeling qualitatively correspond to the erythropoiesis dynamics in other mammalian species during protracted irradiation [22, 32].

Erythropoiesis in rats after acute irradiation at various doses was also modeled. The values of the parameters are listed in table 1.3. The model qualitatively reproduces the basic patterns of postirradiation dynamics of erythropoietic cells in the bone marrow and erythrocytes in the peripheral blood [20, 40, 44]. For example, the model describes a postirradiation decrease in concentration of all the three cell groups. Having decreased to minimal values, the cell concentrations of X_1 and X_2 pools start growing, reach a maximum, decline, and return to the initial level; X_3 cell concentration reaches the normal level practically without oscillations. Dose dependence of the minimal cell concentrations of the pools X_1 and X_2 in the erythropoietic model is the same as in the lymphopoietic and thrombocytopoietic models: the minimal level is lower the higher the radiation dose is.

Modeling results also agree quantitatively with experimental data. This is evident from figure 1.16A, which shows the calculated and experimental concentration changes of the erythrocyte precursors in the bone marrow (cells of the X_1 and X_2 pools) and of the erythrocytes in the blood (X_3 cells) of rats following acute irradiation at a sublethal dose [20, 40]. However, the model does not describe a peculiar feature of postirradiation dynamics of the bone marrow erythrocyte precursors, which is an elevation of cell concentration shortly after irradiation ("abortive" elevation). At present, there is no consensus of opinion as to the nature of the abortive concentration elevation. Many authors explain it by the existence of weakly damaged cells that do not belong to the groups of cells termed damaged and heavily damaged in this work. It is suggested that these weakly damaged cells (X_{wd1} cells) divide and differentiate as ordinary intact X_1 cells for the first few days, whereupon they die together with their progeny [20].

The theory of abortive elevation has been taken into account in the model in the following way. In addition to X_i, X_{di}, and X_{hdi} cells we have introduced X_{wdi} cells ($i = 1, 2, 3$). Their concentration x_{wdi} in the time interval from onset of irradiation to the time of maximum abortive elevation ($t = t_{ae}$) is described by equations identical to those for the X_i cell concentrations. Next we assumed for the sake of simplicity that, at time t_{ae}, cells from the X_{wdi} group pass to the X_{hdi} group and die at a specific rate ν_2. Expression 1.12 was transformed to take into account the contribution of X_{wdi} cells to chalone production. The initial conditions for solving the modified system of equations were also changed. Two new parameters, D_1', and D_c, were substituted for the coefficient D_1. The parameter D_1' is the dose after which the total number of undamaged and weakly damaged cells is 37% of the initial number of X_1 cells. The parameter D_c is the dose after which the number of weakly damaged cells is 37% of the initial number of X_1 cells (see table 1.3).

Figure 1.16B presents the dynamics of erythropoiesis calculated within the framework of the modified model for the same dose as in figure1.16A. In figure 1.16B the model reproduces the abortive elevation of erythroid cell concentration in the bone marrow. As shown by model studies, the magnitude of the secondary depletion is determined by the number of X_1 cells left intact after irradiation, and the amplitude of the abortive elevation depends on the size of the X_{wd1} cell population.

The models described do not include the contribution of erythropoietin to the regulatory processes. This simplification is explained by the following considerations. It is believed that erythropoietin substantially affects erythropoiesis in mammals in conditions of emergency (hemorrhages, hypoxia, etc.) when a quick response of the blood system is needed to provide required oxygen to the organism. In the experimental conditions we deal with, no such emergencies are likely to arise. With low and moderate doses D of acute radiation and dose rates N of chronic radiation, hemorrhages do not occur, and hypoxia is very weak if at all present, because the reduction of erythrocyte concentration

in the blood is insignificant. At high D and N, animals die either before a hemorrhage takes place or at the time of hemorrhage.

In the course of the preliminary computer study of the model, all the parameters were varied. It was found that the basic indices of radiation-induced damage of the erythropoietic system—the minimal concentrations of X_1, X_2, and X_3 cells—are largely determined by the parameters D_1 and D_2 that specify the radiosensitivity of X_1 and X_2 cells, as well as by the radiation dose D. The magnitude of secondary depletion depends to a large extent on D, D_1', and D_c.

The results of modeling we obtained are qualitatively consistent with the observed postirradiation patterns of erythropoiesis in different mammalian species [20].

1.6. Granulocytopoiesis

Granulocytes are a class of leukocytes. Their function in the organism is a nonspecific immune protection by digestion of foreign substances with the help of hydrolytic enzymes. The first morphologically identifiable granulocyte precursor cells in the bone marrow are myeloblasts. The dividing cells of the granulocyte series also include promyelocytes and myelocytes. Reproduction of the granulocyte precursors is controlled by the granulocytic chalone [16, 17]. At subsequent stages of differentiation and maturation (metamyelocyte, granulocyte) the cells do not divide. For some time mature cells remain in the bone marrow, in the so-called bone marrow depot, then pass into the blood. There is a negative feedback between the rate of granulocyte emergence from the bone marrow and the number of granulocytes in the peripheral blood. From the blood the granulocytes migrate to the tissues; tissue granulocytes no longer circulate, and this is the final stage of their life.

First we constructed a simplified model. We denote by X_1 the bone marrow precursor cells, from stem cells in the respective microenvironment to myelocytes; by X_2, the metamyelocytes and the mature bone marrow granulocytes, and by X_3, the mature granulocytes outside the bone marrow. With equations 1.1-1.3 and relation 1.6, the changes in cell concentrations x_1, x_2, and x_3 can be described as follows:

$$\frac{dx_1}{dt} = \frac{\alpha x_1}{1 + \beta (x_1 + \theta_2 x_2 + \theta_3 x_3)} - \gamma x_1, \tag{1.30}$$

$$\frac{dx_2}{dt} = \gamma x_1 - F x_2, \tag{1.31}$$

$$\frac{dx_3}{dt} = F x_2 - \psi x_3. \tag{1.32}$$

The block diagram of system 1.30-1.32 is illustrated in figure 1.2C. The constant coefficients α, β, θ_2, θ_3, $\gamma \equiv C$, $\psi \equiv E$ have the same meaning as in equations 1.1-1.6. The specific rate of granulocyte supply to the blood flow, with consideration for the bone marrow depot, we represent as a decreasing function of the concentration x_3:

$$F = \delta(1 + Mx_3^2)/(1 + Lx_3^2). \tag{1.33}$$

The quantities δ and δ M/L are the maximal and minimal specific rates of granulocyte output from the bone marrow, respectively. The constants L and M are related by inequality $L > M$.

System 1.30-1.32 has two singular points. The first point is trivial. The second singular point $\bar{x}_1$ $\bar{x}_2$, $\bar{x}_3$ is in the positive octant if $\alpha > \gamma$, as in the preceding cases. This point corresponds to the normal state of granulocytopoiesis. The trivial singular point is either a stable node ($\alpha < \gamma$) or a saddle ($\alpha > \gamma$). When $\alpha > \gamma$, the second singular point located in the positive octant can be unstable (saddle-focus), and then, apart from unstable singular points, the system has one more particular solution: a stable limit cycle. The algebraic equations defining in the space of the parameters the bifurcation of the stable limit cycle generation are similar to those derived in the models of other hematopoietic lines and have the same physical meaning. Figure 1.3D-F shows projections onto the phase planes $\{\tilde{x}_1\, \tilde{x}_2\}$, $\{\tilde{x}_3\, \tilde{x}_1\}$ $\{\tilde{x}_2\, \tilde{x}_3\}$of the integral curves of system 1.30-1.32 converging to the limit cycle. Computations were performed with $\alpha = 2.4$ day^{-1}, $\gamma = 0.5$ day^{-1}, $\psi = 0.15$ day^{-1}, $\delta = 0.2$ day^{-1}, $m = M\bar{x}_3^2 = 0.33$, $l = L\bar{x}_3^2 = 1.12$, $\theta_2 = 0.5$, and $\theta_3 = 10$. The initial conditions were $\tilde{x}_1(0) = \tilde{x}_2(0) = \tilde{x}_3(0) = 2$ and $\tilde{x}_1(0) = 2.2$, $\tilde{x}_2(0) = 2.05$, $\tilde{x}_3(0) = 1.25$. The chosen parameters are such that the period and amplitude of oscillations of dimensionless cell X_3 concentration ($T = 51$ day, $A = 0.43$) coincide by the order of magnitude with the corresponding characteristics of granulocyte concentration oscillations in the blood of healthy men and women [45].

In cases when the second singular point becomes stable, it can be either a node or a focus. That means that when the variables $\tilde{x}_1, \tilde{x}_2, \tilde{x}_3$ deviate from this point, the kinetic curves return to it either aperiodically or with oscillations, and this was observed in experiments.

Researchers often restrict study to only two indices: the concentration of granulocytes in the peripheral blood and the total number of granulopoietic elements in the bone marrow. For an effective comparison of modeling results and experimental data, system 1.30-1.32 should be modified. Instead of 1.32 we introduce two equations for granulocytes in the peripheral blood and those in tissues (cells X_4 and X_5 and their respective concentrations x_4 and x_5). We assume that the specific rate of granulocyte output from the bone marrow depot is largely determined by the granulocyte concentration in the bloodstream. Finally, the model takes the form

$$\frac{dx_1}{dt} = \frac{\alpha x_1}{1 + \beta (x_1 + \theta_2 x_2 + \theta_4 x_4 + \theta_5 x_5)} - \gamma x_1, \tag{1.34}$$

$$\frac{dx_2}{dt} = \gamma x_1 - \delta \frac{1 + M x_4^2}{1 + L x_4^2} x_2, \tag{1.35}$$

$$\frac{dx_4}{dt} = \delta \frac{1 + M x_4^2}{1 + L x_4^2} x_2 - \kappa x_4, \tag{1.36}$$

$$\frac{dx_5}{dt} = \kappa x_4 - \psi x_5. \tag{1.37}$$

In equations 1.36 and 1.37, the parameter κ is the specific rate of passage of cells from group X_4 to group X_5. The block diagram of system 1.34-1.37 is shown in figure 1.2D. System 1.34-1.37 has two singular points. The first singular point is trivial, and the coordinates $\bar{x}_i$ of the second point are identical to normal concentrations of X_i cells ($i = 1, 2, 4, 5$).

Experiments have shown that all cells of the granulocytic series exhibit radiosensitivity though in varying degrees [46]. Therefore, models of granulocytopoiesis dynamics in irradiated mammals based on system 1.34-1.37 comprise 12 differential equations that describe the concentrations of undamaged, damaged, and heavily damaged cells X_i, X_{di}, X_{hdi} ($i = 1, 2, 4, 5$).

We modeled the granulocytopoiesis dynamics in chronically irradiated mice. The values of the coefficients θ_2, θ_4, θ_5, Φ were selected during a numerical computer study of the model. The rest of the parameters were determined from the available hematologic and radiobiological data [16, 20, 21, 22, 46]. All these parameters are presented in table 1.4. The dynamics of dimensionless concentrations of X_1, X_2, X_4, X_5 cells ($\tilde{x}_1 = x_1/\bar{x}_1$, $\tilde{x}_2 = x_2/\bar{x}_2$, $\tilde{x}_4 = x_4/\bar{x}_4$, $\tilde{x}_5 = x_5/\bar{x}_5$) calculated on a computer for low dose rates of chronic irradiation and the corresponding experimental values of granulocyte concentration in the blood [28] are demonstrated in figure 1.17. The modeling results quantitatively agree with experimental data. The calculated value of $\chi^2 = 0.458$ does not exceed its critical value $\chi^2_{0,05} = 18.307$ ($n = 10$). Figure 1.17 shows that after the onset of irradiation the concentrations of X_1, X_2, X_4 and X_5 cells first decrease to certain minimal values but later increase and reach new stationary levels. The relationships between the new stationary dimensionless concentrations of these cells ($\bar{\tilde{x}}_1, \bar{\tilde{x}}_2, \bar{\tilde{x}}_4, \bar{\tilde{x}}_5$) and dose rate N are shown in figure 1.18. Within certain ranges of variation of chronic irradiation dose rate N, the concentrations $\bar{\tilde{x}}_1, \bar{\tilde{x}}_2, \bar{\tilde{x}}_4$ can be higher than normal. This result was experimentally confirmed [32, 37]. New stationary concentrations of X_5 cells drop below the normal level as N increases.

The effect of chronic irradiation on granulocytopoiesis also manifests itself in enhanced mitotic activity of X_1 cells, which agrees with experimental data [37, 47].

The elevated concentrations of X_1 cells and their nondividing X_2 cell progeny in the bone marrow and of granulocytes X_4 in the blood can be manifestations of the granulocytopoietic system adaptating to prolonged irradiation at low dose rates. This finding can be classed with the effects of radiation hormesis.

It follows from figure 1.18 that the stationary concentrations of X_1, X_2, X_4, and X_5 cells become equal to zero at $N \geq N_c$. The critical dose rate in the granulocytopoiesis model is determined by formula 1.26, as in previously described models, but has the highest value: $N_c = 5.1$ Gy/day.

At N values close to or exceeding N_c, granulocytopoiesis dynamics has an aperiodic character, as in the models of other hematopoietic lines. The concentrations of cells of the granulocytic series drop to low levels at $N \sim N_c$ and to zero at $N \geq N_c$. Such solutions can be identified with an irreversible depletion of the granulocytopoietic system, which was observed in mammals at high doses of chronic irradiation. The results of modeling (fig. 1.19) agree with the corresponding experimental data not only qualitatively but also quantitatively [30].

Also modeled was the granulocytopoiesis dynamics in rats exposed to acute irradiation (table 1.4). As with models of other hematopoietic lines, concentrations of cells of the granulocytic series decrease postirradiation to minimal values, which are smaller the larger the dose. Thereafter a recovery process ensues, which has the character of rapidly damped oscillations. When this process is over, the concentrations of all cell groups return to initial levels.

Concentrations of granulopoietic cells of the bone marrow and of granulocytes in the blood measured in rats at various time intervals after irradiation at

Table 1.4. Parameters of the granulocytopoiesis model.

Symbol	α	γ	δ	κ	ψ	ν_1	ν_2	
Value	2.4	0.36	0.33	2.4	0.03	0.5	6	
Unit	day^{-1}	day^{-1}	day^{-1}	day^{-1}	day^{-1}	day^{-1}	day^{-1}	
Symbol	m	l	θ_2	θ_4	θ_5	Φ	D_1	D_{m1}
Value	0.33	2	0.01	0.06	0.23	1.01	2.5	5
Unit	-	-	-	-	-	-	Gy	Gy
Symbol	D_2	D_4	D_5	D_{m2}	D_{m4}	D_{m5}	D_1'	D_c
Value	10	10	10	100	100	100	4	1.5
Unit	Gy	Gy	Gy	Gy	Gy	Gy	Gy	Gy

moderate doses are presented in figure 1.20 [40, 48]. The figure also shows the corresponding calculated curves. One can see that the model adequately reproduces experimental results [40, 48], except that it does not describe the abortive elevation of concentrations of these cells. The model was therefore improved to account for this peculiar feature of the dynamics of postirradiation granulocytopoiesis (see section 1.5). The results of the modified model calculations at the same dose as before are also given in figure 1.20. The modified model does reproduce the abortive elevation of concentrations. It should be noted that a comparison of experimental concentration dynamics for blood granulocytes with the two calculated versions (curves II and IV, fig. 1.20) yielded $\chi^2 = 7.384$ and $\chi^2 = 6.732$ that do not exceed their critical values $\chi^2_{0,05} = 18.307$, ($n = 10$), i.e, there is quantitative agreement in both cases.

Of interest are model results for the cases when mammals previously exposed to chronic irradiation at low dose rates N later underwent acute irradiation. The initial conditions were specified by formulas 1.16 (see section 1.2). Figure 1.20 shows the concentration dynamics for bone-marrow granulocytopoietic cells and blood granulocytes of rats after acute irradiation following prolonged radiation exposure. It is evident that a preliminary radiation exposure at a low dose rate has a stimulating effect on the recovery process in populations of bone marrow granulocytic cells and peripheral blood granulocytes. Calculations have shown that as N increases, the stimulating effect, just as in the lymphopoiesis model, first grows and then decreases. The maximum of the recovery process stimulation correlated well with the maximum stationary concentration of granulocyte precursors capable of dividing in the bone marrow of mammals previously exposed to continuous irradiation. A similar result was also obtained in the lymphopoiesis model (see section 1.4). The prediction of the model is consistent with data indicating an enhanced capability for tissue self-repair in mammals exposed first to elevated radiation levels [39, 41]. Modeling results show that there is no need to account for the stimulating effect by resorting to any additional hypotheses concerning mechanisms of radiation effect at low dose rates on granulocytopoiesis. The stimulating effect is described in the model in terms of the chalone theory.

1.7. Conclusion

Thus, based on a generalized model of the dynamics of an individual hematopoietic line, we have elaborated mathematical models that describe the dynamics of thrombocytopoiesis, lymphopoiesis, erythropoiesis, and granulocytopoiesis under ordinary conditions and during acute and chronic irradiation. These models are systems of nonlinear differential equations whose variables are represented by concentrations of mature cells in the blood and their precursor cells in the bone marrow. The models include the chalone mechanism of hematopoiesis regulation. They account for the principal stages of development of hematopoietic cells and make allowance for individual

features of separate lines: the existence of a bone marrow depot of granulocytes and the variable average megakaryocyte ploidy. The radiation dose and dose rate are variable parameters of the models, and the constant coefficients have the meanings generally adopted in hematology and radiobiology.

The models reproduce the dynamics of hematopoiesis recovery in nonirradiated mammals and describe stable oscillations of the concentrations of cells in the blood and their precursors in the bone marrow (limit cycles). The models describe the dynamics of damage and recovery of pools of mature blood cells and their precursors in the bone marrow after acute irradiation, simulate depletion of individual hematopoietic lines during chronic irradiation at high dose rates, and reproduce the ability of the hematopoietic system to adapt itself to protracted exposures at low and moderate dose rates. In the lymphopoiesis and granulocytopoiesis systems we reproduced the effect of stimulation of adaptive processes at low dose rates of continuous irradiation and the activation of recovery processes after acute irradiation in mammals exposed first to prolonged radiation at low dose rates. Modeling results demonstrate that to explain the above-mentioned stimulating effects of radiation at low doses it is sufficient to use the chalone theory of hematopoiesis regulation. This is a very important conclusion because the effects of radiation hormesis do not so far conclusively interpret the radiobiology.

Reproduction of a wide range of experimentally observed processes by the models indicates that they do take into account the main cause-effect relationships that govern the function of the hematopoietic system both in the absence and in the presence of ionizing radiation. It also proves the fact that when the models were being constructed, the chosen parameters and variables were indeed the key ones characterizing the dynamics of hematopoiesis. A small number of equations make it possible to carry out a bifurcation analysis of the models of separate hematopoietic lines under normal conditions and to find the values of the constant coefficients of the hematopoiesis dynamics models for nonirradiated and irradiated mammals. This allows comparison of modeling results with experimental data at qualitative and quantitative levels. The agreement obtained bears witness to the validity of these models for simulating hematopoiesis dynamics in nonirradiated mammals and in mammals exposed to acute and continuous radiation.

FIGURES

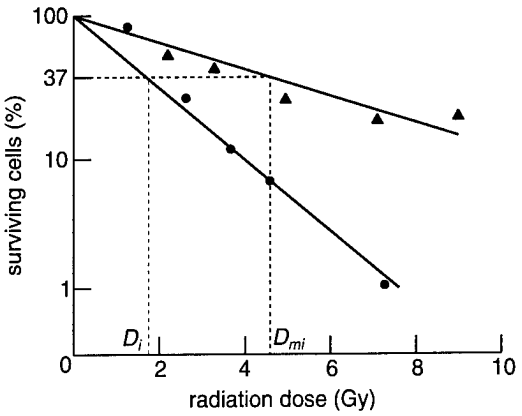

Fig. 1.1. Dose dependence of lymphoid cell damage in rat bone marrow 7 hours (▲) and 48 hours (•) after exposure to radiation [22].

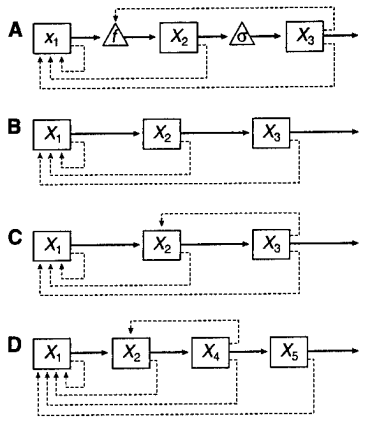

Fig. 1.2. Block diagrams of (A) thrombocytopoiesis, (B) lymphopoiesis and erythropoiesis, and (C, D) granulocytopoiesis models.

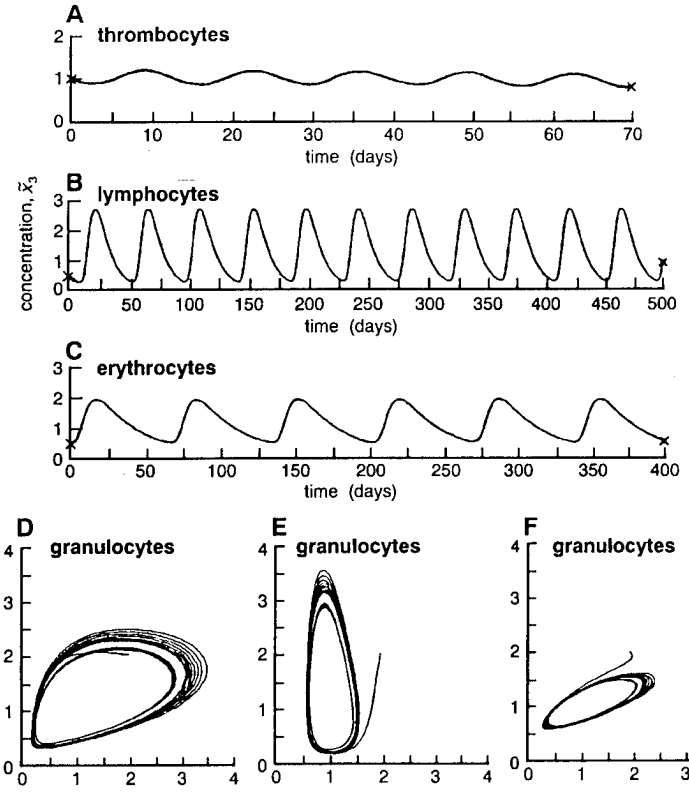

Fig. 1.3. Stable oscillations in hematopoiesis models. (A, B, C) Cyclic kinetics of thrombocytes, lymphocytes, and erythrocytes in blood. (D, E, F) Projection of two integral curves of the granulocytopoiesis model onto the plane of states $\{\tilde{x}_1\,\tilde{x}_2\}$, $\{\tilde{x}_3\,\tilde{x}_1\}$,$\{\tilde{x}_2\,\tilde{x}_3\}$ (closed curve shows limit cycle).

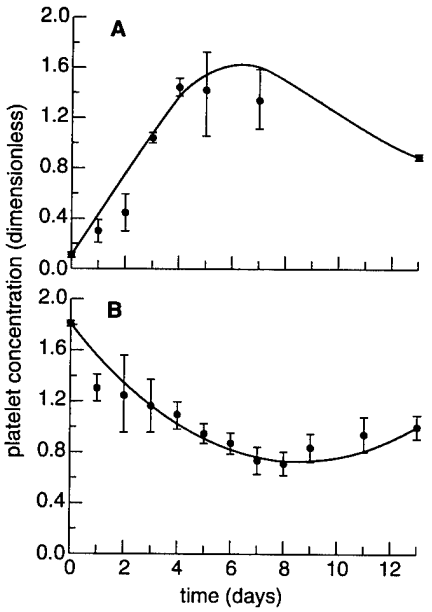

Fig. 1.4. Dynamics of platelet concentration in the blood of unirradiated rats. Results presented are from a computer calculation of equations 1.21-1.23, with (A) the initial values of $\tilde{x}_1(0) = 1$, $\tilde{x}_2(0) = 1$, $\tilde{x}_3(0) = 0.1$; and (B) $\tilde{x}_1(0) = 1$, $\tilde{x}_2(0) = 1$, $\tilde{x}_3(0) = 1.8$, and also the experimental values of platelet concentration in the blood of rats, with concentration first deliberately reduced to 10% (A), then increased to 180% (B) of the initial level [26, 27].

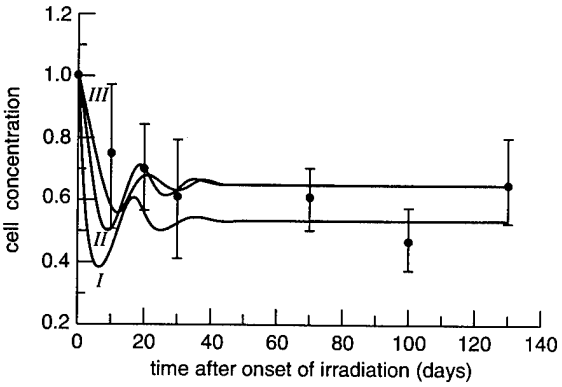

Fig. 1.5. Dynamics of thrombocytopoiesis during continuous irradiation at a dose rate $N = 0.25$ Gy/day. The calculated X_1, X_2, X_3 cell concentrations are represented by curves *I, II,* and *III*. Experimental data are given as average concentrations of platelets in the blood of mice and root-mean-square deviations from these values [29].

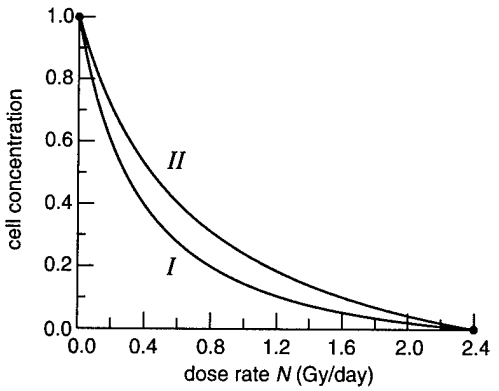

Fig. 1.6. New stationary concentrations of X_1 cells (curve *I*) and X_2 and X_3 cells (curve *II*) as functions of the dose rate N of continuous irradiation in the thrombocytopoiesis model.

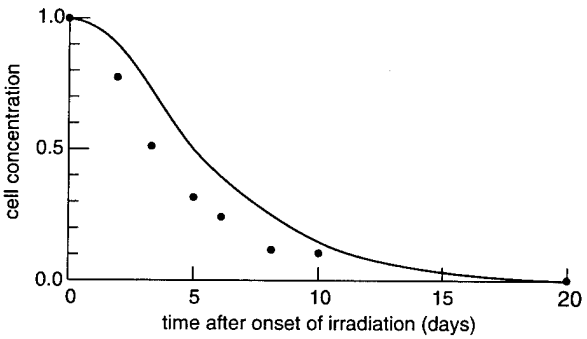

Fig. 1.7. Dynamics of platelet concentration in the blood of mice in continuous irradiation at a dose rate $N = 6$ Gy/day. Modeling results (solid curve); experimental data (•) [30].

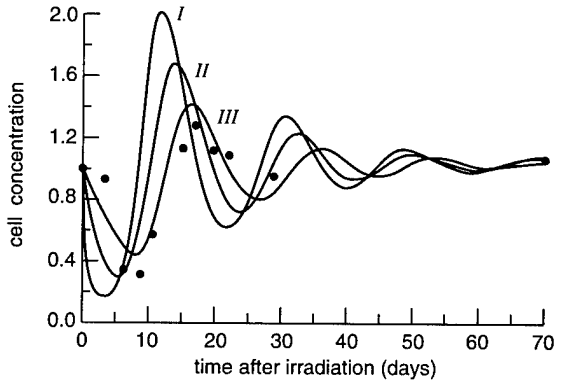

Fig. 1.8. Platelet dynamics following acute irradiation at a dose $D = 4$ Gy. Curve *I* represents the concentration of cells from the X_1 pool; curves *II* and *III* represent concentrations of radioresistant X_2 and X_3 cells, respectively; (•) represents the experimental values [20] of platelet concentration in the blood of mice.

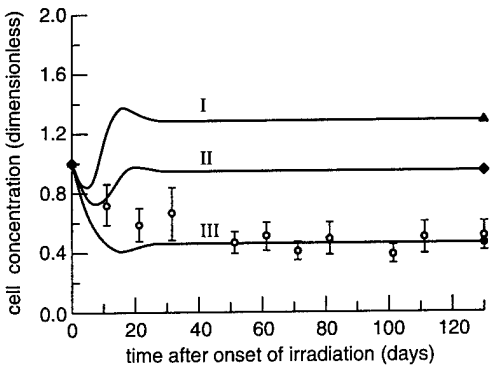

Fig. 1.9. Lymphopoiesis dynamics during continuous irradiation at a dose rate $N = 0.1$ Gy/day. Modeling results (curves *I, II,* and *III* correspond to concentrations of X_1, and X_2, and X_3 cells, respectively) and experimental data [29] on the dynamics of blood lymphocytes in mice.

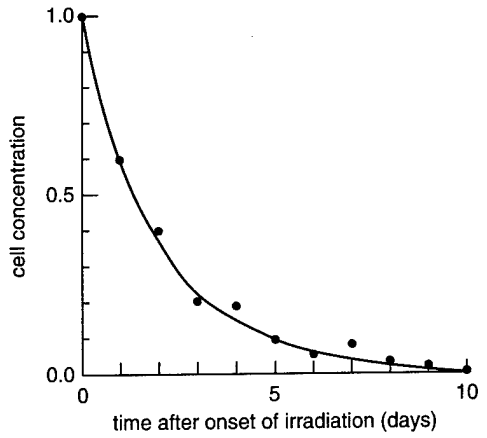

Fig. 1.11. Dynamics of lymphocyte concentrations in the blood of mice during continuous irradiation at a dose rate $N = 6$ Gy/day. Modeling results (solid curve) and experimental data (•) [30].

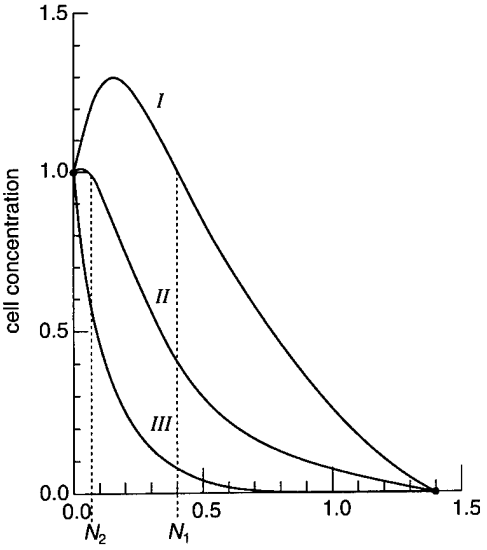

Fig. 1.10. New stationary concentrations of X_1, and X_2, and X_3 cells as functions of the dose rate N of continuous irradiation (curves *I, II,* and *III*) in the model of lymphopoiesis.

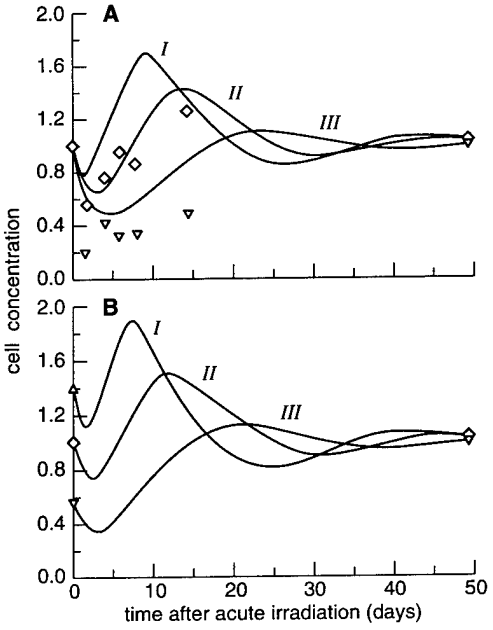

Fig. 1.12. Lymphopoiesis dynamics after acute irradiation at a dose $D = 1$ Gy (A) in the absence of preliminary radiation and (B) after preliminary continuous irradiation at a dose rate $N = 0.1$ Gy/Day. Curves *I, II,* and *III* represent the calculated concentrations of cells from pools X_1, and X_2, and X_3, respectively. Experimental [40] concentrations of lymphoid elements in the bone marrow (◊) and lymphocytes in the peripheral blood ∇ of rats that had not been irradiated previously.

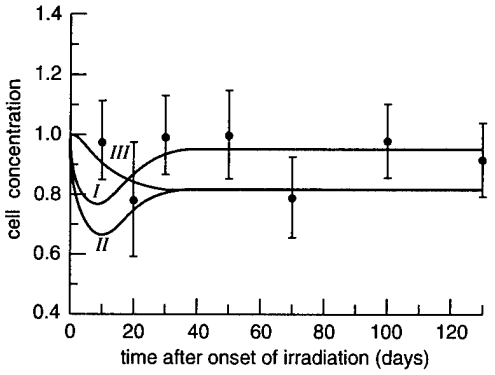

Fig. 1.13. Erythropoiesis dynamics during continuous irradiation at a dose rate $N = 0.1$ Gy/day. Modeling results (curves *I, II,* and *III* represent the concentrations of X_1, X_2, and X_3 cells, respectively) and experimental data [29] on blood erythrocyte dynamics in mice.

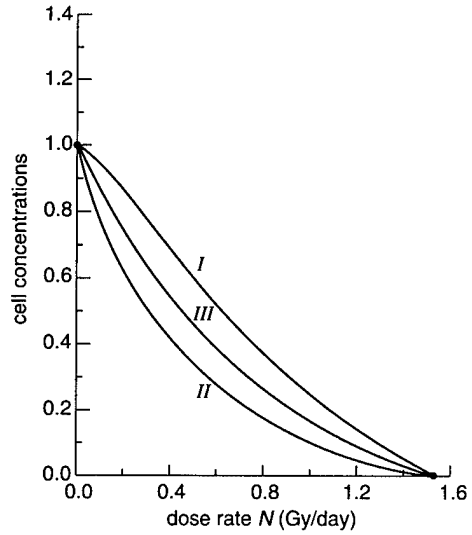

Fig. 1.14. New stationary concentrations of X_1 cells (curve *I*), X_2 and X_3 cells (curve *II*), and the total concentration of X_1 and X_2 cells (curve *III*) versus the dose rate N of continuous irradiation in the model of erythropoiesis.

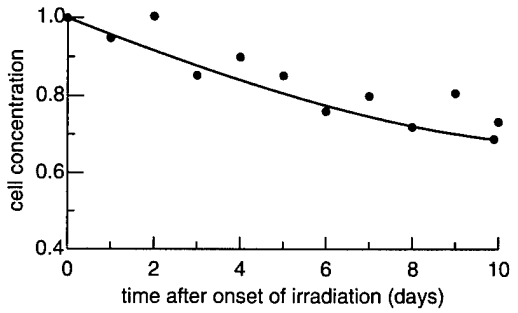

Fig. 1.15. Dynamics of erythrocyte concentration in the blood of mice during continuous irradiation at dose rate $N = 3$ Gy/day. Modeling results (solid line) and experimental data (•) [30].

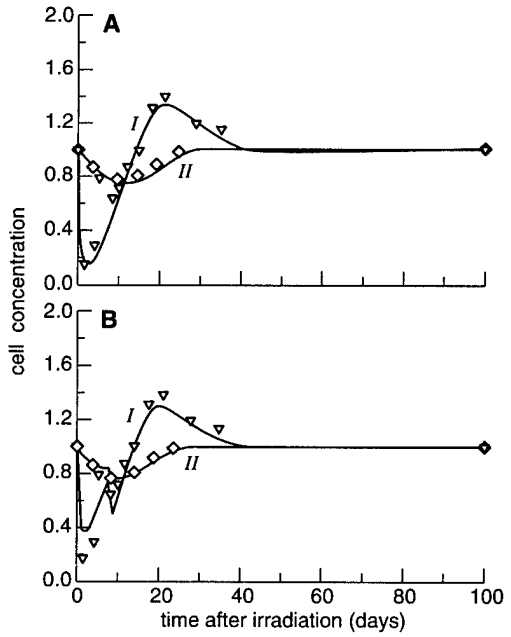

Fig. 1.16. Erythropoiesis dynamics after acute irradiation at dose $D = 4$ Gy. Results of model calculations (A) without allowance for the abortive concentration elevation and (B) with allowance for this elevation. Curves *I* and *II* represent the total concentration of cells from pools X_1 and X_2 and the concentration of X_3 cells, respectively. Symbols ∇ and ◊ indicate experimental values [20, 40] of erythroid cell concentration in the bone marrow and of erythrocyte concentration in the blood of mice, respectively.

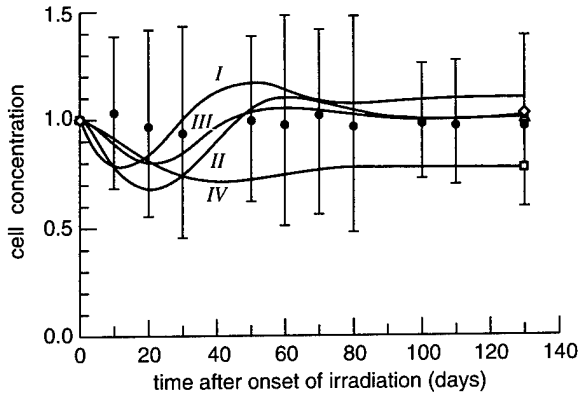

Fig. 1.17. Granulocytopoiesis dynamics during continuous irradiation at a dose rate $N = 0.1$ Gy/day. Modeling results (curves *I, II, III,* and *IV* correspond to concentrations of X_1, X_2, X_4, and X_5 cells, respectively) and experimental data [28] on the granulocyte dynamics in mice.

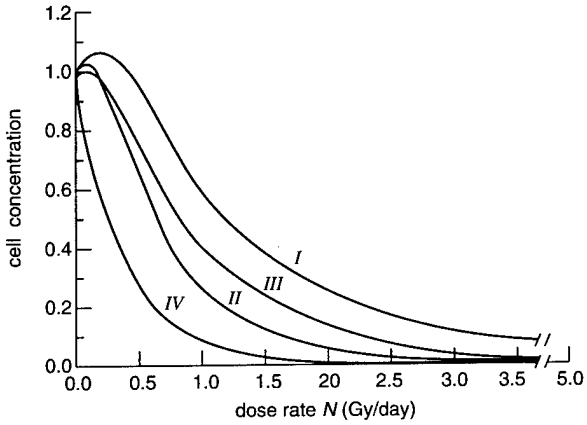

Fig. 1.18. Stationary concentrations of X_1, and X_2, X_4, and X_5 cells (curves *I* - *IV*) of the granulocytopoiesis system versus the dose rate N of continuous irradiation (in Gy/day).

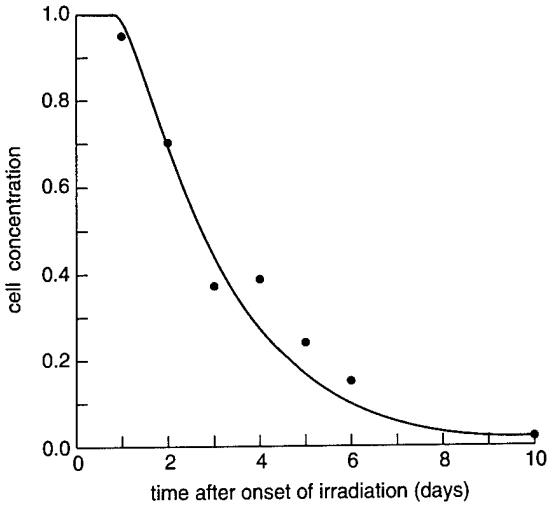

Fig. 1.19. Dynamics of granulocyte concentration in the blood of mice during continuous irradiation at a dose rate $N = 10$ Gy/day. Modeling results (solid curve) and experimental data (•) [30].

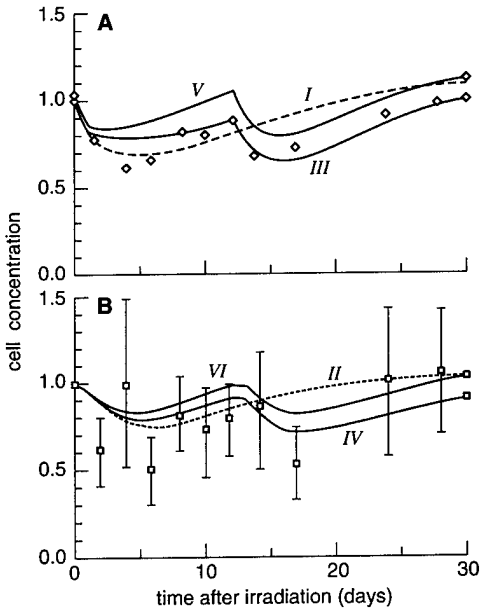

Fig. 1.20. Granulocytopoiesis dynamics after acute irradiation at $D = 2$ Gy. Experimental concentrations of cells of the (A) granulocytic line in the bone marrow and (B) neutrophils in the blood of rats [40, 48], as well as the results of model calculations without allowance for the abortive elevation of concentration (curves *I* and *II*) and with allowance for elevation (curves *III* and *IV*). Curves *V* and *VI* correspond to the case when acute irradiation is preceded by continuous irradiation with a dose rate $N = 0.18$ Gy/day.

REFERENCES

1. Lajtha LG, Oliver R, Gurney CW (1962) Model of a bone-marrow stem cell population. British Journal of Haematology 8:442-460

2. Wichmann HE (1983) Computer modeling of erythropoiesis. In: Dunn CDR (ed) Current concepts in erythropoiesis. Chichester; New York; Brisbane-Toronto; Singapore: John Wiley and Sons, Ltd.

3. Marchuk GI (1980) Mathematical models in immunology. Moscow: Nauka, pp. 134-206 (Russian)

4. Verigo VV (1987) Systemic methods in cosmic biology and medicine. Problems of cosmic biology. Moscow: Nauka, pp. 132-150 (Russian).

5. Wichmann HE, Loeffler M (1985) Mathematical modeling of cell proliferation: Stem cell regulation in hemopoiesis. Boca Raton, CRC Press, first edition, vol 1-2

6. Kirk J, Orr JS, Wheldon TE, Gray WM (1970) Stress cycle analysis in the biocybernetic study of blood cell populations. Journal of Theoretical Biology 26:265-276

7. Wheldon TE (1975) Mathematical model of oscillatory blood cell production. Mathematical Biosciences 24:289-305

8. Gray WM, Kirk J (1971) Analysis of analogue and digital computers of bone marrow stem cell and platelet control mechanisms. Computers for analysis and control in medical and biological research. IEEE publication, pp. 120-124

9. King-Smith EA, Morley A (1970) Computer simulation of granulopoiesis: Normal and impaired granulopoiesis. Blood 36(2):254-262

10. Kazarinoff ND, Driessche P (1979) Control of oscillations in hematopoiesis. Science 203:1348-1349

11. Monichev AJ (1984) Dynamics of haemopoiesis. Moscow: Meditsina (Russian)

12. Tyazelova VG (1988) Kinetic principle in interspecies extrapolations. Moscow: Nauka (Russian)

13. Vakha I, Znoil V (1975) The mathematical model of erythropoiesis application for investigation of the postradiation recovery process in mice. Biofizika 20:827-879 (Russian)

14. Sacher GA, Trucco E (1966) Theory of radiation injury and recovery in self-renewing cell populations. Radiation Research 29:236-256

15. Shafirkin AV (1989) Some regularities of hemopoietic stem cell dynamics under continuous irradiation with different values of dose rate. Radiobiologiya 23:630-636 (Russian)

16. Fedorov NA (1976) Normal haemopoiesis and its regulation. First edition, Moscow: Meditsina (Russian)

17. Romanov JA, Ketlinsky SA, Antokhin AI, Okulov VB (1984) Chalones and regulation of cell division. Moscow: Meditsina (Russian)

18. Kozlov VA, Zhuravkin IN, Tsirlova IG (1982) Stem haemopoietic cell and immune response. Novosibirsk: Nauka (Russian)

19. Romanovsky JM, Stepanova NV, Chernavsky DS (1984) Mathematical biophysics. Moscow: Nauka (Russian)

20. Bond VP, Fliendner TM, Archambeau JO (1965) Mammalian radiation lethality: A disturbance in cellular kinetics. New York: Academic Press

21. Yarmonenko SP (1974) Radiation haematology hand-book. Moscow: Meditsina (Russian)

22. Belousova OI, Gorizontov PD, Fedorova MI (1979) Radiation and haemopoietic system. Moscow: Atomizdat (Russian)

23. Kudryashov JB, Berenfeld BS (1982) Bases of radiation biophysics. Moscow: Moscow State University Press (Russian)

24. Smirnova OA, Govorun RD, Ryshov NI (1982) Investigation of the postirradiation lymphopoiesis dynamics by mathematical modelling. Radiobiologiya 22(4):488-493 (Russian)

25. Patt HM, Lund JE, Maloney MA (1973) Cyclic hematopoiesis in grey collie dogs: a stem-cell problem. Blood 42:873-884

26. Matter M, Hartmann JR, Kautz J, De Marsh QB, Finch CA (1960) A study of thrombopoiesis in induced acute thrombocytopenia. Blood 15(1):174-185

27. De Gabriele G, Penington DG (1967) Physiology of the regulation of platelet production. British Journal of Haematology 13:202-209

28. Kalina I, Praslichka M (1977) Changes in haemopoiesis and survival of continuously irradiated mice. Radiobiologiya 17:849-853 (Russian)

29. Praslichka M, Kalina I (1976) Influence of low dose-rate radiation on the change of CFC and peripheral blood in mice. Radiobiologiya 16:376-380 (Russian)

30. Kalina I, Praslicka M, Marko L, Hudak S (1975) Hämatologische veränderungen und überlebensdauer bei mäusen nach kontinuierlicher bestrahlung. Radiobiologia Radiotherapia 16(3):S347-354

31. Fabrikant JI (1987) Adaptation of cell renewal systems under continuous irradiation. Health Physics 52(5)561-570

32. Muksinova KN, Mushkacheva GS (1990) Cellular and molecular bases of haemopoiesis transformation under continuous irradiation. Moscow: Energoatomizdat (Russian)

33. Dale DS, Alling DW, Wolff SM (1972) Cyclic hematopoiesis: The mechanism of cyclic neutropenia in grey collie dogs. Journal of Clinical Investigations. 51:2197-2204

34. Lange RD, Jones JB (1983) Erythropoiesis in dogs and humans with cyclic hematopoiesis. In: Dunn CDR (ed) Current concepts in erythropoiesis. Chichester; New York; Brisbane-Toronto; Singapore: John Wiley & Sons Ltd., 144-165

35. Hulse EV (1959) Lymphocyte depletion of the blood and bone marrow of the irradiated rat: A quantitative study. British Journal of Haematology 5:278-283

36. Zukhbaya TM, Smirnova OA (1991) An experimental and mathematical analysis of lymphopoiesis dynamics under continuous irradiation. Health Physics 60:87-95

37. Lamerton LF, Pontifex AH, Blackett NM, Adams K (1960) Effects of protracted irradiation: I. Continuous exposure. British Journal of Radiology 33:287-301

38. Kuzin AM (1977) Stimulation effect of ionizing radiation on biological processes. Moscow: Atomizdat (Russian)

39. Luckey TD (1982) Physiological benefits from low levels of ionizing radiation. Health Physics 43(6):771-789

40. Hulse EV (1963) Lymphocytic recovery after irradiation and its relation to other aspects of haemopoiesis. British Journal of Haematology 9:376-384

41. Vahsmann F (1987) Are small doses of radiation so dangerous? Atomnaya tekhcnika za rubeshom 5:30-32 (Russian)

42. Morley A, Stohlman F (1968) Erythropoiesis in the dog: The periodic nature of the steady state. Science 165:1025-1027

43. Hulse EV (1957) Quantitative studies on the depletion of the erythropoietic cells in the bone marrow of the irradiated rat. British Journal of Haematology 3:348-358

44. Hulse EV (1963) Recovery of erythropoiesis after irradiation: A quantitative study in the rat. British Journal of Haematology 9:365-375

45. Morley A (1966) A neutrophil cycle in healthy individuals. Lancet 2:1220-1222

46. Hulse EV (1959) The depletion of the myelopoietic cells of the irradiated rat. British Journal of Haematology 5:369-378

47. Smirnova OA Zukhbaya TM (1991) The stimulating effect of prolonged irradiation with low dose rates on granulocytopoiesis. Kosmicheskaya Biologiya i Aviakosmicheskaya Meditsina 3:40-42 (Russian)

48. Hulse EV (1961) The recovery of myelopoietic cells after irradiation: A quantitative study in the rat. British Journal of Haematology 7:430-441

CHAPTER 2

Mathematical Model of the Small Intestine Epithelium System

2.1. Introduction

As far as we know, there are only a few published works concerned with modeling the dynamics of the small intestine epithelium system in nonirradiated mammals [1-3] and in mammals exposed to acute radiation doses [4-9]. Our purpose was to construct models based on current concepts that would illustrate the principal mechanisms of the system in the absence of radiation and under acute/continuous irradiation. It was important that the models include explicitly the characteristics of ionizing radiation and the basic dynamic and radiobiological parameters of the system studied. We wanted the models to reproduce the principal dynamic conditions of functioning of the intestinal epithelium in nonirradiated mammals and to describe quantitatively the kinetics of concentration of villus cells and their precursors in the crypt under conditions of acute and continuous irradiation. The results are described below.

2.2. Model of Dynamics of the Small Intestine Epithelium System in Nonirradiated Mammals

The model is based on modern concepts of the structure and functioning of the small intestine epithelium system [10, 11]. A schematic representation of renewal of the small intestine epithelium is given in figure 2.1*.

First, we built a basic model of the dynamics of the intestinal epithelium in nonirradiated mammals. The object of modeling is a population of basic (cylindrical) cells of the crypt-villus system.

*Figures begin on page 50.

We divided the major cell types of the intestinal epithelium into three groups according to degree of maturity and differentiation:

- Group X, proliferating precursor cells, from the stem cell to the dividing maturing crypt cell,
- Group Y, nondividing maturing crypt cells, and
- Group Z, functional villus cells.

The concentrations of cells x, y, z and the concentration of the specific chalone I are used as variables of the model. The dynamics of the crypt-villus system can be described by the system of nonlinear differential equations similar to system 1.1-1.4 used in the hematopoiesis model (chapter 1):

$$\frac{dx}{dt} = Bx - \gamma x, \tag{2.1}$$

$$\frac{dy}{dt} = \gamma x - Fy, \tag{2.2}$$

$$\frac{dz}{dt} = Fy - Ez, \tag{2.3}$$

$$\frac{dI}{dt} = G(x + \theta_1 y + \theta_2 z) - HI. \tag{2.4}$$

In system 2.1-2.3, the coefficients β, γ, F, and E are the specific rates of X cell division, cell passage from group X to group Y, cell displacement from crypt to villus, and cell exfoliation from the villus into the intestinal lumen, respectively. In 2.4, the multipliers G, $G\theta_1$, and $G\theta_2$ determine the specific rates of chalone production by X, Y, and Z cells during their vital activity and death, and H is the rate of natural chalone decomposition.

The model takes account of the functioning peculiarities of the intestinal epithelium system relating to the motion of cells over the crypt and villus in the course of their division and maturation. It has been found that the specific rates of cell displacement from crypt to villus, F, and from villus to intestinal lumen, E, increase as the mitotic activity of X cells increases, i.e., as B increases [12]. The exact form of these relationships has not been determined experimentally. As a first approximation we assume them to be linear:

$$F = \delta(1 + L_1 B), \quad E = \psi(1 + L_2 B). \tag{2.5}$$

Here, δ and ψ are the specific rates of cell displacement from crypt to villus and from villus to intestinal lumen, respectively, when mitosis of the crypt cells is suppressed ($B = 0$); L_1 and L_2 are constants.

The relationship between the specific rate of reproduction of X cells, B, and the concentration of the specific inhibitor I is given, as in chapter 1, by the Ierusalimskii equation [13]:

$$B = \alpha(1 + I/K)^{-1}, \tag{2.6}$$

where α is the maximum specific rate of cell division and K is a constant.

In view of the fact that the chalones keep their activity for a few hours [11] whereas the intestinal epithelial cells live, differentiate, and maturate over tens of hours [10], equation 2.4 can be considered "rapid" when compared to equations 2.1-2.3. Then, according to the Tikhonov theorem [13], equation 2.4 can be replaced by its stationary solution $I = (G/H)\,(x + \theta_1 y + \theta_2 z)$, by virtue of which equation 2.6 acquires the form

$$B = \alpha[1 + \beta\,(x + \theta_1 y + \theta_2 z)]^{-1}, \quad \beta = G/(HK). \tag{2.7}$$

The model of the crypt-villus system in its final version includes three nonlinear differential equations that are fully specified by eight independent parameters, α, γ, δ, ψ, L_1, L_2, θ_1, and θ_2. Six of them are found from experimental data. The last two parameters, θ_1 and θ_2, remain unknown. Their values can be obtained by fitting the model to the experimental data on the dynamics of the crypt-villus system when this system's stationary state is upset by some external factor. A schematic diagram of the model of the crypt-villus system is given in figure 2.2.

System 2.1-2.3 has two singular points. The first singular point is trivial. The coordinates of the second point are

$$\bar{x} = [(\alpha/\gamma) - 1]\beta^{-1} \times$$

$$\left\{1 + \theta_1\gamma/[\delta\,(1 + L_1\gamma)] + \theta_2\gamma/[\psi\,(1 + L_2\gamma)]\right\}^{-1}, \tag{2.8}$$

$$\bar{y} = \bar{x}\gamma/[\delta(1 + L_1\gamma)], \quad \bar{z} = \bar{x}\gamma/[\psi(1 + L_2\gamma)].$$

Relations 2.8 imply that the second singular point is in the positive octant ($\bar{x} > 0, \bar{y} > 0, \bar{z} > 0$) if $\alpha > \gamma$. Then $\bar{x}$, $\bar{y}$, and $\bar{z}$ can be regarded as crypt-villus cell concentrations in the normal state. The trivial singular point is unstable (saddle) if $\alpha > \gamma$ and stable (node) if $\alpha < \gamma$. The second singular point can also be both stable (focus) and unstable (saddle-focus). The corresponding ranges of parameter variation are determined in the course of numerically solving the characteristic equation. Analysis of these results have shown that the second singular point loses stability if the X cell reproduction is predominantly controlled by the inhibitor produced by Z cells and if the cells stay in the Y group for a sufficiently long time. In the case when the first and second points are unstable, there is one more particular solution: stable oscillations of the x, y, z variables (limit cycle). Stable oscillations of the dimensionless concentra-

tion of villus cells ($\tilde{z} = z/\bar{z}$) and that of crypt cells ($(x + y)/(\bar{x} + \bar{y})$) are shown in figure 2.3. The oscillation period is 10.6 days. The values fluctuate at levels higher than normal. Note that the parameters θ_1 and θ_2 were chosen to be 0.01 and 10, respectively. The values of the other coefficients are given in section 2.3.

When the second singular point is a stable focus, the dynamics of intestinal epithelium recovery has the form of damped oscillations of crypt and villus cell concentrations. On completion of this transition process, concentrations of all cells return to initial levels.

The model developed reproduces all the basic dynamic regimes of the crypt-villus system in nonirradiated mammals and can be used when modeling the effects of ionizing radiation on the small intestine epithelium system.

2.3. Model of Intestinal Epithelium Dynamics Under Continuous Irradiation

Experimental studies have shown that X cells of the crypt capable of division and maturation are radiosensitive to some extent, while nondividing Y cells of the crypt and functional Z cells of the villus are radioresistant [10]. The radiosensitive X cells are divided into two groups according to their response to radiation. One group includes undamaged X cells, and the other includes damaged X_d cells. The concentration of the latter cells is denoted by x_d. In this particular model there is no distinction between damaged and heavily damaged cells, as in the hematopoiesis models (section 1.2), because the effect on radiosensitive cells of the crypt in the two cases is similar: practically all cells damaged by radiation undergo so-called interphase death [10].

We introduce the dimensionless variables $\tilde{x} = x/\bar{x}$, $\tilde{y} = y/\bar{y}$, $\tilde{z} = z/\bar{z}$, $\tilde{x}_d = x_d/\bar{x}$ and the dimensionless parameters $l_1 = \gamma L_1$ and $l_2 = \gamma L_2$. Then, according to the one-target-one-hit theory of cell radiation injury [14], the dynamics of dimensionless concentrations of crypt-villus cells in mammals exposed to continuous radiation at dose rate N can be described by the equations

$$\frac{d\tilde{x}}{dt} = \gamma\tilde{x}(B'' - 1) - \frac{N}{D_1}\tilde{x}, \tag{2.9}$$

$$\frac{d\tilde{y}}{dt} = \delta[(1 + l_1)\tilde{x} - (1 + l_1 B'')\tilde{y}], \tag{2.10}$$

$$\frac{d\tilde{z}}{dt} = \psi\left\{\frac{1 + l_2}{1 + l_1}(1 + l_1 B'')\tilde{y} - (1 + l_2 B'')\tilde{z}\right\}, \tag{2.11}$$

$$\frac{d\tilde{x}_d}{dt} = \frac{N}{D_1}\tilde{x} - \nu\tilde{x}_d. \qquad (2.12)$$

In equations 2.9 and 2.12, the term $(N/D_1)\tilde{x}$ is the rate of X cell transition into the damaged state X_d, and $\nu\tilde{x}_d$ in equation 2.12 is the death rate of damaged X_d cells. The coefficient D_1, having the dimensionality of radiation dose, characterizes the radiosensitivity of X cells and is equivalent to the conventionally measured quantity D_0.

In modifying equation 2.7, which describes the rate B of X cell reproduction, we allow for the contribution of radiation damage-induced death of X_d cells to the chalone production. Then the dimensionless specific rate of X cell reproduction is

$$B'' = B/\gamma = a/\left\{1 + b[\tilde{x} + \Phi\tilde{x}_d + \theta_1\tilde{y}/(g(1+l_1)) + \theta_2\tilde{z}/(c(1+l_2))]\right\}. \qquad (2.13)$$

Here, $a = \alpha/\gamma$, $g = \delta/\gamma$, $c = \psi/\gamma$, $b = \beta\bar{x} = (a-1)/\{1 + \theta_1[g(1+l_1)]^{-1} + \theta_2[c(1+l_2)]^{-1}\}$ are dimensionless parameters. The initial conditions for solving system 2.9-2.12 are the preirradiation concentrations of X, Y, Z, and X_d cells:

$$\tilde{x}(0) = 1, \quad \tilde{y}(0) = 1, \quad \tilde{z}(0) = 1, \quad \tilde{x}_d(0) = 0. \qquad (2.14)$$

It should be noted that the use of the concentration of undamaged cells as a variable in the model of the small intestine epithelium system and also the allowance for the contribution of these cells to regulatory processes (equation 2.13) constitute a novel approach to modeling the dynamics of this system during irradiation. It seems important to stress that when implementing this approach and modifying model 2.1-2.3 in order to describe the effects of continuous radiation on the dynamics of the crypt-villus system, apart from the variable parameter N, we introduced only three new independent coefficients, D_1, ν, and Φ. The parameter D_1 specifies the radiosensitivity of X cells; the coefficient ν gives the specific death rate of damaged X_d cells; and the dimensionless multiplier Φ expresses the dissimilar contributions of undamaged X and damaged X_d cells to chalone production. D_1 and ν are conventionally measured radiobiological parameters. The total number of independent coefficients in system 2.9-2.12 is 10, and most of them, as will be shown below, can be directly determined from experimental data.

Model 2.9-2.12 was used to simulate experiments with chronic irradiation of mice and rats. The initial parameters were determined from the data obtained in experimental studies of the small intestine epithelium of these mammals in the absence of radiation and under acute irradiation. For example, in experiments on estimating mitotic activity, the mitotic index M was measured [15]. Mitotic index M is related to the specific rate B by the formula

$$M = B \cdot T \cdot 100\%. \qquad (2.15)$$

In equation 2.15, the parameter T is the true time of mitosis. Bearing in mind that in nonirradiated mice the mitotic index of dividing cells of the crypt is 5.3% and $T = 0.8$ hour [16], from equation 2.15 we derive the value of specific division rate for X cells: $B = 1.6$ day^{-1}. It follows from equation 2.1 that the normal specific rates of cell passage from pool X to pool Y and of X cell division are equal, hence $\gamma = B = 1.6$ day^{-1}.

As shown by analysis of experimental data [12], when the mitotic activity is suppressed ($B = 0$), the specific rates of cell migration from crypt to villus and of villus cell exfoliation are $F = 0.8$ day^{-1} and $E = 0.28$ day^{-1}, whereas under normal condition ($B = \gamma$), these quantities are $F = 2.4$ day^{-1} and $E = 0.86$ day^{-1}. It follows from equation 2.5 that when $B = 0$ we have $F = \delta$, $E = \psi$, and when $B = \gamma$, then $F = \delta (1 + l_1)$ and $E = \psi (1 + l_2)$. Hence it follows that $\delta = 0.8$ day^{-1}, $l_1 = 2$, $\psi = 0.28$ day^{-1}, and $l_2 = 2$. Three more coefficients were determined from experimental data: $\alpha = 5.6$ day^{-1}, $D_1 = 1.12$ Gy, $v = 2$ day^{-1} [10, 12, 17]. The parameters θ_1, θ_2, and Φ, which could not be measured experimentally, were chosen in the course of the numerical study of system 2.9-2.12 to be $\theta_1 = 0.1$, $\theta_2 = 1$, and $\Phi = 20$.

The dynamics of the crypt-villus system was studied within model 2.9-2.12 at various dose rates N of chronic irradiation. Calculations have shown that at low N the intestinal epithelium remains practically intact. For instance, at $N = 0.001 \div 0.1$ Gy/day the loss of crypt-villus cells is less than $0.05 \div 5\%$ of the normal level. At higher radiation dose rates, $N = 0.1 \div 10$ Gy/day, the pattern of injury of the crypt-villus system has two stages: the first stage is an oscillatory transition process; the second stage is a new stationary state of the crypt-villus system.

The dynamics of the mitotic index M of X cells, calculated by formulas 2.13 and 2.15, and also the overall concentration of crypt cells (X and Y) and villus cells (Z) at $N = 0.84$ Gy/day and $N = 1.76$ Gy/day are presented in figures 2.4 and 2.5. The figures also show the corresponding experimental concentrations of villus cells in rats [18]. One can see that within the first 3 days after the onset of irradiation the crypt cell concentration decreases. The reduction of villus cell concentration starts 1 day after the beginning of irradiation and ends within 5 days. Thereafter, concentrations of crypt and villus cells increase somewhat but do not reach the normal level. A new though less pronounced reduction of these concentrations then occurs, and the transition process is actually completed. The concentrations of crypt and villus cells take on new stationary values, which decrease (compared to the normal level) as dose rate N increases. These results are consistent with the experimental values [18]. For example, after 20 days of continuous irradiation at $N = 0.84$ Gy/day and $N = 1.76$ Gy/day, the new stationary levels of villus cell concentration in rats were 0.83 ± 0.15 and 0.67 ± 0.2, respectively. The corresponding calculated values are 0.75 and 0.56. The steady reduction of the number of crypt cells under continuous irradiation is also reproduced rather well by the model. For example, at $N = 4$ Gy/day the new stationary levels of crypt cell concentrations in irradiated rats [19] and in the model are 0.37 ± 0.16 and 0.34, respectively.

Thus, the model provides a theoretical description of the ability of the intestinal epithelium to adapt itself to protracted radiation exposure, which has been observed in experiments by several authors [18, 19].

The state of stable dynamic equilibrium (homeostasis) maintained by the crypt-villus system under conditions of chronic irradiation is accompanied by an enhanced (compared to normal) mitotic activity of the dividing crypt cells. Figures 2.4A and 2.5A show that within 1 day after the onset of irradiation the mitotic index M of X cells decreases. The decrease is greater as dose rate N increases. Then M increases and reaches a maximum. Later, the mitotic index M decreases, and the transition process is practically over. As a result, the mitotic index assumes a new stationary value, which exceeds the normal value. This stationary value is higher with higher dose rate N. These results show qualitative agreement with experiments [20].

As the dose rate of chronic irradiation increases from $N = 10$ Gy/day to $N = N_c = 44.8$ Gy/day and higher, the shapes of the kinetic curves undergo a change. There is a rapid reduction of cell concentration, first in the crypt and then in the villus, to lethal levels at $N < N_c$ and to 100% lethality at $N \geq N_c$. This can be regarded as model simulation of the intestinal form of radiation-induced injury at high dose rate levels of chronic irradiation. Note that the critical dose rate N_c in the intestinal epithelium model is defined by the same formula (1.27) as in the models of all hematopoietic lines. The critical dose rate N_c is equal to the product of the parameter D_1 (characterizing the radiosensitivity of precursor cells for functioning cells of these systems) and the difference between the maximum possible and the normal division rate of precursor cells. This means that the level of radiosensitivity and the proliferative potential of dividing cells of the intestinal epithelium and of the above-mentioned hematopoietic systems alone determine the dose rate of continuous irradiation that is critical for their vital activity. It should be noted that formula 1.27 can be used to obtain an approximate cautious estimate of life-threatening dose rates of continuous irradiation, since lethal dose rates are associated with low but not necessarily zero concentrations of functioning cells of the vital organs.

During the preliminary computer study of model 2.9-2.12 it has been found that the minimal concentrations of X, Y, and Z cells are mainly determined by the parameter D_1 characterizing the radiosensitivity of X cells. The parameter D_1 and the coefficients l_1, l_2, θ_1, θ_2, and Φ affect the levels of new stationary concentrations of X, Y, and Z cells. Obviously, these quantities also depend on the variable parameter N—the dose rate of continuous irradiation.

2.4. Model of Intestinal Epithelium Dynamics Under Acute Irradiation

We use equations 2.9-2.12 as an initial model to simulate the effect of acute irradiation on the crypt-villus system. We can simplify the model because the characteristic times in equations 2.9-2.12 substantially exceed the duration of radiation exposure T. The duration of acute radiation exposure is not sufficient for radioresistant Y and Z cells to change in number, therefore

$$\tilde{y}(T) = 1, \quad \tilde{z}(T) = 1. \tag{2.16}$$

The concentrations of undamaged X and damaged X_d cells, $\tilde{x}(T)$ and $\tilde{x}_d(T)$, respectively, are determined by solving the rapid equations

$$\frac{d\tilde{x}}{dt} = -\frac{N}{D_1}\tilde{x}, \quad \frac{dx_d}{dt} = \frac{N}{D_1}\tilde{x} \tag{2.17}$$

with the initial conditions $\tilde{x}(0) = 1$ and $\tilde{x}_d(0) = 0$. With N = constant, system 2.17 can be easily integrated:

$$\tilde{x}(T) = \exp(-D/D_1), \quad \tilde{x}_d(T) = 1 - \exp(-D/D_1), \tag{2.18}$$

where $D = NT$ is the total dose of acute irradiation. In view of the small value of T, the dynamics of postirradiation injury and recovery of the crypt-villus system can be described by equations 2.9-2.12 with $N = 0$ and the initial conditions by equations 2.16 and 2.18.

The calculated dynamics of the mitotic index M of X cells, the dimensionless total concentration of crypt cells (X, X_d, and Y), and the dimensionless concentration of villus cells (Z) for a high dose of acute irradiation, D = 30 Gy, are shown in figure 2.6. Also given in the figure are corresponding experimental data [21] on radiation-induced changes of crypt and villus cell concentrations in mice of the CFW strain. The model reproduces the experimentally observed rapid depletion of the crypt cellular pool. As early as the second day after irradiation, the number of crypt cells is less than 20% of the normal cell number. On the first day, the reduction of cell concentration in the villus proceeds more slowly than in the crypt, but already by the second day, the number of cells is reduced almost by half and continues to drop rapidly to a level incompatible with life. This level is usually reached on the third day after irradiation, and all mice die [21]. The use of the statistical χ^2-test demonstrated quantitative agreement between the modeling results and the experimental data given in figure 2.6B (the calculated values of $\chi^2 = 0.844$ and $\chi^2 = 1.839$ did not exceed the critical value of $\chi^2_{0,05} = 5,991$ (number of degrees of freedom $n = 2$).

The dynamics of the crypt-villus system at lower radiation doses was also calculated, in particular $D = 7$ Gy (fig. 2.7). Figure 2.7 also shows corresponding experimental data obtained in a study of the intestinal epithelium in white mice [20, 21]. The model reflects the radiation-induced decrease in cell numbers in the crypt and villus—the decrease is greater as dose D increases. The depletion stage is followed by the repair stage when the number of cells start growing first in the crypt and then in the villus. Intestinal epithelium regeneration in mice irradiated at doses lower than 10 Gy and surviving the first three days was also observed in experiments [20, 21].

The calculated dynamics of mitotic index M for X cells after acute irradiation at above-indicated doses is presented in figure 2.7A. The mitotic activity decreases within the first few hours. Thereafter the mitotic index starts increasing and returns to normal. The mitotic activity of the cells continues to grow to a certain maximum value. As shown by the calculations, the dynamics of the mitotic index has the form of damped oscillations later and finally returns to the initial level. The calculated dynamics of the mitotic index M of X cells qualitatively corresponds to the experimentally observed changes of the mitotic index of crypt cells in mice [17] and rats [10] after irradiation at doses of 6-10 Gy. It should be noted that this is the first time that the pattern of changes of the mitotic activity of crypt cells in the course of postirradiation injury and regeneration of the intestinal epithelium is reproduced by a dynamic model at the qualitative level.

When varying the parameters of the model it was found that the principal characteristics of radiation injury of the intestinal epithelium system—minimal concentrations of X, Y, and Z cells—are mainly determined by the parameter D_1, which provides the radiosensitivity of X cells, and by the radiation dose D.

2.5. Conclusion

The models thus reproduce a broad range of experimentally observed processes specific to the dynamics of the small intestine epithelium in nonirradiated and irradiated mammals. This proves the fact that the models properly incorporate the main cause-effect relationships governing the functioning of the crypt-villus system in the presence and the absence of ionizing radiation. As in the modeling of hematopoiesis, we performed a bifurcation analysis of the base system of equations to reveal the specific features of its behavior. Also found were the values of the constant coefficients, which allowed a quantitative comparison of the modeling results and experimental data. The agreement obtained makes it feasible to use the models to simulate and predict the behavior of the intestinal epithelium in mammals exposed to acute or chronic radiation in broad ranges of doses and dose rates.

FIGURES

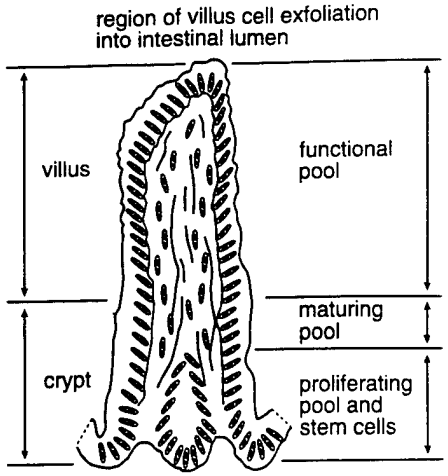

Fig. 2.1. Schematic diagram of the renewal of the small intestine epithelium system.

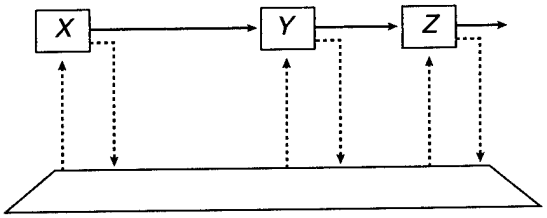

Fig. 2.2. Block diagram of the crypt-villus system. Rectangles, cell compartments; trapezium, unit of control signal formation; solid lines with arrows, cell flows; dashed lines with arrows, information flows.

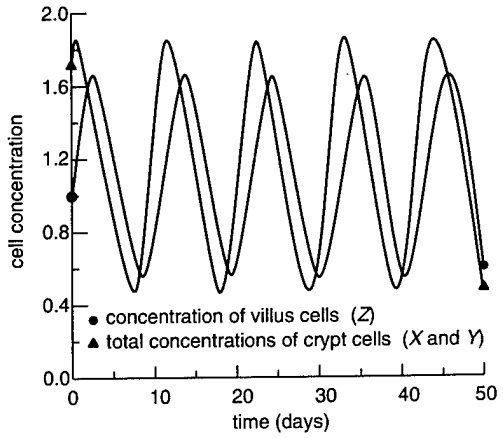

Fig. 2.3. Cyclic kinetics of the crypt-villus system in nonirradiated mammals.

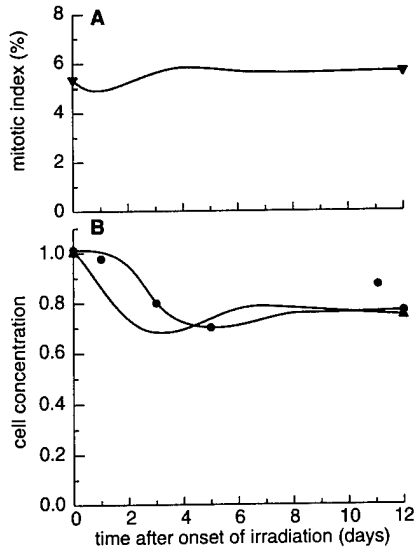

Fig. 2.4. Dynamics of the crypt-villus system under chronic irradiation at a dose rate of 0.84 Gy/day. Symbols ▼, ▲, and • at the initial ($t = 0$) and final ($t = 12$ days) points mark the curves representing calculated values of (A) the mitotic index of X cells and (B) the total concentration of crypt cells (X and Y) and the concentration of villus cells (Z). The symbol • also represents experimental values of villus cell concentration in rats at various periods of time after irradiation [16].

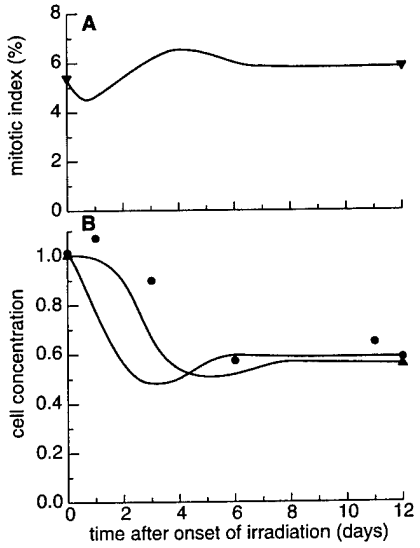

Fig. 2.5. Dynamics of the crypt-villus system under chronic irradiation at a dose rate of 1.76 Gy/day. Symbols ▼, ▲, and • at the initial ($t = 0$) and final ($t = 12$ days) points mark the curves representing calculated values of (A) the mitotic index of X cells and (B) the total concentration of crypt cells (X and Y) and the concentration of villus cells (Z). The symbol • also represents experimental values of villus cell concentration in rats at various periods of time after irradiation [16].

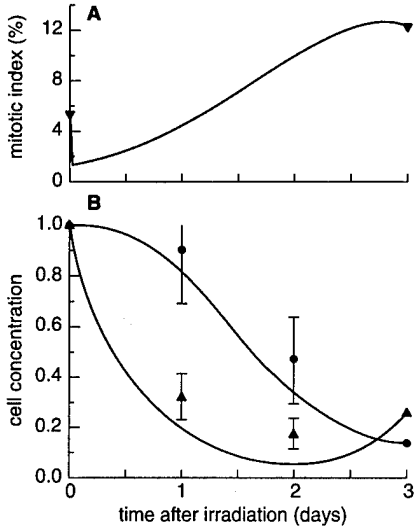

Fig. 2.6. Dynamics of the crypt-villus system after acute irradiation at a dose of 30 Gy. Symbols ▼, ▲, and • at the initial ($t = 0$) and final ($t = 3$ days) points mark the curves representing calculated values of (A) the mitotic index of X cells and (B) the total concentration of crypt cells (X and Y) and the concentration of villus cells (Z). The symbols ▲ and • also represent the mean cell concentrations for crypt and villus of mice in experiments [19]. Vertical bars represent the mean square deviations from these values.

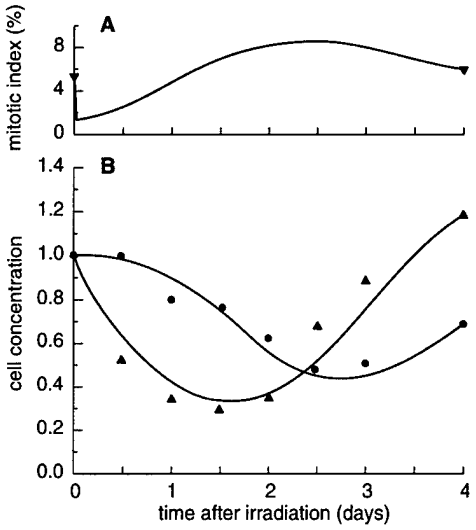

Fig. 2.7. Dynamics of the crypt-villus system after acute irradiation at a dose of 7 Gy. Symbols ▼, ▲, and • at the initial ($t = 0$) and final ($t = 4$ days) points mark the curves representing calculated values of (A) the mitotic index of X cells and (B) the total concentration of crypt cells (X and Y) and the concentration of villus cells (Z). The symbols ▲ and • also represent mean cell concentrations for crypt and villus in experimental mice [19]. Modeling results and experimental data [20, 21].

REFERENCES

1. Loeffler M, Stein R, Wichmann HE, et al. (1986) Intestinal crypt proliferation: I. A comprehensive model of steady-state proliferation in the crypt. Cell and Tissue Kinetics 19:627-645

2. Loeffler M, Potten CS, Paulus U, et al. (1988) Intestinal crypt proliferation: II. Computer modelling of mitotic index data provides further evidence for lateral and vertical cell migration in the absence of mitotic activity. Cell and Tissue Kinetics 21(4):247-248

3. Potten CS, Loeffler M (1987) A comprehensive model of the crypts of the small intestine of the mouse provides insight into the mechanisms of cell migration and the proliferation hierarchy. Journal of Theoretical Biology 127:381-391

4. Tyazelova VG (1988) Dynamics of haemopoiesis. Moscow: Meditsina (Russian)

5. Gozenbuk VL, Keirim-Markus IB (1988) Dosimetric criteria of the severity of acute man irradiation. Moscow: Energoatomizdat (Russian)

6. Sato F, Muramatsu S, Tsuchihashi S, et al. (1972) Radiation effects on cell populations in the intestinal epithelium of mice and its theory. Cell and Tissue Kinetics 5:227-235

7. Shiragai A, Sato F, Hiraoka T, et al. (1976) Kinetics of cell populations in the intestinal epithelium of mice after partial-body irradiations with X-rays and neutrons. International Journal of Radiation Biology 29:377-383

8. Bond VP, Fliedner TM, Archambeau JO (1965) Mammalian radiation lethality: A disturbance in cellular kinetics. New York: Academic Press

9. Romanov JA, Ketlinsky SA, Antokhin AI, Okulov VB (1984) Chalones and regulation of cell division. Moscow: Meditsina (Russian)

10. Strdzidzovsky AD (1975) Quantitative analysis of the cellular aspects of the intestinal syndrome under ionizing radiation action. Theoretical premises and the models of the radiation damage processes in organism system. Pushchino, 50-57 (Russian)

11. Romanovsky JM, Stepanova NV, Chernavsky DS (1975) Mathematical modelling in biophysics. Moscow: Nauka (Russian)

12. Kudryashov JB, Berenfeld BS (1982) Bases of radiation biophysics. Moscow: Moscow State University Press (Russian)

13. Gruzdev GP (1968) Problems of haemopoietic tissue damage under acute radiation pathology. Moscow: Meditsina (Russian)

14. Lesher S (1967) Compensatory reactions in intestinal crypt cells after 300 roentgens of ^{60}Co gamma irradiation. Radiation Research 32(3):510-519

15. Lesher J, Lesher S (1970) Effects of single-dose, whole-body, ^{60}Co gamma irradiation on number of cells in DNA synthesis and mitosis in the mouse duodenal ephithelium. Radiation Research. 43(2):429-438

16. Quastder H, Bensted JPM, Chir B (1959) Adaptation to continuous irradiation: Observations on the rat intestine. The British Journal of Radiology 32(380):501-512

17. Fabrikant JI (1987) Adaptation of cell renewal systems under continuous irradiation. Health Physics 52(5):561-570

18. Cairnie AB (1967) Cell proliferation studies in the intestinal epithelium of the rat: Response to continuous irradiation. Radiation Research 32:240-264

19. Matsuzawa T, Wilson R (1965) The intestinal mucosa of germfree mice after whole-body X-irradiation with 3 kiloroentgens. Radiation Research 25(1):15-24

20. Kononenko AM (1968) On the influence of cell abnormal growth on crypt cell population kinetics in irradiated intestinal epithelium. Citologiya 10:1425-1431 (Russian)

21. Kononenko AM, Pharaphonov GV (1969) On changes in the amount of epithelium cells on small intestine fibers of irradiated mice. Radiobiologiya 9:209-212

Task II

Mathematical Models of Mortality Dynamics for Irradiated Mammalian Populations

E. E. Kovalev, principal investigator
O. A. Smirnova, senior researcher

Abstract

Mathematical models were developed to describe radiation-induced mortality dynamics for homogeneous and nonhomogeneous (in radiosensitivity) mammalian populations. These models relate statistical biometric functions with statistical and dynamic characteristics of critical systems in specimens belonging to these populations. The model of mortality for the nonhomogeneous population involves normal and log-normal distributions of its specimens with respect to the index of radiosensitivity for cells of the critical system. When the small intestine is the critical system, the mortality model for the homogeneous population quantitatively reproduces the mortality rate of laboratory mice after exposure to very high doses of pulsed or continuous radiation. This model also quantitatively describes the mortality of the same animals chronically irradiated at low dose rates when the hematopoietic system (specifically, thrombocytopoiesis) is the critical one. The mortality model for the nonhomogeneous population exposed to the same irradiation conditions predicts a higher mortality rate and a lower survival than could have been predicted from the averaged values of the radiosensitivity index of critical system cells. The level of doses and dose rates of acute and chronic exposures presenting a hazard to nonhomogeneous mammalian populations decreases as the variance of the corresponding distributions increases. These modeling results provide a clue to understanding the experimental information collected in the area of the Chernobyl catastrophe.

CHAPTER 3

Mathematical Model of Mortality for a Homogeneous Mammalian Population

3.1. Introduction

A new approach is presented to model mortality of mammals exposed to acute and chronic radiation in a broad range of doses and dose rates. The mortality of a population is the ultimate result of exposing a population to particular conditions of radiation. Our concept of population mortality is essentially different than that used in "black box" models [1-3].

The principal cause of death of an exposed organism is failure of one of its vital systems, which manifests itself in the disruption of cellular kinetics and a decrease in the number of functional cells of the particular system below the level required for survival. For each of the studied dose and dose rate intervals there seems to be a specific critical system, and its damage determines the mechanism of development of radiation sickness and ultimately the death of mammals [4, 5, 6]. For example, exposure to a sublethal dose, D = 2-7 Gy, has the greatest effect on the bone-marrow hematopoietic system. Death occurs within 14 to 20 days after irradiation [4].

With a lethal dose of D = 10-200 Gy, the first system to be injured is the epithelium of the small intestine, which leads to loss of liquid (water) by the organism, blood thickening, and collapse. Death occurs within 3-5 days after irradiation when the effects of damage to blood-forming and other systems have not yet had time to develop [4, 6].

Very high radiation doses, $D > 200$ Gy, damage the central nervous system by destroying cortical neurons and disrupting blood flow. Depending on the dose, death occurs within hours or even minutes after irradiation [4].

The three different mechanisms of lethality for irradiated mammals and their time intervals are well illustrated by the dose dependence of the average life span of irradiated mice (fig. 3.1*) [4]. The figure shows that within the first two dose intervals, the average life span of laboratory mice was 15 days and 4 days, respectively.

In addition to average life span, three statistical biometric functions are usually measured in radiobiological experiments. The first is life span probability $v(t)$, which represents the ratio of the number of animals that have survived to time t, $\theta(t)$, to their initial number θ_0: $v(t) = \theta(t)/\theta_0$. The second function is the life span probability density $w(t)$, which is the ratio of the fraction of animals that die at time t to their initial number: $w(t) = -(d\theta/dt)/\theta_0$. The third biometric function is the mortality rate $\rho(t)$, which is the ratio of the fraction of animals that die at time t to the number of animals that survived to time t: $\rho(t) = -(d\theta/dt)/\theta(t)$.

The studies that are reported in this chapter were aimed at finding an algorithm that would adequately describe the relationship between statistical biometric functions and the state of critical systems in irradiated mammals.

3.2. Model of Mortality for Acutely and Chronically Irradiated Mammals

At the first stage, we have used the method proposed by Sacher [7, 8] to find the relationship between biometric functions and the dynamic and statistical characteristics of critical systems. Sacher modeled a homogeneous population, in which every individual was characterized by the same average values of all physiological variables and their fluctuation parameters, and described this population by a random variable ξ, which was an index of physiological state. It was also assumed that the deviation μ of the random variable ξ from its mean value m ($\mu = \xi - m$) obeys the stochastic differential equation

$$\frac{d\mu}{dt} + \omega\mu = \eta(t), \tag{3.1}$$

where $\eta(t)$ is a Gaussian random process with a zero mean value and the spectral density $4\Omega = 4S^2\omega$ (ω^{-1} is the mean relaxation time in system 3.1; S^2 is the variance of the random variable μ).

The distribution function of the variable μ, $P(\mu_0 \mid \mu, t)$, is a solution to the Fokker-Planck partial differential equation

$$\frac{\partial P}{\partial t} = \omega\frac{\partial}{\partial\mu}(\mu P) + \Omega\frac{\partial^2 P}{\partial\mu^2}. \tag{3.2}$$

*Figures begin on page 67.

The function $P(\mu_0 \mid \mu, t)$ in equation 3.2 is the conditional probability that μ should be observed in system 3.1 at time (t) if μ_0 was observed at $t = 0$. Stationary solution to equation 3.2 has the form

$$P(\mu) = (2\pi S^2)^{-1/2} \exp(-\mu^2/2S^2). \tag{3.3}$$

It was assumed further that the situation, when the variable ξ characterizing a specimen reaches or exceeds the critical value L, could serve as a death analog. Such specimens then left the population. In accordance with this assumption, the distribution $P(\mu)$ was modified:

$$P_M(\mu) = \begin{cases} \dfrac{(2\pi S^2)^{-1/2} \exp(-\mu^2/2S^2)}{(2\pi S^2)^{-1/2} \int_{-\infty}^{\lambda} \exp(-\mu^2/2S^2)\, d\mu} & \text{for } \mu < \lambda, \\ 0 & \text{for } \mu \geq \lambda, \end{cases} \tag{3.4}$$

$$\lambda = L - m. \tag{3.5}$$

By virtue of equation 3.4 it was found that the rate at which individuals leave the population, i.e., the mortality rate, is determined by the expression

$$\rho = \omega (2\pi S^2)^{-1/2} \lambda \exp(-\lambda^2/2S^2)/\Phi(U), \tag{3.6}$$

$$\Phi(U) = (2\pi)^{-1/2} \int_{-\infty}^{U} e^{-u^2/2} du.$$

Here, $u = \mu/S$ is a standardized random variable, $U = \lambda/S$ is a dimensionless constant, and $\Phi(U)$ is the standard normal distribution [9]. When $\lambda \geq 2S$, the mortality rate can be described by the approximate relationship

$$\rho = \omega (2\pi S^2)^{-1/2} \lambda \exp(-\lambda^2/2S^2). \tag{3.7}$$

The table of the numerical value of the function $\Phi(U)$ [9] shows that the error in the ρ estimate is then less than 2.3%.

The physical meaning of the index of physiological state was not specified by Sacher; therefore, he used formula 3.7 only to approximate experimental data [7]. In our model, attempts are made to relate mortality to particular characteristics of the vital systems of the organism. We first take as ξ the random variable that describes the deviation of the index of physiological state from its normal level, because when this deviation reaches a critical value the organism usually dies [4-6]. The quantity describing the averaged physiological state index of a young and healthy organism is denoted by z_0, and the same quantity at time t by $z(t)$; then

$$m(t) = z_0 - z(t). \tag{3.8}$$

We assume that, under conditions of natural aging, $z(t)$ decreases linearly with time:

$$z(t) = z_0 - \kappa t, \tag{3.9}$$

and

$$\kappa t \ll z_0 \quad \text{for } t < t_v. \tag{3.10}$$

Here κ = constant, and t_v is the average life span. These assumptions are justified by the notion well known in biology and medicine that many physiological indices undergo gradual degradation with age.

By substituting 3.8 and 3.9 into 3.5 and 3.6, we obtain

$$\rho(t) = \omega\,(2\pi S^2)^{-1/2}\,(L - \kappa t)\exp\left\{-\frac{(L-\kappa t)^2}{2S^2}\right\} / \Phi(U), \tag{3.11}$$

$$U = (L - \kappa t)/S.$$

The dimensionless parameter $Q = S/L$ and the coefficient $k = \kappa/L$ with dimension T^{-1} are introduced. Then

$$\rho(t) = \omega\,(2\pi Q^2)^{-1/2}\,(1 - kt)\exp[-(1-kt)^2/2Q^2]\,/\Phi(U), \tag{3.12}$$

$$U = (1 - kt)/Q.$$

Relation 3.10 enables one to neglect the linear term in 3.12—kt, in front of exponent and in U. Obviously the quadratic term $k^2t^2/(2Q^2)$ in the exponent argument can also be neglected. The formula for $\rho(t)$ assumes a form

$$\rho(t) = \rho_0 \exp(R_0\, t), \tag{3.13}$$

where

$$\rho_0 = \omega\,(2\pi Q^2)^{-1/2}\exp(-1/2Q^2)/\Phi\,(1/Q),\quad R_0 = k/Q^2. \tag{3.14}.$$

Thus we have, in this approximation, Gompertz' well-known formula 3.13, which is often applied to describing the mortality rate in mammals [1, 2]. It is a convincing confirmation of the validity of our first step in specifying the random variable ξ.

Equations 3.6, 3.8, and 3.9 are taken as the basis for modeling the mortality of irradiated mammals. The fact that there are three different mechanisms that lead to death of irradiated animals within three nonoverlapping time intervals

enables us to make a second step in specifying the random variable ξ. We use as ξ the deviation of the index of the physiological state of the critical system (for particular doses and dose rates) from its normal level. As the index of the physiological state of a critical system, we take the concentration of its functional cells. We denote the mean concentration of critical system functional cells at time t after the onset of irradiation by $z_R(t)$, and the mean concentration of the same cells in a young and healthy organism by z_0. Then, formula 3.9 can be rewritten as follows:

$$z(t) = \begin{cases} z_0 - \kappa t & \text{for } t < t_R, \\ z_R(t) - \kappa t & \text{for } t \geq t_R, \end{cases} \tag{3.15}$$

where t_R is the onset of irradiation.

In accordance with 3.15, relation 3.8 changes to

$$m(t) = \begin{cases} \kappa t & \text{for } t < t_R, \\ z_0 - z_R(t) + \kappa t & \text{for } t \geq t_R. \end{cases} \tag{3.16}$$

Substituting 3.16 into 3.6, we obtain

$$\rho(t) = \omega\,(2\pi)^{-1/2} U \exp(-U^2/2)/\Phi(U), \tag{3.17}$$

$$U = \begin{cases} (L - \kappa t)/S & \text{for } t < t_R, \\ [\,L - (z_0 - z_R(t)) - \kappa t]/S & \text{for } t \geq t_R. \end{cases}$$

Besides the earlier defined coefficients Q and k, a dimensionless parameter $q = z_0/L$ and a dimensionless variable $\tilde{z}_R(t) = z_R(t)/z_0$ are introduced. Equation 3.17 assumes the form

$$\rho(t) = \rho_1 R \exp[(1 - R^2)/2Q^2]\,, \tag{3.18}$$

where

$$R = R(t) = 1 - q[1 - \tilde{z}(t)] - kt, \tag{3.19}$$

$$\rho_1 = \rho_0\, \Phi(1/Q)\, /\Phi\,(R/Q), \tag{3.20}$$

$$\tilde{z}(t) = \begin{cases} 1 & \text{for } t < t_R, \\ \tilde{z}_R(t) & \text{for } t \geq t_R\,. \end{cases} \tag{3.21}$$

The parameter ρ_0 in formula 3.20 is defined by equation 3.14. The function $R(t)$ in 3.19 is proportional to the difference between the critical deviation of the functional cell concentration from its normal level and the mean value of this deviation at time t. The function $R(t)$ is always positive because of the assumptions adopted in deriving formulas 3.18-3.21.

Note that when $R > 2Q$, formula 3.20 in model 3.18-3.21 can be replaced by the approximate relation

$$\rho_1 = \omega\,(2\pi Q^2)^{-1/2} \exp(-1/2Q^2). \tag{3.22}$$

The inaccuracy in the estimate of ρ_1 is less than 2.3%, as seen from the table of numerical values of the function $\Phi(U)$ [9].

Using the explicit expression 3.18 for the mortality rate $\rho(t)$, the other two biometric functions can be calculated: the probability density $w(t)$ and the probability $v(t)$ of the life span [3]:

$$w(t) = \rho(t) \exp\left\{-\int_0^t \rho(\tau)\, d\tau\right\}, \tag{3.23}$$

$$v(t) = \exp\left\{-\int_0^t \rho(\tau)\, d\tau\right\}. \tag{3.24}$$

These three modeling biometric functions will be compared, where possible, to experimental data for various mechanisms of death.

3.3. Intestinal Form* of Mortality of Irradiated Mammals

The developed model, 3.18-3.21, 3.23, and 3.24, was used for computer calculations of mortality probability characteristics for mice acutely and chronically irradiated within dose and dose rate ranges critical to the crypt-villus system. The dynamics of functional villus cells was determined within models described in chapter 2. The time interval within which the dynamics of the small intestine epithelium and mortality were simulated was 12 days. The duration in real experiments [10] was the same.

The parameters $\rho_0 = \exp(-11{,}7)$ day^{-1} and $k = 0{,}0005$ day^{-1} in formula 3.13 were calculated by the least squares method from experimental data on the mortality rate of nonirradiated mice of the BCF_1 and LAF_1 strains [1]. The following experimental data were used when estimating the coefficients q and Q; irradiated mice die if the concentration of functional villus cells drops to 10% of the normal level (z_0) [6]. Therefore, the critical value L equals $0.9\,z_0$; thus, $q = 1.1$. The mean square deviation from the mean values of the villus cell concentration in nonirradiated and irradiated mice is about $0.175\,z_0$ [11]; consequently, we have $Q^2 = 0.038$.

*Many American scientists use the term "gastrointestinal subsyndrome" of the acute radiation syndrome.

Figures 3.2 to 3.4 present computer-calculated mortality dynamics for 100-day-old mice after acute exposure to three different radiation doses. Figure 3.2 shows that after exposure the mortality rate $\rho(t)$ increases to a maximum level; the higher the dose, the greater the maximum level becomes. This is followed by a decrease of $\rho(t)$ and then by a new ascent. These model results are qualitatively consistent with experimental data [10].

The life span probability density $w(t)$ (fig. 3.3) during the first day after acute irradiation does not practically vary, while by day 100, $w(t)$ vanishes. The function $w(t)$ then increases to a maximum level; the higher the dose, the greater the maximum level becomes. The time to reach the maximum value is only weakly dependent upon the dose. After reaching its maximum value, the function $w(t)$ decreases, and by the end of the fifth day it returns to the initial value. The subsequent variations of $w(t)$ are insignificant and cannot be shown in the figure. These calculation results qualitatively agree with the diagram of the function $w(t)$ built from experimental observations of mice after an acute exposure to doses of 10-20 Gy [4]. It should be noted that the time parameters obtained in the model are consistently smaller than corresponding experimental quantities by about 24 hours. For example, in the experiments with the dose of 14 Gy, mice started dying at $t_1 = 2$ days, and all mice were dead at $t_2 = 5$ days after irradiation, with the maximum number of deaths at $t_3 = 3.5$ days [4]. The calculated values of t_1, t_2, and t_3 are 1.2, 4.3, and 2.5 days, respectively. This discrepancy seems to be due to a delay between the final stage of sickness (severe impairment of the small intestine epithelium) and death. Experiments suggest that this delay is a little less than 24 hours [4]. This also means that there is quantitative agreement, between the model and experimental data.

Within 1.5 days after radiation exposure, the life span probability function $v(t)$ does not practically deviate from its initial value (fig. 3.4). For 100-day-old mice this value is unity. Then the function $v(t)$ goes down and by the end of the fourth day arrives at the stationary level, which is lower for greater radiation doses D. This means that in the first 4 days after irradiation surviving animals decrease as D increases.

At $D = 9$ Gy, mortality is 50%. This result practically coincides with experimental data [12], which indicates that the dose that induces death of 50% of 12-week-old mice of the *C*5761/6 strain within 4 days after exposure ($LD_{50/4}$) is 8.8 ± 0.13 Gy. The estimates of mean lethal doses $LD_{50/5}$, and $LD_{50/6}$, and $LD_{50/7}$ by other authors are rather similar: 8.5-13 Gy [13].

It should be noted that the function $v(t)$ remains constant as long as the intestinal form of mortality prevails. At given intervals of doses D, this period is restricted to 5-7 days, according to experimental data [10].

Figures 3.5-3.7 show the calculated dynamics of mice mortality under chronic irradiation with three dose rates N. The age of animals at the onset of irradiation was 100 days. The mortality rate $\rho(t)$ (fig. 3.5) does not practically vary during the first day after onset of irradiation. The function $\rho(t)$ grows, then decreases, and increases again, arriving at higher values at higher dose rates N.

The function of life span probability density, $w(t)$, remains at the initial level during the first 2 days after the onset of irradiation (fig 3.6). On the third day, $w(t)$ starts to increase and arrives at a maximum; the lower the dose rate, the later the maximum is reached. The maximum value of $w(t)$ is greater with higher dose rate N. Then function $w(t)$ decreases.

In its turn, the function of the life span probability, $v(t)$, does not practically deviate from its initial value for the last two days after the onset of chronic irradiation (fig. 3.7). Furthermore, as N increases, $v(t)$ decreases more rapidly and attains lower minimum values. These results qualitatively (in the time interval 0-7 days quantitatively) coincide with experimental data [10]. Here and in chapter 4, experimental data [10] are presented with correction to one-day delay, discovered in experiments [4] between the final stage of sickness (severe impairment of the small intestine epithelium) and death. Calculated fractions of specimens surviving after 9 and 11 days exposure to the dose rate $N = 2$ Gy/day exceed corresponding experimental values. The discrepancy probably indicates that during this period the damaged small intestine is already not the sole reason for the animal's death.

Thus, modeling results agree qualitatively and, in most cases, also quantitatively with experimental observations.

3.4. Bone Marrow Form* of Mortality

The model described above is also suitable to simulate the dynamics of mortality of mice exposed from age t of 100 days to continuous radiation at dose rates $0 \leq N \leq 0.088$ Gy/day. The critical system in this case is the bone-marrow blood-forming system—the thrombocytopoiesis [5]. The dynamics of platelets, the functional elements of this system, was determined using the model developed in chapter 1. The time interval within which the dynamics of the critical system and mortality were simulated was 1,000 days, as in actual experimentation [7].

The parameters $\rho_0 = \exp(-11, 7)$ day^{-1} and $k = 0.0005$ day^{-1}, as before, were calculated by the least squares method from experimental mortality rates for nonirradiated mice of the BCF_1 and LAF_1 strains [1]. The following experimental facts were used when estimating the coefficients q and Q. Irradiated

*Many American scientists use the term "hematopoietic subsyndrome" of the acute radiation syndrome.

mice die when platelet concentration is 10% of the normal level [5]. Therefore the critical value L equals 0.9 z_0 and $q = 1.1$. The mean square deviation from the mean platelet concentrations for irradiated and nonirradiated mice is about $0.2z_0$ [5]; consequently, $Q = 0.05$.

The calculations of thrombocytopoiesis dynamics have shown that with the chosen values of the coefficients in the range of chronic irradiation dose rates $0 \leq N \leq 0.088$ Gy/day, the minimal value of R/Q is 4. Consequently, the inequality of $R > 2Q$ is valid, and instead of formula 3.20, the approximate relation 3.22 can be used.

Figures 3.8-3.10 present the functions $\rho(t)$, $w(t)$, and $v(t)$, calculated within the model 3.18, 3.19, and 3.21-3.24, and corresponding, experimental data [7] on mortality rate dynamics for nonirradiated and irradiated LAF_1 mice from age $t_R = 100$ days at three different dose rates. Figure 3.8 shows that the model adequately reproduces experimental results [7]. The mortality rate for nonirradiated mice increases with increasing the age t. Two phases can be distinguished in the dynamics of the mortality rate of irradiated mice. During the first phase, the values of $\rho(t)$ oscillate with damping near by a permanently rising level. This phase corresponds to the oscillating transitional process in the dynamics of thrombocytopoiesis and precedes the establishment of a new homeostasis in the system under consideration (see chapter 1). During the second phase, the function $\rho(t)$ increases. As in the experiments [7] for a fixed age t, the mortality rate during prolonged irradiation exceeds that for nonirradiated mice by a quantity that increases with increasing dose rate N. In contrast to Gompertz' widely applied formula 3.13, the model describes the experimentally observed deviation of the function $\rho(t)$ from the exponential curve in the region of high values of t.

Life span probability density for nonirradiated mice increases to a maximum then decreases (fig. 3.9). The function $w(t)$ describing life span probability density of mice exposed to chronic radiation has, as the function $\rho(t)$, (mortality rate) two characteristic regions. From the onset of irradiation, $w(t)$ reproduces the oscillating transitional process. After radiation exposure is ended, the values of $w(t)$ are greater at higher dose rate N. Further, $w(t)$ increases, arrives at the maximum level, and then decreases. As the dose rate increases, the time it takes $w(t)$ to reach the maximum level diminishes, i.e., the mortality peak occurs earlier.

Figure 3.10 shows that the function $v(t)$, which describes the life span probability of animals exposed to chronic radiation, decreases since the onset of irradiation and takes the smaller values $v(t)$ as dose rate N increases.

Experimental data are not presented in figs. 3.9 and 3.10 because in the experiments imitated here [7] only the biometric function $\rho(t)$ was measured. Such additional experimental data are not really required because the function $\rho(t)$ uniquely determines two other biometric functions, $w(t)$ and $v(t)$ (see equations 3.23 and 3.24).

The model was used to calculate the average shortening of life span:

$$s = \int_0^\infty t\, w_0(t)\, dt \; - \; \int_0^\infty t\, w_R(t)\, dt. \tag{3.25}$$

In 3.25, $w(t)$ and $w_R(t)$ are the life span probability densities (3.23) for nonirradiated and irradiated mammals, and t is time. For N of 0.013, 0.026, and 0.06 Gy/day we obtained the life span shortening s values of 30, 64, and 166 days, respectively, which are fairly close to experimental estimates of 34, 67, and 146 days [1].

3.5. Conclusion

A mathematical model of mortality dynamics for homogeneous population of mammals exposed to acute and continuous radiation was developed. It relates the statistical biometric functions (mortality rate, life span probability density, and life span probability) with the statistical characteristics and the kinetics of the organism's critical systems. The thrombocytopoietic system and the small intestine epithelium system were selected as critical systems. The number of functional elements in these systems (platelets and villus cells) were found by solving the respective mathematical models described in chapters 1 and 2. Modeling results agree qualitatively and quantitatively with experimental data on mortality dynamics and average life span shortening for acutely and chronically irradiated mice.

FIGURES

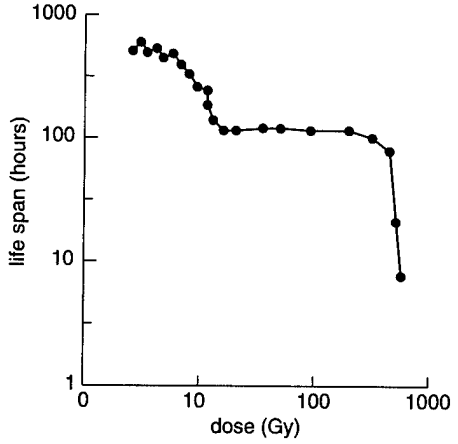

Fig. 3.1. Average life span of LAF_1 mice as a function of dose of acute irradiation [4].

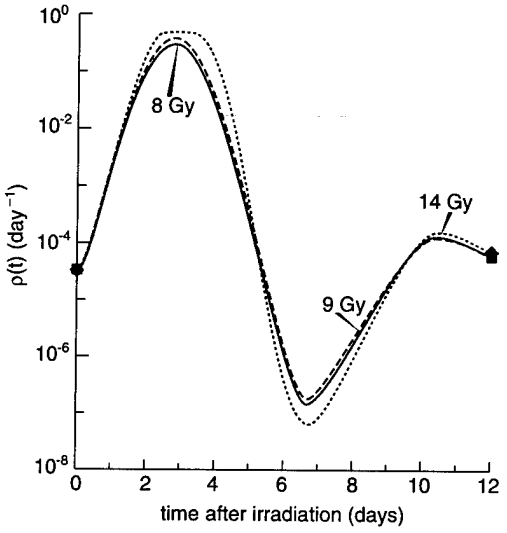

Fig. 3.2. Biometric function $\rho(t)$ characterizing the mortality rate of mice exposed to acute radiation.

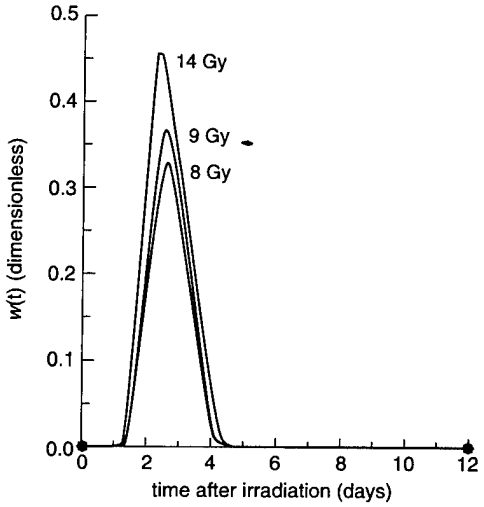

Fig. 3.3. Biometric function $w(t)$ characterizing life span probability density of mice exposed to acute radiation.

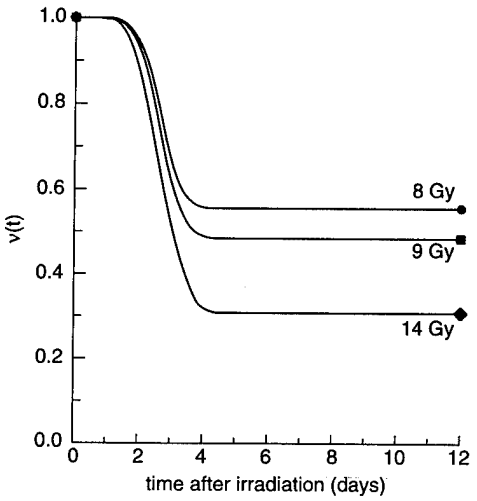

Fig. 3.4. Biometric function $v(t)$ characterizing life span probability of mice exposed to acute radiation.

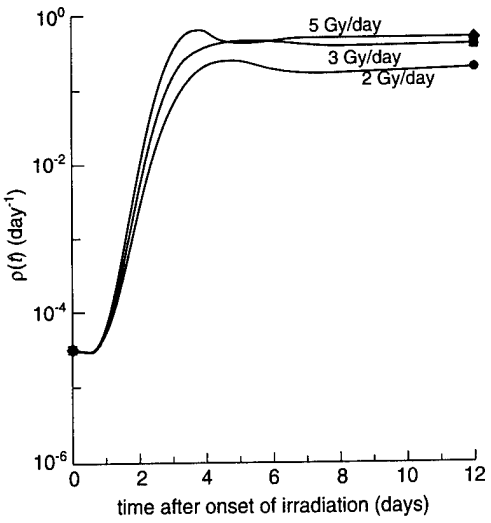

Fig. 3.5. Biometric function $\rho(t)$ describing the mortality rate of chronically irradiated mice.

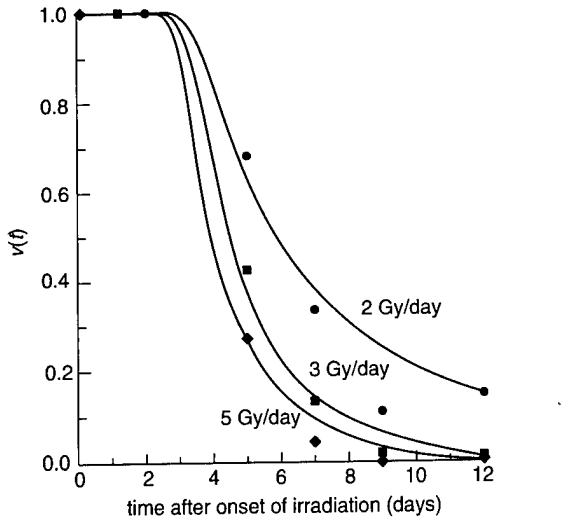

Fig. 3.7. Biometric function $v(t)$ describing life span probability of chronically irradiated mice.

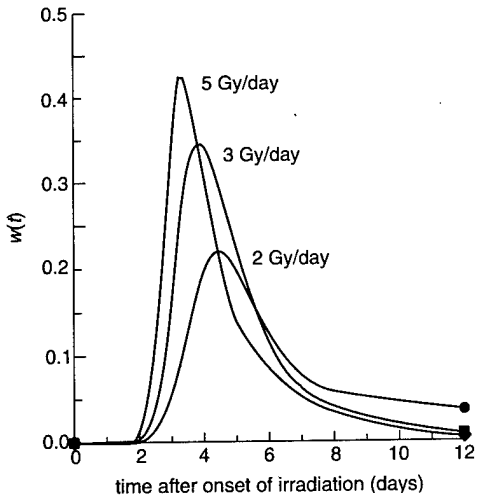

Fig. 3.6. Biometric function $w(t)$ describing life span probability density of chronically irradiated mice.

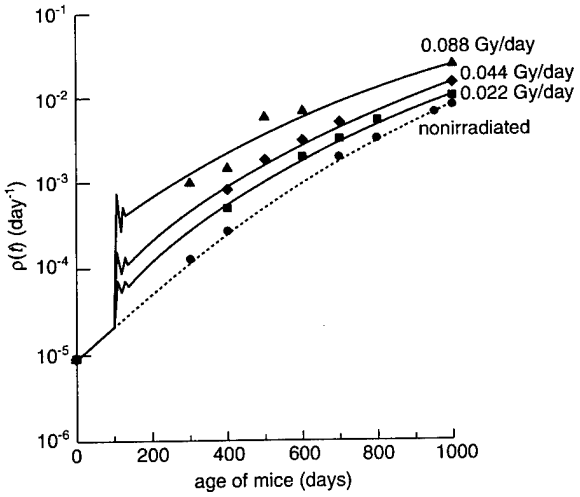

Fig. 3.8. Biometric function $\rho(t)$ describing the mortality rate of mice.

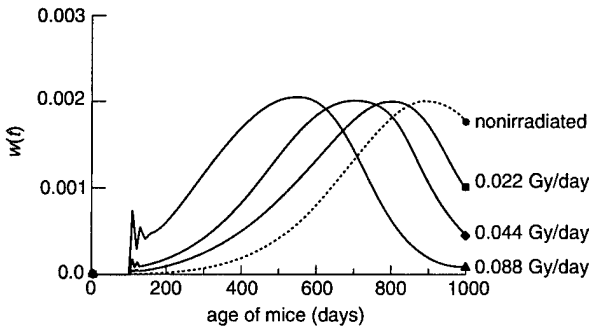

Fig. 3.9. Biometric function $w(t)$ describing life span probability density of mice.

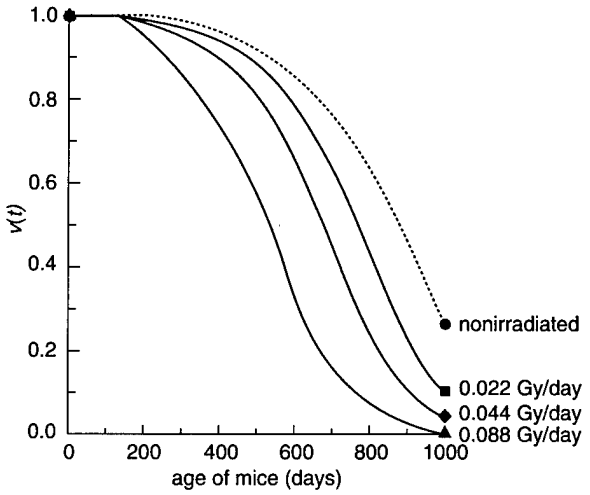

Fig. 3.10. Biometric function $v(t)$ describing life span probability of mice.

REFERENCES

1. Ionizing radiation: Sources and biological effects, Vol II (1982) Report to the General Assembly, United Nations Scientific Committee on the Effects of Atomic Radiation, New York: United Nations Organization

2. Cox DR, Oakes D (1984) Analysis of survival data. London; New York: Chapman and Hall

3. Boleslawski L (1977) Cohort tables of life span. Moscow: Statistika vol. 12-38 (Russian)

4. Bond VP, Fliedner TM, Archambeau JO (1965) Mammalian radiation lethality: A disturbance in cellular kinetics. New York: Academic Press

5. Kalina I, Praslichka M (1977) Changes in haemopoiesis and survival of continuously irradiated mice. Radiobiologiya 17:849-853 (Russian)

6. Matsuzawa T, Wilson R (1965) The intestinal mucosa of germfree mice after whole-body X-irradiation with 3 kiloroentgens. Radiation Research 25:15-24

7. Sacher GA (1955) On the statistical nature of mortality with a special reference to chronic radiation mortality. Radiology 67:250-258

8. Sacher GA, Trucco E (1962) The stochastic theory of mortality. Annals of the New York Academy of Sciences 96:985-1007

9. Korn GA, Korn TM (1968) Mathematical handbook. New York; San Francisco; Toronto; London: Sydney: McGraw-Hill Book Company

10. Iberall AS (1967) Quantitative modeling of the physiological factors in radiation lethality. Annals of the New York Academy of Sciences 147:1-81

11. Lesher S (1967) Compensatory reaction in intestinal crypt cells after 300 roentgens of cobalt-60 gamma irradiation. Radiation Research 32(3)510-519

12. Konoplyannikova OA, Konoplyannikov AG (1984) Age-related changes in radiosensitivity of animals and critical cell systems: Survival of stem cells of small intestine epithelium, and 4-5-day death of mice of different age after irradiation. Radiobiologiya 24:249-252 (Russian)

13. Potten CS (1987) Radiosensitivity and kinetics of target cells in relation to tissue responses—as exemplified by the epidermis and the intestine. In: Radiation Research. Proceedings of the 8th International Congress of Radiation Research, Edinburgh. London; New York; Philadelphia: Taylor & Francis, pp 782-788

CHAPTER 4

Mathematical Model of Mortality for a Nonhomogeneous Mammalian Population

4.1. Introduction

The development of the mathematical model of mortality dynamics for mammals described in chapter 3 was based on the assumption that mean values and fluctuations of major physiological parameters and cell radiosensitivity of critical systems are identical for all members of the population. Mortality dynamics of laboratory mice irradiated with acute doses and chronic dose rates that affect the critical systems of hematopoiesis (thrombocytopoiesis) and the small intestine epithelium are reproduced fairly well in this model. However, new evidence indicating that there are human subpopulations hypersensitive to radiation [1, 2] calls for model investigations of mortality dynamics for a nonhomogeneous population. This chapter describes the extension and modification of the model presented in chapter 3 and applies it to the analysis of mortality in irradiated nonhomogeneous mammalian populations.

4.2. Generalized Model of Mortality for Nonhomogeneous Population

To apply the mathematical models in chapters 1-3 to describe radiation-induced mortality of a nonhomogeneous population, it is necessary to represent the population as a collection of a finite number of homogeneous subpopulations. Within the context of this approach, it is reasonable to assume that the nonhomogeneity of a mammalian population to radiation exposure is principally due to the dissimilar radiosensitivity of critical system cells. In our models (chapters 1 and 2), the parameter D_1 characterizes the radiosensitivity of division-capable precursor cells in the thrombocytopoietic system and in the crypts of the small intestine epithelium system. The specimen distribution

in the radiosensitivity index of the critical system cells, D_1, in a nonhomogeneous mammalian population will be described by a continuous function $\varphi(D_1)$. Then, by definition, $\varphi(D_1)\,dD_1$ is the fraction of specimens whose index of critical system cell radiosensitivity lies between D_1 and $D_1 + dD_1$. The range of the continuous random variable D_1 breaks into a finite number of intervals I. Thus, we have I groups of specimens whose critical cell radiosensitivity index D_1 belongs to the respective ith interval $(D'_{1i},\ D''_{1i})$ $(i = 1, \ldots, I)$. The fraction of animals constituting the ith group is expressed through the probability density function $\varphi(D_1)$ as follows [3]:

$$n_i = \int_{D'_{1i}}^{D''_{1i}} \varphi(D_1)\,dD_1. \tag{4.1}$$

The mean value of D_1 for animals of the ith group is

$$\overline{D}_{1i} = \frac{1}{n_i} \int_{D'_{1i}}^{D''_{1i}} D_1\,\varphi(D_1)\,dD_1. \tag{4.2}$$

The initial continuous distribution $\varphi(D_1)$ is then approximated by a discrete distribution in the following way. Assume that the random variable D_1 takes on discrete values $\overline{D}_{1i}$ (equation 4.2) with the probability

$$\varphi_i(\overline{D}_{1i}) = n_i \quad (i = 1, \ldots, I), \tag{4.3}$$

where the probabilities n_i are determined by equation 4.1. This operation is equivalent to the representation of the initial nonhomogeneous population as a set of a finite number of homogeneous subpopulations. The number of specimens in the ith homogeneous subpopulation coincides with the number of specimens in the ith group of the initial population whose D_1 belongs to the ith interval. The parameter $\overline{D}_{1i}$ that shows the radiosensitivity of the critical system cells for individuals of the ith homogeneous subpopulation is equal to the mean value of D_1 for the individuals of the ith group of the initial population. It should be noted that with any method of subdivision of the range of continuous random variable D_1 into intervals and, regardless of the number of the latter, the mean values of the radiosensitivity index of the critical system cells for individuals of the initial nonhomogeneous population and for individuals of the nonhomogeneous population, which is a set of the homogeneous subpopulations (with parameters n_i and $\overline{D}_{1i}$ $(i = 1, \ldots, I)$), are equal. This follows from the equality of the expected value of the random variable D_1 described by the continuous distribution $\varphi(D_1)$ and of the expected value of the random variable D_1 described above by the derived discrete distribution $\varphi_{i(}\overline{D}_{1i)}$ (equation 4.3).

The dynamics of radiation-induced mortality of each ith homogeneous subpopulation, whose members have their particular value of the radiosensitivity

index $\overline{D}_{1i}$, can be calculated by the model described in chapter 3. This will yield a set of values of the biometric functions (mortality rate $\rho_i(t)$, probability density $w_i(t)$, and life span probability $v_i(t)$) that describe the mortality dynamics of the ith subpopulation under a given irradiation regime.

The biometric functions $\rho_\Sigma(t)$, $w_\Sigma(t)$, and $v_\Sigma(t)$, characterizing the mortality dynamics of the population as a whole, are expressed through the biometric functions $\rho_i(t)$, $w_i(t)$ and $v_i(t)$ ($i = 1, \ldots, I$). As indicated in chapter 3, the biometric function $v_\Sigma(t)$ represents the ratio of animals that survived to time t, $N_\Sigma(t)$, to their initial number $N_{0\Sigma}$ in the population:

$$v_\Sigma(t) = \frac{N_\Sigma(t)}{N_{0\Sigma}}. \tag{4.4}$$

For each instant time t, the values of the functions $v_i(t)$ ($i = 1, \ldots, I$) are known. They are equal to the ratio of the number of specimens of the ith subpopulation that survived to time t, $N_i(t)$, to their initial number $N_{0i} = N_{0\Sigma} \cdot n_i$:

$$v_i(t) = \frac{N_i(t)}{N_{0i}} = \frac{N_i(t)}{N_{0\Sigma} \cdot n_i}. \tag{4.5}$$

It follows from 4.5 that

$$N_i(t) = N_{0\Sigma} \cdot v_i(t) \cdot n_i. \tag{4.6}$$

Hence, the total number of animals surviving to time t in the population composed of I homogeneous subpopulations is

$$N_\Sigma(t) = \sum_{i=1}^{I} N_i(t) = N_{0\Sigma} \sum_{i=1}^{I} v_i(t) \cdot n_i. \tag{4.7}$$

Substitution of 4.7 into 4.4, yields

$$v_\Sigma(t) = \sum_{i=1}^{I} v_i(t)\, n_i. \tag{4.8}$$

The biometric function $w_\Sigma(t)$ is equal to the ratio of the number of animals in the population that die at time t, dN_Σ/dt, to the initial number of animals $N_{0\Sigma}$:

$$w_\Sigma(t) = -\frac{dN_\Sigma}{dt} \cdot \frac{1}{N_{0\Sigma}}. \tag{4.9}$$

For every instant time t, the values of the functions $w_i(t)$ ($i = 1, \ldots, I$) are known. They are equal to the ratio of the number of animals belonging to the

ith subpopulation that die at time t, dN_i/dt, to the initial number of animals in this subpopulation $N_{0i} = N_{0\Sigma} \cdot n_i$:

$$w_i(t) = -\frac{dN_i}{dt} \cdot \frac{1}{N_{0i}} = -\frac{dN_i}{dt} \cdot \frac{1}{N_{0\Sigma} \cdot n_i}. \tag{4.10}$$

It follows from 4.10 that

$$-\frac{dN_i}{dt} = N_{0\Sigma} \cdot w_i(t) \cdot n_i. \tag{4.11}$$

In accordance with 4.11, the total number of specimens in the entire population that die at time t is defined by the expression

$$-\frac{dN_\Sigma}{dt} = -\sum_{i=1}^{I} \frac{dN_i}{dt} = N_{0\Sigma} \sum_{i=1}^{I} w_i(t)\, n_i. \tag{4.12}$$

Substitution of 4.12 into 4.9 yields

$$w_\Sigma(t) = \sum_{i=1}^{I} w_i(t)\, n_i. \tag{4.13}$$

The biometric function $\rho_\Sigma(t)$ represents the ratio of the number of animals in the population that die at time t, dN_Σ/dt, to the number of animals of the same population that survived to time t, $N_\Sigma(t)$:

$$\rho_\Sigma(t) = -\frac{dN_\Sigma}{dt} \cdot \frac{1}{N_\Sigma(t)}. \tag{4.14}$$

By the relations described in 4.7, 4.8, 4.12, and 4.13 the following formula is obtained:

$$\rho_\Sigma(t) = \frac{N_{0\Sigma} \sum_{i=1}^{I} w_i(t)\, n_i}{N_{0\Sigma} \sum_{i=1}^{I} v_i(t)\, n_i} = \frac{w_\Sigma(t)}{v_\Sigma(t)}. \tag{4.15}$$

Another version of the formula is suitable for calculating function $\rho_\Sigma(t)$. Values of the function $\rho_i(t)$ $(i = 1, \ldots, I)$ are known for each instant t. They are equal to the ratio of the number of animals that die at time t, dN_i/dt, to the number of animals that survived to time t in the ith subpopulation $N_i(t)$:

$$\rho_i(t) = -\frac{dN_i}{dt} \cdot \frac{1}{N_i(t)}. \tag{4.16}$$

From 4.16,

$$-\frac{dN_i}{dt} = \rho_i(t) \cdot N_i(t). \tag{4.17}$$

According to 4.6 and 4.17, the total number of animals in the whole population that die at time t is

$$-\frac{dN_\Sigma}{dt} = -\sum_{i=1}^{I} \frac{dN_i}{dt} = \sum_{i=1}^{I} \rho_i(t) \cdot N_i(t) = N_{0\Sigma} \sum_{i=1}^{I} \rho_i(t) \cdot v_i(t) \cdot n_i. \tag{4.18}$$

In turn, according to formulas 4.7 and 4.8, N_Σ is defined by the expression

$$N_\Sigma(t) = N_{0\Sigma} \sum_{i=1}^{I} v_i(t) \cdot n_i = N_{0\Sigma} \cdot v_\Sigma(t). \tag{4.19}$$

Substitution of 4.18 and 4.19 into 4.14, yields

$$\rho_\Sigma(t) = \frac{\sum_{i=1}^{I} \rho_i(t)\, v_i(t)\, n_i}{\sum_{i=1}^{I} v_i(t)\, n_i} = \frac{1}{v_\Sigma(t)} \cdot \sum_{i=1}^{I} \rho_i(t)\, v_i(t)\, n_i. \tag{4.20}$$

Thus, a mathematical model in the general form was built to enable the calculation of statistical biometric functions that describe mortality dynamics in irradiated mammals from a population that is nonhomogeneous in radiosensitivity.

4.3. Normal and Log-Normal Distributions of Animal Populations and the Radiosensitivity Index of Their Critical System Cells

The mathematical model in section 4.2 was refined to describe a nonhomogeneous population by using two types of distribution: normal (Gaussian) and log-normal, most frequently used in biology. Examined first was the case where the distribution of animals of a nonhomogeneous population in the radiosensitivity index of the critical system cells, D_1, obeyed the Gauss law [3]:

$$\varphi_N(D_1) = \frac{1}{\sigma\sqrt{2\pi}} \exp\left\{-\frac{(D_1 - \overline{D}_1)^2}{2\sigma^2}\right\}. \tag{4.21}$$

In formula 4.21 the parameter $\overline{D}_1$ is the expected value of the random variable D_1 (the mean of the density $\varphi_N(D_1)$), and σ^2 is equal to the variance $V(D_1)$ of the probability density function $\varphi_N(D_1)$. The range of the variable D_1 in 4.21

covers real numbers from -∞ to +∞; however, in practice, a finite range of the normal random variable is taken. In many cases, the range is restricted by a tripled standard deviation from the mean value in both sides, and no renormalization of the normal probability density function is performed. This is acceptable because the probability for a normal random variable to assume a value that is outside the indicated region is negligible (0.0027) [4]. Because the ratio of the standard deviation to the mean for many biological indices described by normal distribution does not exceed 0.3 [5], our consideration was also restricted to the interval $(\overline{D}_1 - 3\sigma, \overline{D}_1 + 3\sigma)$. It is in this region that the random variable D_1 is positive, having a real physical meaning.

When passing to discrete distribution (equation 4.3), the studied range of the continuous random variable D_1 is subdivided into six symmetric intervals relative to $\overline{D}_1$ with the following boundaries:

$$\overline{D}_1 - 3\sigma, \overline{D}_1 - 2\sigma, \overline{D}_1 - \sigma, \overline{D}_1, \overline{D}_1 + \sigma, \overline{D}_1 + 2\sigma, \overline{D}_1 + 3\sigma. \quad (4.22)$$

According to equations 4.1, 4.2, and 4.21, n_i and $\overline{D}_{1i}$ in 4.3 are defined by the formulas

$$n_i = \Phi(U_i'') - \Phi(U_i'), \text{ and} \quad (4.23)$$

$$\overline{D}_{1i} = \overline{D}_1 - \frac{1}{n_i}\frac{\sigma}{\sqrt{2\pi}}\left[\exp\left\{-\frac{(U_i'')^2}{2}\right\} - \exp\left\{-\frac{(U_i')^2}{2}\right\}\right]. \quad (4.24)$$

In 4.23 and 4.24, U_i' and U_i'' are expressed through the boundary values of the intervals D_{1i}' and D_{1i}'':

$$U_i' = (D_{1i}' - \overline{D}_1)/\sigma; \quad U_i'' = (D_{1i}'' - \overline{D}_1)/\sigma. \quad (4.25)$$

In 4.23, Φ(U) is the standard normal distribution [3]:

$$\Phi(U) = \frac{1}{\sqrt{2\pi}}\int_{-\infty}^{U}\exp\left\{-u^2/2\right\}du. \quad (4.26)$$

With the chosen values of D_1' and D_{1i}'' (equation 4.22), the parameters n_i and $\overline{D}_{1i}$ $(i = 1, \ldots, 6)$ are respectively equal to

$$\begin{aligned} n_1 &= 0.02140, \quad n_4 = 0.34134, \\ n_2 &= 0.13591, \quad n_5 = 0.13591, \\ n_3 &= 0.34134, \quad n_6 = 0.02140, \end{aligned} \quad (4.27)$$

and

$$\begin{aligned}
\overline{D}_{11} &= \overline{D}_1 - \sigma \cdot 2.31585, \quad \overline{D}_{14} = \overline{D}_1 + \sigma \cdot 0.45986, \\
\overline{D}_{12} &= \overline{D}_1 - \sigma \cdot 1.38312, \quad \overline{D}_{15} = \overline{D}_1 + \sigma \cdot 1.38312, \\
\overline{D}_{13} &= \overline{D}_1 - \sigma \cdot 0.45986, \quad \overline{D}_{16} = \overline{D}_1 + \sigma \cdot 2.31585.
\end{aligned} \tag{4.28}$$

In calculating n_i, the table of the function $\Phi(U)$ was used [4].

In the approximation applied, the initial nonhomogeneous population with a normal distribution of specimens in the radiosensitivity index of the critical system cells can indeed be represented as a set of the six homogeneous subpopulations. The number of specimens in each of the subpopulations is determined by n_i (4.27). The index of individual radiosensitivity of critical system cells in each of the six subpopulations, $\overline{D}_{1i}$ (4.28), is uniquely expressed by the parameters $\overline{D}_1$ and σ of the normal distribution $\varphi_N(D_1)$ (4.21).

Examined next was log-normal distribution of specimens of the population in the radiosensitivity index D_1 of the critical system cells, which means that the logarithm of the random variable D_1, $X = \ln D_1$, and not the random variable D_1 itself, is distributed by normal law. The probability density function $\varphi_{LN}(D_1)$ of the random variable D_1 is expressed through the expected value m and the standard deviation σ of the normal random variable X [3]:

$$\varphi_{LN}(D_1) = \frac{1}{\sigma\sqrt{2\pi}} \frac{1}{D_1} \exp\left\{-\frac{(\ln D_1 - m)^2}{2\sigma^2}\right\}. \tag{4.29}$$

The parameters m and σ also define the expected value $\overline{D}_1$ of the random variable D_1 and the variance $V(D_1)$ of the probability density function $\varphi_{LN}(D_1)$ (4.29).

$$\overline{D}_1 = \exp\left\{m + \frac{\sigma^2}{2}\right\}. \tag{4.30}$$

$$V(D_1) = \exp(2m + \sigma^2)\left[\exp(\sigma^2) - 1\right]. \tag{4.31}$$

The range of the normal random variable X includes real numbers from $-\infty$ to $+\infty$. The corresponding range of the random variable D_1 includes positive real numbers. Therefore, the random variable D_1 described by log-normal distribution (4.29) has a real physical meaning within the domain of its definition.

In passing to discrete distribution (4.3), it is more convenient first to deal with the normal random variable $X = \ln D_1$. As before, we restrict the consideration to its finite range. Now, however, X must not be necessarily positive, so we can set its wider range: $(m - 5\sigma, m + 5\sigma)$. In this case, the probability for a normal random variable to take on values lying outside the indicated limits of the given region is practically equal to zero $(5.734 \cdot 10^{-7})$ [4]. So there is no need for a renormalization of the corresponding distribution functions. The indicated range of the normal random variable X was broken up as in the first

version into six symmetrical intervals relative to the expected value m and having the same internal boundaries:

$$m - 5\sigma,\ m - 2\sigma,\ m - \sigma,\ m,\ m + \sigma,\ m + 2\sigma,\ m + 5\sigma. \tag{4.32}$$

The corresponding boundaries D'_{1i}, and D''_{1i} of the intervals of the range of the random variable D_1 are expressed in terms of the parameters m and σ in the following way:

$$e^{m-5\sigma},\ e^{m-2\sigma},\ e^{m-\sigma},\ e^{m},\ e^{m+\sigma},\ e^{m+2\sigma},\ e^{m+5\sigma}. \tag{4.33}$$

According to 4.1, 4.2, and 4.29, n_i and $\overline{D}_{1i}$ are defined in 4.3 by the formulas

$$n_i = \Phi(U'') - \Phi(U'), \text{ and} \tag{4.34}$$

$$\overline{D}_{1i} = \frac{1}{n_i}\frac{e^m}{\sqrt{2\pi}}\int_{U'_i}^{U''_i} \exp\left\{-\frac{u^2}{2} + \sigma u\right\} du\,. \tag{4.35}$$

In equations 4.34 and 4.35, U'_i and U''_i are expressed by the boundary values of the intervals D'_{1i} and D''_{1i}:

$$U'_i = (\ln D'_{1i} - m)/\sigma, \quad U''_i = (\ln D''_{1i} - m)/\sigma\,. \tag{4.36}$$

In 4.34, $\Phi(U)$ is the standard normal distribution as defined in equation 4.26.

With the chosen values of D'_{1i} and D''_{1i} in 4.33, the parameters of n_i ($i = 1, \ldots, 6$) are as follows [4]:

$$\begin{aligned} n_1 &= 0.02275 \quad n_4 = 0.34134 \\ n_2 &= 0.13591 \quad n_5 = 0.13591 \\ n_3 &= 0.34134 \quad n_6 = 0.02275 \end{aligned} \tag{4.37}$$

and the lower and upper integration limits in formula 4.35 (which defines $\overline{D}_{1i}$ ($i = 1, \ldots, 6$)) are set by the following pairs of numbers:

$$\begin{matrix} [-5, -2] & [0, 1] \\ [-2, -1] & [1, 2] \\ [-1, 0] & [2, 5] \end{matrix} \tag{4.38}$$

Thus, in the stated approximation above, the initial nonhomogeneous population with a log-normal distribution of animals in the radiosensitivity index of critical system cells can be represented as a nonhomogeneous population formed by six homogeneous subpopulations. The fraction of animals in each subpopulation is determined by n_i (4.37). The index of individual radiosensitivity of critical system cells for specimens of these subpopulations, $\overline{D}_{1i}$ (4.35)

is uniquely expressed by the parameters m and σ of the log-normal distribution φ_{LN} (4.29).

We have thus proposed two versions for calculating the quantities n_i and $\overline{D}_{1i}$ ($i = 1, \ldots, I$), which are parameters of the model of radiation-induced mortality in a nonhomogeneous mammalian population. These versions are used when the distribution $\varphi(D_1)$ of specimens of the population in the cell radiosensitivity index D_1 is, respectively, normal or log-normal. However, the study of the relationship between the mortality dynamics and the type of probability density function $\varphi(D_1)$ was not the only objective of our investigations. It was also our intention to examine the correlation between radiation-induced mortality and degree of nonhomogeneity of the population, i.e., the spread of values of the random variable D_1 about a fixed mean $\overline{D}_1$. As a measure of nonhomogeneity can serve a dimensionless quantity κ, which is equal to the ratio of the square root of the variance $\sqrt{V(D_1)}$ to the mean $\overline{D}_1$ of the probability density function $\varphi(D_1)$ of the radiation variable D_1, then

$$\kappa = \sqrt{V(D_1)}/\overline{D}_1. \tag{4.39}$$

If the random variable D_1 is described by the normal distribution $\varphi N(D_1)$ (equation 4.21), κ is uniquely related to the parameters of this distribution [3]:

$$\sigma = \kappa \overline{D}_1. \tag{4.40}$$

Therefore, according to 4.40, the variation of κ in a model study of the effect of population nonhomogeneity on the dynamics of radiation-induced mortality will be manifested in changes of the parameter σ in formulas 4.28 for calculating $\overline{D}_{1i}$.

If the random variable D_1 is described by the log-normal distribution $\varphi_{LN}(D_1)$ (4.29), then in accordance with 4.30 and 4.31, the dimensionless quantity κ is determined by only one parameter σ of the log-normal distribution $\varphi_{LN}(D_1)$:

$$\kappa = \sqrt{V(D_1)}/\overline{D}_1 = [\exp(\sigma^2) - 1]^{1/2}. \tag{4.41}$$

Hence we find

$$\sigma = [\ln(\kappa^2 + 1)]^{1/2}. \tag{4.42}$$

According to 4.30, the second parameter, m, of the distribution $\varphi_{LN}(D_1)$ (4.29) can be expressed by σ and by a fixed expected value $\overline{D}_1$ of the random variable D_1 as follows:

$$m = \ln \overline{D}_1 - \sigma^2/2. \tag{4.43}$$

Substitution of 4.42 into 4.43 yields

$$m = \ln \overline{D}_1 - \frac{1}{2}\ln(\kappa^2 + 1). \tag{4.44}$$

Consequently, in this case, when modeling the dependence of population mortality on the degree of its nonhomogeneity, the variation of κ leads to changes in both parameter σ (4.42) and parameter m (4.44) in the $\overline{D}_{1i}$ calculation formula (4.35).

This model was used in studies of the gastrointestinal and bone-marrow syndromes of radiation-induced mortality in radiosensitive, nonhomogeneous mammalian populations. Results of these studies are given in subsequent sections of this chapter.

4.4. Intestinal Form* of Radiation-Induced Mortality of Mammals

The generalized model described in the preceding sections was used to study mortality dynamics of a nonhomogeneous mammalian population exposed to chronic or acute radiation conditions with the small intestine epithelium as the critical system. Accordingly, the mathematical model of the dynamics of the crypt-villus system (section 2.3) and the model simulating the intestinal form of mortality of a homogeneous mammalian population (section 3.3) were used. As in sections 2.3 and 3.3, mice were used for the modeling. All the parameters of the above models were kept unchanged. The numerical value of the averaged index of radiosensitivity for the division-capable precursor cells of the crypts was given to the parameter $\overline{D}_1$, a key parameter of the nonhomogeneous population mortality model. In this case, $\overline{D}_1$ denotes the expected value of the random variable D_1 (index of radiosensitivity of the cells of the crypt-villus system for members of a nonhomogeneous population).

Parameters n_i were determined first, and the parameters $\overline{D}_{1i}$ $(i = 1, \ldots, 6)$ were calculated from the given $\overline{D}_1$ and the chosen value of κ (4.39). Equations 4.27, 4.28, and 4.40 were used for normal distribution $\varphi_N(D_1)$ (4.21) of the random variable $\overline{D}_1$, and equations 4.35-4.38, 4.42, and 4.44 were used for log-normal distribution $\varphi_{LN}(D_1)$ (4.29). The values of $\overline{D}_{1i}$ obtained are listed in table 4.1. Next, the model 2.9-2.12 was used to find the dynamics of the small intestine epithelium for six subpopulations of mice in the chosen radiation conditions and the corresponding values of $\overline{D}_{1i}$ $(i = 1, \ldots, 6)$. Recall that the latter describe the individual radiosensitivity of intestinal epithelium precursor cells in specimens of the ith subpopulation. The values of the functional cell concentration of the crypt-villus system thus obtained were substituted into formula 3.21 of the mortality model 3.18-3.21, 3.23, and 3.24. The biometric functions $v_i(t)$, $w_i(t)$, and $\rho_i(t)$ $(i = 1, \ldots, 6)$, which describe the mortality of mice in each of

*Many American scientists use the term "gastrointestinal subsyndrome" of the acute radiation syndrome.

Table 4.1. Index of individual radiosensitivity $\overline{D}_{1i}$ ($i = 1, \ldots, 6$) of small intestine epithelium precursor cells for specimens of six subpopulations that constitute the nonhomogeneous population. Normal and the log-normal distributions of animals of the initial nonhomogeneous population in the radiosensitivity index D_1 were examined. The distributions have equal means, $\overline{D}_1 = 11.2$ Gy, and different variances $V(D_1)$. The parameter κ is defined by formula 4.39: $\kappa = \sqrt{V(D_1)}/\overline{D}_1$.

	Distribution				
Parameter	Normal			Log-normal	
κ	0.15	0.3	0.3	1.0	1.5
$\overline{D}_{11}$	7.309	3.419	5.370	1.137	0.500
$\overline{D}_{12}$	8.876	6.553	7.170	2.565	1.441
$\overline{D}_{13}$	10.427	9.655	9.405	5.549	3.948
$\overline{D}_{14}$	11.973	12.745	12.321	11.942	10.731
$\overline{D}_{15}$	13.524	15.847	16.151	25.711	29.161
$\overline{D}_{16}$	15.091	18.981	21.643	59.815	88.725

the six subpopulations for the chosen irradiation conditions, were calculated in the framework of this model. Further, using the values of $v_i(t)$, $w_i(t)$, $\rho_i(t)$, and n_i ($i = 1, \ldots, 6$) and formulas 4.8, 4.13, and 4.20, the functions $v_\Sigma(t)$, $w_\Sigma(t)$, and $\rho_\Sigma(t)$ were found. These functions characterize the mortality dynamics for the nonhomogeneous population as a whole. Parameter κ, chronic radiation dose rate, and acute radiation dose were varied in the model studies. As in section 3.3, the chosen time of the model experiment was 12 days, and the age of the animals at the onset of radiation was 100 days.

When analyzing the results of modeling mortality dynamics in the nonhomogeneous population of mice exposed to continuous radiation, normal specimen distribution in the radiosensitivity index of the intestinal epithelium precursor cells was considered first. Figures 4.1-4.3* show the biometric functions $\rho_\Sigma(t)$, $w_\Sigma(t)$, and $v_\Sigma(t)$, and describe mortality in the nonhomogeneous population of mice chronically irradiated with three different dose rates N. The value of the parameter κ (equation 4.39) is close to the maximum possible value for this particular distribution type (section 4.2). These figures (and other similar ones) also include functions $\rho(t)$, $w(t)$, and $v(t)$ and specify the mortality for the homogeneous population of mice under the same radiation conditions. The radiosensitivity index of the intestinal epithelium precursor cells in the specimens of this population is equal to the expected value $\overline{D}_1$ of the random variable D_1 that describes this radiosensitivity index in animals of the initial nonhomogeneous population. Figure 4.3 also shows corresponding experi-

*Figures begin on page 97.

mental data on mortality dynamics of laboratory mice [6]. The results demonstrate that the inclusion of population nonhomogeneity in the model does not result in a qualitative change of the dependence of the mortality rate, life span probability density, and life span probability on time t at a constant N and on N at constant t. At the same time, some specific features are observed at the quantitative level. For instance, comparison of functions $\rho\Sigma(t)$ and $\rho(t)$ in figure 4.1 and functions $w\Sigma(t)$ and $w(t)$ in figure 4.2 shows that the model of nonhomogeneous population mortality at the two lower N values predicts mortality rate and life span probability density higher over the entire time period studied than the model of homogeneous population mortality: $\rho\Sigma(t) > \rho(t)$ and $w\Sigma(t) > w(t)$. At the highest of the three dose rates N, the differences between $\rho\Sigma(t)$ and $\rho(t)$, as well as between $w\Sigma(t)$ and $w(t)$, are small. Within the earlier time intervals after onset of radiation, the relationship between functions $\rho\Sigma(t)$ and $\rho(t)$, as well as between $w\Sigma(t)$ and $w(t)$, is of the same type as with lower N values, whereas in the later time intervals it is the reverse: $\rho\Sigma(t) < \rho(t)$, and $w\Sigma(t) < w(t)$. However, the changed relation between the functions in the final time interval produces no qualitative changes of the relationship between the corresponding life span probability functions $v\Sigma(t)$ and $v(t)$. With all three dose rates N used in the calculations, the nonhomogeneous population mortality model predicts a lower survival of animals than that suggested by the experimental data obtained on laboratory mice [6] and the one predicted by the homogeneous population mortality model: $v\Sigma(t) < v(t)$.

It is important that the calculation results demonstrate substantial distinctions in mortality dynamics of the subpopulations constituting the nonhomogeneous population. Comparison of the functions $\rho_i(t)$ ($i = 1, \ldots, 6$) reveals that, at each of the three dose rates N, the mortality rate increases and reaches greater values the greater the individual radiosensitivity of the critical system precursor cells for a particular subpopulation, i.e., the lower $\overline{D}_{1i}$. In turn, the maximum values of the life span probability density function $w_i(t)$ are higher and occur earlier when $\overline{D}_{1i}$ values are lower. Accordingly, survival at time t ($0 < t \leq 12$ days) is higher in a subpopulation whose specimens have higher $\overline{D}_{1i}$. In particular, after 12 days of continuous irradiation at a dose rate $N = 1.5$ Gy/day, 0.41% and 88.12% of animals in the first and sixth subpopulations, respectively, survived. Members of these subpopulations have the lowest and the highest indices of radiosensitivity of the intestinal epithelium precursor cells D_{11} and D_{16}. Therefore, the survival of mice with the most radioresistant critical system cells differs from the survival of mice with the most radiosensitive cells by nearly 215 times.

Qualitatively similar results were obtained when modeling mortality of the nonhomogeneous population at other values of the parameter κ ($0 < \kappa < 1/3$) and at other values (but of the same order of magnitude) of N. It was found that, at the same N, differences in the predicted mortality for nonhomogeneous and homogeneous populations and also for individual subpopulations are less pronounced when the variance $V(D_1)$ is lower, i.e., when parameter κ is smaller. This is confirmed by the modeling results for the biometric func-

tions $\rho\Sigma(t)$ and $\rho(t)$, $w\Sigma(t)$ and $w(t)$, and $v\Sigma(t)$ and $v(t)$ in figures 4.4-4.6. They reproduce the mortality of nonhomogeneous and homogeneous populations of mice exposed to continuous radiation at the same dose rates shown in figures 4.1-4.3. The parameter κ in this particular calculation is half of κ used in the preceding calculation. It is evident from figures 4.4-4.6 that, for chosen dose rates N, the differences between functions $\rho\Sigma(t)$ and $\rho(t)$, $w\Sigma(t)$ and $w(t)$, and $v\Sigma(t)$ and $v(t)$, as well as between $v\Sigma(t)$ and experimental data [6] obtained on laboratory mice are less pronounced than the differences shown in figures 4.1-4.3. The same applies to mortality dynamics for individual subpopulations. For example, after 12 days of continuous irradiation at a dose rate of 1.5 Gy/day, survival in the first and sixth subpopulations is 6.59% and 74.81%, respectively. The ratio of survivals is 11.35. Consequently, a twofold decrease of the parameter κ leads to a greater than twentyfold reduction of this ratio.

Modeling data obtained for log-normal distribution of population specimens in the radiosensitivity index of the intestinal epithelium precursor cells are now examined. Figures 4.7-4.9 demonstrate biometric functions $\rho\Sigma(t)$, $w\Sigma(t)$, and $v\Sigma(t)$ describing mortality dynamics for the nonhomogeneous population. They were calculated for the same values of chronic irradiation dose rate N, expected value $\overline{D}_1$, and variance $V(D_1)$ (i.e., for the same parameter κ) as the biometric functions in figures 4.1-4.3. Figures 4.7-4.9 show the biometric functions $\rho(t)$, $w(t)$, and $v(t)$ that express the mortality dynamics of the homogeneous population in the same irradiation conditions. Corresponding experimental data [6] are also presented in figure 4.9. Comparison of the results in figures 4.7-4.9 and 4.1-4.3 show that, for the given parameters, the nonhomogeneous population mortality model based on the log-normal specimen distribution manifests the same patterns as the model with normal specimen distribution. There is also a quantitative similarity in the results.

Figures 4.10-4.12 show the biometric functions $\rho\Sigma(t)$ and $\rho(t)$, $w\Sigma(t)$ and $w(t)$, and $v\Sigma(t)$ and $v(t)$ calculated for the three chronic irradiation dose rates N and for a greater parameter κ than was used in the preceding calculation. Comparison of figures 4.7-4.9 and figures 4.10-4.12 demonstrates that, at the same dose rate, the differences between the functions $\rho\Sigma(t)$ and $\rho(t)$, $w\Sigma(t)$ and $w(t)$, and $v\Sigma(t)$ and $v(t)$ are more significant at higher κ. For instance, after 12 days of prolonged radiation exposure with $N = 0.5$ Gy/day, the homogeneous population has 98.20% survival, whereas the nonhomogeneous populations have 96.86% survival ($\kappa = 0.3$) and 78.53% survival ($\kappa = 1.0$). An increase of the parameter κ by a factor of 3.3 brings about a 1.2-fold increase in the ratio of mortality of homogeneous and nonhomogeneous populations. When κ is higher, the greatest difference is observed between the function $v\Sigma(t)$ and corresponding experimental data [6] (figs. 4.9 and 4.12).

The parameter κ is largely responsible for the amount of differences in mortality dynamics between individual subpopulations constituting a particular nonhomogeneous population. This is illustrated by the modeling results in figures 4.13-4.30. The biometric functions $\rho_i(t)$, $w_i(t)$, and $v_i(t)$ ($i = 1, \ldots, 6$) shown were calculated for the same parameters as were functions $\rho\Sigma(t)$, $w\Sigma(t)$,

and $v_\Sigma(t)$ in figures 4.10-4.12. Comparison of the function $\rho_i(t)$ in figures 4.13-4.18 reveals that in the model with log-normal distribution as in the model with normal distribution, the mortality rate increases slower and reaches lesser values as $\overline{D}_{1i}$ increases with each of the three dose rates N. Calculations show that the maximums of functions $w_i(t)$ diminish, and the time required to attain them increases as $\overline{D}_{1i}$ increases. Note that in the model with log-normal distribution, the differences between functions $w_i(t)$ ($i = 1, \ldots, 6$) are quite large at the chosen values of N and κ (figs. 4.19-4.24). These plots, constructed on the same scale, show the functions $w_5(t)$ and $w_6(t)$ (figs. 4.23-4.24) actually merge with the abscissa because their values are much lower than those of function $w_1(t)$ (fig. 4.19) and approach zero at all three dose rates. The difference between functions $v_i(t)$ ($i = 1, \ldots, 6$) (figs. 4.25-4.30) is also quite large. In the first subpopulation,whose members have the lowest radiosensitivity index, $\overline{D}_{11}$, most of the mice die within 12 days of continuous irradiation at any of the chosen dose rates N (fig. 4.25). At the same time, in subpopulations with the highest radiosensitivity indices, $\overline{D}_{15}$ and $\overline{D}_{16}$, mortality is close to zero (figs. 4.29 and 4.30). In particular, after 12 days of continuous irradiation at $N = 0.5$ Gy/day, 0.42% of the animals remain alive in the first subpopulation and 99.92% in the sixth subpopulation. This means that with $\kappa = 1.0$ the survival in the sixth subpopulation is 241 times that observed in the first subpopulation. Note that these quantities calculated for the same continuous irradiation dose rate but at a lower parameter, $\kappa = 0.3$, are 79.51% and 99.66%, respectively, with a ratio of 1.25. Thus, a 3.3-fold increase in the parameter κ brings about a higher than 190-fold increase in the ratio of survival indices between specimens with the most radioresistant and the most radiosensitive precursor cells of the critical system. These results demonstrate that chronic exposure, even to relatively low-dose rates, is particularly dangerous for mammals whose precursor cells of the small intestine epithelium system are hyperradiosensitive.

Higher values of the parameter κ at a given N lead to even more pronounced differences between the functions $\rho_\Sigma(t)$ and $\rho(t)$, $w_\Sigma(t)$ and $w(t)$, and $v_\Sigma(t)$ and $v(t)$ (figs. 4.31-4.33), and also between the functions $\rho_i(t)$, $w_i(t)$, and $v_i(t)$ ($i = 1, \ldots, 6$).

A curious relationship has been found in the model study of the effect of chronic radiation on the intestinal syndrome of mortality in the nonhomogeneous population. Similar mortality dynamics in nonhomogeneous populations with both normal and log-normal specimen distributions are observed at dose rates N that decrease as variances $V(D_1)$ of these distributions increase, i.e., as parameter κ increases. This is better illustrated by the mortality of populations with log-normal distribution. With continuous radiation at dose rates $N = 0.75$ Gy/day, $N = 0.3$ Gy/day, and $N = 0.2$ Gy/day, mortality dynamics for mice of three nonhomogeneous populations ($\kappa = 0.3$, $\kappa = 1.0$, and $\kappa = 1.5$) are roughly similar (figs. 4.7-4.9, 4.10-4.12, and 4.31-4.33). In particular, 12 days after the onset of the irradiation, the survival of mice was 88.48%, 91.00%, and 88.59%, respectively (figs. 4.9, 4.12, and 4.33).

The studies performed suggest an important conclusion. As the scatter becomes wider in the values of the individual radiosensitivity indexes of the critical system precursor cells in nonhomogeneous populations with both normal and log-normal distributions (i.e., as variance $V(D_1)$ increases), the level of continuous radiation dose rates hazardous for these populations decreases. This is illustrated by the results of mortality modeling for a nonhomogeneous population of mice with log-normal distribution and a fairly high variance $V(D_1)$ ($\kappa = 1.5$). After 12 days of chronic irradiation at the dose rate $N = 0.1$ Gy/day, this population had a survival of 96.68% (fig. 4.33), with 92.30% and 7.62% of animals dying in the first and second subpopulations, respectively. However, this radiation regime presents an incomparably smaller threat for a nonhomogeneous population with low $V(D_1)$ ($\kappa = 0.15$): most of the mice (99.908%) survived, whereas the first and second subpopulations of this population lost 0.13% and 0.11% of the mice, respectively. Note that for the homogeneous population under similar radiation conditions the survival is nearly the same: 99.91%.

The results of modeling the effect of acute radiation on the intestinal syndrome of mortality in nonhomogeneous populations are examined next. Figures 4.34-4.36 show the biometric functions $\rho\Sigma(t)$ and $\rho(t)$, $w\Sigma(t)$ and $w(t)$, and $v\Sigma(t)$ and $v(t)$. They describe the mortality dynamics for the nonhomogeneous and homogeneous populations of mice at three different doses of acute radiation. In the nonhomogeneous population the specimen distribution in the radiosensitivity index of the intestinal epithelium precursor cells obeys the Gauss law with the same values of the mean $\overline{D}_1$ and the variance $V(D_1)$ as those in figures 4.1-4.3. Comparison of the functions $\rho\Sigma(t)$ and $\rho(t)$, $w\Sigma(t)$ and $w(t)$, and $v\Sigma(t)$ and $v(t)$ shows that inclusion of the specimen nonhomogeneity in the model produces no qualitative changes in the character of postirradiation mortality dynamics of the population as a whole. But there are quantitative differences in the mortality of the homogeneous and nonhomogeneous populations. The differences are roughly similar to those found above when considering the mortality of the analogous nonhomogeneous population exposed to chronic radiation (figs. 4.1-4.3). For instance, as shown by figures 4.34 and 4.35, the mortality rate and the life span probability density for the nonhomogeneous population are higher than for the homogeneous population at all three doses D: $\rho\Sigma(t) > \rho(t)$ and $w\Sigma(t) > w(t)$. However, in contrast to chronic radiation, the times of reaching maximum values by functions $w\Sigma(t)$ and $w(t)$ practically coincide, which means that with acute radiation the peaks of mortality in homogeneous and nonhomogeneous populations occur simultaneously. According to these results, survival is lower in the nonhomogeneous population: $v\Sigma(t) < v(t)$ (fig. 4.36).

Calculations reveal that biometric functions $\rho_i(t)$, $w_i(t)$, and $v(t)$ ($i = 1, \ldots, 6$), which reflect mortality dynamics for six subpopulations constituting the nonhomogeneous population, differ appreciably. Survival is lower in subpopulations whose members have lower radiosensitivity indices $\overline{D}_{1i}$ for the critical system precursor cells, as with chronic irradiation. For example, 12 days after acute irradiation at $D = 5$ Gy, survival in the first and sixth

subpopulations (with the lowest ($\overline{D}_{11}$) and the highest ($\overline{D}_{16}$) individual radiosensitivity indexes) is 27.80% and 95.46%, respectively, with a ratio of 3.43.

In calculations by the same model but with other values of κ and other doses D of the same order of magnitude, results were qualitatively similar. Their quantitative comparison revealed that, as in the case of chronic radiation and under the same exposure conditions, the differences in mortality predictions for nonhomogeneous and homogeneous populations diminish with decreasing variance $V(D_1)$ of normal distribution, i.e., with decreasing κ. This is confirmed by figures 4.37-4.39 that show mortality dynamics of nonhomogeneous and homogeneous populations for three different doses D. Parameter κ is half the κ in the preceding calculation (figs. 4.34-4.36). At the same dose D, functions $\rho\Sigma(t)$ and $\rho(t)$, $w\Sigma(t)$ and $w(t)$, and $v\Sigma(t)$ and $v(t)$ are closer to each other in figures 4.37-4.39 than in figures 4.34-4.36.

With acute irradiation as with chronic irradiation the differences in mortality dynamics between different subpopulations in the nonhomogeneous population also decrease with decreasing κ. For instance, when $\kappa = 0.15$ the survival of mice in the first and sixth subpopulations 12 days after acute exposure to 5 Gy is 57.60% and 91.14%, respectively; their ratio is 1.58, which is about half the ratio in the model where the same dose D and the doubled value of κ were used.

The results of modeling using the log-normal distribution type are examined next. Figures 4.40-4.42 demonstrate the biometric functions $\rho\Sigma(t)$ and $\rho(t)$, $w\Sigma(t)$ and $w(t)$, and $v\Sigma(t)$ and $v(t)$ that describe the mortality dynamics for nonhomogeneous and homogeneous populations of mice exposed to three different radiation doses D. The values of D and κ are the same used earlier in the model based on normal specimen distribution in the nonhomogeneous population (figs. 4.34-4.36). Comparison of these figures reveals rather similar patterns. Results obtained by the two models are also quantitatively close, as with chronic irradiation (figs. 4.1-4.3 and 4.7-4.9).

Figures 4.43-4.45 depict mortality dynamics for the nonhomogeneous and homogeneous populations of mice exposed to three doses D of acute radiation; κ is higher in this calculation than in the preceding one. Comparison of figures 4.40-4.42 and 4.43-4.45 shows that with both acute and chronic irradiation the difference in predicted mortality for nonhomogeneous and homogeneous populations increases with increasing variance $V(D_1)$ of the log-normal distribution, i.e., with increasing κ. For example, 12 days after acute radiation at a dose of $D = 1.5$ Gy, survival in the homogeneous and two nonhomogeneous populations is 99.39%, 99.03% ($\kappa = 0.3$), and 92.02% ($\kappa = 1.0$), respectively. Thus, when κ increases 3.3-fold, the ratio of survivals between the homogeneous and nonhomogeneous populations increases 1.1-fold (figs. 4.42 and 4.45).

Figures 4.46-4.63 show the biometric functions $\rho_i(t)$, $w_i(t)$, and $v_i(t)$ ($i = 1, \ldots, 6$), calculated for the same parameters as functions $\rho_\Sigma(t)$, $w_\Sigma(t)$, and $v_\Sigma(t)$ in figures 4.43-4.45. Figures 4.46-4.63 describe postirradiation mortality dynamics of six subpopulations of the nonhomogeneous population. The differences between the corresponding functions $\rho_i(t)$, $w_i(t)$, and $v_i(t)$ ($i = 1, \ldots, 6$) are considerable, as was the modeling of the chronic radiation effect on the identical nonhomogeneous population.

Calculations indicate that, with dose D being the same, the difference in the predicted mortality for individual subpopulations grows with increasing variance $V(D_1)$ of the log-normal distribution describing the original nonhomogeneous population, i.e., with increasing κ. For example, 12 days after acute irradiation at a dose of $D = 1.5$ Gy, survival in the first and sixth subpopulations is 99.55% and 99.86%, respectively, if $\kappa = 0.3$, and 29.45% and 99.95%, respectively, if $\kappa = 1.0$. Thus, a 3.3-fold increase in κ brings about a 3.2-fold increase in the survival ratio between specimens with the most radioresistant and the most radiosensitive cells of the critical system in the radiation conditions indicated.

It should be noted that the results in figures 4.13-4.30, 4.46-4.63, and similar calculations with both types of D_1 distribution at other values of κ suggest a direct correlation between the variability of individual radiosensitivities of intestinal epithelium precursor cells and the variability of the organism's overall radiosensitivity, which manifests itself in different death probabilities at high doses and dose rates of acute and continuous radiation.

The model demonstrated that the dose of acute radiation—at which nonhomogeneous populations with both normal and log-normal distributions have close mortality dynamics—decreases as the variance $V(D_1)$ of these distributions increases, i.e., as κ increases. This is especially evident for mortality of populations with log-normal distribution. For example, similar mortality dynamics for three populations ($\kappa = 0.3$, $\kappa = 1.0$, and $\kappa = 1.5$) were observed at doses of 1.5 Gy, 0.5 Gy, and 0.25 Gy (figs. 4.40-4.42, 4.43-4.45, and 4.64-4.66). Twelve days after exposures, survival in these populations was 99.03%, 99.22%, and 99.20%, respectively (figs. 4.42, 4.45, and 4.66).

Posirradiation mortality of populations with both normal and log-normal distributions shows a feature similar to that observed in the analysis of mortality of nonhomogeneous populations exposed to chronic radiation. The level of hazardous doses of acute radiation lowers with increasing scatter in the values of the individual radiosensitivity index of the intestinal epithelium precursor cells in the nonhomogeneous population. In particular, when modeling mortality dynamics for two nonhomogeneous populations with log-normal specimen distribution, 3% of the animals died in one population ($\kappa = 1.5$) and 0.08% of the animals in the other population ($\kappa = 0.15$) 12 days after acute radiation at 0.5 Gy. Accordingly, mortality in the first subpopulation was 62.12% and 10.05%, respectively, and in the second subpopulation was 0.12% and 0.10%, respectively. Mortality of the corresponding homogeneous popu-

lation was 0.08%. These data demonstrate that acute exposures to relatively low radiation doses are particularly dangerous for specimens whose intestinal epithelium precursor cells show hyperradiosensitivity.

4.5. Bone-Marrow Form* of Mammalian Mortality

Mortality dynamics for a nonhomogeneous mammalian population after irradiation with very high doses at pulsed or constant dose rates were described in the preceding section. Duration of the exposure was incomparably shorter than the maximum life span of intact animals. Nonhomogeneous population mortality dynamics for the duration of radiation, which is comparable to the maximum age of intact animals, are reported in this section. The critical system for these radiation conditions, characterized by low dose rates, is bone-marrow blood formation, specifically thrombocytopoiesis (see chapter 3). Therefore, the constituent parts of the nonhomogeneous population mortality model are the thrombocytopoiesis dynamics model (section 1.3) and the model describing the bone-marrow form of mortality for the homogeneous mammalian population (section 3.4). As before, mice were used, and all model parameters were left unchanged. The numerical value of one parameter, D_1, which is the averaged radiosensitivity index of bone-marrow thrombocyte precursor cells capable of dividing (table 1.1), was given to the parameter $\overline{D}_1$. Here it denotes the expected value of the random variable D_1 that describes the radiosensitivity index of the cells in the members of the nonhomogeneous population.

For the calculation procedure the parameters n_i were found first, and, proceeding from the given value of $\overline{D}_1$ and the chosen value of κ (equation 4.39), the parameters $\overline{D}_{1i}$ ($i = 1, \ldots, 6$) were calculated. Formulas 4.27, 4.28, and 4.40 for normal distribution $\varphi_N(D_1)$ (4.21) of the random variable D_1 and formulas 4.35-4.38, 4.42, and 4.44 for log-normal distribution $\varphi_{LN}(D_1)$ (4.29) were used. The values of $\overline{D}_{1i}$ obtained are summarized in table 4.2.

The dynamics of this system in mice of six subpopulations for chosen irradiation conditions and corresponding values of $\overline{D}_{1i}$ ($i = 1, \ldots, 6$) were calculated in the framework of the thrombocytopoiesis model (section 1.3). Using the found concentrations of the functional elements, thrombocytes, the biometric functions $v_i(t)$, $w_i(t)$, and $\rho_i(t)$ ($i = 1, \ldots, 6$) were determined by formulas 3.18, 3.19, and 3.21-3.24. These functions describe the mortality dynamics for each of the six subpopulations under the chosen radiation conditions. In turn, the values of these functions and of n_i served to calculate the functions $v_\Sigma(t)$, $w_\Sigma(t)$, and $\rho_\Sigma(t)$ by formulas 4.8, 4.13, and 4.20. These functions reproduce mortality dynamics for the nonhomogeneous population as a whole. In the course of model studies, parameter κ and the chronic radiation dose rate N were varied.

*Many American scientists use the term "hematopoietic subsyndrome" of the acute radiation syndrome.

Table 4.2. Index of individual radiosensitivity $\overline{D}_{1i}$ ($i = 1, \ldots, 6$) of thrombocyte precursor cells for specimens of six subpopulations constituting the nonhomogeneous population. Normal and log-normal distributions of animals of the initial nonhomogeneous population in the radiosensitivity index D_1 were considered. These distributions have equal means $\overline{D}_1 = 2.4$ Gy and different variances $V(D_1)$. The parameter κ is defined by formula 4.39: $\kappa = \sqrt{V(D_1)}/\overline{D}_1$.

	Distribution				
Parameter	Normal		Log-normal		
κ	0.15	0.3	0.3	1.0	1.5
$\overline{D}_{11}$	1.566	0.733	1.151	0.244	0.107
$\overline{D}_{12}$	1.902	1.404	1.536	0.550	0.309
$\overline{D}_{13}$	2.235	2.069	2.015	1.189	0.846
$\overline{D}_{14}$	2.566	2.731	2.640	2.559	2.300
$\overline{D}_{15}$	2.898	3.396	3.461	5.509	6.249
$\overline{D}_{16}$	3.234	4.067	4.638	12.818	19.013

As in section 3.4, the duration of the "model experiment" and the age of the animals at the onset of irradiation were 1,000 days and 100 days, respectively.

The results of modeling mortality dynamics of the nonhomogeneous population of irradiated and nonirradiated mice for normal distribution of specimens in the radiosensitivity index of the thrombocytopoiesis system precursor cells were examined first. Figures 4.67-4.69 show biometric functions $\rho_\Sigma(t)$, $w_\Sigma(t)$, and $v_\Sigma(t)$ and describe mortality of nonhomogeneous populations of mice in the absence of radiation and under chronic irradiation with three different dose rates N. Parameter κ (formula 4.39) in this calculation is close to the maximum possible for the distribution type considered (see section 4.2). These and similar figures below show the functions $\rho(t)$, $w(t)$, and $v(t)$. They define mortality in homogeneous populations of mice nonexposed and exposed to chronic radiation at the same dose rates as mice of the nonhomogeneous population. The radiosensitivity index of the thrombocyte precursor cells for specimens from the homogeneous population is equal to the expected value $\overline{D}_1$ of the random variable D_1, which describes this index for specimens of the initial nonhomogeneous population. Figure 4.67 also demonstrates experimental data on mortality rate dynamics for nonirradiated and irradiated LAF_1 mice [7].

Figures 4.67-4.69 reveal that mortality dynamics in homogeneous and nonhomogeneous populations in the absence of radiation are the same. This could not be otherwise because, according to model construction conditions, any differences between specimens belonging to the homogeneous and nonhomo-

geneous populations manifest themselves only when radiation is involved. It is important to note that model mortality dynamics for nonirradiated mammals quantitatively agree with experimental data [7] (fig. 4.67).

The results in figures 4.67-4.69 indicate that allowance in the model for specimen nonhomogeneity with respect to the radiosensitivity index of the critical system precursor cells does not lead to a qualitative change in the dependence of life span probability density and life span probability on time t at a constant N and on N at t = const. For the N values chosen, the biometric functions calculated within the framework of the nonhomogeneous and homogeneous population mortality models are rather close at the quantitative level also. Yet there are certain differences between the two populations.

Comparison of biometric functions $\rho\Sigma(t)$ and $\rho(t)$ (fig. 4.67) shows that, with the lowest of the dose rates used in the calculations, the mortality model for the nonhomogeneous population over the total time period considered predicts higher mortality rates than the mortality model for the homogeneous population: $\rho\Sigma(t) > \rho(t)$. With the other two dose rates N the relationship between $\rho\Sigma(t)$ and $\rho(t)$ is similar to that described above for stage 1, whereas at stage 2 this relationship is reversed: $\rho\Sigma(t) < \rho(t)$. However, the differences between $\rho\Sigma(t)$ and $\rho(t)$ are very small, so these functions agree with experimental values of the mortality rate for LAF_1 mice [7].

It is evident from figure 4.68 and from calculations that, at stage 1 after the onset of irradiation, the mortality model for the nonhomogeneous population predicts higher life span probability densities than the mortality model for the homogeneous population: $w\Sigma(t) > w(t)$. At stage 2, the relation between these biometric functions is reversed: $w\Sigma(t) < w(t)$. At stage 3, it is the same as at stage 1: $w\Sigma(t) > w(t)$. With the lowest of the three dose rates N, only the first two of the indicated relation types between $w\Sigma(t)$ and $w(t)$ were obtained.

In accordance with data above, the mortality model with the lowest N for the nonhomogeneous population predicts lower survival levels than the mortality model for the homogeneous population: $v\Sigma(t) < v(t)$ (fig. 4.69). At the other two dose rates N, the same relationship between $v\Sigma(t)$ and $v(t)$ is observed for most of the duration of the "model experiment." It is only at the final stage that the relationship between functions $v\Sigma(t)$ and $v(t)$ is reversed: $v\Sigma(t) > v(t)$. However, the difference between $v\Sigma(t)$ and $v(t)$ is so small in absolute value that the change of its sign does not affect the ratio between the average life spans of specimens in the nonhomogeneous and homogeneous populations: the former have a shorter average life span than the latter at each dose rate N used. Accordingly, shortening of average life spans (formula 3.25) for animals of the nonhomogeneous population is greater than for animals of the homogeneous population. With dose rates of 0.022 Gy/day, 0.044 Gy/day, and 0.088 Gy/day, the average life span shortening for the nonhomogeneous population is 61, 132, and 266 days, respectively, and for the homogeneous population 53,116, and 250 days, respectively.

Calculations demonstrated that there are appreciable differences in radiation-induced mortality of individual subpopulations constituting the nonhomogeneous population. Comparison of the functions $\rho_i(t)$ ($i = 1, \ldots, 6$) reveals that with the dose rates N chosen the mortality rate is higher at any time after the beginning of irradiation for the subpopulation with a lower index of radiosensitivity of the thrombocytopoiesis system precursor cells (i.e., a higher radiosensitivity of these cells). An exception is the function $\rho_1(t)$ calculated for the highest dose rate N. During the final two months of the "model experiment" the function $\rho_1(t)$ was lower than $\rho_2(t)$ because the fraction of surviving animals in the first subpopulation at that time dropped nearly to zero, thereby reducing function $\rho_1(t)$. For instance, during continuous irradiation at $N = 0.088$ Gy/day, only 24×10^{-10} (24 of 10 billion) specimens in the first subpopulation will survive to age $t = 1{,}000$ days. In turn, at the same values of N, the maximum life span probability density function $w_i(t)$ is higher and is achieved earlier at lower $\overline{D}_{1i}$. Accordingly, survival at any time after onset of irradiation is higher in a subpopulation whose members have a higher $\overline{D}_{1i}$. For example, 900 days after the beginning of continuous exposure to a dose rate of $N = 0.022$ Gy/day, the first and sixth subpopulations have respectively 0.51% and 14.39% of animals surviving. Consequently, the survival of mice with the most radioresistant and the most radiosensitive thrombocyte precursor cells differs by more than a factor of 28 after 900 days. The average life span shortening for specimens of these two subpopulations under these particular irradiation conditions is 203 and 30 days, respectively—a quite appreciable difference of 173 days.

Qualitatively similar data were obtained when modeling nonhomogeneous population mortality at other values of κ ($0 < \kappa < \frac{1}{3}$). At the same N, distinctions in the mortality prediction between nonhomogeneous and homogeneous populations, as well as between individual subpopulations, are less pronounced with a lower variance $V(D_1)$, i.e., with lower κ. This is illustrated by the modeling results presented in figures 4.70-4.72. Parameter κ in this calculation was half of κ used in the preceding calculation. The biometric functions $\rho_\Sigma(t)$ and $\rho(t)$, $w_\Sigma(t)$ and $w(t)$, and $v_\Sigma(t)$ and $v(t)$ depicted in the figures describe the mortality dynamics for the nonhomogeneous and the homogeneous populations of nonirradiated mice and of mice chronically irradiated at dose rates equal to those shown in figures 4.67-4.69. Also shown in figure 4.70 are the mortality rates for nonirradiated and irradiated LAF_1 mice [7]. The differences between the functions $\rho_\Sigma(t)$ and $\rho(t)$, $w_\Sigma(t)$ and $w(t)$, and $v_\Sigma(t)$ and $v(t)$ in figures 4.70-4.72 are even smaller than those in figures 4.67-4.69. Therefore, functions $\rho_\Sigma(t)$ and $\rho(t)$ are both consistent with experimental data [7] (fig. 4.70). Accordingly, average life span shortening values for the nonhomogeneous and homogeneous populations under similar irradiation conditions practically coincide. For instance, at the above indicated dose rates, survival is 54 days, 120 days, 254 days and 53 days, 116 days, 250 days, respectively.

Differences in mortality dynamics between various subpopulations are also smaller than they were in the preceding calculation. For example, after 900

days of continuous irradiation at $N = 0.022$ Gy/day, the survival percentage in the first and sixth subpopulations are 5.41% and 12.48%, respectively. Their ratio, 2.3, is 12 times lower than the similar ratio corresponding to a parameter κ twice as large. When κ decreases, so does the difference between the values of average life shortening for different subpopulations at the same dose rates of chronic irradiation. For instance, at $N = 0.022$ Gy/day, the average life span shortening is 86 and 48 days for the first and the sixth subpopulations, respectively. This time the difference is smaller by 125 days than was the case in the preceding calculation.

The modeling results for log-normal distribution of specimens in the radiosensitivity index of thrombocytopoietic system precursor cells are now examined. Figures 4.73-4.75 show biometric functions $\rho\Sigma(t)$, $w\Sigma(t)$, and $v\Sigma(t)$ calculated for the same values of the chronic irradiation dose rate N and the same $\overline{D}_1$ and $V(D_1)$ (same parameter κ) as were used to calculate these functions in figures 4.67-4.69. Figures 4.73-4.75 also show biometric functions $\rho(t)$, $w(t)$, and $v(t)$ defining mortality dynamics of the corresponding homogeneous population in the absence of radiation and under continuous radiation at the same dose rates. Figure 4.73 also demonstrates experimental data on mortality of nonirradiated and irradiated LAF_1 mice [7]. Comparison of biometric functions $\rho\Sigma(t)$, $w\Sigma(t)$, and $v\Sigma(t)$ in figures 4.67-4.69 and 4.73-4.75 reveals a qualitative and quantitative similarity of mortality dynamics of these two nonhomogeneous populations at chosen conditions of irradiation. In turn, at each of the three dose rates chosen, the average life shortening for the nonhomogeneous population with log-normal distribution practically coincides with the quantity for the nonhomogeneous population with normal distribution and the same $\overline{D}_1$ and $V(D_1)$. Specifically, calculations for dose rates 0.022 Gy/day, 0.044 Gy/day, and 0.088 Gy/day yield average life span shortening of 59, 129, and 265 days, respectively.

Figures 4.76-4.78 show the biometric functions $\rho\Sigma(t)$ and $\rho(t)$, $w\Sigma(t)$ and $w(t)$, and $v\Sigma(t)$ and $v(t)$ describing mortality dynamics for mice of nonhomogeneous and homogeneous populations in the absence of radiation and for mice exposed to continuous radiation at three dose rates N. Figure 4.76 also presents experimental mortality rate data for LAF_1 mice [7]. The parameter κ in this particular calculation is higher than in the preceding calculation. Comparison of figures 4.73-4.75 and 4.76-4.78 suggests the following conclusions. At the same dose rate, the differences between the functions $\rho\Sigma(t)$ and $\rho(t)$, $w\Sigma(t)$ and $w(t)$, and $v\Sigma(t)$ and $v(t)$ are more pronounced with higher κ, are particularly large within the first year after onset of irradiation, and nearly disappear toward the end of the "model experiment." Therefore, the differences between the function $\rho\Sigma(t)$ and the experimental data on the mortality rate for LAF_1 mice (which practically coincide with corresponding values of the function $\rho(t)$) also diminish with time (fig. 4.76). In turn, as κ increases, the differences in average life span shortening between the homogeneous and nonhomogeneous populations also grow under the same irradiation conditions. For example, at a dose rate of 0.022 Gy/day, the average life span shortening for mice of a

homogeneous population and two nonhomogeneous populations is 53 days, 59 days ($\kappa = 0.3$) and 113 days ($\kappa = 1.0$), respectively.

Figures 4.79-4.96 show the biometric functions $\rho_i(t)$, $w_i(t)$, and $v_i(t)$, ($i = 1, \ldots, 6$) calculated at the same parameters as $\rho_\Sigma(t)$, $w_\Sigma(t)$, and $v_\Sigma(t)$ in figures 4.76-4.78. Comparison of the functions $\rho_i(t)$ ($i = 1, \ldots, 6$) in figures 4.79-4.84 reveals that, at the chosen dose rates, the mortality rate is higher in the subpopulation with a lower radiosensitivity index for thrombocytopoietic system precursor cells. The one exception, as in the case considered earlier, is the function $\rho_1(t)$ calculated for the highest dose rate. Function $\rho_2(t)$ exceeds $\rho_1(t)$ in the final 12 weeks of the "model experiment," and function $\rho_3(t)$ exceeds $\rho_1(t)$ in the final 2 weeks of the "model experiment" (figs. 4.79-4.81) for the reason indicated above.

Figures 4.85-4.90 show that, for each of the three dose rates, $w_i(t)$ maximums increase, and the times of reaching the maximums decrease with decreasing $\overline{D}_{1i}$. Accordingly, at any time after onset of irradiation at any of the dose rates used in the calculations, survival is lower in the subpopulation having a lower value of $\overline{D}_{1i}$.

It should be noted that in this particular calculation the differences in mortality dynamics between subpopulations are quite high in the first months of the "model experiment" and diminish toward its concluding stages. At each of the three dose rates, mortality dynamics of the sixth subpopulation, characterized by the highest critical system radiosensitivity index, $\overline{D}_{16}$, is close to mortality dynamics for nonirradiated mammals (figs. 4.84, 4.90, and 4.96). For example, at $N = 0.022$ Gy/day, the average life span shortening for the first and sixth populations is 494 days and 9 days, respectively. Note that analogous quantities survival, calculated for the same dose rate and a lower parameter ($\kappa = 0.3$) differ much less from each other: 122 and 26 days, respectively.

It is important to keep in mind that the results shown in figures 4.79-4.96 and similar calculations with both types of D_1 distributions demonstrate a direct relationship between variability of individual radiosensitivity of precursor cells of the critical system (bone-marrow thrombocytopoiesis) and variability of overall radiosensitivity of the organism. The latter characteristic is manifested in a higher or lower probability of survival to a certain age under conditions of continuous exposure to low dose rates.

When parameter κ is higher, distinctions between functions $\rho_\Sigma(t)$ and $\rho(t)$, $w_\Sigma(t)$ and $w(t)$, and $v_\Sigma(t)$ and $v(t)$ are even greater (figs. 4.97-4.99). As κ grows (figs. 4.73, 4.76, and 4.97) so does the difference from $\rho_\Sigma(t)$ of the experimental mortality rate data on LAF_1 mice [7], which practically coincide with corresponding calculated values of the mortality rate $\rho(t)$ for the homogeneous population of mice.

As κ increases so does the difference between average life shortening for specimens from the nonhomogeneous and homogeneous populations. For

example, at N = 0.022 Gy/day and κ = 1.5, survival is 160 and 53 days, respectively. The difference is greater by 47 and 101 days than the difference between the same quantities calculated for the same dose rate N with κ equal to 1.0 and 0.3, respectively.

In turn, differences in mortality dynamics of the subpopulations constituting the nonhomogeneous population also increase with increasing κ. For example, with N = 0.022 Gy/day and κ = 1.5, average life shortening for the first subpopulation is 611 days and for the sixth subpopulation 6 days. The difference between these subpopulations is respectively greater by 120 and 509 days than that between the same quantities for survival calculated with κ = 1.0 and κ = 0.3. These data demonstrate that continuous irradiation at relatively low dose rates can be very harmful for specimens whose thrombocyte precursor cells are hyperradiosensitive (table 4.2).

In simulating the bone-marrow form of mortality for nonhomogeneous populations a pattern similar to the gastrointestinal form of mortality of irradiated mammals was observed. Similar mortality dynamics for nonhomogeneous populations with both normal and log-normal distributions of specimens take place at dose rates N that decrease as variance $V(D_1)$ of these distributions increases, i.e., as parameter κ increases. For example, during chronic irradiation with N = 0.033 Gy/day and N = 0.022 Gy/day, mortality dynamics for two nonhomogeneous populations with log-normal distribution and κ = 1.0 and 1.5 are nearly the same (figs. 4.76-4.78 and 4.97-4.99). The average life span shortening for these populations is also similar: 165 and 160 days.

The results of this model suggest an important conclusion: as the scatter in values of the individual radiosensitivity index of the thrombocytopoietic system precursor cells in a nonhomogeneous population increases, the level of prolonged irradiation dose rate that is dangerous for this population decreases. For example, with chronic irradiation at a dose rate of 0.022 Gy/day, the average life shortening for specimens of a nonhomogeneous population (log-normal distribution, κ = 1.5) is 160 days, or 21% of the average life span for intact animals. The same level of exposure is less dangerous for a nonhomogeneous population with smaller scatter in the values of the individual radiosensitivity index (κ = 0.15). Average life shortening for such a population is 54 days, or 7%.

4.6. Conclusion

The mathematical model of mortality dynamics for a nonhomogeneous population of mammals exposed to radiation described in this chapter is based on models presented in preceding chapters. The model shows the relation of statistical biometric functions (mortality rate, life span probability density, and life span probability) with kinetic and statistical characteristics of critical body

systems. The model considers the nonhomogeneity of specimens for individual radiosensitivity of cells of a critical system. Two types of distribution, normal (Gaussian) and log-normal, most widely encountered in biology, were used to describe the distribution of specimens in the population that is nonhomogeneous with respect to the above index.

The dependence of radiation-induced mortality of the nonhomogeneous population on both the distribution of specimens in the radiosensitivity index of critical system precursor cells and on variance, the most important parameter were studied. Various exposure conditions were simulated: radiation at very high doses with pulsed or constant dose rates, and prolonged radiation at low dose rates where duration is comparable to the maximum life span of intact animals. With radiation at high dose rates the critical system was assumed to be the small intestine epithelium; with prolonged radiation at low dose rates the critical system was assumed to be the thrombocytopoietic system. Mice were used in the modeling.

Investigations primarily revealed the existence of a direct correlation between the variability of specimen survival in the nonhomogeneous population and the variability of individual radiosensitivity of cells of critical systems. Also revealed was that the probability of death from the gastrointestinal syndrome resulting from exposures to extremely high doses of radiation at pulsed and constant rates increases as radiosensitivity of the intestinal epithelium precursor cells increases. In turn, the probability to survive to a certain age for a specimen exposed to prolonged radiation at a low dose rate grows as the radiosensitivity of the bone-marrow thrombocyte precursor cells decreases.

It was established that the models of mortality based on normal and log-normal distributions of specimens of the nonhomogeneous population in the radiosensitivity index predict, under identical radiation conditions, rather similar mortality dynamics if these distributions have equal means and variances and if the latter values are not high.

It is shown that inclusion in the model of normal and log-normal distributions of specimens in the nonhomogeneous population by the index of the radiosensitivity for the critical system precursor cells leads to higher mortality rates and lower survival than could have been predicted from the averaged radiosensitivity index alone. The differences in predictions increase as the variance of the individual radiosensitivity index for critical system precursor cells in the nonhomogeneous population increases. These differences are especially pronounced when log-normal distribution with a high variance value is used. This result of the modeling is of high theoretical significance because it helps gain an insight into the variety of experimental data obtained in the area of the Chernobyl catastrophe.

The model studies suggest an important and practical conclusion: the level of doses and dose rates of acute and chronic exposures that present a certain danger for nonhomogeneous mammalian populations decreases as the spread

of values of the individual radiosensitivity index for the critical system precursor cells in these populations increases, i.e., the greater the variance of corresponding distributions. For animals having hyperradiosensitive precursor cells, even low-level radiation can have fatal consequences. The results thus outline new pathways in the development of methods of radiation risk evaluation and in the strategy of radioprotection.

FIGURES

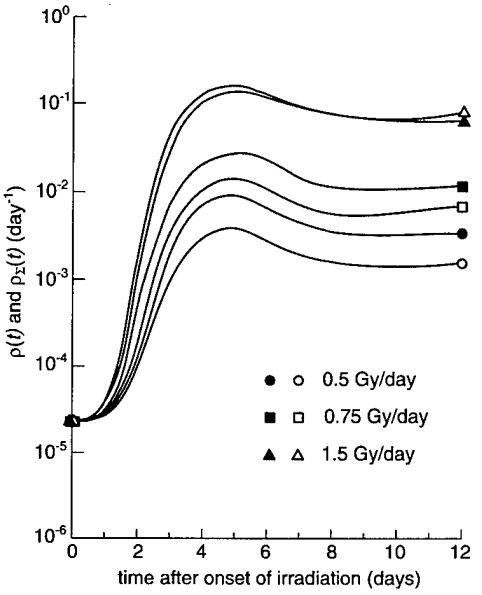

Fig. 4.1. Biometric functions $\rho(t)$ and $\rho\Sigma(t)$ describing mortality rate for mice of homogeneous (o, □, Δ) and nonhomogeneous (•, ■, ▲) populations (normal distribution, $\kappa = 0.3$) exposed to chronic radiation.

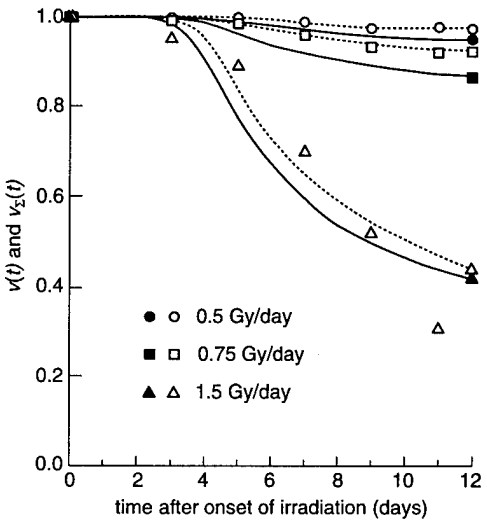

Fig. 4.3. Biometric functions $v(t)$ and $v\Sigma(t)$ describing life span probability for mice of homogeneous (o, □, Δ) and nonhomogeneous (•, ■, ▲) populations (normal distribution, $\kappa = 0.3$) exposed to chronic radiation. Symbols o, □, and Δ also indicate corresponding experimental data on mortality dynamics [6].

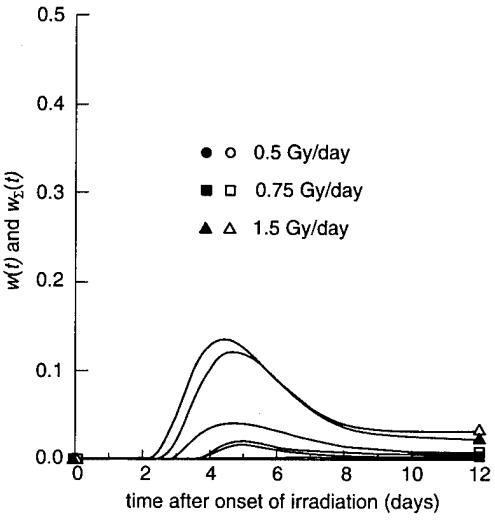

Fig. 4.2. Biometric functions $w(t)$ and $w\Sigma(t)$ describing life span probability density for mice of homogeneous (o, □, Δ) and nonhomogeneous (•, ■, ▲) populations (normal distribution, $\kappa = 0.3$) exposed to chronic radiation.

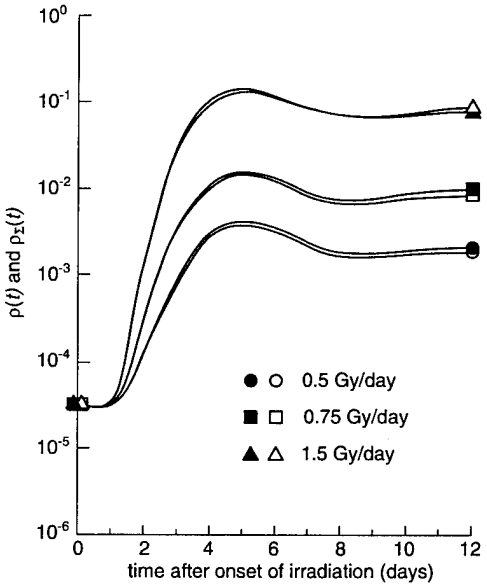

Fig. 4.4. Biometric functions $\rho(t)$ and $\rho\Sigma(t)$ describing mortality rate for mice of homogeneous (o, □, Δ) and nonhomogeneous (•, ■, ▲) populations (normal distribution, $\kappa = 0.15$) exposed to chronic radiation.

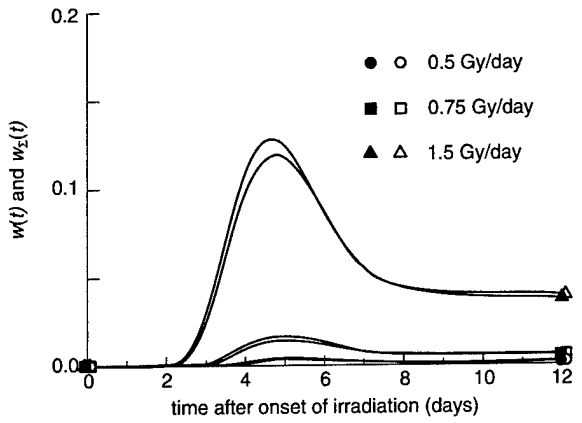

Fig. 4.5. Biometric functions $w(t)$ and $w\Sigma(t)$ describing life span probability density for mice of homogeneous (o, □, Δ) and nonhomogeneous (•, ■, ▲) populations (normal distribution, $\kappa = 0.15$) exposed to chronic radiation.

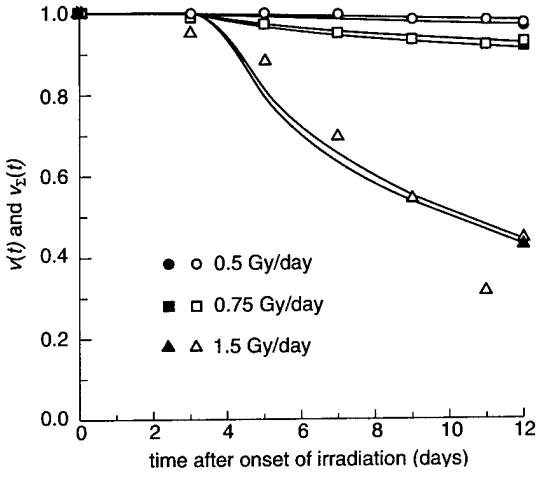

Fig. 4.6. Biometric functions $v(t)$ and $v\Sigma(t)$ describing life span probability for mice of homogeneous (o, □, Δ) and nonhomogeneous (•, ■, ▲) populations (normal distribution, $\kappa = 0.15$) exposed to chronic radiation. Symbols o, □, and Δ also indicate corresponding experimental data on mortality dynamics of mice [6].

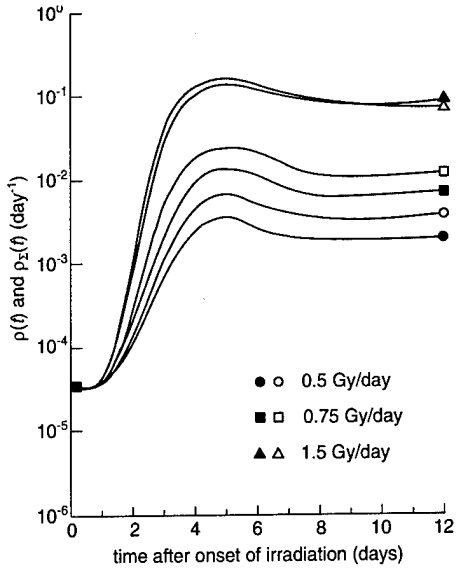

Fig. 4.7. Biometric functions $\rho(t)$ and $\rho\Sigma(t)$ describing mortality rate for mice of homogeneous (o, □, Δ) and nonhomogeneous populations (•, ■, ▲) (log-normal distribution, $\kappa = 0.3$) exposed to chronic radiation.

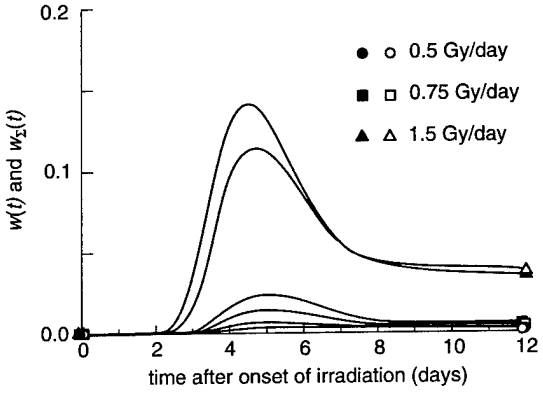

Fig. 4.8. Biometric functions $w(t)$ and $w\Sigma(t)$ describing life span probability density for mice of homogeneous (o, □, Δ) and nonhomogeneous (•, ■, ▲) populations (log-normal distribution, $\kappa = 0.3$) exposed to chronic radiation.

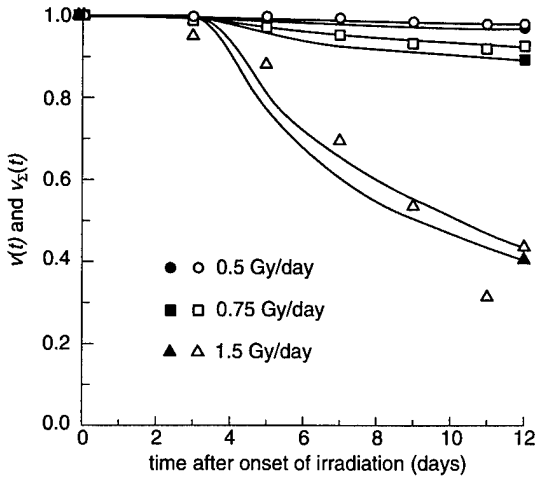

Fig. 4.9. Biometric functions $v(t)$ and $v\Sigma(t)$ describing life span probability for mice of homogeneous (o,□, Δ) and nonhomogeneous (•, ■, ▲) populations (log-normal distribution, $\kappa = 0.3$) exposed to chronic radiation. Symbols o, □, and Δ also indicate corresponding experimental data on mortality [6].

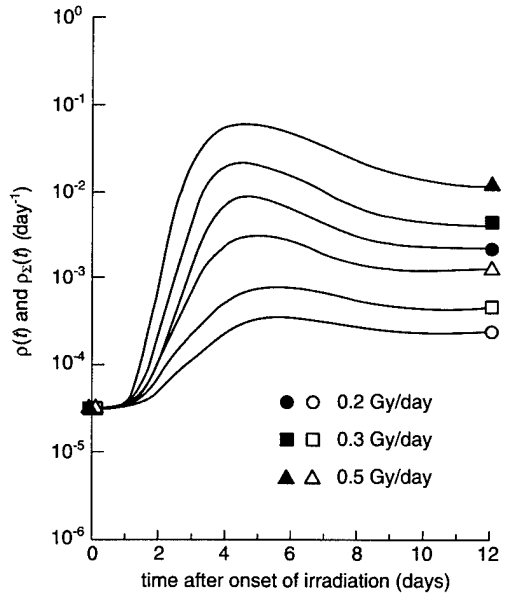

Fig. 4.10. Biometric functions $\rho(t)$ and $\rho\Sigma(t)$ describing mortality rate for mice of homogeneous (o,□, Δ) and nonhomogeneous (•, ■, ▲) populations (log-normal distribution, $\kappa = 1.0$) exposed to chronic radiation.

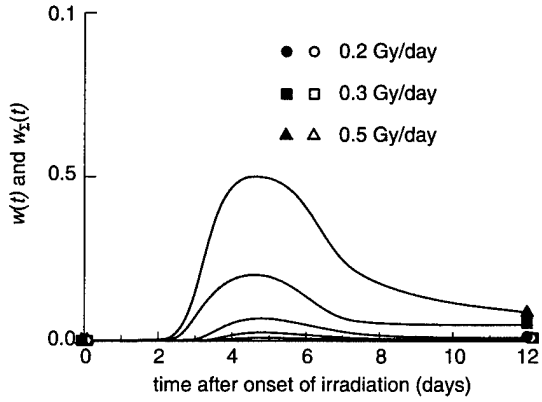

Fig. 4.11. Biometric functions $w(t)$ and $w\Sigma(t)$ describing life span probability density for mice of homogeneous (o,□, Δ) and nonhomogeneous (•, ■, ▲) populations (log-normal distribution, $\kappa = 1.0$) exposed to chronic radiation.

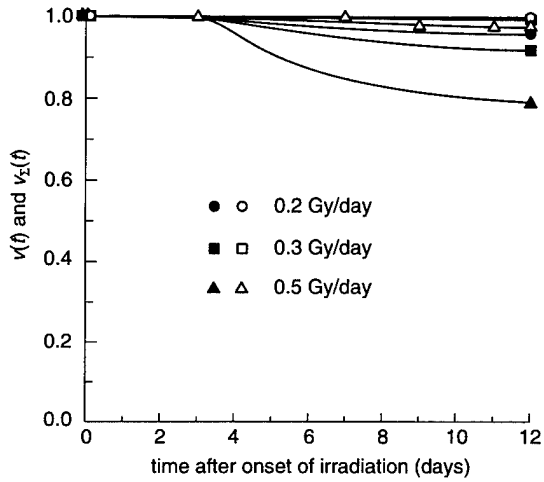

Fig 4.12. Biometric functions $v(t)$ and $v\Sigma(t)$ describing life span probability for mice of homogeneous (o,□, Δ) and nonhomogeneous (•, ■, ▲) populations (log-normal distribution, $\kappa = 1.0$) exposed to chronic radiation. Symbol Δ also indicates experimental data on mortality dynamics of mice exposed to chronic radiation.

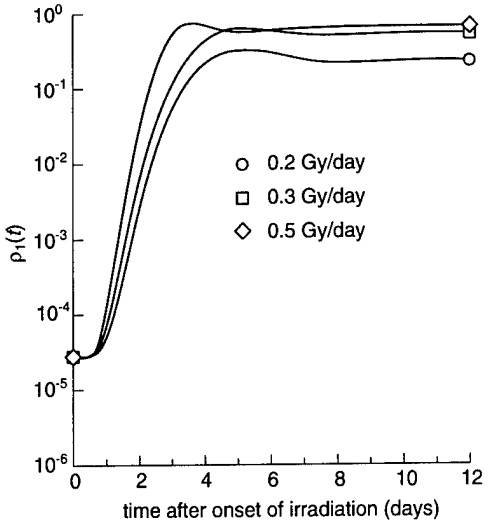

Fig. 4.13. Biometric function $\rho_1(t)$ describing mortality rate for mice of the first subpopulation of the nonhomogeneous population (log-normal distribution, $\kappa = 1.0$) exposed to chronic radiation.

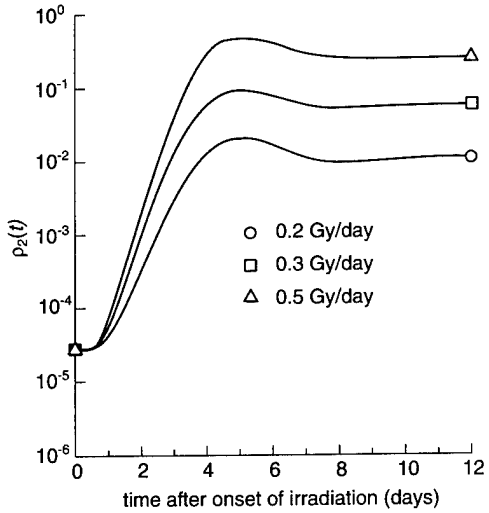

Fig. 4.14. Biometric function $\rho_2(t)$ describing mortality rate for mice of the second subpopulation of the nonhomogeneous population (log-normal distribution, $\kappa = 1.0$) exposed to chronic radiation.

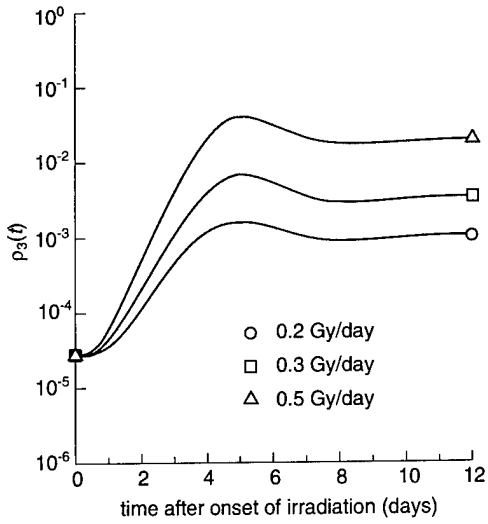

Fig. 4.15. Biometric function $\rho_3(t)$ describing mortality rate for mice of the third subpopulation of the nonhomogeneous population (log-normal distribution, $\kappa = 1.0$) exposed to chronic radiation.

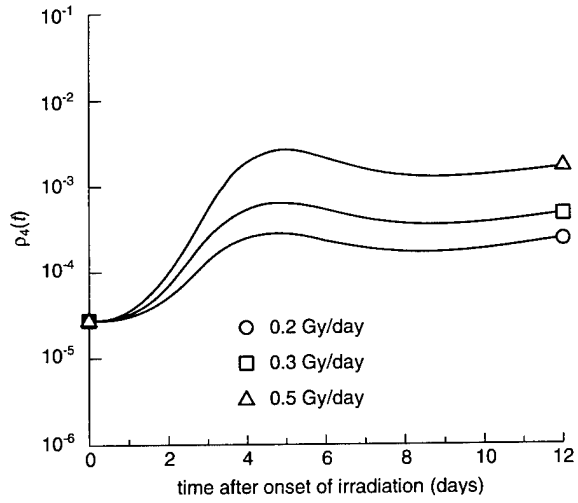

Fig. 4.16. Biometric function $\rho_4(t)$ describing mortality rate for mice of the fourth subpopulation of the nonhomogeneous population (log-normal distribution, $\kappa = 1.0$) exposed to chronic radiation.

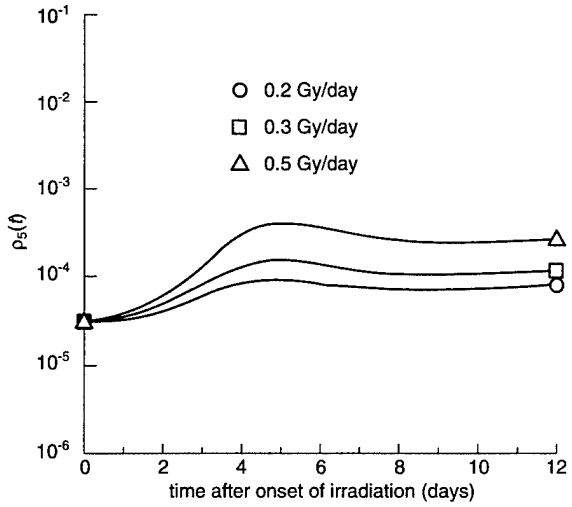

Fig. 4.17. Biometric function $\rho_5(t)$ describing mortality rate for mice of the fifth subpopulation of the nonhomogeneous population (log-normal distribution, $\kappa = 1.0$) exposed to chronic radiation.

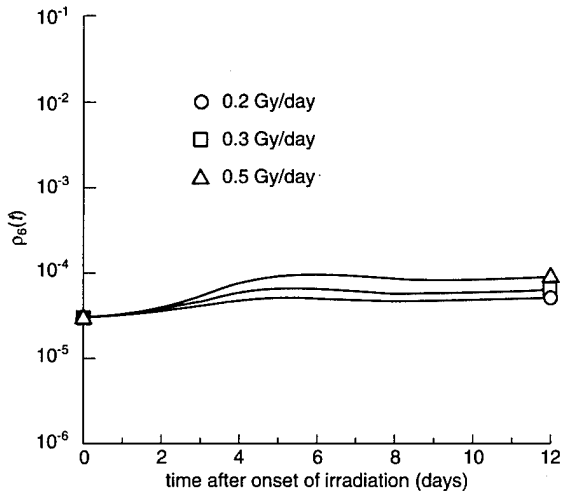

Fig. 4.18. Biometric function $\rho_6(t)$ describing mortality rate for mice of the sixth subpopulation of the nonhomogeneous population (log-normal distribution, $\kappa = 1.0$) exposed to chronic radiation.

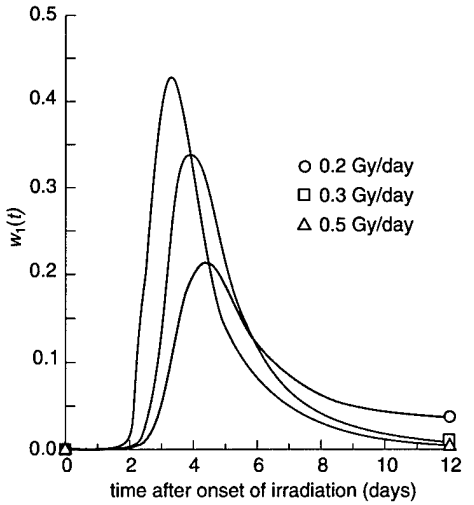

Fig. 4.19. Biometric function $w_1(t)$ describing life span probability density for mice of the first subpopulation of the nonhomogeneous population (log-normal distribution, $\kappa = 1.0$) exposed to chronic radiation.

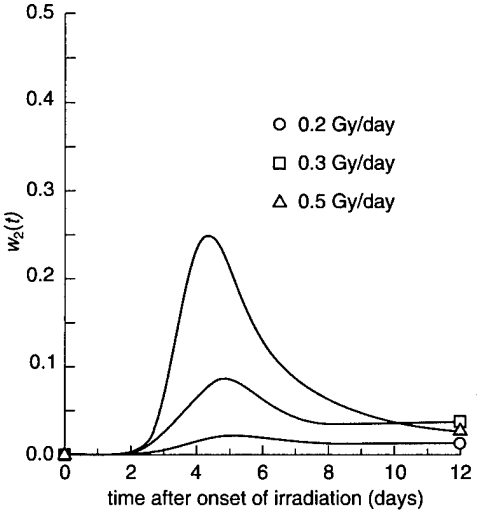

Fig. 4.20. Biometric function $w_2(t)$ describing life span probability density for mice of the second subpopulation of the nonhomogeneous population (log-normal distribution, $\kappa = 1.0$) exposed to chronic radiation.

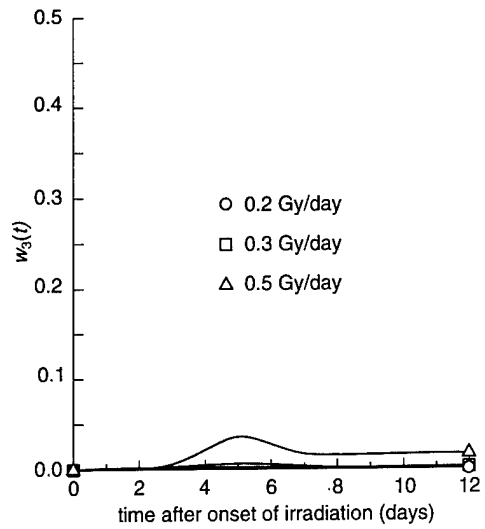

Fig. 4.21. Biometric function $w_3(t)$ describing life span probability density for mice of the third subpopulation of the nonhomogeneous population (log-normal distribution, κ = 1.0) exposed to chronic radiation.

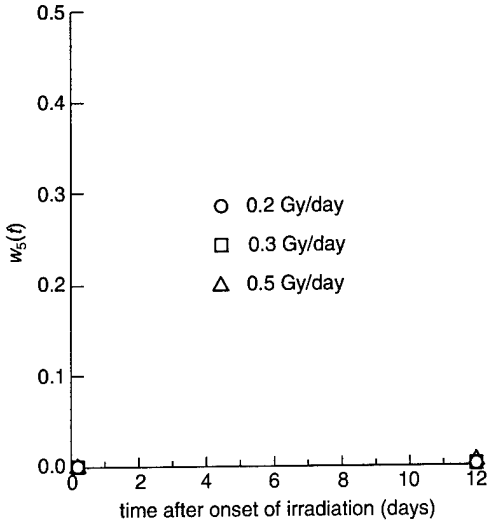

Fig. 4.23. Biometric function $w_5(t)$ describing life span probability density for mice of the fifth subpopulation of the nonhomogeneous population (log-normal distribution, κ = 1.0) exposed to chronic radiation.

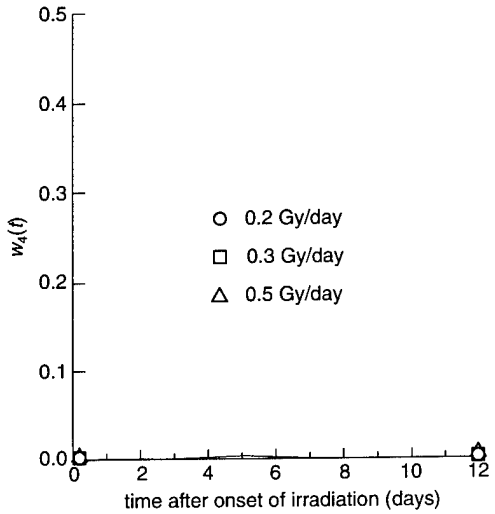

Fig. 4.22. Biometric function $w_4(t)$ describing life span probability density for mice of the fourth subpopulation of the nonhomogeneous population (log-normal distribution, κ = 1.0) exposed to chronic radiation.

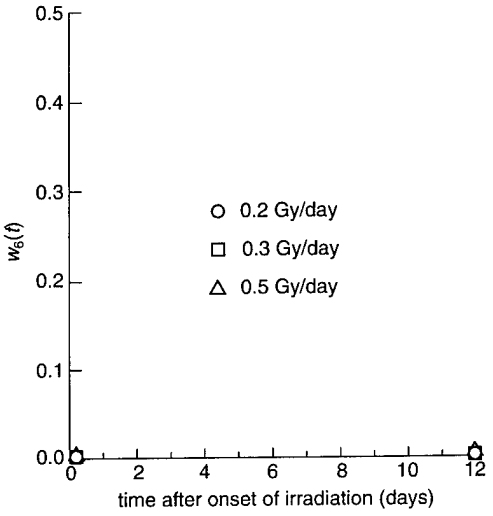

Fig. 4.24. Biometric function $w_6(t)$ describing life span probability density for mice of the sixth population of the nonhomogeneous population (log-normal distribution, κ = 1.0) exposed to chronic radiation.

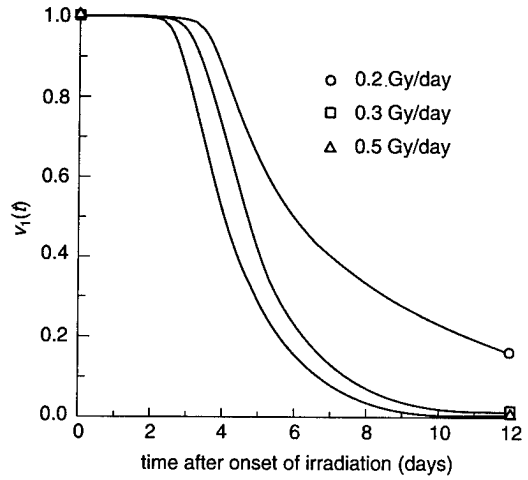

Fig. 4.25. Biometric function $v_1(t)$ describing life span probability for mice of the first subpopulation of the nonhomogeneous population (log-normal distribution, $\kappa = 1.0$) exposed to chronic radiation.

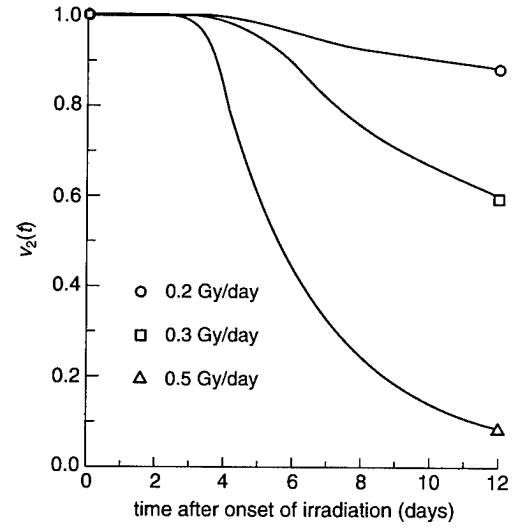

Fig. 4.26. Biometric function $v_2(t)$ describing life span probability for mice of the second subpopulation of the nonhomogeneous population (log-normal distribution, $\kappa = 1.0$) exposed to chronic radiation.

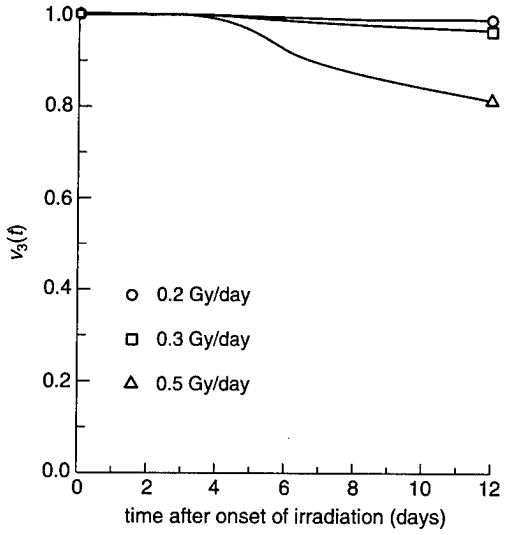

Fig. 4.27. Biometric function $v_3(t)$ describing life span probability for mice of the third subpopulation of the nonhomogeneous population (log-normal distribution, $\kappa = 1.0$) exposed to chronic radiation.

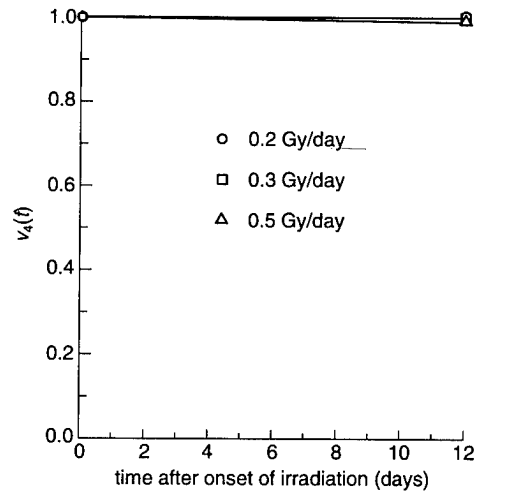

Fig. 4.28. Biometric function $v_4(t)$ describing life span probability for mice of the fourth subpopulation of the nonhomogeneous population (log-normal distribution, $\kappa = 1.0$) exposed to chronic radiation.

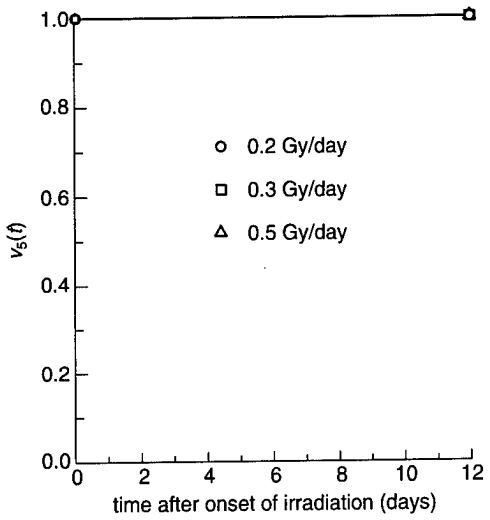

Fig. 4.29. Biometric function $v_5(t)$ describing life span probability for mice of the fifth subpopulation of the nonhomogeneous population (log-normal distribution, $\kappa = 1.0$) exposed to chronic radiation.

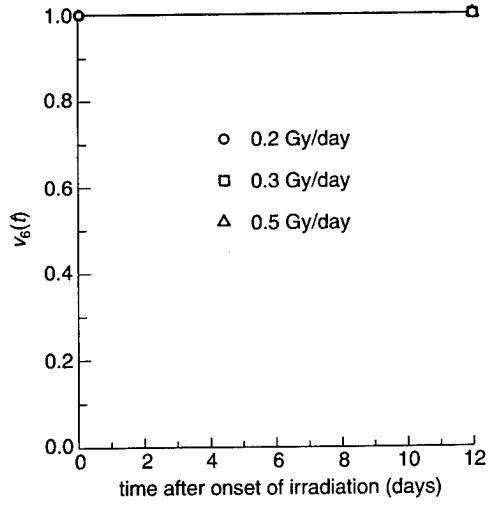

Fig. 4.30. Biometric function $v_6(t)$ describing life span probability for mice of the sixth subpopulation of the nonhomogeneous population (log-normal distribution, $\kappa = 1.0$) exposed to chronic radiation.

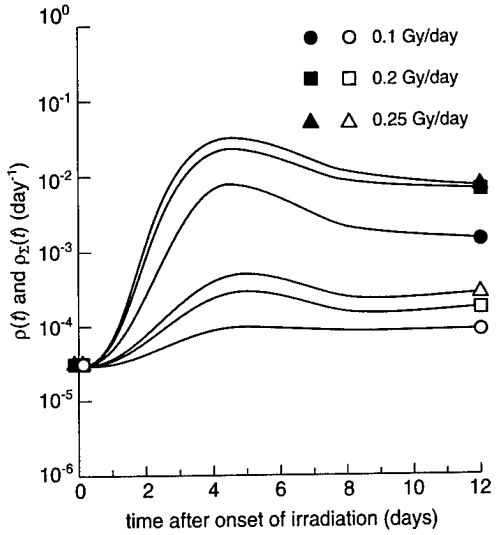

Fig. 4.31. Biometric functions $\rho(t)$ and $\rho\Sigma(t)$ describing mortality rate for mice of homogeneous (o, □, Δ) and nonhomogeneous (•, ■, ▲) populations (log-normal distribution, $\kappa = 1.5$) exposed to chronic radiation.

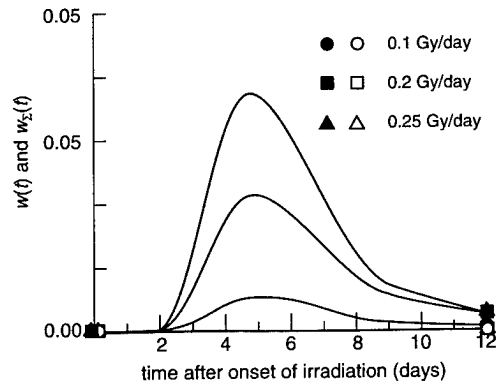

Fig. 4.32. Biometric functions $w(t)$ and $w\Sigma(t)$ describing life span probability density for mice of homogeneous (o, □, Δ) and nonhomogeneous (•, ■, ▲) populations (log-normal distribution, $\kappa = 1.5$) exposed to chronic radiation.

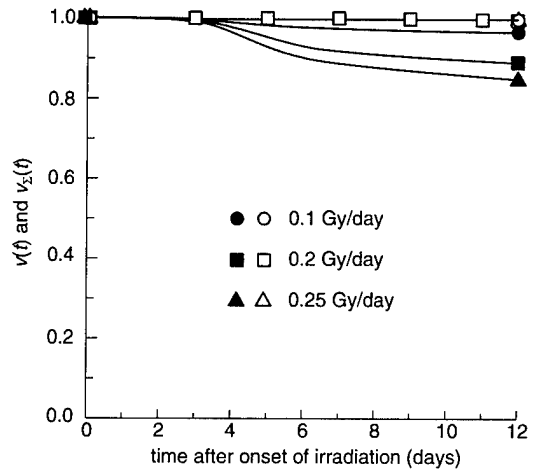

Fig. 4.33. Biometric functions $v(t)$ and $v\Sigma(t)$ describing life span probability for mice of homogeneous (o, □, Δ) and nonhomogeneous (•, ■, ▲) populations (log-normal distribution, $\kappa = 1.5$) exposed to chronic radiation. Symbol □ also represents experimental data on mortality dynamics of mice exposed to chronic radiation at a dose rate of 0.2 Gy/day [6].

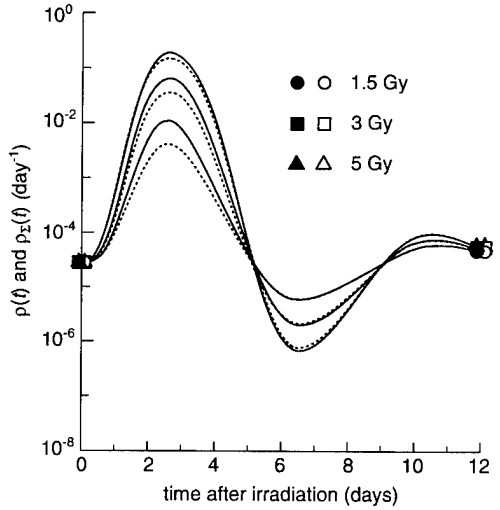

Fig. 4.34. Biometric functions $\rho(t)$ and $\rho\Sigma(t)$ describing mortality rate for mice of homogeneous (o, □, Δ) and nonhomogeneous (•, ■, ▲) populations (normal distribution, $\kappa = 0.3$) exposed to acute radiation.

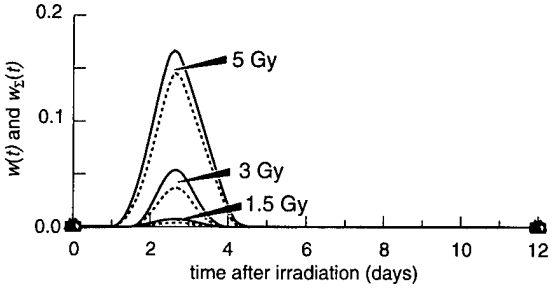

Fig. 4.35. Biometric functions $w(t)$ and $w\Sigma(t)$ describing life span probability density for mice of homogeneous (o, □, Δ) and nonhomogeneous (•, ■, ▲) populations (normal distribution, $\kappa = 0.3$) exposed to acute radiation.

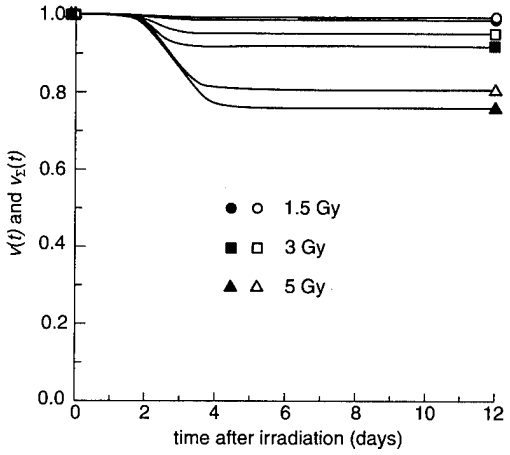

Fig. 4.36. Biometric functions $v(t)$ and $v\Sigma(t)$ describing life span probability for mice of homogeneous (o, □, Δ) and nonhomogeneous (•, ■, ▲) populations (normal distribution, $\kappa = 0.3$) exposed to acute radiation.

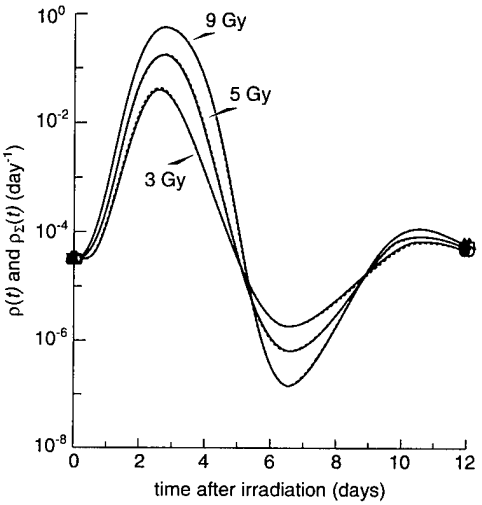

Fig. 4.37. Biometric functions $\rho(t)$ and $\rho\Sigma(t)$ describing mortality rate for mice of homogeneous (o, □, Δ) and nonhomogeneous (•, ■, ▲) populations (normal distribution, $\kappa = 0.15$) exposed to acute radiation.

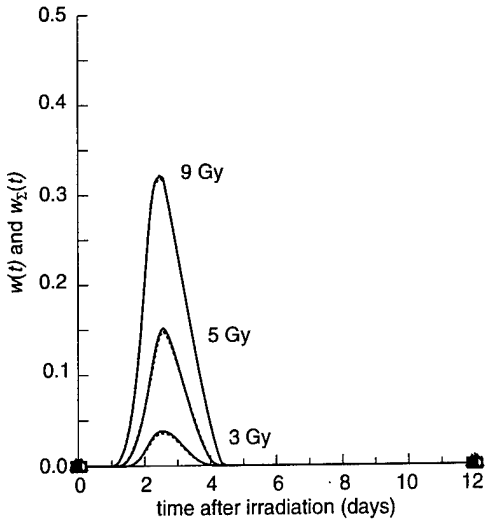

Fig. 4.38. Biometric functions $w(t)$ and $w\Sigma(t)$ describing life span probability density for mice of homogeneous (o, □, Δ) and nonhomogeneous (•, ■, ▲) populations (normal distribution, $\kappa = 0.15$) exposed to acute radiation.

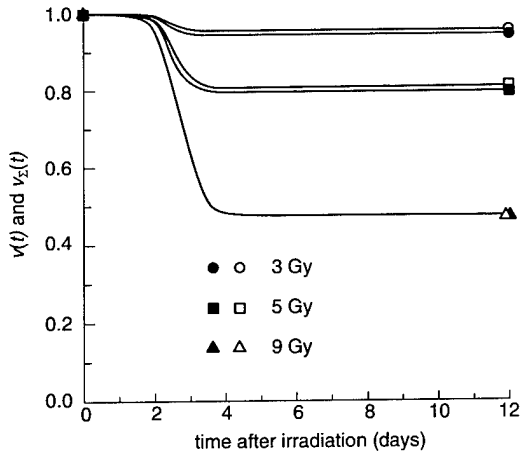

Fig. 4.39. Biometric functions $v(t)$ and $v\Sigma(t)$ describing life span probability for mice of homogeneous (o, □, Δ) and nonhomogeneous (•, ■, ▲) populations (normal distribution, $\kappa = 0.15$) exposed to acute radiation.

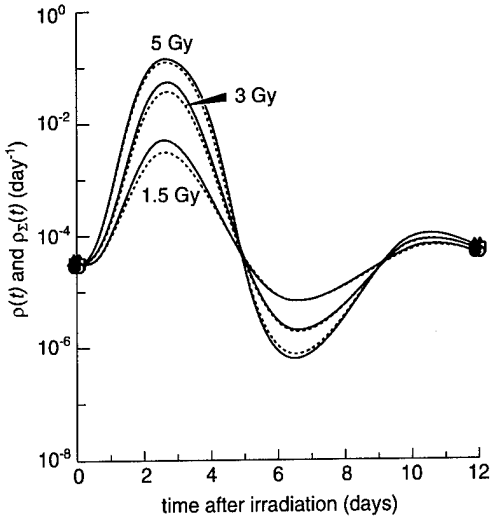

Fig. 4.40. Biometric functions $\rho(t)$ and $\rho\Sigma(t)$ describing mortality rate for mice of homogeneous (o, □, Δ) and nonhomogeneous (•, ■, ▲) populations (log-normal distribution, $\kappa = 0.3$) exposed to acute radiation.

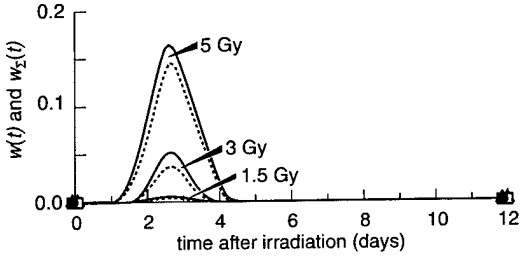

Fig. 4.41. Biometric functions $w(t)$ and $w\Sigma(t)$ describing life span probability density for mice of homogeneous (o, □, Δ) and nonhomogeneous (•, ■, ▲) populations (log-normal distribution, $\kappa = 0.3$) exposed to acute radiation.

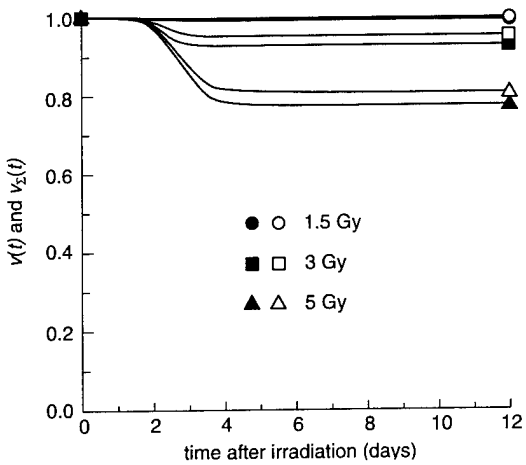

Fig. 4.42. Biometric functions $v(t)$ and $v\Sigma(t)$ describing life span probability for mice of homogeneous (o, □, Δ) and nonhomogeneous (•, ■, ▲) populations (log-normal distribution, $\kappa = 0.3$) exposed to acute radiation.

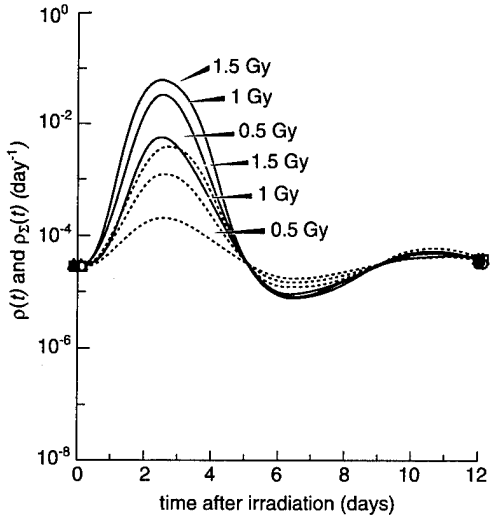

Fig. 4.43. Biometric functions $\rho(t)$ and $\rho_\Sigma(t)$ describing mortality rate for mice of homogeneous (o, □, Δ) and nonhomogeneous (•, ■, ▲) populations (log-normal distribution, $\kappa = 0.1$) exposed to acute radiation.

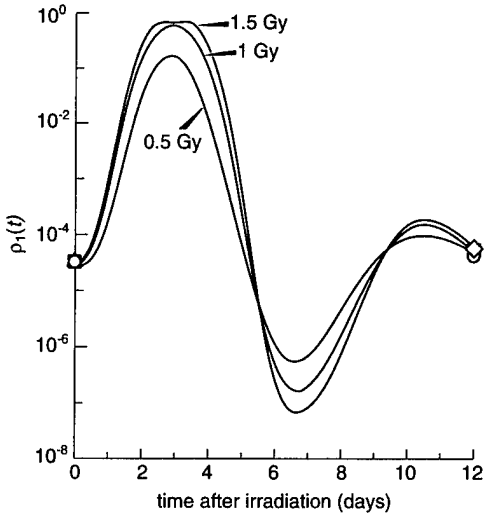

Fig. 4.46. Biometric function $\rho_1(t)$ describing mortality rate for mice of the first subpopulation of the nonhomogeneous population (log-normal distribution, $\kappa = 1.0$) exposed to acute radiation.

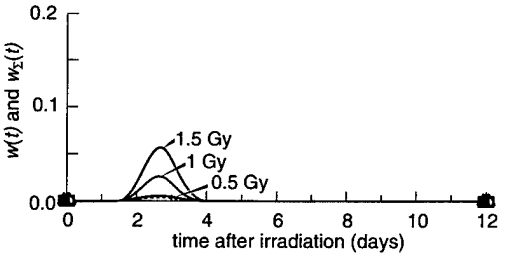

Fig. 4.44. Biometric functions $w(t)$ and $w_\Sigma(t)$ describing life span probability density for mice of homogeneous (o, □, Δ) and nonhomogeneous (•, ■, ▲) populations (log-normal distribution, $\kappa = 1.0$) exposed to acute radiation.

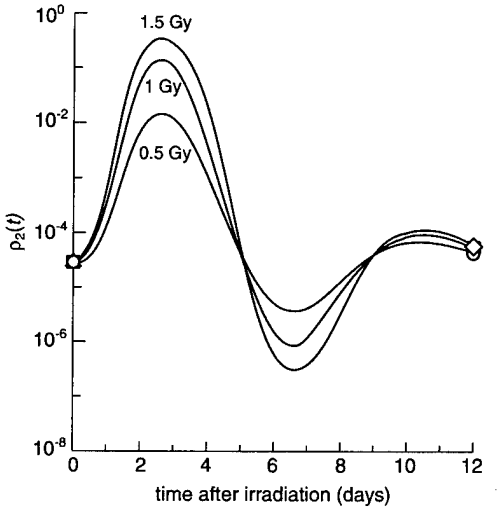

Fig. 4.47. Biometric function $\rho_2(t)$ describing mortality rate for mice of the second subpopulation of the nonhomogeneous population (log-normal distribution, $\kappa = 1.0$) exposed to acute radiation.

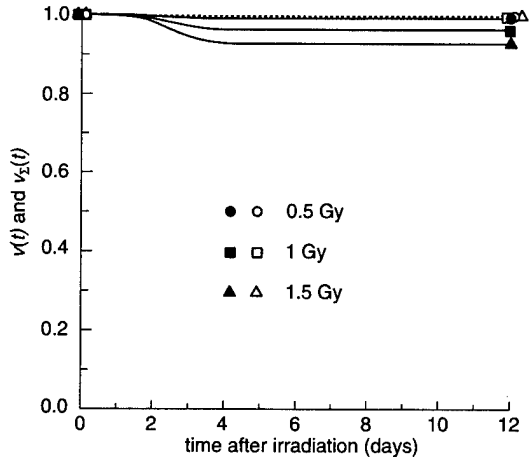

Fig. 4.45. Biometric functions $v(t)$ and $v_\Sigma(t)$ describing life span probability for mice of homogeneous (o, □, Δ) and nonhomogeneous (•, ■, ▲) populations (normal distribution, $\kappa = 1.0$) exposed to acute radiation.

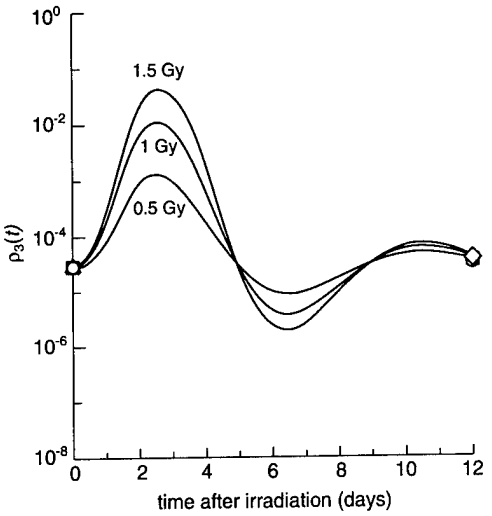

Fig. 4.48. Biometric function $\rho_3(t)$ describing mortality rate for mice of the third subpopulation of the nonhomogeneous population (log-normal distribution, $\kappa = 1.0$) exposed to acute radiation.

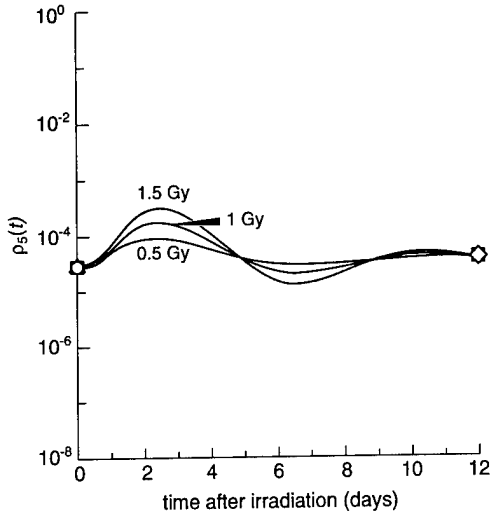

Fig. 4.50. Biometric function $\rho_5(t)$ describing mortality rate for mice of the fifth subpopulation of the nonhomogeneous population (log-normal distribution, $\kappa = 1.0$) exposed to acute radiation.

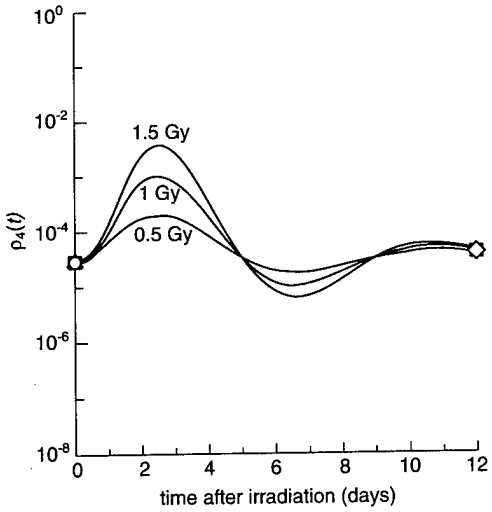

Fig. 4.49. Biometric function $\rho_4(t)$ describing mortality rate for mice of the fourth subpopulation of the nonhomogeneous population (log-normal distribution, $\kappa = 1.0$) exposed to acute radiation.

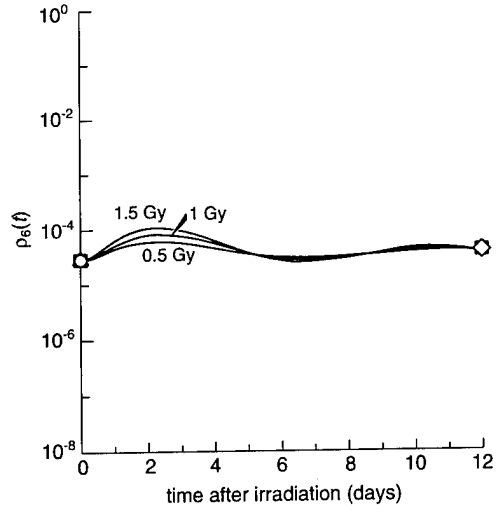

Fig. 4.51. Biometric function $\rho_6(t)$ describing mortality rate for mice of the sixth subpopulation of the nonhomogeneous population (log-normal distribution, $\kappa = 1.0$) exposed to acute radiation.

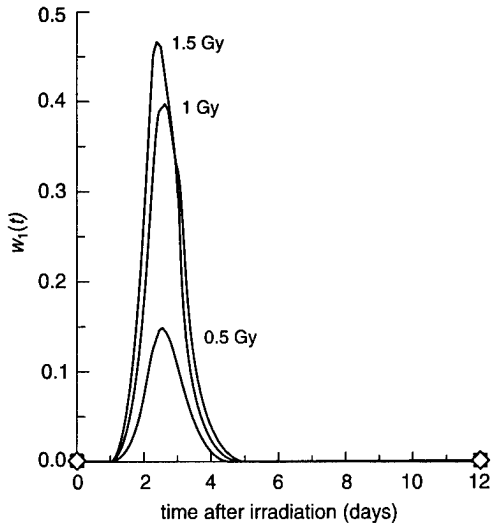

Fig. 4.52. Biometric function $w_1(t)$ describing life span probability density for mice of the first subpopulation of the nonhomogeneous population (log-normal distribution, κ = 1.0) exposed to acute radiation.

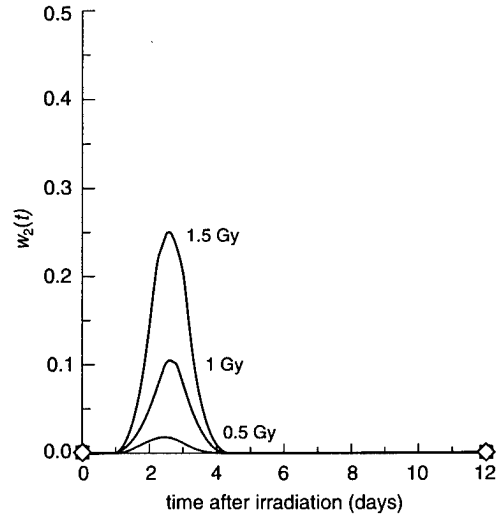

Fig. 4.53. Biometric function $w_2(t)$ describing life span probability density for mice of the second subpopulation of the nonhomogeneous population (log-normal distribution, κ = 1.0) exposed to acute radiation.

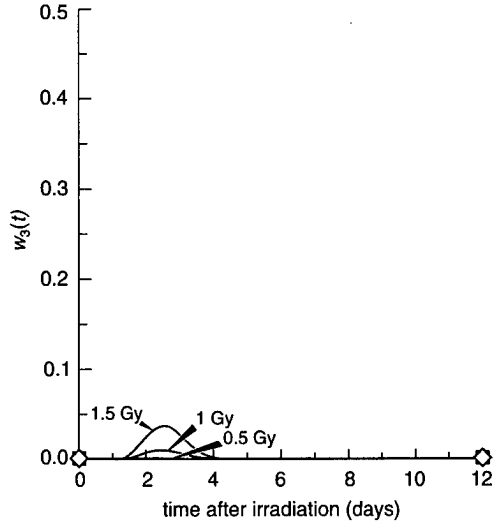

Fig. 4.54. Biometric function $w_3(t)$ describing life span probability density for mice of the third subpopulation of the nonhomogeneous population (log-normal distribution, κ = 1.0) exposed to acute radiation.

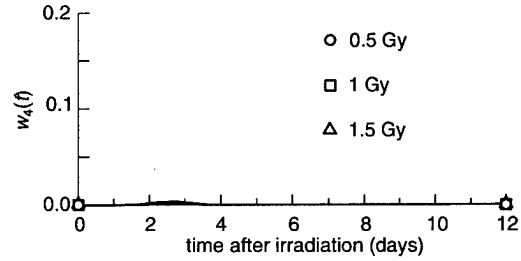

Fig. 4.55. Biometric function $w_4(t)$ describing life span probability density for mice of the fourth subpopulation of the nonhomogeneous population (log-normal distribution, κ = 1.0) exposed to acute radiation.

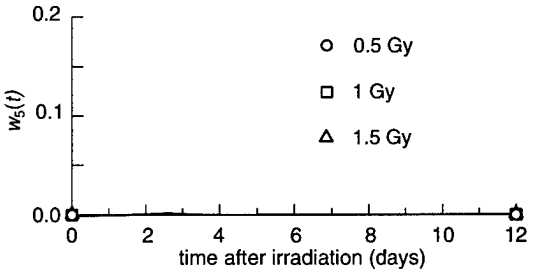

Fig. 4.56. Biometric function $w_5(t)$ describing life span probability density for mice of the fifth subpopulation of the nonhomogeneous population (log-normal distribution, κ = 1.0) exposed to acute radiation.

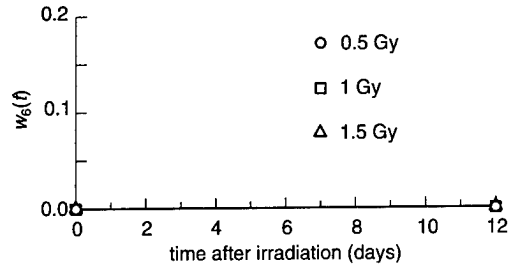

Fig. 4.57. Biometric function $w_6(t)$ describing life span probability density for mice of the sixth subpopulation of the nonhomogeneous population (log-normal distribution, κ = 1.0) exposed to acute radiation.

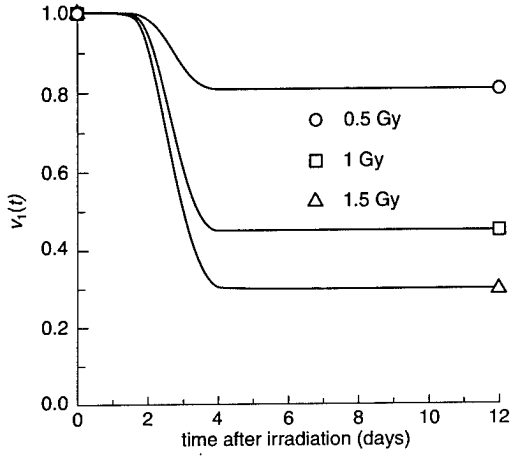

Fig. 4.58. Biometric function $v_1(t)$ describing life span probability for mice of the first subpopulation of the nonhomogeneous population (log-normal distribution, κ = 1.0) exposed to acute radiation.

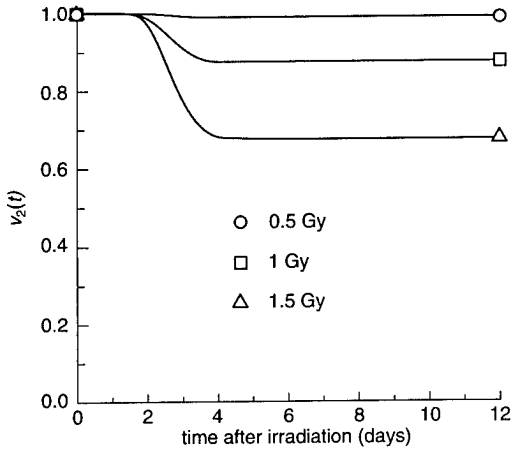

Fig. 4.59. Biometric function $v_2(t)$ describing life span probability for mice of the second subpopulation of the nonhomogeneous population (log-normal distribution, κ = 10) exposed to acute radiation.

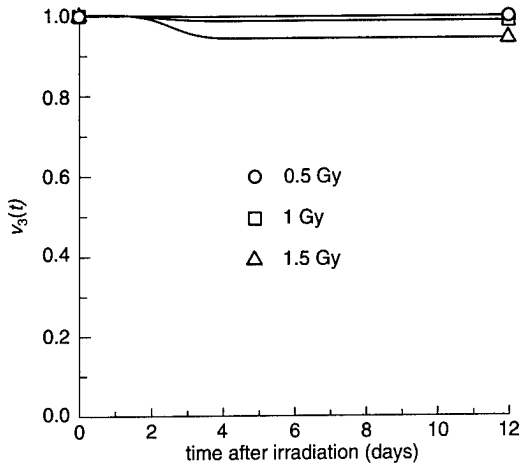

Fig. 4.60. Biometric function $v_3(t)$ describing life span probability for mice of the third subpopulation of the nonhomogeneous population (log-normal distribution, κ = 1.0) exposed to acute radiation.

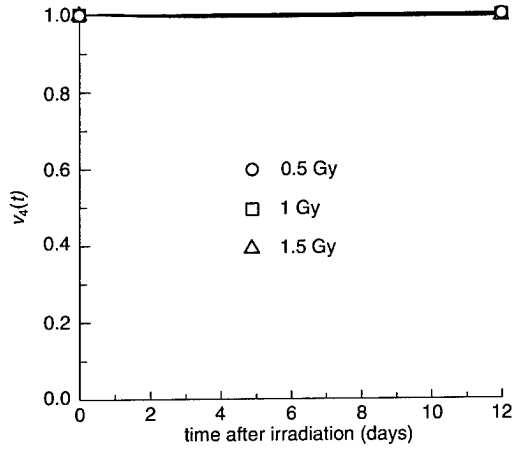

Fig. 4.61. Biometric function $v_4(t)$ describing life span probability for mice of the fourth subpopulation of the nonhomogeneous population (log-normal distribution, κ = 1.0) exposed to acute radiation.

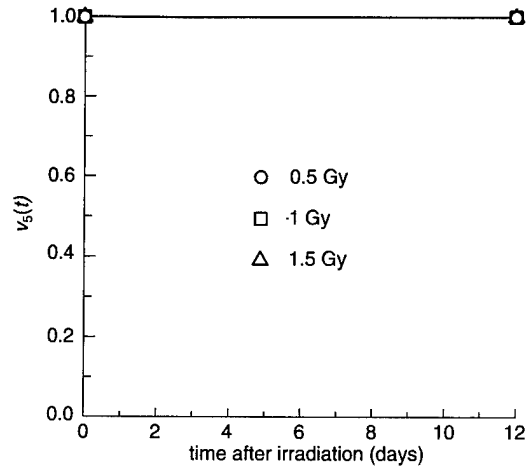

Fig. 4.62. Biometric function $v_5(t)$ describing life span probability for mice of the fifth subpopulation of the nonhomogeneous population (log-normal distribution, $\kappa = 1.0$) exposed to acute radiation.

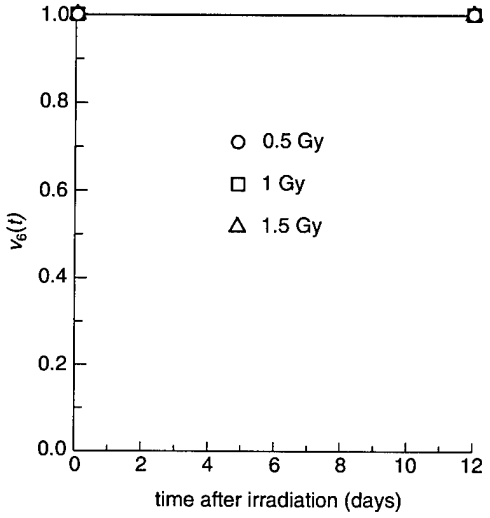

Fig. 4.63. Biometric function $v_6(t)$ describing life span probability for mice of the sixth subpopulation of the nonhomogeneous population (log-normal distribution, $\kappa = 1.0$) exposed to acute radiation.

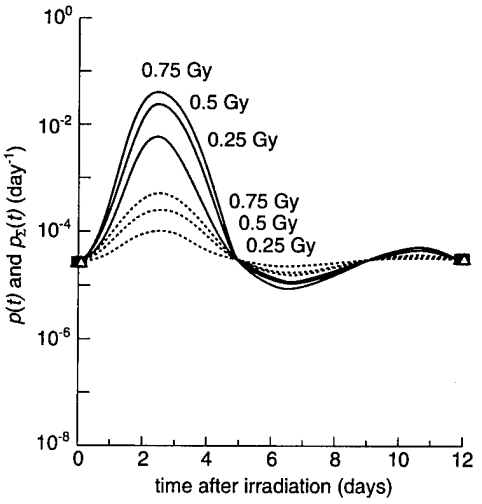

Fig. 4.64. Biometric functions $\rho(t)$ and $\rho_\Sigma(t)$ describing mortality rate for mice of homogeneous (o, □, Δ) and nonhomogeneous (•, ■, ▲) populations (log-normal distribution, $\kappa = 1.5$) exposed to acute radiation.

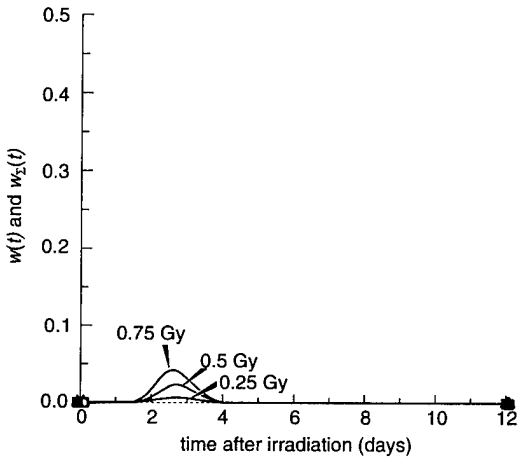

Fig. 4.65. Biometric functions $w(t)$ and $w_\Sigma(t)$ describing life span probability density for mice of homogeneous (o, □, Δ) and nonhomogeneous (•, ■, ▲) populations (log-normal distribution, $\kappa = 1.5$) exposed to acute radiation.

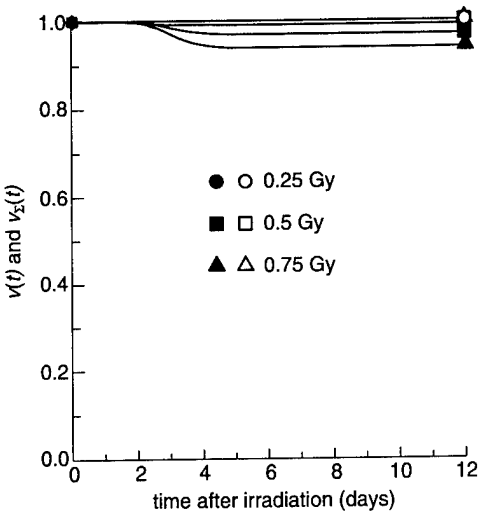

Fig. 4.66. Biometric functions $v(t)$ and $v\Sigma(t)$ describing life span probability for mice of homogeneous (o, □, Δ) and nonhomogeneous (●, ■, ▲) poulations (log-normal distribution, $\kappa = 1.5$) exposed to acute radiation.

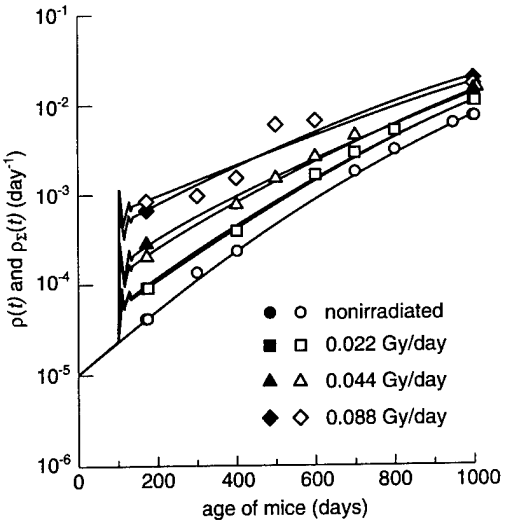

Fig. 4.67. Biometric functions $\rho(t)$ and $\rho\Sigma(t)$ describing mortality rate for mice of homogeneous (□, Δ, ◊) and nonhomogeneous (■, ▲, ◆) populations (normal distribution, $\kappa = 0.3$) not exposed (o, •) and exposed to chronic radiation. Symbols o, □, Δ, ◊ indicate corresponding experimental data on mortality rate of LAF_1 mice [7].

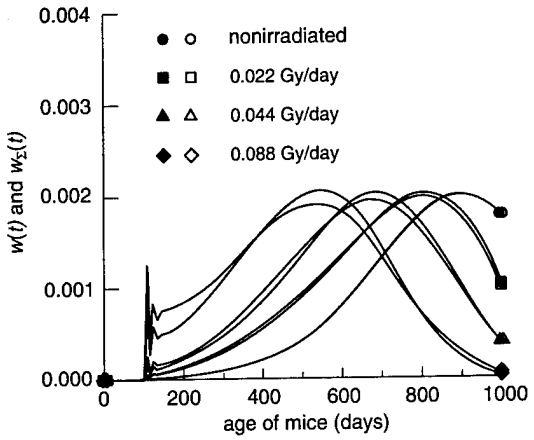

Fig. 4.68. Biometric functions $w(t)$ and $w\Sigma(t)$ describing life span probability density for mice of homogeneous (□, Δ, ◊) and nonhomogeneous (■, ▲,◆) populations (normal distribution, $\kappa = 0.3$) not exposed (o, •) and exposed to chronic radiation.

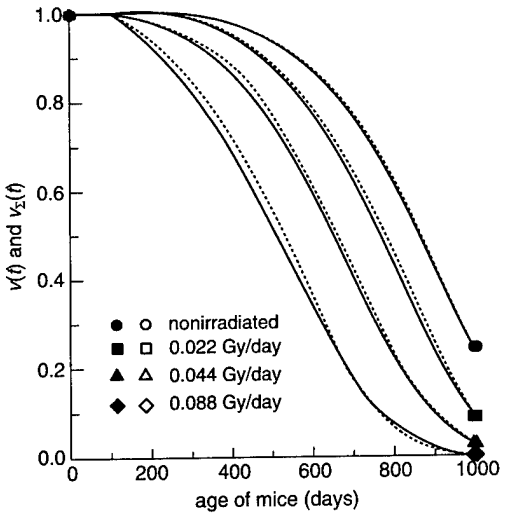

Fig. 4.69. Biometric functions $v(t)$ and $v\Sigma(t)$ describing life span probability for mice of homogeneous (□, Δ, ◊) and nonhomogeneous (■, ▲,◆) populations (normal distribution, $\kappa = 0.3$) not exposed (o, •) and exposed to chronic radiation.

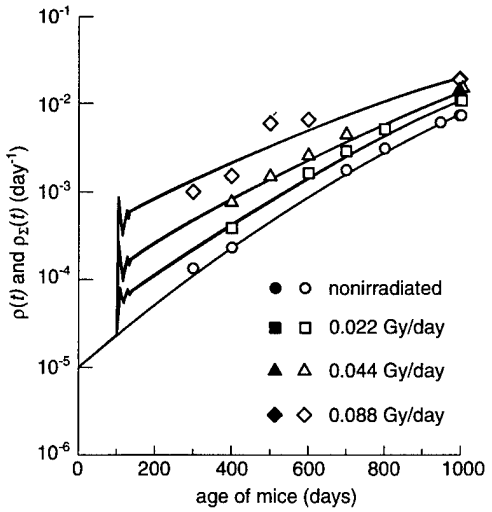

Fig. 4.70. Biometric functions $\rho(t)$ and $\rho\Sigma(t)$ describing mortality rate for mice of homogeneous (□, △, ◊) and nonhomogeneous (■, ▲, ◆) population (normal distribution, $\kappa = 0.15$) not exposed (o, •) and exposed to chronic radiation. Symbols o, □, △, ◊ indicate corresponding experimental data on the mortality rate of LAF_1 mice [7].

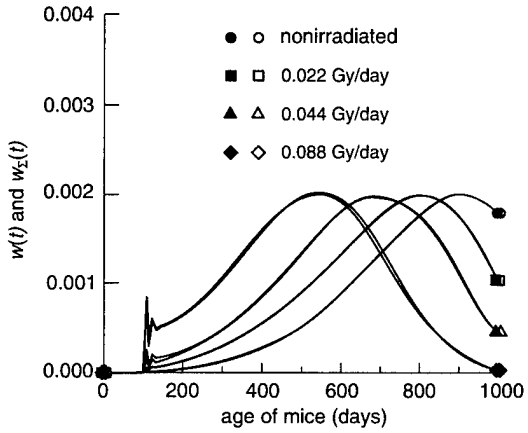

Fig. 4.71. Biometric functions $w(t)$ and $w\Sigma(t)$ describing life span probability density for mice of homogeneous (□, △, ◊) and nonhomogeneous (■, ▲, ◆) populations (normal distribution, $\kappa = 0.15$) not exposed (o, •) and exposed to chronic radiation.

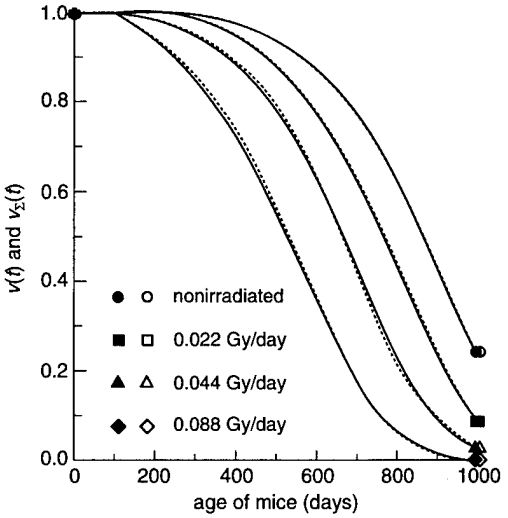

Fig. 4.72. Biometric functions $v(t)$ and $v\Sigma(t)$ describing life span probability for mice of homogeneous (□, △, ◊) and nonhomogeneous (■, ▲, ◆) populations (normal distribution, $\kappa = 0.15$) not exposed (o, •) and exposed to chronic radiation.

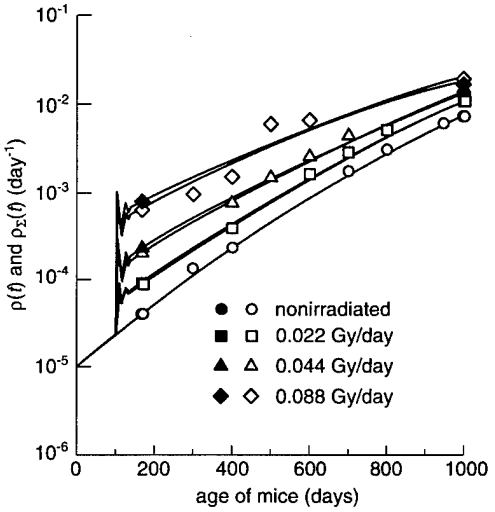

Fig. 4.73. Biometric functions $\rho(t)$ and $\rho\Sigma(t)$ describing mortality rate for mice of homogeneous (□, △, ◊) and nonhomogeneous (■, ▲, ◆) populations (log-normal distribution, $\kappa = 0.3$) not exposed (o, •) and exposed to chronic radiation. Symbols o, □, △, ◊ indicate corresponding experimental data on mortality rate of LAF_1 mice [7].

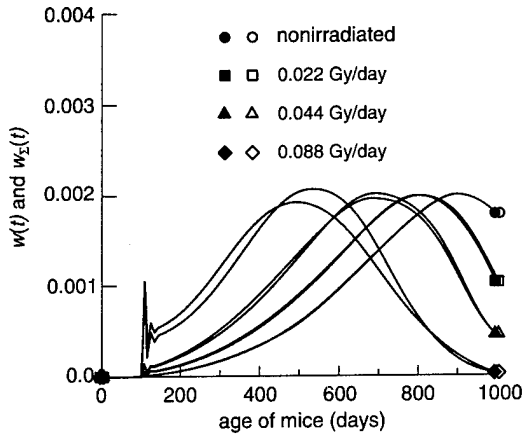

Fig. 4.74. Biometric functions $w(t)$ and $w_\Sigma(t)$ describing life span probability density for mice of homogeneous (□, ∆, ◊) and nonhomogeneous (■, ▲, ◆) populations (log-normal distribution, $\kappa = 0.3$) not exposed (o, •) and exposed to chronic radiation.

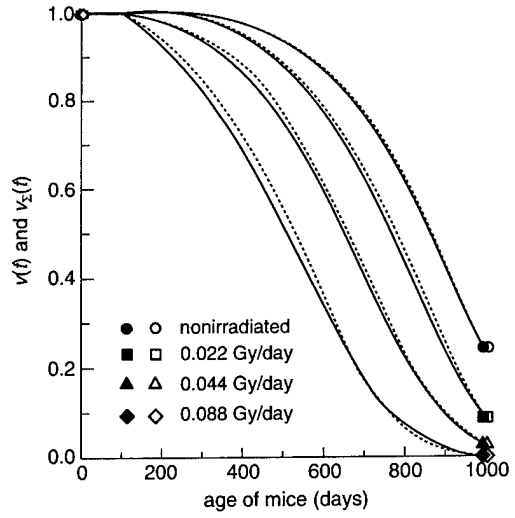

Fig. 4.75. Biometric functions $v(t)$ and $v_\Sigma(t)$ describing life span probability for mice of homogeneous (□, ∆, ◊) and nonhomogeneous (■, ▲, ◆) populations (log-normal distribution, $\kappa = 0.3$) not exposed (o, •) and exposed to chronic radiation.

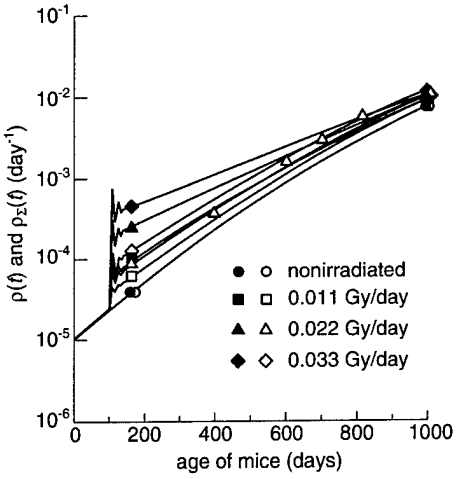

Fig. 4.76. Biometric functions $\rho(t)$ and $\rho_\Sigma(t)$ describing mortality rate for mice of homogeneous (□, ∆, ◊) and nonhomogeneous (■, ▲, ◆) populations (log-normal distribution, $\kappa = 1.0$) not exposed (o, •) and exposed to chronic radiation. The symbol ∆ indicates corresponding experimental data on mortality rate of LAF_1 mice exposed to chronic radiation at 0.022 Gy/day [7].

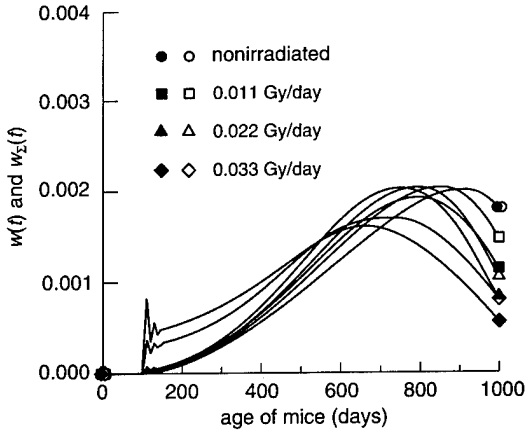

Fig. 4.77. Biometric functions $w(t)$ and $w_\Sigma(t)$ describing life span probability density for mice of homogeneous (□, ∆, ◊) and nonhomogeneous (■, ▲, ◆) populations (log-normal distribution, $\kappa = 1.0$) not exposed (o, •) and exposed to chronic radiation.

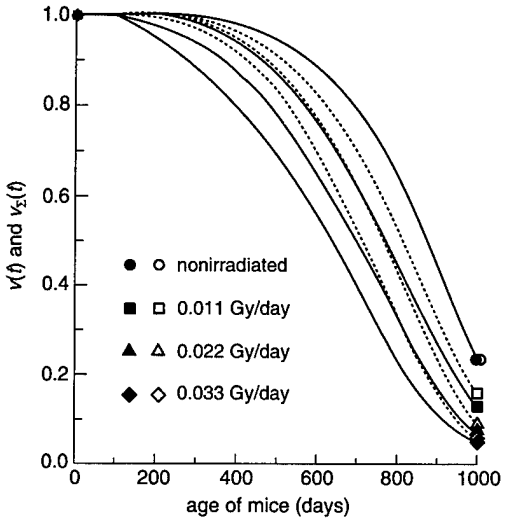

Fig. 4.78. Biometric functions $v(t)$ and $v_\Sigma(t)$ describing life span probability for mice of homogeneous (□, △, ◊) and nonhomogeneous (■, ▲, ◆) populations (log-normal distribution, $\kappa = 1.0$) not exposed (o, •) and exposed to chronic radiation.

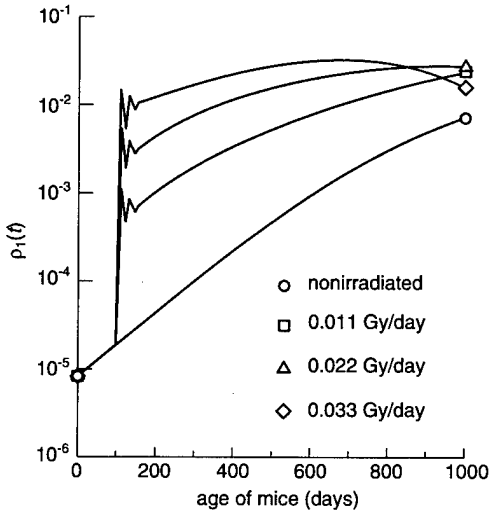

Fig. 4.79. Biometric function $\rho_1(t)$ describing mortality rate of the first subpopulation of nonirradiated mice (o) and mice exposed to chronic radiation (□, △, ◊). Distribution of specimens of the initial nonhomogeneous population according to parameter D_1 is log-normal; parameter $\kappa = 1.0$.

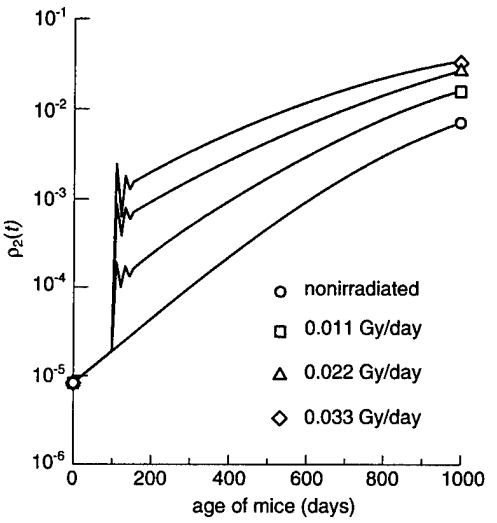

Fig. 4.80. Biometric function $\rho_2(t)$ describing mortality rate of the second subpopulation of nonirradiated mice (o) and mice exposed to chronic radiation (□, △, ◊). Distribution of specimens of the initial nonhomogeneous population according to parameter D_1 is log-normal; parameter $\kappa = 1.0$.

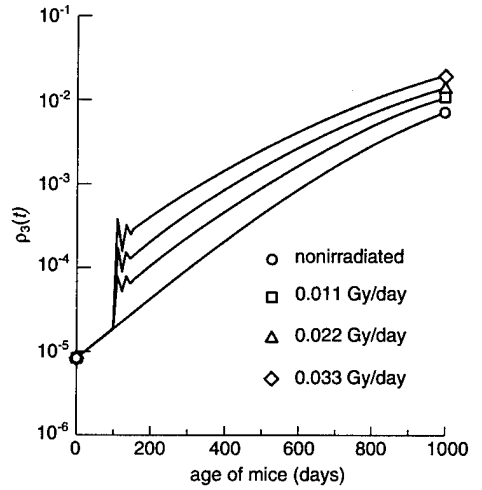

Fig. 4.81. Biometric function $\rho_3(t)$ describing mortality rate of the third subpopulation of nonirradiated mice (o) and mice exposed to chronic radiation (□, △, ◊). Distribution of specimens of the initial nonhomogeneous population according to parameter D_1 is log-normal; parameter $\kappa = 1.0$.

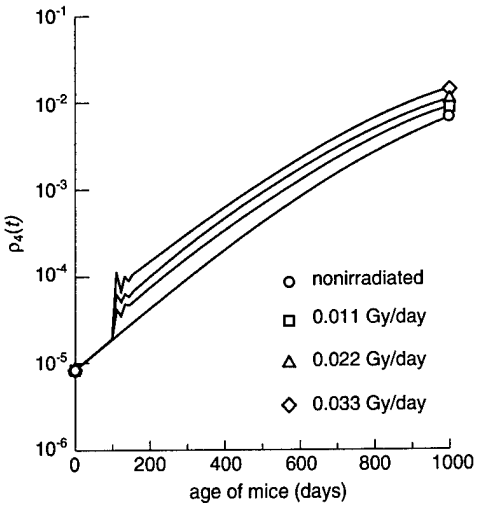

Fig. 4.82. Biometric function $\rho_4(t)$ describing mortality rate of the fourth subpopulation of nonirradiated mice (o) and mice exposed to chronic radiation (□, △, ◊). Distribution of specimens of the initial nonhomogeneous population according to parameter D_1 is log-normal; parameter $\kappa = 1.0$.

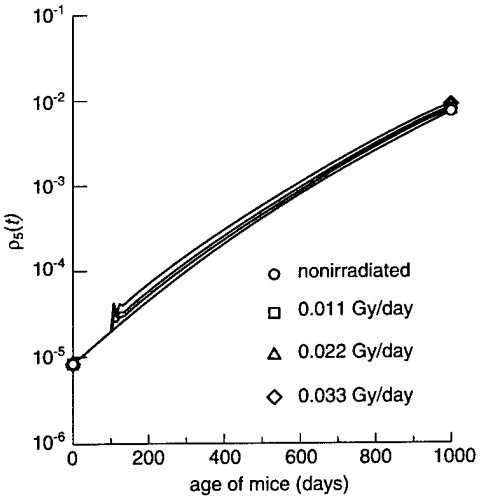

Fig. 4.83. Biometric function $\rho_5(t)$ describing mortality rate of the fifth subpopulation of nonirradiated mice (o) and mice exposed to chronic radiation (□, △, ◊). Distribution of specimens of the initial nonhomogeneous population according to parameter D_1 is log-normal; parameter $\kappa = 1.0$.

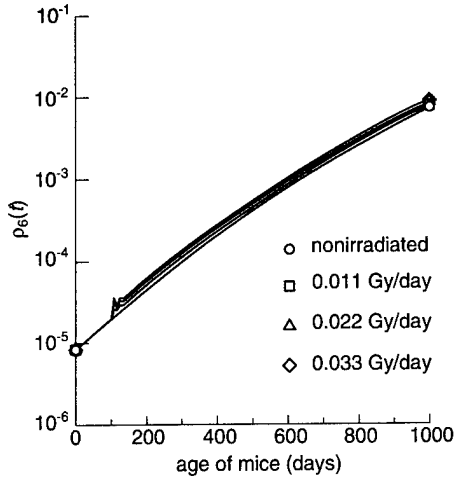

Fig. 4.84. Biometric function $\rho_6(t)$ describing mortality rate of the sixth population of nonirradiated mice (o) and mice exposed to chronic radiation (□, △, ◊). Distribution of specimens of the initial nonhomogeneous population according to parameter D_1 is log-normal; parameter $\kappa = 1.0$.

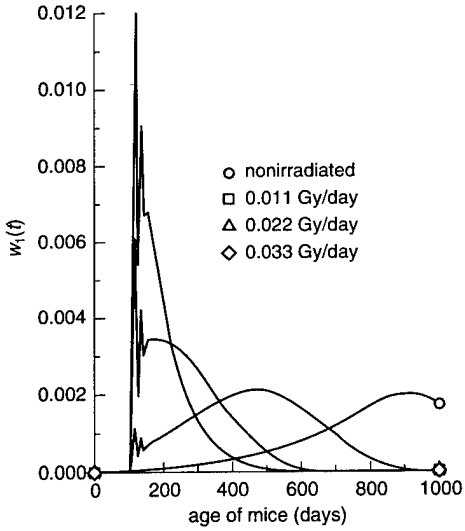

Fig. 4.85. Biometric function $w_1(t)$ describing life span probability density of the first subpopulation of nonirradiated mice (o) and mice exposed to chronic radiation (□, △, ◊). Distribution of specimens of the initial nonhomogeneous population according to parameter D_1 is log-normal; parameter $\kappa = 1.0$.

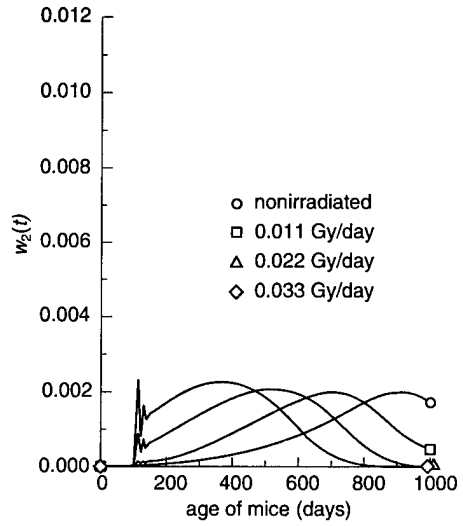

Fig. 4.86. Biometric function $w_2(t)$ describing life span probability density of the second subpopulation of nonirradiated mice (o) and mice exposed to chronic radiation (□, △, ◊). Distribution of specimens of the initial nonhomogeneous population according to parameter D_1 is log-normal; parameter $\kappa = 1.0$.

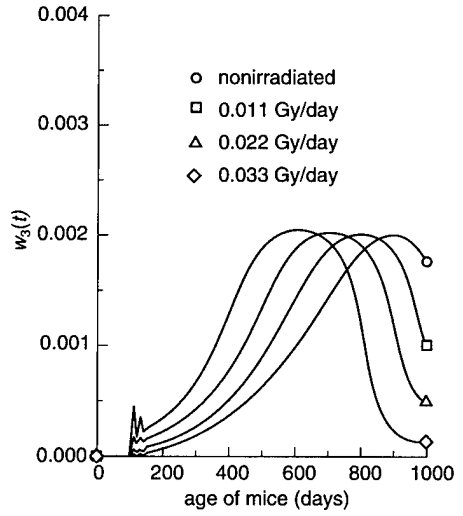

Fig. 4.87. Biometric function $w_3(t)$ describing life span probability density of the third subpopulation of nonirradiated mice (o) and mice exposed to chronic radiation (□, △, ◊). Distribution of specimens of the initial nonhomogeneous population according to parameter D_1 is log-normal; parameter $\kappa = 1.0$.

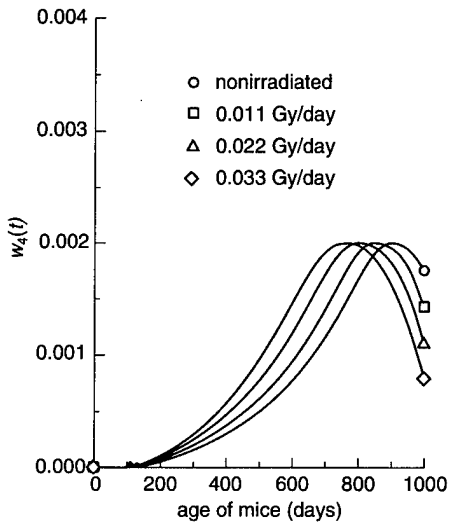

Fig. 4.88. Biometric function $w_4(t)$ describing life span probability density of the fourth subpopulation of nonirradiated mice (o) and mice exposed to chronic radiation (□, △, ◊). Distribution of specimens of the initial nonhomogeneous population according to parameter D_1 is log-normal; parameter $\kappa = 1.0$.

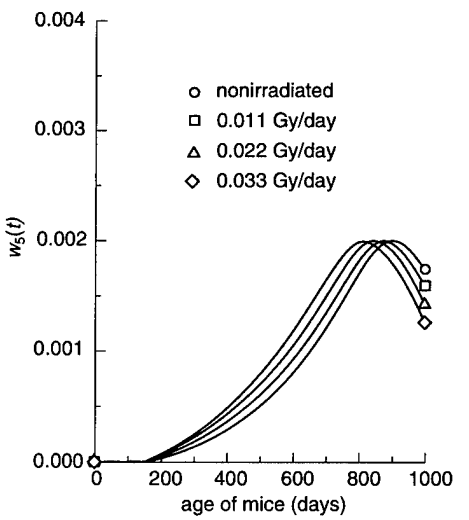

Fig. 4.89. Biometric function $w_5(t)$ describing life span probability density of the fifth subpopulation of nonirradiated mice (o) and mice exposed to chronic radiation (□, △, ◊). Distribution of specimens of the initial nonhomogeneous population according to parameter D_1 is log-normal; parameter $\kappa = 1.0$.

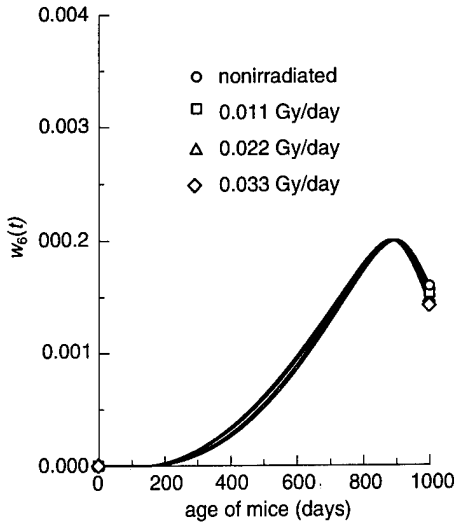

Fig. 4.90. Biometric function $w_6(t)$ describing life span probability density of the sixth subpopulation of nonirradiated mice (o) and mice exposed to chronic radiation (□, △, ◊). Distribution of specimens of the initial nonhomogeneous population according to parameter D_1 is log-normal; parameter $\kappa = 1.0$.

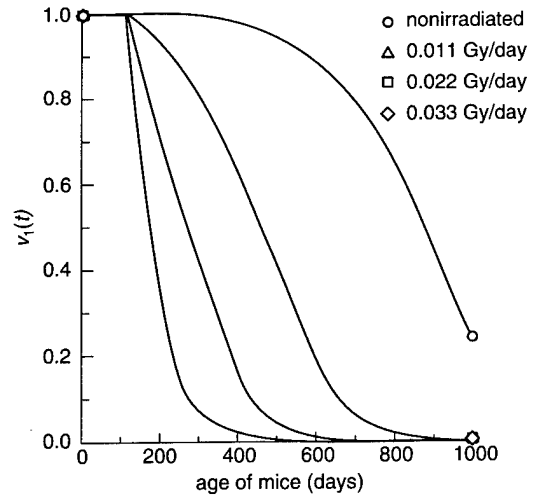

Fig. 4.91. Biometric function $v_1(t)$ describing life span probability of the first subpopulation of nonirradiated mice (o) and mice exposed to chronic radiation (□, △, ◊). Distribution of specimens of the initial nonhomogeneous population according to parameter D_1 is log-normal; parameter $\kappa = 1.0$.

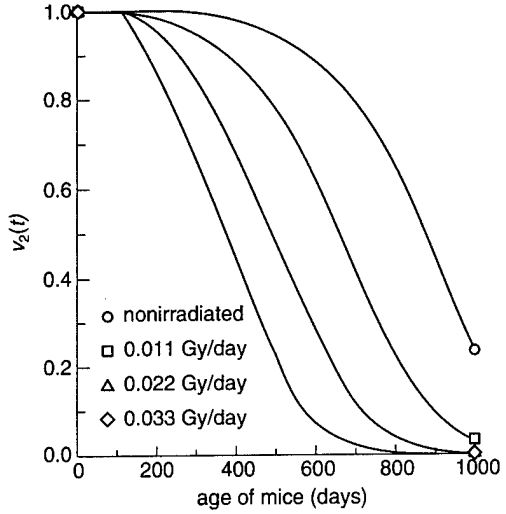

Fig. 4.92. Biometric function $v_2(t)$ describing life span probability of the second subpopulation of nonirradiated mice (o) and mice exposed to chronic radiation (□, △, ◊). Distribution of specimens of the initial nonhomogeneous population according to parameter D_1 is log-normal; parameter $\kappa = 1.0$.

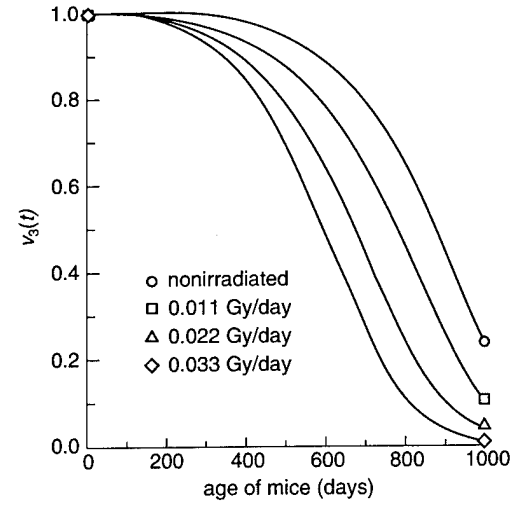

Fig. 4.93. Biometric function $v_3(t)$ describing life span probability of the third subpopulation of nonirradiated mice (o) and mice exposed to chronic radiation (□, △, ◊). Distribution of specimens of the initial nonhomogeneous population according to parameter D_1 is log-normal; parameter $\kappa = 1.0$.

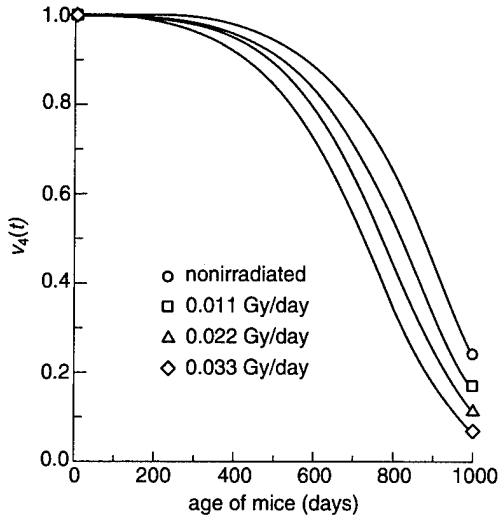

4.94. Biometric function $v_4(t)$ describing life span probability of the fourth subpopulation of nonirradiated mice (o) and mice exposed to chronic radiation (□, △, ◊). Distribution of specimens of the initial nonhomogeneous population according to parameter D_1 is log-normal; parameter $\kappa = 1.0$.

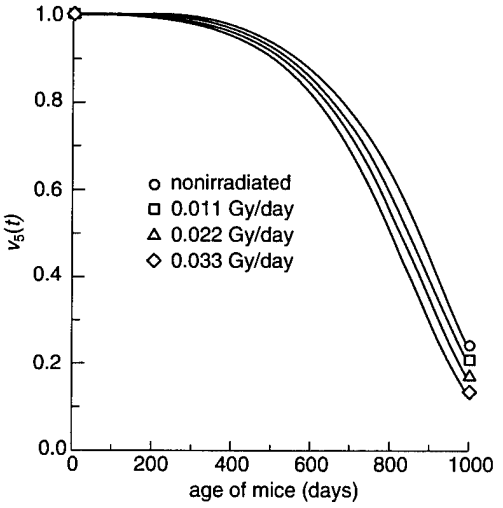

Fig. 4.95. Biometric function $v_5(t)$ describing life span probability of the fifth subpopulation of nonirradiated mice (o) and mice exposed to chronic radiation (□, △, ◊). Distribution of specimens of the initial nonhomogeneous population according to parameter D_1 is log-normal; parameter $\kappa = 1.0$.

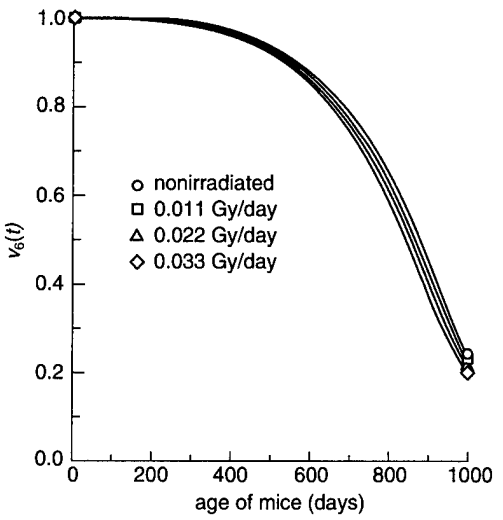

Fig. 4.96. Biometric function $v_6(t)$ describing life span probability of the sixth subpopulation of nonirradiated mice (o) and mice exposed to chronic radiation (□, △, ◊). Distribution of specimens of the initial nonhomogeneous population according to parameter D_1 is log-normal; parameter $\kappa = 1.0$.

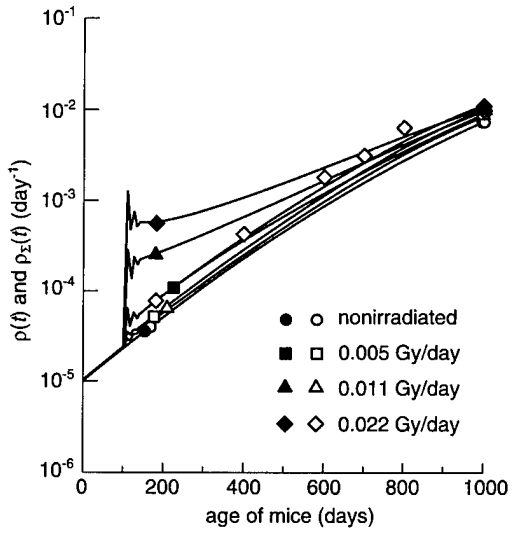

Fig. 4.97. Biometric functions $\rho(t)$ and $\rho_\Sigma(t)$ describing mortality rate for mice of homogeneous (□, △, ◊) and nonhomogeneous (■, ▲, ◆) populations (log-normal distribution, $\kappa = 1.5$) not exposed (o, •) and exposed to chronic radiation. Symbol ◊ indicates corresponding experimental data on mortality rate of LAF_1 mice exposed to chronic radiation at 0.022 Gy/day [7].

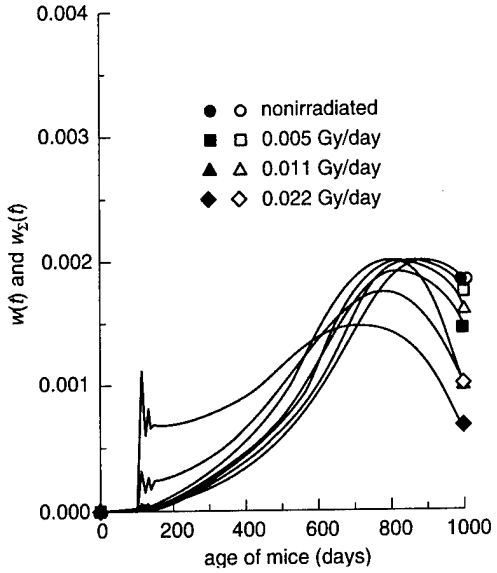

Fig. 4.98. Biometric function $w(t)$ and $w\Sigma(t)$ describing life span probability density for mice of homogeneous (□, △, ◊) and nonhomogeneous (■, ▲, ◆) populations (log-normal distribution, $\kappa = 1.5$) not exposed (o, •) and exposed to chronic radiation.

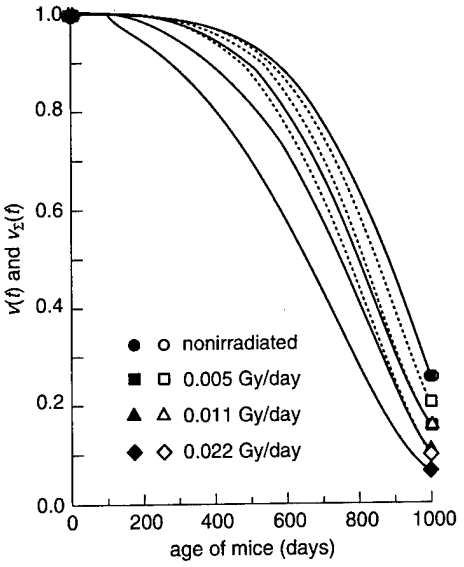

Fig. 4.99. Biometric functions $v(t)$ and $v\Sigma(t)$ describing life span probability for mice of homogeneous (□, △, ◊) and nonhomogeneous (■, ▲, ◆) populations (log-normal distribution, $\kappa = 1.5$) not exposed (o, •) and exposed to chronic radiation.

REFERENCES

1. Arlett CF, Cole J, Green MHL (1989) Radiosensitive individuals in the population. In: Baverstock KF, Stather JW (eds) Low dose radiation: Biological bases of risk assessment. London; New York; Philadelphia: Taylor and Francis, 240-252

2. Gentner NE, Morrison DP (1989) Determination of the proportion of persons in the population-at-large who exhibit abnormal sensitivity to ionizing radiation. In: Baverstock KF, Stather JW (eds) Low dose radiation: Biological bases of risk assessment. London; New York; Philadelphia: Taylor and Francis, 259-268

3. Eadie WT, Drijard D, James FE, et al. (1971) Statistical methods in experimental physics. Amsterdam; London: North-Holland Publishing Company

4. Korn GA, Korn TM (1968) Mathematical handbook. New York; San Francisco; Toronto; London; Sydney: McGraw-Hill Book Company

5. Report of the Task Group on Reference Man ICRP Publication 23 (1975) Oxford; New York; Toronto; Sydney; Braunschweig: Pergamon Press

6. Iberall AS (1967) Quantitative modeling of the physiological factors in radiation lethality. Annals of the New York Academy of Sciences 147(1):1-81

7. Sacher GA (1955) On the statistical nature of mortality with a special reference to chronic radiation mortality. Radiology 67(2)250-258

Task III

Analysis of Experimental and Clinical Data

E. E. Kovalev, principal investigator
N. G. Darenskaya, senior researcher
O. A. Smirnova, senior researcher

Abstract

An analysis of the experimental and clinical data relating to species-specific and individual radiosensitivity of mammals, including humans, is presented. The analysis is based on our concepts underlying the mortality model. Convincing evidence in support of a correlation between the radiosensitivity of the body, its critical systems, and the cells making up the systems is presented. The important role of individual radiosensitivity in the development of the responses of an individual and a population as a whole to radiation is shown. Special attention is paid to the analysis of the responses to low-dose irradiation of the cleanup crew who took part in the elimination of the consequences of the Chernobyl disaster. Additional experimental studies aimed at the development of tests detecting risk groups are outlined.

CHAPTER 5

Variability of the Radiosensitivity of Mammals: Experimental Data

5.1. Introduction

A vast body of experimental data on the different radiosensitivity levels of normal tissues, organs, and systems of animals and humans has been accumulated. The substantial differences found in the responses of various tissues to irradiation were caused by their physiological, morphological, and functional features.

Of particular interest in this context are studies of the causal relations between the initial changes in tissues and the final radiobiological effect, i.e., elucidation of the key links in a complex system of radiation injuries at different levels of the biological organization of structures and regulatory processes.

An essential advance in this field is understanding that acute radiation damage to the body is determined by the injury to critical cell systems. As noted in previous chapters, the hematopoietic and intestinal syndromes caused by radiation damage to hematopoietic tissue and the intestinal epithelium deserve special attention. Both tissues are self-renewing systems. Stem cells that have survived radiation damage to the body are the only sources for full restoration of relevant cell systems. The first successful attempt at generalizing the results of uniform whole-body irradiation by comparing the cell kinetics of tissues responsible for the development of the principal radiation syndromes and body damage was made in 1965 [1]. An analysis and generalization of the available radiobiological literature resulted further in developing the concept of cellular determinants of the outcome of acute radiation damage to the body [2-6].

This chapter generalizes and analyzes the radiobiological literature and the original experimental data on species-specific and individual radiosensitivity of mammals and the relation between the radiosensitivity of the body, its critical systems, and the constituent cells of these systems.

5.2. Species-Specific and Individual Radiosensitivity of Mammals and Their Critical Systems

The damage to the body according to irradiation dose can be described by two functions: effects of irradiation dose on mortality and on average life span [1, 7]. As the dose increases, the mortality of animals increases until it reaches 100%. A comparison of the dose dependence of mortality for different animal species makes it possible to detect not only the species-specific features but also the individual variability of radiosensitivity. It is difficult to compare reported data because of dissimilar conditions of exposure and animal upkeep in different laboratories and radiobiology centers. Moreover, it is not always clear whether the detected dissimilarities were due to species-specific and individual features of radiosensitivity of animals or to differences in experimental conditions, such as radiation type and energy, dose rate, irradiation geometry, character of distribution of the absorbed doses in the body, sex, body weight, age of animals, etc.

Of much interest to us are the data obtained by Professor N. G. Darenskaya for seven animal species multilaterally irradiated under identical conditions of a uniform distribution of absorbed γ radiation doses using an experimental γ unit EGO-2 [7]. Irradiation under these conditions revealed differences between the functional dependences of the mortality of the test animals on the irradiation dose (fig. 5.1)*. These differences are caused by both species-specific and individual features of the radiosensitivity of the animals. It can be seen that the dose-effect dependences thus obtained can be represented to a first approximation by linear functions. It is also noteworthy that the dose-effect curves for mice, rats, and dogs have a larger slope, whereas the slope is smaller for guinea pigs, rabbits, and sheep. The smallest slope is peculiar to the dose-effect curve for rabbits. These data were used in calculating the damaging dose values, which made it possible to arrange the animal species in the following decreasing order of radiosensitivity: dogs, monkeys, pigs, sheep, guinea pigs, rabbits, mice, and rats.

It should be emphasized that the slope of the dose-effect curve represents the variability of the individual radiosensitivity of the animal species. The larger the slope of the curve (therefore the broader the dose range covering the death rate of animals of a certain species from 0 to 100%), the more distinct are the differences in the individual radiosensitivity in the particular animal species.

A comparison of the LD_{50} values obtained by Domshlak et al. [8] and the data presented by other authors (table 5.1) points to some discrepancies. The most notable discrepancies were found for mice, rats, rabbits, and sheep, whereas a rather good agreement was observed for guinea pigs, dogs, monkeys, and pigs.

*Figures are on page 143.

Table 5.1. Lethal doses, $LD_{50/30-60}$ (Gy), for different animal species under uniform γ-irradiation.

Species	$LD_{50/30-60}$ (Gy)	
	Darenskaya's data [7]	Bond et al. data [1]
Mice	5.28 (5.1 - 5.45)	6.4
Rats	5.9 (5.8 - 5.96)	7.1
Guinea pigs	3.6 (3.1 - 4.0)	4.5
Rabbits	5.3 (4.3 - 5.8)	7.5
Monkeys	5.5 (4.8 - 6.2)	6.0
Dogs	2.5 (2.4 - 2.6)	2.5
Sheep	3.2 (1.7 - 3.4)	-
Suckling pigs (2.5 months old)	2.82 (1.7 - 3.4)	2.5

The second important feature revealing the species-specific differences in the responses of animals to irradiation in a broad dose range is the change in their average life span with irradiation dose. Such dependences were generalized for different animals in references 1, 7, 9, and 10. For most animal species, the relationship of dose to the average life span is complex.

The observations [8] of the manifestations of responses of experimental animals irradiated in the same γ unit within a broad dose range (2-450 Gy) made it possible to obtain the dose dependence of the average life span for six mammalian species (fig. 5.2). Three specific segments can be distinguished in the dose-effect curves presented in the figure. The average life span in the first and third segments is dose dependent—life span decreases with dose. In the second segment, the average life span is virtually independent of dose.

The clinical manifestations of radiation damage caused by exposure to the doses corresponding to the three segments in the dose-effect curve are indicative of the development of different radiation sickness forms. The first segment represents the development of the acute or hematopoietic form of radiation sickness. In this case, the dose range for different animal species is 3-10 Gy. It should be noted that this segment of the dose-effect curves for guinea pigs, monkeys, and dogs covers lower doses than in the curves for mice, rats, and rabbits. These findings testify to a higher radiosensitivity in the first group of animals.

The species-specific differences in life span are less pronounced in the second section of the dose curve, which is a plateau. The life span of animals of different species varies within comparatively narrow limits—3 to 7 days. The species-specific differences manifest themselves in different lengths of the

plateau, i.e., in dissimilar values of the dose range leading to development of the intestinal form of radiation sickness. Thus, the plateau extends from 10 to 200 Gy in mice, whereas in monkeys it ranges from 8 to 60 Gy, and in dogs from 6 to 100 Gy. The $LD_{50/3-8}$ for animals of different species also varies (table 5.2).

The species-specific differences in radiosensitivity are exhibited markedly at the level of doses exceeding 60-200 Gy that lead to the development of the cerebral form of radiation sickness. These doses are represented by the third segment of the dose-effect curve in figure 5.2. It can be seen that the highest radiosensitivity in the development of this damage is shown by monkeys, guinea pigs, and dogs [11-13].

Thus, the stepwise character of the dependence of life span on irradiation dose is peculiar to almost all animal species, presumably except donkeys. The dose-effect curves for the latter animal species have no plateau. The three different segments of the dose curve represent the hematopoietic, intestinal, and cerebral forms of radiation sickness, respectively.

It is well known that the response of an animal to irradiation is a result of the interaction of destructive and repair processes in many organs and systems of the body; the extent of damage is determined by different inherent radiosensitivity levels. However, there are "critical" systems whose damage is mainly responsible for the death of animals and for the development of certain forms of radiation sickness in specific dose ranges. Therefore, each form of radiation sickness is the result of damage to one of the body's critical systems in a certain dose range.

The basis for the development of each of the syndromes above is the damage to different critical tissue systems possessing dissimilar radiosensitivities. As the dose increases, the dose threshold of the injury to a certain critical system is attained; the physiological features of the system and the peculiarity of its cell kinetics determine the time of the development of symptoms and the specific character of the clinical picture of the particular form of radiation sickness.

The critical system responsible for the damage in the dose range represented by the first segment of the dose curve is the hematopoietic system. Data testifying to the leading role of the damage to the hematopoietic system have accumulated and are supported by data indicating the possibility of preventing the death of animals by bone marrow transplantation [39-41]. As a result, the animals survive after exposure to lethal doses. The role of the hematopoietic system in the development of this form of radiation sickness is also evidenced by the data [42] on irradiation of rats whose body parts containing active red

Table 5.2. Lethal doses ($LD_{50/3\text{-}8}$) for different animal species under whole-body irradiation.

	Condition of exposure			
Species	Radiation type	Dose rate (Gy/min)	Lethal dose (Gy)	Reference
Mouse	X-ray, 200 keV		$LD_{50/5} = 12.6$	[14]
	γ-ray, ^{60}Co	6.3	$LD_{50/3} = 12.0$	[7]
	X-ray, 250 keV		$LD_{50/8} = 20.0$	[15]
	γ-ray, ^{137}Cs	0.01	$LD_{50/5} = 25.0$	[16]
	γ-ray, ^{60}Co	0.56	$LD_{50/5} = 9.92$	[17]
		0.49	$LD_{50/5} = 15.2$	[18]
		0.24	$LD_{50/5} = 16.83$	[18]
	Neutrons		$LD_{50/5} = 5.2$	[18]
	X-ray		$LD_{50/5} = 12.28$	[18]
	Neutrons		$LD_{50/5} = 3.57$	[19]
	γ-ray, ^{60}Co		$LD_{50/5} = 10.0$	[19]
	X-ray		$LD_{50/5} = 10.81$	[20]
	γ-ray		$LD_{50/5} = 13.65$	[21]
	Neutrons		$LD_{50/5} = 2.52$	[21]
	γ-ray, 4 MeV		$LD_{50/6} = 12.77$	[21]
	Electrons, 8 MeV	60.0	$LD_{50/5} = 13.3$	[22]
Rat	X-ray, 250 keV		$LD_{50/5} = 8.08$	[23]
	γ-ray, ^{60}Co	4.7 - 6.3	$LD_{50/3} = 10.0$	[7]
	X-ray		$LD_{50/3} = 10.5$	[24]
Mongolian gerbil	X-ray		$LD_{50/8} = 12.0$	[25]
Hamster	X-ray, 200 keV		$LD_{50/8} = 10.0$	[23]
	X-ray, 250 keV		$LD_{50/6} = 20.0$	[26]
Guinea pig	X-ray, 200 keV		$LD_{50/8} = 15.0$	[27]
	γ-ray, ^{60}Co	4.7 - 6.3	$LD_{50/5} = 15.0$	[7]
			$LD_{50/5} = 15.0$	[28]
			$LD_{50/5} = 10.0$	[29]
Monkey	γ-ray, 1.1 MeV	0.06	$LD_{50/8} = 15.0$	[30]
	γ-ray, ^{60}Co	4.7 - 6.3	$LD_{50/5} = 12.0$	[7]
	γ-ray, ^{60}Co	8.03	$LD_{50/5\text{-}6} = 20.0$	[31]
Dog	X-ray, 2,000 keV		$LD_{50/3} = 10.0$	[32]
	γ-ray, ^{60}Co	4.7 - 6.3	$LD_{50/3} = 10.0$	[7]
	γ-ray, ^{60}Co	0.06	$LD_{50/5} = 13.0$	[33, 34]
	γ-ray, ^{60}Co		$LD_{50/3} = 10.0$	[35]
	γ-ray, 0.54 MeV		$LD_{50/3} = 12.0$	[36]
Pig	X-ray, 1,000 keV	0.33	$LD_{100/5} = 15.5$	[37]
	γ-ray, ^{60}Co	1.0	$LD_{100/5} = 17.0$	[38]

Table 5.3. LD_{50} for rats under different irradiation conditions [42].

Condition of exposure	LD_{50} (Gy)	Part of bone marrow shielded (%)
Whole body	4.8 (4.5 - 5.1)	-
Pelvis shielded	5.8 (5.3 - 6.3)	15
Chest shielded	6.0 (5.5 - 6.5)	11
Head shielded	7.0 (6.5 - 7.5)	14
Hind extremity shielded	7.4 (6.8 - 8.0)	15

bone marrow were shielded (table 5.3). It is evident that with 8%-15% of the bone marrow maintained intact, the LD_{50} value increased from 4.9 Gy to 7.4 Gy. Of importance in these experiments were both the activity of the unirradiated portion of the bone marrow and the rate of migration of hematopoietic stem cells from the shielded part of the body [43, 44].

The clinical manifestations in the second segment of the dose curve (the plateau) suggest that the gastrointestinal tract is affected, consequently intestinal damage develops. The critical system responsible for intestinal damage is the small intestine, primarily the epithelium, and damage to the stomach [45] and the large intestine [46] is also involved.

The role of intestinal damage in developing the intestinal form of radiation sickness is confirmed by data indicating that irradiation of the total body, abdomen, and exposed intestine [50, 52-55] resulted in identical times of death and similar clinical manifestations in animals (table 5.4). The contribution of the damage to the gastrointestinal tract on exposure to doses corresponding to the plateau in the dose curve is also attested by experiments with the abdominal area shielded [42, 50, 51]. In this case, deaths of the animals on days 3-4 as a result of the development of the intestinal form of radiation sickness were not observed. The animals died on days 6-8 after irradiation because of severe damage to the bone marrow and the development of the hematopoietic form of radiation sickness. Surgical removal of the irradiated loops of the small intestine also prevented early death [56, 57].

The damage threshold of the third critical system, the central nervous system (CNS), is attained by increasing the dose of whole-body irradiation, which develops into the cerebral form of radiation sickness [1, 11, 13, 23, 54, 58, 59]. The species-specific differences are particularly evident in this case. Monkeys, guinea pigs, and rabbits were found to be most vulnerable in this dose range.

The role of CNS damage in the development of the cerebral form of radiation sickness can be judged from such specific manifestations as the spastic syndrome and other neurologic symptoms. It should be noted that this form also develops after irradiation of the head only [60-64]. Shielding the head prevents development of the cerebral form of radiation sickness [11, 60, 62, 65, 66].

We have discussed the principal features of development of radiation damage in different mammalian species after exposure to ionizing radiation in a broad range of doses and have also indicated the principal forms of radiation sickness that develop after uniform irradiation. Wherever possible, we tried to underscore the importance of the individual radiosensitivity of the body. However, the individual radiosensitivity of mammals belonging to the same species manifests itself most clearly on exposure to doses bringing about transitional forms of radiation sickness. Two regions of such doses are located at the boundaries of the dose ranges that result in the bone-marrow and intestinal forms and also in the intestinal and cerebral forms of radiation sickness, respectively. Because of different individual radiosensitivity levels of the critical systems, different forms of damage may develop in animals exposed to the above-mentioned dose ranges. Thus, after irradiation in doses corresponding to the first region, the most resistant animals die as a result of developing very grave hematopoietic damage. As the dose is increased above the absolutely minimal lethal level, life span decreases further. As this takes place, the clinical picture of the disease manifests the signs of intestinal damage more and more intensely. A hematopoietic-intestinal form of radiation

Table 5.4. $LD_{50/3}$ for intestinal form of radiation sickness of rats and mice under different irradiation conditions.

Condition of irradiation	$LD_{50/3}$ (Gy)	Reference
Whole body	9.35 ± 0.75	[47]
Hind extremity shielded	8.4 ± 0.55	[42]
Head shielded	9.2 ± 0.6	[42]
Pelvis shielded	9.45 ± 0.3	[42]
Chest shielded	9.85 ± 0.65	[42]
Hind extremity	9.45	[47, 48]
Whole abdomen	13.1 ± 1.2	[47, 48]
Front part of abdomen	18.55 ± 0.5	[47, 48]
Hind part of abdomen	17.6 ± 1.3	[47, 48]
Exteriorized intestine	13.5 16.2	[49, 50] [51]

sickness develops in those animals with medium radiosensitivity, resulting in death within the period between the limits peculiar to the hematopoietic and intestinal forms of radiation sickness; in other words, transitional or mixed forms of radiation damage arise, with signs of injury to both critical systems simultaneously. The most radiosensitive animals die on day 3 or 4 as a result of the intestinal form of radiation sickness.

After irradiation with doses of the second region, animals of the same species also manifest the development of other forms of radiation sickness because of the different radiosensitivity levels of their critical systems: the intestine and CNS. Some of the most radioresistant animals have the intestinal form of radiation sickness, whereas the most sensitive animals already manifest the cerebral form. Animals with medium radiosensitivity have a mixed intestinal-cerebral form of radiation sickness, with signs of injuries to the intestine and CNS. Death occurs within 1.5-2 days.

In cases of uniform and nonuniform whole-body radiation exposures, account should be taken not only of the major radiation syndromes resulting from action on the principal critical systems but also of the simultaneous effect on other tissues and systems, primarily those with regulatory functions. The extent of the involvement of these tissues and systems in the pathological process is determined both by their radiosensitivity and their dose loads. Thus, it is well known that in doses leading to the development of the intestinal syndrome, severe damage to the hematopoietic system occurs, which affects the development of the intestinal syndrome [49, 50, 67-71]. These processes manifest themselves in a decrease in the threshold dose of the onset of the intestinal syndrome on total-body irradiation as compared with the dose on partial exposure of the abdominal zone.

Thus, the bone marrow and intestine are two critical systems where radiation injury determines the development of the hematopoietic and intestinal forms of radiation sickness [3, 4, 72-76]. A direct relation was found between changes in these critical systems and the value of the absorbed radiation energy. The death of animals takes place against the background of the depletion of the relevant cell system and, hence, the deficit of mature functional elements.

5.3. The Cell Factor in the Development of Species-Specific and Individual Radiosensitivity of Mammals

Convincing experimental data indicate that one of the most important factors determining the radiosensitivity of the critical systems and therefore of the body as a whole is the radiosensitivity of the cells of a particular critical system: most importantly, the stem cells.

As noted above, the hematopoietic organs rank among the most radiosensitive systems in mammals. Damage to the bone marrow, thymus, lymph nodes, and spleen is the first phase in developing radiation sickness in the initial range of lethal doses [74-77]. The population of hematopoietic stem cells plays an important part in the development of radiosensitivity in animals exposed to radiation doses that result in the hematopoietic form of radiation sickness [1, 43, 78-80].

The survival curves of the colony-forming stem cells of the bone marrow are usually characterized by the D_0 value and the extrapolation number n. Data on the radiosensitivity of different colony-forming cells in animals of different species are summarized in table 5.5 and indicate that a correlation exists between the species-specific radiosensitivity of hematopoietic stem cells and the species-specific radiosensitivity of the same mammals at the whole-body level (see figure 5.2).

It follows from table 5.5 that the D_0 values for the precursor bone-marrow cells of the same type in animals belonging to the same species vary within rather broad limits [81, 89-91, 97, 102-104, 108, 109, 113, 115, 117]. The D_0 values of different specialized hematopoietic precursors change within a still wider range: the granulocytic-monocytic precursors manifest a higher resistance than the pluripotent hematopoietic stem cells. Experiments with fractional gamma irradiation also revealed a higher rate of postirradiation repair of CFU-GEMM cells, whereas no repair of CFU-C cells was observed [126].

The D_0 for CFU-C cells was about 1 Gy, thus testifying to a high radiovulnerability of these cells. Changes in the radiosensitivity of *T*- and *B*-lymphocytes in the course of their differentiation were detected [127]. For the precursors of *B* cells, $D_0 = 0.89$ Gy; for *B* cells at the differentiation stage, $D_0 = 1.25$ Gy, and for the functioning *B* cells, $D_0 = 2.23$ Gy. For the precursors of *T* cells, $D_0 = 1.6$ Gy; for *T* cells at the differentiation stage, $D_0 = 4.41$ Gy; and for the functioning *T* cells, $D_0 = 10.95$ Gy.

The character of the process of recovery of the CFU population after radiation damage was similar to the change in radiosensitivity of the body that was evaluated from the survival rate of animals on repeated radiation exposure. Thorough studies of the dynamics of recovery after irradiation showed that within the first 24 hours pronounced variations of the effective dose (D_{eff}) occurred. A hypothesis was put forward [128] suggesting that these variations represent the process of repair of sublethal radiation injuries in the cells of hematopoietic tissues and, possibly, the effect of their partial synchronization. The further changes in D_{eff} are caused by proliferation of these cells. These ideas have found support in studies of the dynamics of the recovery of the CFU-C population after irradiation; the studies were based on the method of endocolonies [128, 129]. The character of D_{eff} changes during the acute period of radiation sickness correlates with the dynamics of the number of CFU-C cells [130-132]. Simultaneously using the survival criterion and the number of stem cells, comparison of the data obtained, showed that the recovery of the

Table 5.5. Radiosensitivity of the colony-forming cells of the bone marrow.

Species	Type of cells	Type of radiation	D_0 (Gy)	n	Reference
Mice					
	CFU-S	γ-ray	1.0	1.5-2.0	[81]
		X-ray	0.81	0.9	[82]
$B6D2F_1O$		γ-ray, 4.5 Gy/min	0.9	1	[83]
$C_{57}Bx$ BAαB/C		X-ray, 1.2 Gy/min	0.79	1.59	[84]
		X-ray, 300 keV	1.18 ± 0.01	1	[85]
		Fast neutrons	0.48 ± 0.05	1	[85]
$C_{57}Bα$		g-ray, ^{60}Co, 0.55 Gy/min	0.99 ± 0.04	0.82 ± 0.02	[86]
		Neutrons	0.55 ± 0.05	0.73 ± 0.24	[96]
		γ-ray, ^{60}Co	0.94	1	[87]
		γ-ray	1.11	1	[88]
		γ-ray	1.11 - 1.22	1	[89]
		γ-ray	1.15 - 1.26	1	[90, 91]
		γ-ray 0.08; 0.25; 0.48 Gy/min	0.75	1	[92]
BAαB/C		g-ray, ^{60}Co, 0.45 Gy/min	1.13	1	[93]
		0.045 Gy/min	0.87	1	[93]
BAαB/C	$CFU-S_7$	X-ray, 300 keV	0.79	1	[94]
		Neutrons 1 MeV	0.31	1	[94]
F_1/CBAx $C_{57}Bα/6$		γ-ray, ^{137}Cs	0.78	1	[95]
	$CFU-S_8$	γ-ray, ^{137}Cs	0.99 - 1.03	1	[96]
	$CFU-S_{11}$	γ-ray, ^{137}Cs	1.25 ± 0.08	1	[95]
	$CFU-S_{12}$	γ-ray, ^{137}Cs	1.13 - 1.16	1	[96]
		X-ray, 300 keV	0.95	1	[94]
		Neutrons, 1 MeV	0.36	1	[94]
	CFU-GM	γ-ray	1.79	0.94	[81]
			1.6 - 2.4	0.6-1.0	
		γ-ray	1.28	1	[97]
		X-ray	1.57	1.1	[82]
		γ-ray	1.19 ± 0.13	0.74 ± 0.47	[98]

Continued on next page.

Table 5.5. Radiosensitivity of the colony-forming cells of the bone marrow (continued).

Species	Type of cells	Type of radiation	D_0 (Gy)	n	Reference
	CFU-GM	γ-ray, ^{137}Cs, 5.4 Gy/min	0.9	2-3	[99]
		γ-ray, ^{137}Cs, 4.4 Gy/min	0.91-1.08	1	[100]
		Acute	0.42-1.14	1	[101]
		Fractional	0.72-0.94	1	[101]
		Acute	1.57-1.97	1	[89]
		Acute	1.04 ± 0.07	1	[102]
	Radiosensitive	γ-ray	0.1-0.5	1	[90, 91]
	Radioresistant	γ-ray	1.15-1.26	1	[90, 91]
		γ-ray, ^{137}Cs	1.03-1.18	1	[103]
		γ-ray, ^{60}Co, 0.45-0.83 Gy/min	1.10-1.30	1-1.2	[104]
		X-ray, 300 keV	0.72 ± 0.17	2.47 ± 0.28	[105]
		γ-ray, ^{60}Co, ^{137}Cs	0.91 ± 0.24	2.47 ± 0.28	[105]
		Neutrons	0.63 ± 0.22	1.34 ± 0.16	[105]
			0.78 ± 0.21	1.34 ± 0.16	[105]
9-day-old mice	CFU-GM		1.15 ± 0.01	1.34 ± 0.16	[105]
90-day-old mice			0.72 ± 0.07	1.34 ± 0.16	[106]
		γ-ray	0.89	1	[107]
	CFU-DC	γ-ray	1.37-1.97	1.0-1.2	[81]
		γ-ray	1.31-1.35	1.4	[108, 109]
		γ-ray, ^{60}Co	0.93	1	[110]
		Neutrons, 0.85 MeV	0.4 ± 0.03	0.7	[110]
		Neutrons, 0.35 MeV	0.25 ± 0.02	0.7	[110]
	CFU-DC_{bm}		1.2	1.8	[111]
	CFU-DC_s		1.2	2.0	[111]
	CFU-Er	X-ray	0.68	0.9	[82]
	CFU-Er	X-ray	0.74	1.8	[81]
		X-ray	0.53	0.8	[82]
	CFU-M	X-ray	1.2-1.3	1	[97, 102]
	CFU-K	γ-ray	2.01 ± 0.01	0.51 ± 0.008	[86]
		Neutrons	0.80 ± 0.01	0.95 ± 0.042	[86]
		γ-ray	1.6		[112]

Continued on next page.

Table 5.5. Radiosensitivity of the colony-forming cells of the bone marrow (continued).

Species	Type of cells	Type of radiation	D_0 (Gy)	n	Reference
	CFU-F	γ-ray, ^{137}Cs, 4.5 Gy/min	1.7	1	[83]
		X-ray, 200 keV	2.15-2.3	1.2-1.6	[113]
		X-ray	1.64	0.2	[114]
		Neutrons	1.36	1.0	[114]
Rats					
	CFU-GM	γ-ray, ^{137}Cs	0.94-0.97	4.1-5.2	[115]
	CFU-F	γ-ray, ^{60}Co			
	Type of colonies:				
	mixed		1.87	1.4	[116]
	solid		0.65	6.7	[116]
	crumbly		4.27	1.0	[116]
			1.67-1.79	1	[117]
	mixed		1.79	1	[118]
	solid		1.24	1	[118]
	crumbly		2.09	1	[118]
Guinea pigs					
	CFU-F	γ-ray, 2.0 Gy/min			
	mixed		1.22-1.28	2.5-3.5	[119]
	solid		1.41	1.0	[120, 121]
	crumbly		2.39	1.0	[120, 121]
Monkeys					
	CFU-GM	X-ray, 6 MeV	1.1	1	[122]
			0.9-1.6	1	[122]
		X-ray, 300 keV	0.6	1	[122]
Dogs					
	CFU-GM	γ-ray	0.64	0.98	[81]
			0.59-0.70	(0.8-1.1)	[81]
		X-ray			
	Blood		0.25 ± 0.26	1	[123]
	Bone marrow		0.60 ± 0.02	1	[123]
		X-ray, 0.56 Gy/min	0.61	1	[124]
		γ-ray, 1.20 Gy/min	0.70	1	[125]

Continued on next page.

Table 5.5. Radiosensitivity of the colony-forming cells of the bone marrow (continued).

Species	Type of cells	Type of radiation	D_0 (Gy)	n	Reference
	BFU-Er	X-ray	0.15 ± 0.002	1	[123]
	CFU-DC	γ-ray	1.44 ± 0.15	0.8	[124]
	CFU-F	X-ray	4.68 ± 0.36	0.8	[121]
			2.41 ± 0.38	1	[125]
			2.61 ± 0.4	1	[125]

CFU-S - CFU settling and growing in spleen
CFU-GM - CFU granulocyte-macrophage type
CFU-DC - CFU giving colonies in diffusion chambers
BFU-Er - erythrocyte burst-forming units
CFU-Er - CFU giving small erythrocyte colonies
CFU-M - CFU giving colonies of megakaryocytes
CFU-C - CFU forming colonies in cultures on agar
CFU-F - CFU forming colonies of fibroblasts in monolayer cultures in the bone marrow

body after irradiation with sublethal doses has three characteristic stages [133]. Several schemes describing the dynamics of radiosensitivity assessed from the response to repeated exposures have been proposed by now [134, 135]. Noteworthy is the scheme [133, 136] according to which the first stage of body recovery, lasting about 24 hours, involves the recovery of bone marrow cells after sublethal injuries and activation of the resting part of this population. In the course of the second stage, the pool of stem cells reaches or exceeds the normal level through repopulation. As a result, the radiosensitivity of the body recovers completely. Finally, damping oscillations of the number of stem cells about the normal level and, consequently, the corresponding variations of radiosensitivity of the body as a whole occur at the third stage of the recovery process.

It should be emphasized that the repair dynamics studied in detail on rodents is also peculiar to other mammalian species: rabbits, pigs, dogs, sheep, donkeys, monkeys, and presumably man [1, 134, 137-142].

The experiments [143] that have revealed a relationship between the number of hematopoietic stem cells and the individual radiosensitivity of animals deserve attention. It has also been noted that under the conditions of hematopoiesis stimulation by fasting, hemorrhage, or low atmospheric pressure, lower levels of radiosensitivity are manifested by animals possessing a higher hematopoietic activity [144].

Of special interest are studies of the role of sulfhydryl (SH) groups in characterizing of the individual radiosensitivity of the body [145, 146]. Five days before whole-body X-irradiation, the rear extremity of the rat was removed surgically, and the concentration of SH groups in the bone marrow was determined. This operation did not affect to any appreciable extent the

viability or radiosensitivity of the animals. For the purpose of quantitative analysis of the result, the rats were ranked according to the level of SH groups in bone marrow cells for each of the doses used (500-900 roentgen). Individual data on the level of SH groups were divided according to the median of the variation series into two parts: minus and plus groups. The $LD_{50/30}$ values calculated from the data obtained for the two groups of the animals were 559 ± 28 roentgen and 685 ± 30 roentgen. Thus, the existence of a correlation between the radiosensitivity of hematopoietic cells and the individual radiosensitivity of the body was first proved in a direct experiment.

The therapeutic effect of transplantation of syngeneic bone marrow and tissues of other hematopoietic organs to lethally irradiated animals depends mostly on the concentration of stem-type cells in the inoculates [147]. The therapeutic effect of peritoneal exudate cells or the leukocytic mass isolated from peripheral blood also correlates well with the concentration of CFU-C cells in them [148]. The therapeutic effect of irradiated bone marrow depends fully on the CFU-C level [149, 150]. CFU-C concentrates, prepared by centrifuging, enabled morphological characterization of the assumed pluripotent stem cells of mice, monkeys, and man; their high therapeutic efficiency was demonstrated [151, 152].

A comparison of the character of the damage caused by nonuniform and uniform animal body irradiation showed that similar damage to the pool of hematopoietic stem cells led to an identical decrease in survival of animals in both groups [48, 153, 154].

An analysis of the data on the effect of different radioprotectors on the survival of animals and on the extent of damage to hematopoietic stem cells indicated that both the damage to the pool of stem cells and the death rate of animals decreased to an equal extent [155-158].

The existence of a correlation between the radiosensitivity of cells of the hematopoietic tissue and the radiosensitivity of the body on exposure to radiation within a certain dose range is shown by many experimental studies in which the criteria characterizing the condition of the hematopoietic system were used to predict the radiosensitivity of the body [159].

Thus, the data presented above testify to a correlation between the functional activity of the hematopoietic tissue and the response of the body to radiation.

Such correlations were revealed in the analysis of the dynamics of the intestinal form of radiation sickness and the dynamics of the pool of stem cells of the intestinal epithelium [133, 160, 161]. The technique of microcolonies was used for quantitative description of the radiosensitivity of these stem cells [162, 163]. It is now possible to consider the damage to stem cells of the intestinal epithelium as the determining factor in the death of an animal with the intestinal form of radiation sickness. These data corroborate the role of the intestine as the critical system in this form of damage [3, 141, 164, 165]. It

Table 5.6. Radiosensitivity of the colony-forming cells of the intestinal epithelium.

Species	Type of cells	Type of radiation	D_0 (Gy)	n	Reference
Mice					
	Stem cells of intestine	γ-ray	1.0-1.3	15-50	[155, 162, 163, 160-168]
CBA		γ-ray, ^{60}Co, 0.31 Gy/min	1.82 ± 0.3	1	[169]
CBAxC$_{57}$B/6		γ-ray, ^{60}Co, 0.31 Gy/min	1.45 ± 0.14	1	[169]
		γ-ray, ^{60}Co	1.08-1.09	1	[170]
LAF_1		^{4}He ions LTE keV/μm,			
		1.5	1.97	1	[171]
		2.0	2.01	1	[171]
		10.0	1.82	1	[171]
		X-ray	1.58	1	[171]
Hα/JCR		X-ray, 250 keV, 0.6 Gy/min	3.3	1	[172]
		X-ray	1.25	1	[173]
C3H		X-ray	1.61	6.86	[174]
		Neutrons, 6 MeV	0.82	1.47	[174]
		Electrons, 7 MeV	1.25	5.22	[174]
C3H		X-ray, 200 keV, 2.62 Gy/min	1.0	10	[175]
		Neutrons, 2 MeV, 0.92 Gy/min	0.7	1.0	[175]
		γ-ray, ^{60}Co, 0.89 Gy/min	3.75	1	[176]
		γ-ray, ^{137}Cs	1.85	8.43	[177]
Hybrids		X-ray, 200 keV, 1.3 Gy/min	1.07-1.09	58	[163]
		γ-ray, ^{137}Cs, 1.02 Gy/min	1.09	55	[178]

Continued on next page.

Table 5.6. Radiosensitivity of the colony-forming cells of the intestinal epithelium (continued).

Species	Type of cells	Type of radiation	D_0 (Gy)	n	Reference
Rats					
	Monolayer culture	X-ray, 1.8 Gy/min	0.2-5.0	1	[179]
		X-ray	1.1	1	[180]
	Epithelial stem cells of removed intestine	X-ray	1.8-2.4	1	[181]
Hamsters					
		X-ray	1.4	1	[180]
Gophers					
Awake	Stem cells	X-ray	1.33 ± 0.12	1	[182]
Hibernating or the first hour after waking		X-ray	4.87 ± 0.92	1	[182]

should be noted that the experimental D_0 values for the stem cells of the intestinal epithelium of animals of one species and of animals of different species vary within rather broad limits in different studies [155, 162, 163, 166-184] (table 5.6). As with CFU-C cells, the effect on stem cells of the intestine depends on the dose rate [185], oxygen [186, 187], radioprotection, and radiosensitization [155, 188, 189].

A comparison of the dynamics of residual damage in the intestinal syndrome by the method of repeated $LD_{50/7}$ exposures [133] with the dynamics of the number of stem cells in the crypts of the small intestine [184] revealed a strict correlation between the variations in the radiosensitivity of the body and the changes in the number of stem cells in the intestinal epithelium. This correlation is similar to that observed for CFU-C cells [167, 168]. A small number of highly radiosensitive cells ($D_0 \approx 0.1$ Gy) was found among the crypt-base cells, just as in bone marrow stem cells. It is possible that hyperradiosensitivity of the former cells is due to a certain stage of the cell cycle [190]. These data thus point to a correlation between the condition of the pool of stem cells in the crypts of the small intestine and the survival of the body on exposure to radiation in doses leading to the development of the intestinal form of radiation sickness.

With different forms of damage the responses of the critical systems to irradiation do have common features. Thus, RBE coefficients of different

radiation types correspond with the criteria of the hematopoietic and the intestinal forms of radiation sickness and the survival of corresponding stem cells [190-197]. The radiosensitivity of the body on exposure to radiation in doses leading to the development of the hematopoietic and intestinal forms of radiation sickness can also be judged from the $LD_{50/30}$ and $LD_{50/4}$ values for mice exposed to gamma and neutron radiation [191]. These values were 6.6 and 10.8 Gy for gamma irradiation and 2.3 and 2.9 Gy for neutron irradiation. The RBE coefficients on exposure to high-LET radiation in the intestinal form of radiation damage and the RBE coefficients for the hematopoietic form were 3.8 and 2.5, respectively [191-193, 195, 198].

Deaths of animals that involve damage to stem-type cells in the hematopoietic system correlate with deaths of animals that involve damage to stem-type cells in the intestinal system. The dose rate effect provides additional evidence for the validity of a correlation. It was shown that the change in the survival of animals depends completely on weakening the damage to stem cells in relevant cell systems at lower dose rates [134, 199-203]. It is noteworthy that on exposure to high-LET radiation with irradiation time not exceeding 24 hours, no dose rate effect was found as determined from mortality criteria [204, 205] nor from CFU-C cell survival criteria [194-206].

Different radiosensitivities of the critical systems manifested themselves in the analysis of threshold dose rates that led to the development of various forms of radiation sickness. Thus, the threshold or critical dose rates for the development of the hematopoietic, intestinal, and cerebral forms of radiation sickness are 0.06-0.07 roentgen/min, 0.6-0.8 roentgen/min, and 15-20 roentgen/min, respectively [207, 208].

An evaluation of the damage to stem cells on exposure to ionizing radiation within the lethal dose range LD_{10} - LD_{90} in both critical systems showed that the survival of stem cells in each system is 10^{-3}-10^{-2} [3, 209, 210]. The existence of the dependence between the level of stem cells that have retained their viability in the critical systems and the survival rate of animals after irradiation within a sufficiently broad range of doses is indicative of the stability of the initial proliferation rate of stem cells of the critical systems of the irradiated body. This rate appears to be almost independent of exposure dose or other factors [3, 210, 211].

5.4. Conclusion

Experimental data dealing with the species-specific and individual radiosensitivity of mammals and the relationship between the radiosensitivity of the body, its critical systems, and constituent cells have been analyzed in this chapter. The experimental material supports the validity of the models developed in chapters 1-4 of this report. This material also points to the possibility

of using the models to predict the effect of ionizing radiation on the population death rate not only of small laboratory animals but also of large mammals, including man.

The material presented in this chapter also makes it possible to outline the direction of further experimental studies aimed at comparing the radiosensitivity of critical systems with that of the whole body for different forms of radiation sickness. The need for gathering experimental data on the mutual influence of damage to the critical systems should be emphasized once more. These data will be of much importance in understanding the pathogenesis of radiation sickness for different types of radiation exposure and, hence, in predicting courses and outcomes.

Determining the radiosensitivity of stem cells of the critical systems of man involves certain difficulties, and it would be wise to determine in parallel loading tests the initial functional state of the critical system and its significance in the development of the initial individual radiosensitivity of the body. Already available are some data on forecasting individual radiosensitivity from the characteristics of the initial functional state of critical and regulatory systems and also on evaluating initial reactivity from the response to preliminary non-radiation influences [8, 212-215]. A continuation of these studies would confirm the approaches and direct ways to assess individual risk.

FIGURES

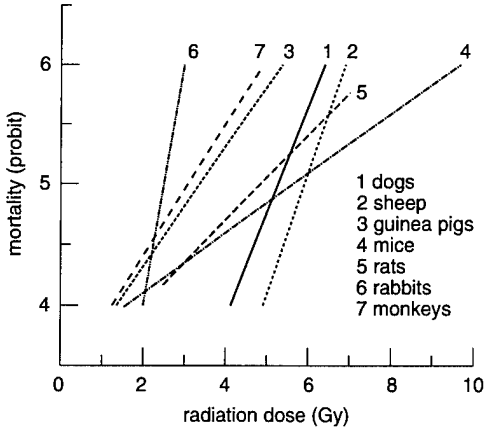

Fig. 5.1. The dose dependence of the mortality for different animals. The abscissa: the dose in Gy; the ordinate: the mortality (probit).

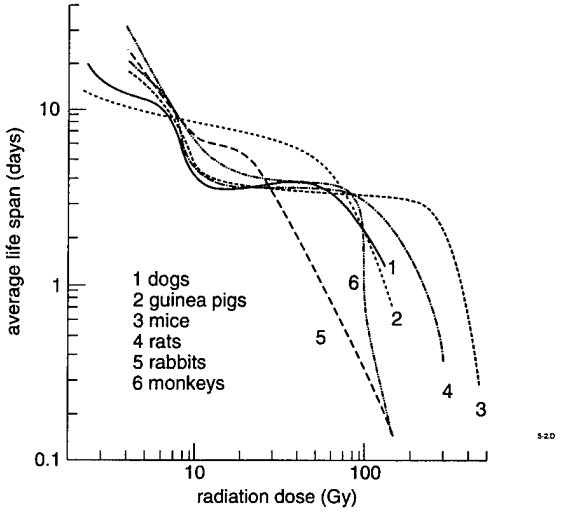

Fig. 5.2. The dose dependence of the average life-span for different animals. The abscissa: the dose in Gy; the ordinate: the life span in days.

REFERENCES

1. Bond VP, Fliedner TM, Archambeau JO (1965) Mammalian radiation lethality: A disturbance in cellular kinetics. New York: Academic Press

2. Konoplyannikov AG (1966) Some aspects of postirradiation recovery in animals. Informatsionnyi Byulleten Akademii Nauk SSSR; Radiobiologiya 9:108-111 (Russian)

3. Konoplyannikov AG (1978) The kinetics of the bone-marrow and intestinal epithelium cell populations following irradiation. Meditsinskaya Radiologiya 23(1):34-37 (Russian)

4. Konoplyannikov AG (1980) Stem cells of self-renewing systems as determinants of the animal survival in the acute stage of radiation injury. Radiatsionnaia Biologiia, Radioecologiia 3:5-38 (Russian)

5. Bond VP, Robinson CV (1967) A mortality determinant in nonuniform exposures of the mammal. Radiation Research Supplement 7:265-275

6. Robinson CV (1968) Relationship between animal and stem cell dose-survival curves. Radiation Research 35(2):318-334

7. Darenskaya NG (1970) Comparison of dose-effect relationships for different animal species and the importance of these data for human radiobiology. In: Radiobiological experiment and man. Moskalev YM (ed) Moscow: Atomizdat 50-62 (Russian)

8. Domshlak MP, Darenskaya NG, Koznova LB, Khrushchov VG (1954) Objectives of irradiation experiment design and some radiobiological data. Meditsinskaya Radiologiya 4(12):3-11 (Russian)

9. Broerse JJ, MacVittie TJ (eds) (1984) Response of different species to high dose total-body irradiation. Dordrecht: Martinus Nijhoff Publications, p. 286

10. Rajewskij B (1956) Strahlendosis und strahlenwirkung. Stuttgart: Georg Thieme Verlag, p. 280

11. Kimeldorf DJ, Hunt EL (1965) Ionizing radiation: Neuronal function and behavior. New York; London: Academic Press

12. Domshlak MP, Darenskaya NG, Pravdina GM (1960) Clinical features of early response in dogs after very high-dose irradiation. Byulleten Radiatsionnoi Meditsiny 2:33-40 (Russian)

13. Davydov BI, Ushakov IB, Fyodorov VP (1991) Radiation damage to the brain. Moscow: Energoatomizdat (Russian)

14. Quastler H (1956) The nature of intestinal radiation death. Radiation Research 4(2):303-320

15. Wilson BR (1963) Survival studies of whole-body X-irradiated germfree (axenic) mice. Radiation Research 20(3):477-483

16. Semyonov LF, Altukhova LI, Barkaya VS (1975) On the intestinal syndrome during protracted low-dose irradiation. In: Modern problems of radiation medicine and radiobiology. Moscow, pp. 97-98 (Russian)

17. Stiemon-Smoes MR, Ostave-Prignot M, Bandoux A, Wambersie A (1978) Tolerance de l'intestin de la souris à une irradiation par ^{60}Co a'feible debit implications en radiotherapie. Comptes Rendus des Seances de la Societe de Biologie et de Ses Filiales 172(4):774-778

18. Geraci JP, Jackson KL, Christensen GM, et al. (1977) Acute and late damage in the mouse small intestine following multiple fractionations on neutrons or X-rays. International Journal of Radiation Oncology, Biology, Physics 2(7):693-696

19. Guenlette J, Wambersie A (1978) Relation EBR/dose absorbee des neutrons d(50)Be determinee pour la tolerance precoce de la mugueuse intestinale de la souris. Comptes Rendus des Seances de la Societe de Biologie et de Ses Filiales 172(4):787-790

20. Sigdestad CP, Scott RM, Hagemann RF, Darden EB (1972) Intestinal crypt survival: The effect of ^{60}Co, 250 kVep X-rays, and fission neutrons. Radiation Research 52(1):168-178

21. Sigdestad CP, Connor AM, Scott RM (1976) Effect of chemical protectors on the response of the intestine to roentgen or fission neutron irradiation. Acta Radiologica: Therapy, Physics, Biology 15(5):401-409

22. Hornsey SH (1970) The relative biological effectiveness of fast neutrons for intestinal damage. Radiology 97(3):649-652

23. Andrews HL (1958) Species differences in response to high radiation doses. Radiation Research 9(4):469-477

24. Fedorovskii LL (1974) Some data on the contribution of the hemopoietic tissue to the mechanism of rat death within 3.5-5 days under conditions of nonuniform irradiation. Radiobiologiya 14(2):215-219 (Russian)

25. Nelson JM, Shellabarger CJ, Abrams GD (1969) Gastrointestinal radiation injury in the mongolian gerbil. Radiation Research 39(2):526-527

26. Brecher G, Smith WW (1955) Gastrointestinal injury from whole body irradiation in hamsters. Radiation Research 3(2):216

27. Bond VP, Robertson JS (1964) Comparison of the mortality response of different mammalian species to X-rays and fast neutrons. In: Biological effects of neutron and proton irradiation, vol 2. Vienna: International Atomic Energy Agency, pp. 365-373

28. Altukhova LN (1971) Specific features of the intestinal stage of radiation sickness in guinea pigs. Radiobiologiya 11(4):550-554 (Russian)

29. Brace KC, Austin HL, Thompson EC (1954) Early radiation death in guinea pigs. American Journal of Physiology 179(2):386-389

30. Allen RG, Brown FA, Logie LC et al. (1960) Acute effects of X-radiation in primates. Radiation Research 2(5):532-559

31. Wilson SG (1959) Radiation-induced gastrointestinal death in the monkey. American Journal of Pathology 35(6):1233-1251

32. Brecher G, Cronkite EP (1951) Lesions of the alimentary tract of dogs exposed to whole-body X-radiation of 300 to 3,000 r. American Journal of Physiology 27(4):676-677

33. Shively JN, Michaelson SM, Howland JW (1958) The response of dogs to bilateral whole-body ^{60}Co irradiation. I. Lethal dose determination. Radiation Research 9(4):445-450

34. Shively JN, Michaelson SM, Howland JW (1961) The response of dogs to bilateral whole-body ^{60}Co irradiation. II. Pathophysiological manifestations. Radiation Research 15(3):319-328

35. Mao Bingzhi, Chen Dezheng, Zhu Xinhua et al. (1985) Gastrointestinal radiation syndrome in dogs irradiated with 10 Gy ^{60}Co gamma-rays. Chinese Journal of Radiology and Medical Protection 5(1):27-29

36. Cronkite EP (1951) The diagnosis, prognosis, and treatment of radiation injuries produced by atomic bombs. Radiology 56(5):661-668

37. Shively JN, Andrews HL, Miller HP, et al. (1959) Responses of swine to high doses of radiation. Proceedings of the Society of Experimental Biology and Medicine 101(1):74-77

38. Daburon F, Remy J, Nizza P (1972) Etude du syndrome gastrointestinal d'irradiation chez le porc. Strahlentherapie 3:343-361

39. Dygai AM, Buznik DV, Shakhov VP, Goldberg ED (1992) Structural-functional organization of the bone marrow following lethal irradiation and transplantation of syngenic hemopoietic cells. Radiobiologiya 32(4):575-579 (Russian)

40. Dygai AM, Buznik DV, Bogdashin IV, Agafonov VI (1994) The production of *JL*-1, *JL*-3, *CSA* by bone marrow nuclears during bone marrow haemopoiesis after lethal irradiation and syngenic bone marrow transplantation. Radiatsionnaia Biologiia, Radioecologiia 34(2):220-224 (Russian)

41. Marx JL (1989) Bone marrow transplants approved. Science 244(4906):768

42. Kashirin VS (1973) Quantitative features of radiation injury in rats irradiated with various parts of their bodies shielded. Author's summary of candidate's thesis (Medicine). Moscow (Russian)

43. Plotnikova ED (1976) Cell foundation of the bone-marrow syndrome. Radiation injury of man. Moscow: Atomizdat 5:10-21 (Russian)

44. Anokhin YN (1981) Lymphocyte migration in the organism exposed to internal and external irradiation. Author's summary of candidate's thesis (Medicine). Obninsk (Russian)

45. Kostesha NY, Darenskaya NG (1990) Intestinal form of radiation sickness and the contribution of damaged stomach to its development. Tomsk: Tomsk University Press (Russian)

46. Sullivan MF, Ruemmler PP, Beamer JL, Mahony TD (1975) Intestinal radiation injury: The lower bowel syndrome. Radiation Research 62(3):579

47. Zaitseva RN (1974) Quantitative pattern and features of radiation injury to partially exposed rats. Author's summary of candidate's thesis (Biology). Moscow (Russian)

48. Avetisov GM (1976) Specific features of radiation injury to mammals exposed to nonuniform external irradiation. Author's summary of doctoral thesis (Biology). Leningrad (Russian)

49. Fedorovskii LL (1981) Pathogenetic aspects of the postirradiation gastrointestinal syndrome. In: Mechanisms of radiation pathology. Moscow, pp. 71-81 (Russian)

50. Fedorovskii LL (1976) Pathophysiological analysis of the intestinal form of radiation sickness. Radiation injury to the organism. Moscow: Atomizdat 5:22-36 (Russian)

51. Sullivan MF, Marks S, Hackett PL, Thomson RC (1959) X-irradiation of exteriorized or *situ* intestine of the rat. Radiation Research 11(5):653-666

52. Domshlak MP, Sedov VV, Nevskaya GF, Petrov PM (1964) On the mechanism of animal mortality from extremely acute radiation sickness: Pathogenesis, experimental preventive measures and treatment of radiation injury. Moscow: Meditsina, pp. 153-162 (Russian)

53. Nevskaya GF (1966) Acute intestinal radiation mortality: Analysis of the dose curve plateau data. In: Problems of general radiology. Moscow: Atomizdat, pp. 175-180 (Russian)

54. Domshlak MP, Khrushchev VG, Volokhova NA, et al. (1960) Species specific features of the response to high-dose irradiation. Byulleten Radiatsionnoi Meditsiny 2:24-33 (Russian)

55. Kudryavtsev VD (1983) Recovery of the critical systems and delayed effects related to the intestinal form of the acute radiation injury. Author's summary of doctoral thesis (Medicine). Obninsk (Russian)

56. Osborne JW (1962) Modification of intestinal radiation death by surgical means. Radiation Research 17(1):22-33

57. Osborne JW, Prasad KN, Zimmerman GR (1970) Changes in the rat intestine after x-irradiation of exteriorized short segments of ileum. Radiation Research 43(1):131-142

58. Darenskaya NG, Timofeev VI (1960) Comparative characterization of the fulminant form of radiation sickness from exposures to 500 and 2,000 R/min dose-rates. Byulleten Radiatsionnoi Meditsiny 2:53-63 (Russian)

59. Langham W, Woodward KT, Rothermel SM, et al. (1956) Studies of the effect of rapidly delivered massive doses of X-ray on mammals. Radiation Research 5(4):404-432

60. Darenskaya NG (1952) Radiation sickness after whole-body and partial experimental irradiation of rats. Author's summary of candidate's thesis (Medicine). Moscow (Russian)

61. Semyonov LF (1958) On the development of the most acute radiation sickness. Med Radiologiya 3(3):70-77 (Russian)

62. Thorp JW, Chaput RL, Kovacic RT (1970) Performance of miniature pigs after partial body irradiation. Aerospace Medicine 41(4):374-382

63. Thorp JW, Young RW (1971) Monkey performance after partial body irradiation. Aerospace Medicine 42(5):503-507

64. Vogel FS (1962) Effects of high dose gamma radiation on the brain and individual neurons. In: Haley TJ, Snider RS (eds) Response of the nervous system to ionizing radiation. New York; London: Academic Press, 249-260

65. Thorp JW (1969) Head shielding protection for beagles exposed to supralethal doses of pulsed mixed gamma neutron radiations. Aerospace Medicine 40(7):759-761

66. Davydov BI, Ushakov IB (1987) Ionizing radiation and the brain: The behavior and structural-functional patterns. In: Advances of science and technology: Radiation biology. Moscow (Russian)

67. Kuzina VA (1979) The effect of shielding and autotransplantation of the bone marrow on the functional state of the intestines in irradiated rats. Radiobiologiya 19(4):626-630 (Russian)

68. Pozharisskaya TD, Sokolova EN, Teslenko VM, et al. (1979) Quantitative assessment of the effect of intestine shielding on the hemopoietic tissue repair after irradiation. Abstracts of the 7th USSR Conference on Recovery and Compensatory Processes in Radiation Injury. Leningrad, p. 87 (Russian)

69. Fedorovskii LL (1974) The effect of bone-marrow autotransplantation on the postirradiation recovery of the intestine under nonuniform irradiation causing 35- to 5-day death in rats. Biulleten Eksperimentalnoi Biologii i Meditsiny 77(2):28-31 (Russian)

70. Fedorovskii LL (1974) Some data of the role of the hemopoietic tissue in the mechanism of the 3.5- to 5-day rat mortality under nonuniform irradiation. Radiobiologiya 14(2):295-297 (Russian)

71. Carr KE, Hume SP, Nelson AC, et al. (1991) Comparison of partial and whole-body X-irradiated small intestine. International Journal of Radiation Biology 60(6):942

72. Darenskaya NG (1977) The radiosensitivity and critical systems of the organism during exposure to external irradiation. In: Biomedical aspects of radiation safety. Moscow: Institute of Biophysics, pp. 82-92 (Russian)

73. Gudkov IN (1984) Heterogeneity of the critical systems as the principal factor of their radiosensitivity. In: Mechanisms of radiation pathology. Moscow, pp. 103-110 (Russian)

74. Kudryashov YB (1987) Radiation injury to "critical systems." In: Radiation injury. Moscow: Moscow University Press, pp. 5-72 (Russian)

75. Silini D (1972) Cellular aspects of radiation injury to the bone marrow: Primary and initial processes of the biological effect of radiation. Moscow: Nauka, pp. 99-111 (Russian)

76. Konoplyannikov AG (1984) Radiobiology of the stem cell. Moscow: Energoatomizdat (Russian)

77. Belousova OI, Gorizontov PD, Fedotova MI (1979) Radiation and the blood system. Moscow: (Russian)

78. Gruzdev GP (1968) Injury to the blood-forming tissue in acute radiation pathology. Moscow: Meditsina (Russian)

79. Gruzdev GP (1988) Acute radiation-induced bone-marrow syndrome. Moscow: Meditsina (Russian)

80. Zherbin EA, Chukhlovin AB (1989) Radiation hematology. Moscow: Meditsina (Russian)

81. Hendry JH, Lord BJ (1983) The analysis of the early and late response to cytotoxic insults in the haemopoietic cell hierarchy. In: Cytotoxic insult to tissue: Effects on cell lineages. Potten CS, Hendry JH (eds), Edinburgh: Churchill Livingstone, pp. 1-66

82. Jmai J, Nakano J (1987) *In vivo* radiosensitivity and recovery pattern of the hematopoietic precursor cells and stem cells in mouse bone marrow. Experimental Hematology 15(7):890-897

83. Hendry JH, Wang SB, Testa NG (1984) Greater sparing of stromal progenitor cells than of haemopoietic stem cells in -irradiated mouse marrow using low dose-rates. Biomedicine and Pharmacotherapy 38(7):356-358

84. Magauto JC, Bueren JA, Nieto M (1984) Radiosensibilizacion hipertermica de las cellulas cepa hematopoyeticas de medula osea de raton "CFU-S." Reviews of Experimental Oncology 31(1):49-55

85. Meijne EJM, Ploemecher RE, Vos O, Huiskamp R (1990) The radiosensitivity of primitive murine haemopoietic stem cells. International Journal of Radiation Biology 58(6):1051

86. Millard RE, Blackett NM (1981) Radiosensitivity and recovery of two murine haemopoietic progenitor cell populations following gamma rays and neutrons. Acta Haematologica 66(4):226-232

87. Shen Ming-Yan, Chu Jen Bao (1988) Finding threshold values for residual hemopoietic stem cells in mice after a high-dose ^{60}Co irradiation. Acta Biologiae Experimentalis Sinica 21(1):57-62

88. Zhukova NA, Palyga GF, Maksimenko AA, et al. (1983) The effect of sodium chloride solution on the hemopoietic stem cell pool in healthy and irradiated mice. Radiobiologiya 23(3):395-397 (Russian)

89. Shvets VN (1978) Thymocyte-related modification of radiation-induced changes in the hemopoietic stem cell pool. Radiobiologiya 18(6):854-859 (Russian)

90. Shvets VN (1983) Two subpopulations of colony-forming cells with differing radiosensitivities. Radiobiologiya 23(1):94-97 (Russian)

91. Shvets VN, Shafirkin AV (1979) Radiosensitivity of blood-forming stem cells undergoing cloning in the bone-marrow and spleen. Radiobiologiya 19(1):48-53 (Russian)

92. Evans RG, Wheatley CL, Nielsen JR (1988) Modification of radiation-induced damage of bone marrow stem cells by dose rate, dose fractionation, and prior exposure to cytoxan as judged by the survival of CFU: Application to bone marrow transplantation (BMT). International Journal of Radiation Oncology, Biology, Physics 14(3):491-495

93. Glasgow GO, Beetham KL, Mill WB (1981) Dose rate effects on the hematopoietic stem cells of BALB/c mice. International Journal of Radiation Oncology, Biology, Physics 7(9):1257

94. Meijne EJM, Davids JAG, Ploemacher RE, et al. (1989) The effects of 1 MeV fission neutrons and X-rays on murine haematopoietic cells. International Journal of Radiation Biology 55(6):1040

95. Gan OI, Konoplyannikov AG (1989) Comparative radiosensitivity of CFU@ from the bone marrow and embryonic liver of mice forming 7-day and 11-day colonies. Biulleten Eksperimentalnoi Biologii i Meditsiny 107(1):93-95 (Russian)

96. Trishkina AI, Konoplyannikov AG (1992) Radiosensitivity of blood-forming stem cells of mice forming spleen colonies 8 and 12 days after transplantation of bone-marrow cells (CFU-S_8 and CFU-S_{12}). Radiobiologiya 32(2):207-210 (Russian)

97. Nakeff A, McLellan WL, Bryan J, Valeriote FA (1979) Response of megakaryocyte, erythroid and granulocyte-macrophage progenitor cells in mouse bone marrow to gamma-irradiation and cyclophasphamide. In: Experimental hematology today 1979. Baum SJ, Ledney GD (eds) New York: Springer-Verlag, pp. 99-104

98. Butomo NV, Pegov AA (1979) Radiosensitivity of the endogenous colony-formation function in intact and preliminarily irradiated mice. Radiobiologiya 19(1):140-142 (Russian)

99. Hendry JH, Lajtha LG (1975) Response of mouse bone marrow to low dose rates, split acute doses, and multiple daily fractions. In: Cell survival after low doses of radiation: Theoretical and clinical implications. Proceedings of the 6th L. H. Gray Conference. London, 1974; pp. 308-312

100. Hendry JH, Schofield R, Bwire NEB (1986) Radiosensitivity of murine hemopoietic colony-forming units assayed *in situ* in the rib and in other marrow sites. Radiation Research 105(3):370-378

101. Tan S, Huang Q, Zhang S, Xiang R (1984) Radiation injury and restoration of hematopoietic stem cells induced by fractionated and single doses of irradiation. Chinese Journal of Radiology and Medical Protection 4(2):14-17

102. Shvets VN, Chertkov KS, Seslavina LS (1975) Determination of the number and radiosensitivity of bone-marrow cells forming erythroid-, myeloid-, and megakaryocitic-type colonies in the spleen. Radiobiologiya 15(2):197-201 (Russian)

103. Baird MC, Hendry JH, Testa NG (1990) Radiosensitivity increases with differentiation status of murine hemopoietic progenitor cells selected using enriched marrow subpopulations and recombinant growth factors. Radiation Research 123(3):292-298

104. Belletti S, Gallini RE, Magno L (1979) The effects of dose rate on hematopoietic stem cells: Preliminary results. International Journal of Radiation Oncology, Biology, Physics 5(3):403-405

105. Broerse JJ, Engels AC, Lelieveld P, et al. (1971) The survival of colony-forming units in mouse bone-marrow after *in vivo* irradiation with *D-T* neutron, X- and gamma-radiation. International Journal of Radiation Biology 19(2):101-110

106. Gerber GB, Maes J (1981) The *in vitro* radiosensitivity of hemopoietic stem cells from control and preirradiated infant mice. Radiation and Environmental Biophysics 19(3):173-179

107. Lu Zhaoyang, Mao Zijun, Yiu Zhiwei (1989) The effects of the granulocytopoiesis-inhibiting factor on normal and irradiated CFU-GM cells of the mouse brain. Chinese Journal of Radiology and Medical Protection 9(2):107-110

108. Kaplan VP, Kolesnikov AI, Konoplyannikov AG, et al. (1983) Radiosensitivity of CFU-DC in the mouse bone marrow during gamma-irradiation under varying oxygenation conditions. Radiobiologiya 23(4):480-483 (Russian)

109. Kaplan VP, Konoplyannikov AG, Kolesnikova AI (1985) Radiosensitivity and postirradiation dynamics of the granulocyte-macrophage precursors (CFU-DC) in the bone marrow of CBA and BAB/c mice. Radiobiologiya 25(4):536-539 (Russian)

110. Konoplyannikov AG, Kolesnikova AI, Kaplan VP, Mishanskaya NI (1980) The effect of neutrons of two different energies (0.35 and 0.85 MeV) on mouse bone-marrow cells capable of forming granulocytic-macrophagal colonies in diffusion chambers. Radiobiologiya 20(6):911-913 (Russian)

111. Lepekhina LA, Kolesnikova AI, Konoplyannikov AG (1985) Radiosensitivity of clonogenic granulocyte-macrophage precursor cells in the bone marrow and spleen of mice with tumors. Radiobiologiya 25(6):752-755 (Russian)

112. Zherbin EA, Kolesnikova AI, Konoplyannikov AG, Khoptynskaya SK (1978) The study of radiosensitivity of human bone-marrow cells forming colonies in agar cultures. Radiobiologiya 18(4):613-615 (Russian)

113. Werts ED, Gibson DP, Knapp SA, DeGowin RL (1980) Stromal cell migration precedes hemopoietic repopulation of the bone marrow after irradiation. Radiation Research 81(1):20-30

114. Xu CX, Hendry JH, Testa NG (1983) The response of stromal progenitor cells in mouse marrow to graded repeated doses of X-rays or neutrons. Radiation Research 96(1):82-89

115. Comas FV (1979) The radiosensitivity of rat bone-marrow cells. International Journal of Radiation Biology 17(6):549-557

116. Kal'sina SS (1992) Radiobiological characteristic of clonogenic cells of the hemopoetic stroma (CFU-F) in rats and the effects of some modifiers. Author's summary of candidate's thesis (Biology). Obninsk (Russian)

117. Kozhevnikov VV, Baranova LN, Popovskikh AS (1979) Radiosensitivity of bone marrow stromal stem cells and survival of an irradiated organism. In: Radiosensitivity and recovery processes in animals and plants. Tashkent, pp. 61-62 (Russian)

118. Kolesnikova AI, Konoplyannikov AG, Kal'sina SS, et al. (1993) The ability of clonogenic precursor cells of the hemopoietic stroma (CFU-F) in rats to restoration after irradiation. Radiobiologiya 33(2):236-243 (Russian)

119. Konoplyannikov AG, Rudakova SF (1973) Radiosensitivity of guinea pig bone-marrow cells forming fibroblast colonies in single-layer cultures. Radiobiologiya 13(1):138-140 (Russian)

120. Gruzdev GP, Kovrigina AM, Chistopol'skii AS (1989) A study of the pattern of maximal activity and latent potentialities of the bone marrow CFU-F following irradiation. Radiobiologiya 29(5):615-620 (Russian)

121. Kovrigina AM, Gruzdev GP (1991) A study of the pattern of compensatory response of the bone marrow fibroblast precursor cells to ionizing radiation. Patologicheskaia Fiziologiia i Eksperimentalnaia Terapiia 3:20-23 (Russian)

122. Wielenga JJ, Van Gils FCJM, Wagemaker G (1989) The radiosensitivity of primate haemopoietic stem cells based on *in vivo* measurements. International Journal of Radiation Biology 55(6):1041

123. Kreja L, Baltschukat K, Nothdurft W (1989) *In vitro* studies of the sensitivity of canine bone-marrow erythroid burst-forming units (BFU-E) and fibroblast colony-forming units (CFU-F) to X-irradiation. International Journal of Radiation Biology 55(3):435-444

124. Nothdurft W, Steinbach KH, Fliedner TM (1983) *In vitro* studies on the sensitivity of canine granulopoietic progenitor cells (GM-CFC) to ionizing radiation: Differences between steady-state GM-CFC from blood and bone marrow. International Journal of Radiation Biology 43(2):133-140

125. Wilson FD, Stitzel KA, Klein AK, et al. (1978) Quantitative response of bone marrow colony-forming units (CFU-C and PFU-C) in weanling beagles exposed to acute whole-body-γ irradiation. Radiation Research 74(2):289-297

126. Neumann HA, Lohr GW, Fauser AA (1981) Radiation sensitivity of pluripotent hemopoietic progenitors (CFU-GEMM) derived from human bone-marrow. Experimental Hematology 9:742-744

127. Pazderuik TL, Nishimura T (1978) Radiosensitivity of different B and T subpopulations of lymphocyte in the spleen. Agents and Actions 8(3):229-237

128. Till JE, McCulloch EA (1963) Early repair processes in marrow cells irradiated and proliferating *in vivo*. Radiation Research 18(1):96-105

129. Till JE, McCulloch EA (1964) Repair processes in irradiated mouse hematopoietic tissue. Annals of the New York Academy of Sciences 114(1):115-125

130. Kovalev YP, Plotnikova ED, Eidus LK (1971) Studies of the recovery in the mammalian critical systems responsible for various forms of mortality. Radiobiologiya 11(2):105-201 (Russian)

131. Konoplyannikov AG (1972) The effect of actinomycin D on early postirradiation cell repair in irradiated animals. Doklady Akademii Nauk 206(4):978-980 (Russian)

132. Porteous DD, Lajtha LG (1968) Restoration of stem cell function after irradiation. Annals of the New York Academy of Sciences 149(1):151-155

133. Kovalev VV (1971) The mechanism of postirradiation recovery in mammals. Author's summary of candidate's thesis (Biology). (Russian)

134. Akoev IG (1970) Problems of postirradiation recovery. Moscow: Atomizdat (Russian)

135. Darenskaya NG, Koznova LB, Akoev IG, Nevskaya GF (1968) Relative biological effectiveness of radiations: The irradiation time factor. Moscow: Atomizdat (Russian)

136. Corp MJ, Mole RH (1966) The kinetics of recovery during the first few weeks after whole-body X-irradiation of mice. International Journal of Radiation Biology 11(1):69-86

137. Davidson GO (1960) Biological effects of whole-body gamma radiation on human beings. Baltimore: Johns Hopkins Press

138. Ainsworth EJ, Leong GF (1966) Recovery from radiation injury in dogs as evaluated by the split-dose technique. Radiation Research 29(1):131-142

139. Andrews GA (1967) Radiation accidents and their management. Radiation Research 7:S390-S397

140. Kohn HJ, Kallman RF (1957) Acute lethality studies with the rat: The LD_{50} death rate and recovery rate. Radiation Research 7(1):85-97

141. Krebs JS, Brauer RW (1969) Comparative accumulation of injury from X-, gamma- and neutron-irradiation. The position of theory and experiment. In: Biological effects of neutron and proton irradiation. Vienna: JAEA (2):347-364

142. Domshlak MP, Grigor'ev YG, Darenskaya NG, et al. (1966) Repair of radiation injuries in the radiological clinic. Med Radiologiya 11(11):36-40 (Russian)

143. Smith LH, Willard HG (1969) Alteration of haemopoietic tissues as a factor indicating radiosensitivity of the mouse. American Journal of Physiology 216(3):493-498

144. Sugahara T, Tanaka T, Vacek A (1967) Hematopoietic stimulation and radiosensitivity in mice. Journal of Radiation Research 8:152-160

145. Le Suan T (1975) A study of the role of endogenic thiols in body and cell radiosensitivity. Author's summary of doctoral thesis (Biology). Moscow: Institute of Developmental Biology (Russian)

146. Le Suan T (1971) The role of endogenous thiols in mammalian radiosensitivity. Izvestiia Akademii Nauk. Seriia Biologicheskaia 2:212-220 (Russian)

147. Petrov RV, Zaretskaya YM (1970) Radiation immunology and transplantation. Moscow: Atomizdat, p. 544 (Russian)

148. Cole LJ (1963) Hemopoietic restoration in lethally X-irradiated mice injected with peritoneal cells. American Journal of Physiology 204(2):265-267

149. McCulloch EA, Till JE (1960) The radiation sensitivity of normal mouse bone marrow cells, determined by quantitative marrow transplantation into irradiated mice. Radiation Research 13(1):115-125

150. Till JE, McCulloch EA (1961) A direct measurement of the radiation sensitivity of normal mouse bone marrow cells. Radiation Research 14(2):213-222

151. Dicke KA, Löwenberg B, Schaefer UW (1972) Haemopoietic restoration of lethally irradiated monkeys by purified CFU-C concentrates. In: Annual report TNO - Rijswijk: Organization Health Research TNO, pp. 149-150

152. Van Bekkum DW, Dicke KA, Maat B, Van Noord MJ (1970) Isolation and morphological characterization of a candidate haemopoietic stem. In: REP-Annual report. Rijswijk: Organization Health Research TNO, pp. 123-125

153. Bond VP, Robinson CV (1967) A mortality determinant in nonuniform exposures of the mammal. Radiation Research 7:S265-S275

154. Darenskaya NG (ed) (1974) Biological effects of nonuniform exposures. Moscow: Atomizdat (Russian)

155. Abul' YA, Butomo NV (1975) Action of ß-methoxytryptamine, cystamine, and aminopropyl-aminoethylthiophosphate on radiosensitivity of stem haemopoietic cells. Radiobiologiya 15(5):766-775 (Russian)

156. Konoplyannikov AG, Konoplyannikova OA (1974) Comparison of radioprotective effects of ß-methoxytryptamine on mouse survival and yield of spleen colonies. Radiobiologiya 14(4):528-530 (Russian)

157. Cole LJ, Davis WE (1968) Chemical radioprotection of hemopoietic colony-forming cells: Comparative effect of AET, anoxia, and urethan. Radiation Research 36(3):555-562

158. Vacek A, Rotkovska D, Sikulova J, et al. (1978) Protective effect of mixture of radioprotective substances (AET and mexamine) on the haemopoietic stem cells of mice. Strahlentherapie 154(6):424-429

159. Darenskaya NG (1965) On the relationship between radiosensitivity and the overall organism response. Radiobiologiya: Informatsionnyi Byulleten Akademii Nauk SSSR 8:12-14 (Russian)

160. Withers HR (1976) Colony-forming units in the intestine. In: Stem cells renewing cell populations. New York; San-Francisco; London: Academic Press, pp. 33-40

161. Konoplyannikova OA, Konoplyannikov AG (1973) Radiobiology of intestinal epithelium stem cells. Part 1. Assessment of the radioprotective effect of AET from the 4-5-day postirradiation mortality of mice and from intestinal epithelium stem cell survival. Radiobiologiya 13(4):531-536 (Russian)

162. Withers HR, Elkind MM (1968) Dose-survival characteristics of epithelial cells of mouse intestinal mucosa. Radiology 91(5):998-1000

163. Withers HR, Elkind MM (1970) Microcolony survival assay for cells of mouse intestinal mucosa exposed to radiation. International Journal of Radiation Biology 17(3):261-267

164. Hagemann RF, Sigdestad CP, Lesher S (1970) A quantitative description of the intestinal epithelium of the mouse. American Journal of Anatomy 129(1):41-51

165. Konoplyannikov AG (1979) The stem cells of the blood-forming system and of the small intestine epithelium as determinants of survival after the bone-marrow and the intestinal forms of radiation sickness: Radiosensitivity and recovery in animals and humans. Tashkent: FAN, pp. 61-62 (Russian)

166. Masuda L, Withers HR, Mason KB, Chen KY (1977) Single dose-response curves of murine gastrointestinal crypt stem cells. Radiation Research 69(1):65-67

167. Withers HR (1972) Cell renewal system concepts and the radiation response: Radiation effect and tolerance, normal tissue. In: Frontiers of radiation therapy and oncology, vol 6. New York: S. Karger, pp. 93-107

168. Withers HR (1976) Colony-forming units in the intestine. In: Cairnie AB et al. Stem cells renewing cell populations. New York; San Francisco; London: Academic Press, pp. 33-40

169. Konoplyannikova OA (1988) Radiobiology of intestinal epithelium stem cells: The effect of single and repeated preliminary sublethal irradiation on the dose dependence of the survival of small intestine epithelium stem cells. Radiobiologiya 28(1):35-38 (Russian)

170. Konoplyannikova OA, Konoplyannikov AG (1979) Radiobiology of intestinal epithelium stem cells: Part 3. The effect of radiation dose fractionation in mice of two age groups. Radiobiologiya 19(3):398-401 (Russian)

171. Alpen EL, Smith PP, McDonald M (1977) The effects of 910 MeV helium ions on intestinal crypt cells of the mouse. Radiation Research 70(3):643

172. Hagemann RF, Sigdestad CP, Lesher S (1972) Intestinal crypt survival total and per crypt levels of proliferative cellularity following irradiation: Role of crypt cellularity. Radiation Research 50(3):583-591

173. Hendry JH, Potten CS, Roberts NP (1980) The gastrointestinal syndrome and mucosal clonogenic cells: Relationships between target cell sensitivities, LD_{50} and cell survival and their modification by antibiotics. Radiation Research 96(1):100-112

174. Hornsey SH (1973) The effectiveness of fast neutrons compared with low-LET radiation on cell survival measured in the mouse jejunum. Radiation Research 55(1):58-68

175. Shiragai A, Sato F, Hiraoka T, et al. (1976) Kinetics of cell populations in the intestinal epithelium of mice after partial-body irradiation with X-rays and neutrons. International Journal of Radiation Biology 26(4):377-383

176. Thames HD, Withers HR, Mason K, Reid BO (1981) Dose-survival characteristics of mouse jejunal crypt cells. International Journal of Radiation Oncology, Biology, Physics 7(11):1591-1597

177. Tucker SL, Withers HR, Mason KA, Thames HD (1983) A dose-surviving fraction curve for mouse colonic mucosa. European Journal of Cancer and Clinical Oncology 19(3):433-437

178. Yan HC, Cairnie AB (1979) Cell-survival characteristics of intestinal stem cells and crypt of irradiated mice. Radiation Research 80(1):92-107

179. Sierra E, Sahu SK, Chiang YW, et al. (1985) Response of cultured IEC-17 normal rat intestinal epithelial cells to X-radiation. Radiation Research 102(2):213-223

180. Konoplyannikova OA (1979) Radiation injury of small intestine epithelium stem cells in mice of various strains, rats, and hamsters: Radiosensitivity and recovery in animals and humans. Tashkent: FAN, pp. 62-63 (Russian)

181. Hawke CJ, Sharp JG, Wright NA, et al. (1983) Development of intestinal epithelial microcolonies in the exteriorized ileum of the anesthetized rat. Radiation Research 94(3):645-646

182. Jaroslow BN, Fry RJM, Suhrbier KM, Sallese AR (1976) Radiosensitivity of ileum crypt cells in hibernating, arousing, and awake ground squirrels (*Citellus tridecemlineatus*). Radiation Research 66(3):566-575

183. Masuda K, Withers HR, Mason KA, Chen KY (1979) Single dose-response curves of murine gastrointestinal crypt stem cells. Radiation Research 69(1):65-75

184. Withers HR, Elkind MM (1969) Radiosensitivity and fractionation response of crypt cells of mouse jejunum. Radiation Research 38(3):598-613

185. Konoplyannikov AG, Konoplyannikova OA (1973) Radiobiology of intestinal epiphelium stem cells: Part 2. The effect of the gamma-irradiation dose rate on the 4-5-day mortality of mice and survival of small intestine epithelium stem cells. Radiobiologiya 13(6):834-838 (Russian)

186. Sigdestad CP, Hagemann RF, Scott RM (1973) The effects of oxygen on intestinal crypt survival in cobalt-60-irradiated mice. Radiation Research 54(1):102-109

187. Hornsey S (1970) The effect of hypoxia on the sensitivity of the epithelial cells of jejunum. International Journal of Radiation Biology 18(3):539-546

188. Sigdestad CP, Connor AM, Scott RM (1975) The effect of WR-2721 on intestinal crypt survival: Part 1. 4 MeV X-rays. Radiation Research 62(2):267-275

189. Dethlefsen LA, Riley RM (1979) The effects of adriamycin and X-irradiation on the murine duodenum. International Journal of Radiation Oncology, Biology, Physics 5(4):507-513

190. Potten CS, Schofield R, Lajtha LG (1979) A comparison of cell replacement in bone marrow, testis, and three regions of surface epithelium. Biochimica et Biophysica Acta 560(2):281-289

191. Konoplyannikov AG, Konoplyannikova OA (1976) Mortality and damage to stem cells in mice irradiated with fast neutrons: Application of neutrons in medicine. Obninsk: Institute of Medical Radiology, pp. 32-34 (Russian)

192. Sverdlov AG (1974) Biological effects of neutrons and chemical protection. Leningrad: Nauka (Russian)

193. Broerse JJ (1975) RBE values of fast neutrons for damage to organized tissue and physical perspectives: Radiation research, biomedical, chemical, and physical perspectives. New York; San Francisco; London: Academic Press, pp. 1073-1082

194. Davids JAG (1970) Bone marrow syndrome in CBA mice exposed to fast neutrons of 1.0 MeV mean energy: Effects of syngeneic bone marrow transplantation. International Journal of Radiation Biology 17(2):173-185

195. Hendry JH, Gilbert GW, Howard AK (1975) Values and gain factors of fast neutrons and X-rays for a mammalian cell system (CFU) *in vivo*. Radiation Research 61(3):504-512

196. Storer JB, Harris PS, Furchner JE, Langham WH (1957) The relative biological effectiveness of various ionizing radiations in mammalian systems. Radiation Research 6(2):188-288

197. Withers HR (1972) Cell renewal system concepts and the radiation response. In: Radiation effect and tolerance on normal tissue: Frontiers of radiation therapy and oncology, vol 6. New York: S. Karger, pp. 93-107

198. Konoplyannikov AG, Kudryashov YB (1966) On the biological effect of high-energy protons, fission neutrons, and gamma- and X-radiations. Zhurnal Obshchei Biologii 27(2):145-161 (Russian)

199. Konoplyannikov AG, Konoplyannikova OA (1973) The effect of irradiation dose rate on the radiation-induced mortality and survival of hemopoietic stem cells. In: Radiation and the organism. Obninsk: Institute of Medical Radiology, pp. 63-64 (Russian)

200. Puro EA, Clark GM (1972) The effect of exposure rate on animal lethality and spleen colony cell survival. Radiation Research 52(1):115-129

201. Stearner SP, Tyler SA (1963) Radiation mortality in the mouse: Model of the kinetics of injury accumulation. I. Protected doses in the 30-day lethal range. Radiation Research 20(4):619-630

202. Stearner SP, Sanderson MH, Tyler SA (1964) Radiation mortality in the mouse: Model of the kinetics of injury accumulation. II. Protected doses in the supralethal range. Radiation Research 23(1):104-118

203. Wambersie A, Dutreix J, Stienon-Smoes MR, Octave-Prignot M (1978) Influence du debit de dose sur la tolerance intestinale chez souris. Journal of Radiation Electrology 59(5):315-322

204. Clark JW, Jordan DL, Vogel HH (1957) Biological effects of fast neutron and gamma rays. American Journal of Roentgenology 17(3):524-530

205. Vogel HH, Clark JW, Jordan DL (1957) Comparative mortality after 24-hour, whole-body exposures of mice to fission neutron and cobalt-60 gamma-rays. Radiation Research 6(3):460-468

206. Carsten AL, Bond VP, Thompson K (1976) The RBE of different energy neutrons as measured by the haemopoietic spleen-colony technique. International Journal of Radiation Biology 29(1):65-70

207. Koznova LB, Lebedeva GA (1981) On the question of critical radiation dose rates in the development of intestinal radiation sickness form in mice. Radiobiologiya 21(2):293-298 (Russian)

208. Koznova LB (1992) Some data relating to the determination of critical radiation dose rates for certain responses to protracted and chronic radiation exposures. Reports of the Institute of Biophysics. Moscow (Russian)

209. Korogodin VI, Korogodina YV, Kharlamova LA, Kholeva SY (1967) Radiosensitivity of mammals and their cells. In: Radiation and the organism, vol 1. Obninsk: Institute of Medical Radiology, pp. 9-12 (Russian)

210. Blackett NM (1976) Cell cycle characteristics of haemopoietic stem cells. In: Stem cells renewing cell populations. New York; San Francisco; London: Academic Press, pp. 157-164

211. Hagemann RF, Lesher S (1973) Intestinal cytodynamics: Adductions from drug radiation studies. In: Drugs and the cell cycle. New York; London: Academic Press, pp. 195-217

212. Pospisil M, Vacha J (1983) Individual radiosensitivity, its mechanisms and manifestations. Praha: Academia

213. Darenskaya NG (1986) The feasibility of individual radiosensitivity prediction. Meditsinskaya Radiologiya 31(12):47-52 (Russian)

214. Korotkevich AO (1986) The endocrine status in the prediction of individual radiosensitivity. Meditsinskaya Radiologiya 31(12):83-87 (Russian)

215. Graevskaya BM (1972) Some results of the study of mammalian radiosensitivity. Radiobiologiya 12(3):323-325 (Russian)

CHAPTER 6

Variability of the Radiosensitivity of Mammals: Clinical Data

6. 1. Introduction

It is well known that individuals manifest a strong variation in both the characteristics of the initial condition and in the sensitivity to the damaging effects of different environmental factors. However, even now, regardless of the general biological importance of this problem, the knowledge of individual variability is fragmentary. Only a few generalizations of the problem have been reported [1-4] because of the intense labor and diversity of methods that must be used to evaluate individual variability in population studies.

Data on individual sensitivity to ionizing radiation are also available. The individual differences in the responses of animals of different species and of man to acute radiation effects in lethal doses have been covered rather extensively [5-14]. Approaches to forecasting individual responses to acute radiation effects have also been outlined [5, 8, 10, 15-28].

Recently, radiobiology researchers have paid more attention to the responses of the human body to ionizing radiation in low doses. This attention is due to the contact that people have with ionizing radiation in low doses as part of their professional activities in the use and development of nuclear technologies, medical applications, exposure to radiation at nuclear power stations and nuclear testing grounds, and finally, in emergency situations at nuclear power units. The number of studies on the effects of radiation in low doses has therefore increased in recent years. The health of individuals working with ionizing radiation sources (roentgenologists, radiologists, nuclear reactor personnel, employees at nuclear power stations and radiochemical plants, etc.) and of the population living in contaminated areas has been explored thoroughly. In the course of such studies virtually no attention has been paid to the role of individual radiosensitivity in the late response of the body to irradiation in low doses although individual features of the development of delayed effects are quite clearly detected [29, 30].

This chapter is dedicated to the generalization and analysis of clinical data on the effect of ionizing radiation in low doses on human health. Special attention is drawn to the data obtained in examinations of those individuals who had been engaged in eliminating the consequences of the Chernobyl disaster: "the cleanup crew". The analysis was based on the variability of individual radiosensitivity of the body, the principal concept of the mortality model developed in chapter 4 of this report.

6.2. Effect of Man's Individual Radiosensitivity in the Development of Different Radiation Syndromes

The evaluation of individual radiosensitivity to low doses involves a number of problems because the contribution of other nonradiation factors grows under these conditions. It was very difficult to recognize the radiation factor against the background of combined effects. In experimental conditions, however, the individual differences in responses to irradiation with 0.25-1.0 Gy doses can be detected clearly [31] .

Various indicators of the physical condition are used to characterize changes occurring in the human body on exposure to radiation in the low dose range: morbidity; biochemical, immunological, hematological, and physiological parameters; and the frequency and character of chromosomal aberrations. However, it is hard to obtain all these parameters in mass examinations because of the large volume of work involved. The lack of information on irradiation doses below 50 cGy is also noteworthy. The 25-cGy level was established as the maximum permissible dose for individuals recruited to participate in eliminating the consequences of the Chernobyl disaster. This dose is equal to the maximum permissible emergency dose for workers dealing with ionizing radiation sources [32, 33].

Medical surveys of the staffs of nuclear submarines, cosmonauts, roentgenologists, radiologists, operators of gamma-ray testing equipment, and personnel of nuclear power units and radiochemical plants do provide information on the effect of long-term exposure to ionizing radiation in low doses on the health of man. All these individuals experience long-term low-dose exposures to ionizing radiation in the course of their professional activities. Also available are the results of medical examinations of persons subjected to low-dose radiation during their residence in contaminated areas or in the course of eliminating the consequences of failures at nuclear reactors. There are many publications on the results of monitoring the physical condition of the Japanese affected by the explosions of nuclear bombs in Hiroshima and Nagasaki [34-41].

The major portion of the relatively few studies on the individual radiosensitivity of man was initially performed on patients with rare hereditary diseases

[42-44]. However, it soon became clear that the question of the individual radiosensitivity of man is also of importance for the whole population.

Published data on the different radiosensitivities of individuals that were revealed in the course of radiation therapy deserve special attention [45-47]. Unfortunately, only a few publications sufficiently report the large numbers of data that are required to reveal the individual features of the responses. One paper [48] presents interesting data concerning the responses of 263 patients subjected to single whole-body irradiation (15-299 roentgen) at a rate of 3.8 roentgen/min. The largest group (193 patients) was exposed to doses of 15-75 roentgen. All patients except one endured the irradiation well. One patient had a brief episode of vomiting on the day of irradiation. A group of 18 patients was exposed to a 100-roentgen dose, and the general responses of these patients was rather weak. A slight decrease in the lymphocyte count was noted in the blood of these patients. Another group of 12 patients was exposed to 125-175 roentgen; vomiting was noted in 7 patients.

The responses of 30 patients to single 200-roentgen exposures have been described in more detail [48]. The patients were irradiated in a sitting position; half of the dose was received by the right side of the body and the other half of the dose by the left side. Primary responses of nausea and vomiting were observed in 17 of the 30 patients. In two patients, multiple vomiting and drastic dehydration were so strong that hospitalization and therapeutic intervention were needed. The results of this study thus indicate that the differences in individual radiosensitivity of patients can be detected rather distinctly.

The results of observations of the responses of 270 patients subjected to whole-body irradiation for the treatment of various diseases have been published [49]. Fractional irradiation in this study was performed in a single dose of 17 roentgen, with the exposure rate varying between 1.5 and 0.37 roentgen/h. Responses were observed in 20% of the patients irradiated with total doses up to 100-300 roentgen.

Observations on individual radiosensitivity made by Professor N. G. Darenskaya and coworkers [50] are of interest. The authors observed the responses of 132 patients undergoing subtotal fractional X-irradiation in a radiological clinic. The condition of the patients before irradiation was satisfactory and made radiation therapy possible on an outpatient basis. Indications for subtotal irradiation were either the dissemination of lesions indicative of metastatic spreading or the existence of other prognostically unfavorable factors [51]. The dose rate was 3.6-5.0 roentgen/min. Single doses were 15, 25, or 50 roentgen. Patients were irradiated every day or, in a few cases, once in 2-3 days. Total doses were 100-500 roentgen per treatment course. It was found that an increase in total dose from 25 roentgen to 125 roentgen resulted in growth of the response rate from 18.6% to 64.2%. Of special interest are the

Table 6.1. Response incidence after acute subtotal irradiation.

Single dose (roentgen)	Number of patients	Without response	With response
15	6	5	1
25	97	79	18
50	5	1	4

data on responses to the first exposures (table 6.1). On irradiation in 15- and 25-roentgen doses, relevant manifestations were observed only in a small number of the most radiosensitive patients. Irradiation in larger single doses (50 roentgen) induced responses in most of the patients. It should be noted that in some patients the intensity of manifestations was so high after both the first and the repeated exposures that an ambulance had to be urgently called. Because of the high radiosensitivity of these patients, the experimenters had to discontinue the treatment. These observations testify to the existence of high sensitivity to radiation even in such low doses in about 8-10% of individuals. Conversely, about 14% of patients showed a rather high resistance to total doses up to 400-500 roentgen.

The foregoing data on the responses to doses of 15-20 roentgen [50] agree well with other observations [52]. Fifty healthy individuals were exposed to single 15-roentgen doses for the purpose of selecting those suitable for work in hazardous radiation conditions. They were considered radiosensitive if the leukocyte count decreased from the initial level by 33% or more. Decreases in the leukocyte count by 33%-50% were only noted in 15 individuals who showed a higher radiosensitivity than the other 35 people. No symptoms or other signs of general response manifestations were observed.

A comparison of data on fractionated and single-dose acute irradiation showed that the incidence of manifestations of the primary response at higher doses increases much faster and more clearly with single-dose irradiation [53].

Dynamic clinical observation and the results of clinical physiological studies of the nervous system of 80 irradiated children [54] clarify individual variations in the responses to irradiation. The children were subjected to applicational γ therapy for the treatment of skin hemangiomas. The hemangiomas were located in the region of the head in 61 children and on the trunk and extremities in 19 children. At the time of irradiation the age of most of the children (71%) was 2-10 months. Different regions of the brain cortex absorbed different cumulative doses after local γ irradiation of the skin of the head, face, or neck. The doses in the centers of the frontotemporal, parietotemporal, and parieto-occipital regions were determined. After irradiation in doses exceeding 1 Gy (1.1-5.75 Gy) and nonuniform irradiation of other regions in a dose below 1 Gy, the incidence of perturbations in the functional activity of

the nervous system and the incidence of cases with microsymptoms of organic damage to the nervous system were 92% and 63%, respectively. After doses above 0.5 Gy (0.67-0.95 Gy) and less than 0.5 Gy for other brain regions, the respective values were 68% and 31%; after doses exceeding 0.2 Gy (0.24-0.44 Gy) and less than 0.2 Gy for other regions, respective values were 41% and 6%; in doses less than 0.2 Gy and 0.1 Gy, they were 7% and 0%. These data also testify to pronounced differences in the individual radiosensitivity of various structures of the central sections of the nervous system of children under local irradiation conditions. Individual radiosensitivity manifested itself both in the incidence and intensity of manifestation of the changes observed and in their dose dependence.

We decided to focus our attention on the manifestations of individual variability of response to low radiation doses primarily in the cleanup crew, the individuals who had taken part in the elimination of the consequences of the Chernobyl disaster. This choice was made because the conditions of a comparatively short radiation exposure and the influence of other concomitant nonradiation factors (including psychoemotional stress) were almost identical in members of this group. At the first stage, we selected those studies that had provided data on the physical condition of the cleanup crew, referring mostly to somatic nononcologic diseases (table 6.2). We used publications containing any quantitative indicators of the morbidity of the cleanup crew. The data provided by different authors vary in the incidence rates of certain nosologic forms but show rather good agreement in the morbidity structure. However, some discrepancies between the data can be associated with the drawbacks in the methods of evaluating and recording the physical state of the cleanup crew, the use of different examination methods, and the absence of adequate control groups.

Regardless of all difficulties involved in mass examinations of individuals and the shortcomings noted above, these results show convincingly that only some of the cleanup crew had health problems. This fact demonstrates the differences in individual sensitivity to ionizing radiation and other concomitant factors.

Of particular interest are the data on the attitudes of the members of the cleanup crew to their conditions of health [74]. Disposition to intrapsychic feelings (affective emotional mood manifested in a depressed state, erethic asthenia-type reactions, retirement into the disease) was noted in 62% of the individuals examined. The response of an interpsychic tendency type was observed in 21% of the individuals; it was characterized by maladaptive behaviour leading in some instances to disturbances in their social functioning. A harmonic type of response to the disease was detected in 17% of the individuals examined; these individuals were characterized by minimal psychological and social maladaptation. They took a sober view of their conditions and were actively involved in facilitating the success of their treatment.

Table 6.2. Morbidity and performance among personnel engaged in operations to eliminate the Chernobyl disaster aftereffects (hereafter called the cleanup crew).

No.	Category of persons	No. of persons	Dose	Principal results	Reference
				Incidence of syndromes Syndrome — % Asthenia — 45 Neurocirculatory — 32 Gastrointestinal — 42 Hematologic — 69 Irritation of upper respiratory tract — 26	
1	Cleanup crew	-	Average 19 cGy (higher than 25 cGy for 2%)	Incidence of diseases Disease — % Chronic tonsillitis — 16 Chronic bronchitis — 4 Chronic ischemic heart disease — 5 Hypertension — 7 Chronic gastritis — 25 Chronic cholecystitis — 5 Ulcer — 4	[55]
2	Personnel of Chernobyl Nuclear Plant (CNP)	-	25-30 cSv	Before the Chernobyl disaster (1986), 9.9% of persons suffered from chronic diseases. In 1987 the percentage increased to 12%. The percentage of vegetative dystonias increased as did nervous system disorders (29% for acute viral respiratory infections, 29% for vegetative dystonias, 10% for nervous system diseases, 5% for respiratory system diseases, 6% for gastrointestinal diseases, and 3% for ENT diseases).	[56]
3	Cleanup crew group 1: immediately after the end of exposures	643	0.03 - 0.8 Gy	Distribution of diseases, % System affected — Group 1 — Group 2 Gastrointestinal — 12.8 — 37.8 Respiratory — 27.2 — 2.4 Urogenital — 1.0 — 1.6 Cardiovascular — 35.4 — 11.4 Blood-forming — 0.5 — - Tumors — - — 1.2 Others — 23.1 — 45.6	[57]
	Group 2: 1-1.5 years later	246	0.03 - 0.8 Gy	Half of the cleanup crew in group 2 showed the neurological syndromes of asthenia, emotional instability, and hypochondria.	

Continued on next page.

Table 6.2. Morbidity and performance among personnel engaged in operations to eliminate the Chernobyl disaster aftereffects (hereafter called the cleanup crew) (continued).

No.	Category of persons	No. of persons	Dose	Principal results	Reference
4	Cleanup crew (period of activity 1986-1989)	1,043 (aged 20-53 years)	10-45 cSv	Incidence of diseases — % Nervous and cardiovascular systems — 69.0 Gastrointestinal tract — 41.0 Osteochondrosis — 44.0 Respiratory system — 20.0	[58]
		127	Control group	No association was found with radiation dose, time period, duration at CNP, or unhealthy habits. The observed changes mainly included functional disorders of the central nervous system, hypokinetic cardiovascular response to exercise, decreased reserve muscular blood flow, deteriorated immune status, some hematologic and biochemical disorders. The incidence of diseases of organs and systems decreased. From 1987 through 1990 the number of functional disorders gradually diminished while the number of chronic organic diseases of various organs and systems increased.	
5	Cleanup crew	836	10-45 cSv	Clinical immunological tests revealed positive dynamics compared to the results of preceding examinations. Morbidity indices, % Type of disease — Examination: First / After 3 yrs Frequent acute respiratory disorders of viral origin — 11.4 / 6.34 Recurrent bacterial infections of skin and subcutaneous fat — 2.05 / 1.44 Increased fatigue syndrome — 41.6 / 24.52 Neurocirculatory dystonia — 8.92 / 5.36	[59]
6	Cleanup crew	218	0.2-47.8 cSv	Increased volume of the liver and bladder in 76%. Congestion of the pancreas in 20%. Increase of the cicatrization time for stomach and duodenal ulcers from 3 to 4 months.	[60]

Continued on next page.

Table 6.2. Morbidity and performance among personnel engaged in operations to eliminate the Chernobyl disaster aftereffects (hereafter called the cleanup crew) (continued).

No.	Category of persons	No. of persons	Dose	Principal results	Reference
7	Cleanup crew	-	0.1; 0.25-0.5 Gy	60.2% of subjects had the hyperkinetic type of central hemodynamics, 23.2% had the eukinetic type, and 16.6% hypokinetic type.	[61]
8	Cleanup crew	694 (aged 20-56 years)	19-68 cGy	Immediately after leaving the 30-km Chernobyl plant zone: healthy, 49.2%; changed blood composition, 7.2%; diagnosis unknown, 20.6%; chronic diseases, 17.1%; acute diseases, 5.9%. During systematic medical examinations from 1986 through 1991: healthy, 8.2%; changed blood composition, 0.5%; diagnosis unknown, 23.2%; chronic diseases, 68.1%.	[62]
9	Cleanup crew (period of activity 1986-1988)	142 (aged 20-40 years)	-	The vascular-type blood circulation predominated (62%), compared to controls (33%). Bicycle ergometer tests revealed performance deterioration and increased oxygen consumption per unit of work. This suggested a disorder of neurohumoral regulation of vascular tone and myocardial contractility.	[63]
10	Cleanup crew (period of activity 1986-1988)	108 (Control group of 30)	-	Premorbid condition represented by various syndromes found in 88% of subjects: vegatocardial syndrome, 44%; vegetonephrogenic syndrome, 8%; vegetogastroenterological syndrome, 32%; and other syndromes, 4%.	[64]
11	Cleanup crew	>3,000	-	Persons that had been exposed to irradiation in the CNP zone for 6 years showed disorders of the principal regulatory systems: immune, 66.0 ± 4.1%; nervous, 52.2 ± 5.0%; cardiovascular, 31.0 ± 4.1%; urogenital, 35.0 ± 2.2%. Latent disease signs were noted in 70% of cases. The combined effect of the factors of the CNP zone resulted in the decrement of nonspecific protective responses, development of endogenous intoxications, and homeostasis disorders. In 1986, the blood indices showed a dose dependence, while no such dependence was found in 1989.	[65]

Continued on next page.

Table 6.2. Morbidity and performance among personnel engaged in operations to eliminate the Chernobyl disaster aftereffects (hereafter called the cleanup crew) (continued).

No.	Category of persons	No. of persons	Dose	Principal results	Reference
12	Cleanup crew	1,500	Doses producing no acute effects	52% of subjects examined had hematological disorders with damaged white cells and their initial repression.	[66]
13	Cleanup crew	-	25-30 cGy	From 60% to 80% of subjects showed an enhanced (compared to the control) lability of the regulatory systems. It was regarded as an adaptive response to irradiation combined with other environmental factors.	[67]
14	Cleanup crew	8,115	-	Among circulatory diseases, hypertension and ischemia were found in 80% of subjects. The same percentage was noted for gastrointestinal diseases and vegetovascular dystonias.	[68]
15	Cleanup crew	120 aged 40.2 ± 0.3 years	-	Hypertension of 1st and 2nd degrees was found in 12%. Neurocirculatory dystonia was found in 88%, of which 60% suffered from hypertonic dystonias.	[69]
16	Cleanup crew from the North Caucasus Territory	-	-	Data supplied by the health centers of various territories showed considerable differences in the total morbidity among the cleanup crew: 101.4 cases in the Rostov Region and 815.3 cases in the Krasnodar Region per 1,000 persons. Comparison has shown that the level of total morbidity of the cleanup crew is much lower than that of the general population of the same age. Three major groups of diseases were noted in the total morbidity picture of the cleanup crew from the North Caucasus Territory: diseases of the (a) nervous system 34.6%; (b) respiratory system, 19.9%; and (c) skeletal-muscular system and the connective tissue, 10.6%. Analysis of the cardiovascular disorders revealed the young age of the affected cleanup crew, 34.4 ± 4.3 years.	[70]
17	Cleanup crew from Rostov-on-Don	114	-	Principal disorders responsible for temporal incapacitation were cardiovascular diseases (47%) followed by respiratory diseases (30%).	[71]

Continued on next page.

Table 6.2. Morbidity and performance among personnel engaged in operations to eliminate the Chernobyl disaster aftereffects (hereafter called the cleanup crew) (continued).

No.	Category of persons	No. of persons	Dose	Principal results	Reference
18	Cleanup crew from personnel employed in the Russian atomic industry	>15,000	Dose known for 55.4%, of which less than 0.1 Gy for 81.5%, 0.1-0.24 Gy for 17.1%, and 0.25 Gy for 1.4% of examined persons.	In 1991, the recorded total morbidity for the cleanup crew was 1,213.9 diseases per 1,000 persons and 1,123.2 diseases for all workers employed in the Russian atomic industry. Morbidity per 1,000 examined persons System affected — Cleanup crew — Control Respiratory — 430.9 — 348.4 Skeletal-muscular — 169.5 — 98.5 Gastrointestinal — 120.8 — 103.3 Blood circulation — 112.8 — 117.3 Nervous system and sense organs — 99.5 — 139.3 Blood and blood-forming organs — 3.8 — 3.6 No clear-cut correlation with the dose was established.	[72]
19	Cleanup crew of the Russian Federation	102,890	Average dose of 12.5 cGy. Most doses in 1986-1987 exceeded 5 cGy. Average doses were 16.5 cGy for 1986, 9.5 cGy for 1987, and 3.2 cGy for 1988.	Cleanup crew mortality increased from 460.9 in 1990 to 505.4 in 1991 (per 100,000 persons). Traumas, poisoning, circulatory diseases, and neoplasms (88.6% in 1990 and 82.7% in 1991) predominate among the causes of death. The highest percentage was for neoplasms, 95.1% and 80.0%, in 1990 and 1991, respectively. Tumors of the respiratory organs increased from 23.1% to 34.6%, and tumors of the digestive organs decreased from 51.3% to 38.5%.	[73]

Continued on next page.

Table 6.2. Morbidity and performance among personnel engaged in operations to eliminate the Chernobyl disaster aftereffects (hereafter called the cleanup crew) (continued).

No.	Category of persons	No. of persons	Dose	Principal results	Reference

Morbidity indices per 100,000 examined members in the cleanup crew, 1987-1991

Index	1987	1988	1989	1990	1991
No. of members	37,465	64,992	71,394	69,700	60,717
All categories	19,127	30,974	40,443	55,077	71,709
Malignant tumors	59	106	154	209	219
Diseases of endocrine organs	1,919	2,175	2,224	3,577	4,959
Psychic disorders	3,683	3,857	4,295	6,660	8,242
Diseases of digestive organs	1,430	3,381	4,450	6,059	8,363
Diseases of blood and blood-forming organs	216	189	242	333	380

Analysis of the dose dependence of the morbidity indices revealed a statistically significant increase in the relative risk (relative risk per unit of dose) with increasing dose of external irradiation.

When evaluating the medical aftereffects of the Chernobyl disaster, psychoemotional stress must be considered. Specific features of vegetative and psychological changes, disturbances of the central nervous system, changes in the intellectual-mnestic sphere, and the appearance of boundary neuropsychic disorders that play an important part in the development of aftereffects of exposure to radiation and other factors were found in some studies [75-80].

The contributions of radiation and psychoemotional factors were evaluated in studies by N. G. Darenskaya and coworkers [81] who examined a sufficiently large number of the members of the cleanup crew. Depending on the duration of restoration work, the cleanup crew was divided into two groups. The first group included 537 men who had worked during the first 5 days, starting on 25 April 1986: 307 of them were aged 39 and less, and 230 were over 39. The second group included 465 men who worked from May 1986: 224 were aged 39 and less, and 241 were over 39.

The structure and incidence rate of diseases with which the cleanup crew suffered were characterized by indicators such as the number of apparently healthy individuals, the number of members in the cleanup crew with a specific disease, and the number of diseases per cleanup crew member in each group.

Table 6.3. Morbidity dynamics for the most frequently encountered diseases in examined members of the cleanup crew (%). *M* is the mean value for the period of observation.

Affected system	Group	Age: ≤ 39 years old (years) 86	87	88	89	*M*	> 39 years old (years) 86	87	88	89	*M*
Nervous system and sense organs	I	17	46	18	51	33	13	37	43	26	30
	II	9	30	8	5	13	11	29	10	8	15
Gastro-intestinal	I	7	21	20	66	29	9	23	31	30	23
	II	6	8	5	1	5	5	9	16	7	9
Otorhino-laryngo-logical	I	17	25	27	20	22	20	23	27	20	23
	II	11	13	5	4	8	13	9	7	2	8
Musculo-skeletal	I	9	12	10	19	13	14	17	19	25	19
	II	1	4	3	2	3	6	9	9	6	8

Studies showed that most frequent were nervous system and gastrointestinal diseases, and somewhat less frequently, otorhinolaryngological and musculoskeletal diseases (table 6.3). The morbidity structure in both groups of the cleanup crew was virtually identical. Although the morbidity structure was similar, the incidence of all forms of the diseases listed in table 6.3 was significantly higher in the first group than in the second group. The occurrence of diseases only in part of each group testifies to the presence of both radiosensitive and radioresistant individuals in the groups. Thus, all the data presented above are indicative of the variability in the individual radiosensitivity of man.

6.3. Cell Factor in the Origin of Individual Radiosensitivity of Critical Systems and the Body as a Whole

Determination of the radiosensitivity of the precursor cells of critical systems of the human body is extremely difficult and, for some systems such as the epithelium of the small intestine, impossible. Nevertheless, some authors succeeded in obtaining data on the radiosensitivity of some types of precursor cells (table 6.4). Presented in the table are the D_0 and n values that characterize the radiosensitivity of bone marrow CFU cells of different types, blood lymphocytes, and cells of the human skin fibroblast culture. It should be noted that under some irradiation conditions it is the skin that may act as the critical tissue for determining radiation sensitivity. It can be seen from table 6.4 that

Table 6.4. Radiosensitivity of human blood-forming stem cells.

Type of precursor cells	Type of radiation	D_0, Gy	n	Reference
CFU-GEMM	γ-ray	0.91	1.0	[82]
	X-ray	1.44	1.0	[82]
CFU-GM	γ-ray	1.15	1.0	[83]
	γ-ray	1.49	1.0	[84]
		1.37-1.60		
	γ-ray	1.30	1.1	[85, 86]
		1.10-1.55		
	γ-ray	1.63	2.2	[87]
	γ-ray	0.42 ± 0.19	1	[88]
	γ-ray	1.38 ± 0.37	1	[88]
	γ-ray	1.18 ± 0.15	1	[88]
	X-ray	1.0 ± 0.09	1	[89]
CFU-DC	γ-ray	0.85	1.0	[84]
CFU-C	γ-ray, 1.0 Gy/min	1.59 ± 0.12	1.0 ± 0.2	[89]
	γ-ray	1.36	1	[90]
	Neutrons, 0.85 MeV	0.34	1	[90]
	Neutrons, 0.35 MeV	0.21	1	[90]
CFU-Er	X-ray	0.74 ± 0.12	1	[89]
CFU-F	X-ray	0.89	1.4	[91]
	γ-ray, ^{60}Co	1.14	1.5	[92]
	γ-ray, 1.0 Gy/min	1.1	1.4	[93]
		(0.77-1.34)		
	γ-ray	1.3	1.3	[83]
	Neutrons, 14.7 MeV	1.31	0.9	[92]
	γ-ray-neutrons, (^{252}Cf)	0.6 ± 0.11	1	[94]
	Tritium (HTO)	0.92 ± 0.12	1	[94]
	γ-ray	1.24 ± 0.3	1	[94]
	γ-ray	1.44 ± 0.12	1	[44]
		1.21-1.92		
Fibroblast-like cells	γ-ray, 1.0 Gy/min	0.88	3.4	[95]
Stimulated FGA lymphocytes of blood		1.13	1.0	[85]
		1.2	1	[96]
Culture of skin fibroblasts		1.53 ± 0.19	1	[97, 98]
		1.25-1.85		

CFU-GEMM - CFU forming mixed colonies
CFU-GM - CFU granulocyte-macrophage type
CFU-DC - CFU giving colonies in diffusion chambers
CFU-C - CFU forming colonies in cultures on agar
CFU-Er - CFU giving small erythrocyte colonies
CFU-F - CFU forming colonies of fibroblasts

the parameters of radiosensitivity of the precursor cells of the above-mentioned systems and of the functional cells of one of them vary within certain limits, which sometimes are rather broad. This conclusion is consistent with results of clinical observations of the variability of individual radiosensitivity of the body as a whole (section 6.2).

It is noteworthy that studies of healthy individuals reveal a broad range of radiosensitivity in various cells. Thus, it was found [43, 99] that the D_0 range for 29 normal cell strains was 0.98-1.8 Gy. The differences between the D_0 values for relatively radiosensitive (D_0 = 1.24 Gy) and comparatively radioresistant (D_0 = 1.6 Gy) cell strains were statistically significant. The range of the D_0 values characterizing the radiosensitivity of diploid fibroblasts in 6 humans was found to be 1.28-1.67 Gy [46]. Comparable D_0 values for the same cells (1.0-1.6 Gy) were obtained by other authors [100] who noted an asymmetric distribution of individuals over the D_0 parameter characterizing the radiosensitivity of skin fibroblasts. The asymmetry was caused by a higher number of individuals with larger values of the radiosensitivity parameter of these cells. This result is of great importance in the selection of the type of distribution of individuals in a population with respect to the parameter of the radiosensitivity of cells of a relevant critical system. Another important result obtained in these studies [100] is the establishment of a correlation between the radiosensitivity parameter of skin fibroblasts and the radiosensitivity of the individual's body as a whole.

Of interest are the data on changes in the functional activity of stromal stem cells of the human bone marrow after the Chernobyl disaster [101]. The percentage of negative results of CFU-F cloning was about 65% versus 15% before the disaster. Moreover, in the summers of 1987 and 1988, this percentage increased to 100%. A trend towards an increase in the activity of these cells was detected in 1989-1990. The negative results of cloning were only observed in 20% of the cases.

Observations of a family of eight members, each having cancers arising in different locations [102], provided support for the concept of a genetic basis for radiosensitivity and radioresistance. In five members, the D_0 value for the fibroblast cell culture was 25% higher than the normal range.

Individual differences in the radiosensitivity of cultured cells are revealed in various diseases (table 6.5). It can be seen that the D_0 values characterizing the radiosensitivity of fibroblast cells in humans suffering from certain neurologic diseases are located within a range of 1.2-2.0 Gy, which is close to the D_0 range of these cells in healthy individuals. An analysis of some radiosensitivity parameters of cultured leukemic cells also reveals pronounced individual variations, which determine different sensitivities to radiation therapy.

The individual variability of the sensitivity of patients with different malignant tumors to the injuries inflicted on normal tissues (skin and lung response) in

Table 6.5. Radiosensitivity of cultivated human cells in different diseases.

Source of cells	Disease	D_0, Gy	n	Reference
Fibroblasts	Friedreich's ataxia	1.23 ± 0.2	1	[96, 98]
		1.04-1.35		
	Motor neurone disease	1.47 ± 0.06	1	[96, 98]
		1.37-1.55		
	Femillial dysantonomia	1.51 ± 0.07	1	[103, 104]
		1.41-1.71		
	Charcot-Marie-Tooth disease	1.44 ± 0.04	1	[103, 104]
		1.38-1.48		
	Duchenne muscular dystrophy	1.41 ± 0.04	1	[103, 104]
		1.23-1.62		
Lymphoid lines	Burkitt's lymphoma	0.9-1.30	1.1-1.4	[86, 96]
	Acute lymphoid leukosis			
	T-cells	1.13-2.30	1.1-1.6	[86, 96]
	B-cells	0.92	1.0	[86, 96]
Myeloid lines	Acute promyelocytic leukosis	0.64-1.37	1.1-3.45	[86, 96]
	Nondifferentiated hemoblastos	1.39-1.65	1.4-4.5	[86, 96]
Blast cells from patients with acute leukosis	Promyelocytic form	1.23-1.80	1.2-1.3	[86, 96]
	Myelomonocytic form	0.55-2.10	1.0-1.7	[86, 96]
	Monoblastic form	0.85	1.2	[86, 96]
		0.30-1.35	1.0-1.3	

the course of radiation therapy is well known [45, 103]. The lung response was observed in 5%-10% of patients irradiated in the thoracic region, which seems to be due to the elevated sensitivity of pneumocytes in this group of patients, pneumocytes being the critical cell system in radiation damage to the lungs.

6.4. Conclusion

A detailed review is presented in this chapter of the clinical data obtained in examinations of diseased and healthy individuals exposed to radiation. Special attention is paid to the results of observations of a contingent of those people who had participated in eliminating the consequences of the Chernobyl nuclear plant disaster. The analysis is performed from the conceptual standpoint used earlier as the basis for the mortality model (chapters 3 and 4). Therefore, the

present review includes not only the results of clinical observations of irradiated individuals but also data on the radiosensitivity of the precursor cells and the functional cells of some critical systems of the human body. In addition, unique data demonstrating a correlation between the radiosensitivity of the cells of one of the critical tissues (skin) and the radiosensitivity of the human body as a whole are also presented. All these data support the principal conceptual ideas underlying our mortality model, including the major idea of the important role of the variability of the radiosensitivity of cells of the critical systems and the body as a whole in the assessment of radiation risk at the population level. These results point to the possibility of using our mortality model in predicting the aftereffects of radiation exposure on the human population.

The relationship between the radiosensitivity of cells of the critical systems and the radiosensitivity of the body needs further investigations because the activation of compensatory and restorative mechanisms of the regulatory systems at the whole-body level may make its own contribution to the modification of radiosensitivity. It seems promising to use, for predictive purposes, both the parameters characterizing the radiosensitivity of critical cell systems and the parameters representing the reactivity of the body in the normal state as well as under the influence of nonradiation loading factors. Such data will be of great importance in predicting the aftereffects of exposure to low-dose radiation and in assessing the risk of their development with due regard for individual radiosensitivity.

REFERENCES

1. Williams RY (1956) Biochemical individuality. The basis for the genetotropic concept. New York: John Wiley and Sons

2. Khrisanfova EN (1990) The constitution and biological individuality of man. Moscow: Moscow University Press (Russian)

3. Monaenkov AM (1970) Immunological response and the type of nervous system. Moscow: Meditsina (Russian)

4. Monaenkov AM (1963) The factor of individuality in immunity processes. Moscow: Institute of Normal and Pathological Physiology (Russian)

5. Darenskaya NG (1976) Individual radiosensitivity and possible ways of its prediction. In: Modern problems of radiobiology, vol 5. Radiation injury to the organism. Moscow: Atomizdat, pp. 138-161 (Russian)

6. Druzhinin YY, Grigor'ev YG, Podluzhnaya GN, Pospishil M (1974) Individual radiosensitivity and its diurnal variations. In: Functioning of the organism and space flight factors. Moscow: Meditsina, pp. 125-131 (Russian)

7. Nechaev IA, Graevskaya BM, Zolotareva NN, Chudinovskaya GA (1972) Statistical approaches to the assessment of individual radiosensitivity in animals. In: Mathematical methods in biology. Moscow: Moscow State University Press, pp. 117-126 (Russian)

8. Pospisil M, Vacha J (1983) Individual radiosensitivity, its mechanisms and manifestations. Prague: Academia

9. Khil'ko AS (1971) Study of individual sensitivity of the blood-forming system to radiation and radiomimetic drugs. Author's summary of candidate's thesis (Medicine). Kiev (Russian)

10. Grigor'ev AY (1992) Individual radiosensitivity. Moscow: Energoatomizdat (Russian)

11. Druzhinin YL, Zubkova-Mikhailova EI, Podluzhnaya GN (1977) Daily variations of the hypothalamic-pituitary-adrenal system activity in animals with different individual radiosensitivity. Kosmicheskaya Biologiya i Aviakosmicheskaya Meditsina 6:40-45 (Russian)

12. Karpfel Z, Koukalova B, Cincarova J, et al. (1965) To the problem of individual radiosensitivity of bone marrow. Folia Biologica (ChSSR) 11(2):140-146

13. Ueno Y (1967) Radiosensitivity of individual mouse and the polarographic properties of its organs in C57Bl/6J mice. Nippon Acta Radiologica 16(11):1511-1518

14. Gus'kova AK, Baisogolov GD (1971) Radiation sickness in man. Moscow: Meditsina (Russian)

15. Darenskaya NG (1986) The feasibility of prediction of individual radiosensitivity. Meditsinskaya Radiologiya 31(12):47-52 (Russian)

16. Graevskaya VM, Nechaev IA, Zolotareva NN (1969) On the prediction of radiation exposure outcome in mammals. Doklady Akademii Nauk 189(3):655-658 (Russian)

17. Novak L, Pospishil M, Gosek B (1968) The rat radiosensitivity as dependent on the individual difference between the calculated and actual oxygen consumption. Radiobiologiya 8(1):152-154 (Russian)

18. Arlashchenko NI, Oparina DY (1981) On the prediction of changes in the resistance to radiation in animals induced by different factors. Izvestiia Akademii Nauk, Seriia Biologicheskaia 6:891-898 (Russian)

19. Darenskaya NG, Chekhonadskii NA, Kuznetsova SS (1986) Prediction of individual radiosensitivity in animals using the mathematical method of object classification. Meditsinskaya Radiologiya 31(12):62-64 (Russian)

20. Korotkevich AO (1986) The endocrine status in the individual radiosensitivity prediction. Meditsinskaya Radiologiya 31(12):83-87 (Russian)

21. Makarov VP, Pliushchev AK, Chekhonadskii NA, Stefashkin YP (1979) A cybernetic approach to the problem of prediction of the radiation sickness outcome in animals. Patologicheskaia Fiziologiia i Eksperimentalnaia Terapiia 1:36-39 (Russian)

22. Mizina TY (1990) The endocrine status as an indicator of severity of radiation injury. In: Proceedings of the USSR Seminar on Theoretical and Applied Biology. Perm, 1988. Moscow, pp. 126-131 (Russian)

23. Mkrtchyan PG, Ogandzhanyan EE, Ogandzhanyan AA, Ordukhanyan AA (1981) The use of pattern recognition methods in assessment of severity of radiation injury. Radiobiologiya 26(4):535-540 (Russian)

24. Ueno Y (1968) Prediction of individual differences in radiosensitivity in mammals. Cospar Symposium on Biological Effects of Radiations in Space, Tokyo, 10 May 1968. Tokyo

25. Nakamura W, Sato F, Nishimoto Y, Kawashima N (1976) Prediction of radiosensitivity of a mouse from its physiological characteristics before X-irradiation. Radiation Research 65(3):500-510

26. Chekhonadskii NA, Yusupov TM (1986) The feasibility of application of mathematical methods in predicting individual radiosensitivity. Meditsinskaya Radiologiya 31(12):64-66 (Russian)

27. Pospisil M (1975) Individuálni rozdily v radiosensitivitě a možnosti jejich predpovedi. Ceskoslovenika Fysiologie 24(2):121-134

28. Sato F, Kawashima N, Nakamura W, Nishimoto Y (1974) Prediction of individual differences in radiosensitivity in mice with multi-dimensional analysis. Journal of Radiation Research 15(1):42

29. Brilliant MD, Vorob'ev AI, Gogin EE (1987) Late effects of human exposure to low-dose radiation. Terapevticheskii Arkhiv 6:3-8 (Russian)

30. Vladimirov VG (1989) Biological effects of external low-dose irradiation. Voenno-Meditsinskii Zhurnal 4:44-46 (Russian)

31. Darenskaya NG, Malyutina GS, Korotkevich AO (1993) The response of rats with different initial reactivity to single gamma irradiation at doses of 0.25 and 1.0 Gy. In: Abstracts of radiobiological meeting, vol. 2. Kiev, 20-25 September 1993. Pushchino, p. 292 (Russian)

32. Avetisov GM, Buldakov LA, Gordeev KI, Il'in LA (1989) The strategy of the NCRP in justifying the tentative limits to annual radiation doses for the population following the Chernobyl disaster. The concept of life dose. Meditsinskaya Radiologiya 34(8):3-11 (Russian)

33. Buldakov LA (1993) Radiation regulation in time periods following nuclear plant accidents. In: Medical aspects of the elimination of the Chernobyl nuclear plant disaster effects. Bulletin of the Center of Public Information on the Atomic Energy. Moscow: Research Institute of Atomic Information, Suppl 3:4-21 (Russian)

34. Gus'kova AK, Denisova EA, Moiseitsev PI, Korgyanova EA (1966) The working conditions and health status of nuclear plant personnel. Meditsinskaya Radiologiya 11(8):37-42 (Russian)

35. Soldatova VA, Kirsanova GN, Solodova RA (1979) The health status of main groups of medical personnel being professionally in contact with sources of ionizing radiation. In: The working conditions and health of the medical staff. Moscow, pp. 135-141 (Russian)

36. Gembitskii EV (1986) Some questions of clinical manifestations and dynamics of neurocirculatory hypotension as related to prolonged exposure to low-dose radiation. Transactions of the Military Medical Academy, Leningrad 185:105-111 (Russian)

37. Romanov IN, Buldakov LA, Shvedov VL (1990) Irradiation of the population and the medical consequences of an accident. Priroda 5:63-67 (Russian)

38. Komarenko DI, Yakimenko DM (1988) Somatic morbidity in persons that have been exposed to low-dose radiation. In: Problems of radiation medicine, Issue 1. Kiev: Zdorovye, pp. 98-103 (Russian)

39. Beebe GW (1981) The atomic bomb survivors and the problem of low-dose radiation effects. American Journal of Epidemiology 114(6):761-783

40. Kamada N, Shigeta CH, Hayakawa N, et al. (1990) Comprehensive medical examination of the atomic bomb survivors which have been close to the explosion epicentrum. Nagasaki Medical Journal 65:556-560

41. Kishikawa M, Mine M, Okumura Y (1991) Effects of the atomic bomb explosion in Nagasaki: A medical perspective. Acta Medica Nagasaki 36(1-4):191-198

42. Boder E, Sedgwick RP (1963) Atoxia-telangiectasia. A review of 101 cases. In: Walsh G (ed) Little club clinics in developmental medicine. London: Heinemann, pp. 110-118

43. Arlett CF, Harcourt SA (1980) Survey of radiosensitivity in a variety of human cell strains. Cancer Research 40(4):589-620

44. Brennan S, Lewis PD (1983) Studies of cellular radiosensitivity in hereditary disorders of nervous system and muscle. Journal of Neurology, Neurosurgery, Psychiatry 8:1143-1145

45. Domshlak MP (1960) Studies of clinical radiology. Moscow: Medgiz (Russian)

46. Weichselbaum RR, Epstein J, Little JB (1976) *In vitro* radiosensitivity of human diploid fibroblasts from patients with unusual clinical responses to radiation. Radiology 121(3):479-482

47. James SE, Arlett CF, Green MHL, Bridges BA (1983) Radiosensitivity of human *T*-lymphocytes proliferating in long term culture. International Journal of Radiation Biology 44(3):417-422

48. Miller LS, Fletcher GH, Gerstner HB (1958) Radiologic observations on cancer patients treated with whole-body X-irradiation. Radiation Research 8(2):150-165

49. Medinger FG, Craver LF (1942) Total body irradiation. American Journal of Roentgenology 48(5):651-670

50. Darenskaya NG, Domshlak MP, Rayevskaya SA (1971) Specific features of clinical manifestations of the human response to subtotal irradiation in a radiological clinic. In: Problems of general radiobiology (Experimental and clinical data). Moscow: Atomizdat, pp. 254-272 (Russian)

51. Kholdin SA (1962) The part of individual factors and their combinations in predicting the mammary gland cancer. Voprosy Onkologii 8(6)28-35 (Russian)

52. Sgalitzer M, Ungar E (1937) Versuch einer körperlicher Eignungsprüfung zur Beschäftigung mit Röntgenstrahlen. Strahlentherapie 58(6):S701-710

53. Gerstner HB (1958) Acute clinical effects of penetrating nuclear radiation. JAMA 168(4):381-388

54. Tereshchenko NY, Burtseva LI, Gezin AV (1971) The results of a dynamic clinical-physiological investigation of the nervous system in children that have been irradiated in the first postnatal months. In: Problems of general radiobiology. Moscow: Atomizdat, pp. 272-283 (Russian)

55. The lessons and conclusions of Chernobyl nuclear plant disaster for the Army, including the Civil Defense Department. Report No 9284H of the Military Medical Academy, 1987 (Russian)

56. Pirogova EA (1988) Epidemiological aspects under evaluation of health of peoples belonging to the group with higher radiation risk. Problems of radiation medicine, Issue 1. Kiev: Zdorovye, pp. 152-160 (Russian)

57. Komarenko DI, Yakimenko DM (1988) Somatic morbidity in persons that have been exposed to low-dose radiation. In: Problems of radiation medicine, Issue 1. Kiev: Zdorovye, pp. 98-103 (Russian)

58. Virabov VRP, Melikyan IE, Oganesyan RK, et al. (1990) The results of a dynamic observation of residents of Armenia that have participated in the elimination of the Chernobyl disaster aftereffects. Meditsinskaya Radiologiya 35(10):4 (Russian)

59. Petrov RV, Oradovskaya IV, Pinegin BV, et al. (1990) The clinical-immunological and allergologic characterization of persons engaged in the elimination of the Chernobyl disaster aftereffects three years after they left the contaminated zone. Meditsinskaya Radiologiya 35(10)11-12 (Russian)

60. Gubergrits EA, Guchnin AG, Chubenko CC, et al. (1992) On the relationship between vegetovascular dystonia and gastrointestinal pathology in the "restorers" at the Chernobyl power plant. In: Abstracts of the Ukraine Conference on Urgent Problems of Elimination of the Chernobyl Disaster Aftereffects. Kiev, 21-23 April 1992. Kiev, p. 61 (Russian)

61. Kovaleva LI, Lyubchenko PN, Basakova TV (1992) The state of the central hemodynamics in the Chernobyl disaster "restorers" four years after the disaster. Gigiena Truda i Professionalnykh Zabolevaniy 3:15-17 (Russian)

62. Komarenko DI, Maslekha EA (1992) Delayed nonstochastic effects of irradiation in the Chernobyl disaster "restorers." In: Abstracts of the Ukraine Conference on Urgent Problems of Elimination of the Chernobyl Disaster Aftereffects. Kiev, 21-23 April 1992. Kiev, p. 110 (Russian)

63. Koryt'ko SS (1991) The functional state of the cardiovascular system in the Chernobyl disaster "restorers." In: Abstracts of the 8th Congress of the Byelorussian Physiological Society. Minsk, 10-11 September 1991. Minsk, p. 60 (Russian)

64. Nikula TD, Karpenko VV. Kisil' SS, et al. (1992) Noninvasive screening of the health status of the Chernobyl disaster "restorers." In: Abstracts of the Ukraine Conference on Urgent Problems of Elimination of the Chernobyl Disaster Aftereffects. Kiev, 21-23 April 1992. Kiev, p. 163 (Russian)

65. Panchenko NA, Zotov VP (1993) Time dependence of changes of the functional state in the Chernobyl disaster "restorers." In: Abstracts of Radiobiological Meeting, vol 2. Kiev, 20-25 September 1993. Pushchino, p. 759 (Russian)

66. Timchenko VG, Pavlenko VA, Sukhanskaya MM, Lemon VS (1992) The dynamics of injury and restitution of basic homeostatic systems in the Chernobyl disaster "restorers." Results of an assessment of health effects of the Chernobyl power plant disaster. In: Abstracts of the Ukraine Conference on Health Aftereffects of the Chernobyl Disaster. Kiev, 21-23 April 1992. Kiev, p. 215-216 (Russian)

67. Torubarov FS, Nikolayev MK, Dakhno DV (1991) On the vegetovascular dystonia diagnosis in the Chernobyl disaster "restorers." Meditsinskaya Radiologiya 36:54-55 (Russian)

68. Khomazyuk IN (1991) The health status in persons that have been engaged in the elimination of the Chernobyl disaster aftereffects. Vestnik Akademii Meditsinskikh Nauk 11:29-31 (Russian)

69. Kodareva NK, Katel'nitskaya LI, Lushpaeva AO, Shamrai TL (1992) Cardiovascular disorders in the Chernobyl disaster "restorers." In: Abstracts of the Ukraine Conference on Urgent Problems of Elimination of the Chernobyl Disaster Aftereffects. Kiev, 21-23 April 1992. Kiev, p. 236 (Russian)

70. Chernyshev VN, Katel'nitskaya LI, Belyanin VA (1992) Analysis of disease distribution among the Chernobyl disaster "restorer" residents of the North Caucasus Territory. In: Abstracts of the Ukraine Conference on Urgent Problems of Elimination of the Chernobyl Disaster Aftereffects. Kiev, 21-23 April 1992. Kiev, p. 249 (Russian)

71. Shamrai TP, Katel'nitskaya LI, Gatseva TB (1992) The health status of the Chernobyl disaster "restorer" residents of Rostov-on Don, Voroshilov District. In: Abstracts of the Ukraine Conference on Urgent Problems of Elimination of the Chernobyl Disaster Aftereffects. Kiev, 21-23 April 1992. Kiev, p. 249 (Russian)

72. Tukov AR, Dzagoeva LG (1993) Morbidity in the Russian atomic industry personnel that have been employed in the Chernobyl disaster aftereffects elimination works. Bulletin of the Center of Public Information of the Atomic Energy. Moscow: Research Institute of Atomic Information. Suppl 3:97-99 (Russian)

73. Tsib AF, Ivanov VK, Gorski AI, et al. (1993) Evaluation of the morbidity and mortality indices for the Chernobyl disaster "restorers." Bulletin of the Center of Public Information of the Atomic Energy. Moscow: Research Institute of Atomic Information. Suppl 3:114-129 (Russian)

74. Polyvyanaya MY (1992) Specific features of the attitude to disease in the Chernobyl disaster "restorers." In: Abstracts of the Ukraine Conference on Urgent Problems of Elimination of the Chernobyl Disaster Aftereffects. Kiev, 21-23 April 1992. Kiev, p. 181 (Russian)

75. Getmanets RL, Guchnin AG, Zhdanyuk YI, et al. (1992) Some peculiarities of the vegetative and psychological disorders in the Chernobyl disaster "restorers." In: Abstracts of the Ukraine Conference on Urgent Problems of Elimination of the Chernobyl Disaster Aftereffects. Kiev, 21-23 April 1992. Kiev, p. 54 (Russian)

76. Gornichenko II, Imshenetskaya LP, Sokolova MN, Boiko NI (1992) The state of the central nervous system during sexual disorders in men that have been engaged in the elimination of the Chernobyl disaster aftereffects. In: Abstracts of the CIS Conference on the Effects of Ionizing Radiation on the Reproductive Function, Obninsk, 1992. Obninsk: Medical Radiology Science Centre, pp. 16-19 (Russian)

77. Grishayeva IV (1992) Some peculiarities of the intellectual-mnemonic changes in persons that have been injured following the Chernobyl nuclear plant disaster. In: Abstracts of the Ukraine Conference on Urgent Problems of Elimination of the Chernobyl Disaster Aftereffects. Kiev, 21-23 April 1992. Kiev, p. 60 (Russian)

78. Morozov AM (1992) The dynamics of border-line neuropsychic disorders observed in the Chernobyl disaster "restorers." In: Abstracts of the Ukraine Conference on Urgent Problems of Elimination of the Chernobyl Disaster Aftereffects. Kiev, 21-23 April 1992. Kiev, p. 154 (Russian)

79. Chinkina OV (1993) The peculiarities of the perception of ionizing radiation risk and the problems of medical-social preventive measures. Bulletin of the Center of Public Information of the Atomic Energy. Moscow: Research Institute of Atomic Information, Suppl 3:41-44 (Russian)

80. Morozov AM (1993) The biological aspects of border-line neuropsychic disorders in persons suffering from late effects of irradiation. In: Abstracts of Radiobiological Meeting, vol II. Kiev, 20-25 September 1993. Pushchino, p. 690 (Russian)

81. Darenskaya NG, Ivanov AA, Nadezhina NM et al. (1992) The biomedical background for risk groups. The elaboration of methods for prediction and prevention of delayed effects. Report of the Institute of Biophysics, Moscow (Russian)

82. Neumann HA, Lohr GW, Fauser AA (1981) Radiation sensitivity of pluripotent hemopoietic progenitors (CFU-GEMM) derived from human bone marrow. Experimental Hematology 9(6):742-744

83. Laver J, Ebell W, Casto-Malaspina H (1986) Radiobiological properties of the human hematopoietic microenvironment: Contrasting sensitivities of proliferative capacity and hematopoietic function to *in vitro* irradiation. Blood 67(4):1090-1097

84. Hendry JH, Lord BJ (1983) The analysis of the early and late response to cytotoxic insults in the haemopoietic cell hierarchy. In: Potten CS, Hendry JH (eds) Cytotoxic insult to tissue: Effects on cell lineages. Edinburgh, pp. 1-66

85. Lehnert S, Rybka WB, Sulssa S, Giambattista D (1986) Radiation response of haematopoietic cell lines of human origin. International Journal of Radiation Biology 49(3):423-431

86. Osawa K, Yasusads M, Suda T, et al. (1983) Radiation sensitivity of leukemic progenitor cells in acute nonlymphocytic leukemia. Cancer Research 43:2339-2341

87. Peacock JL, Steel GG, Stephens TC (1986) Radiation dose-rate dependent differences in cell kill and repopulation in murine bone marrow CFU-S and CFU-C. British Journal of Cancer 53(Suppl 17):171-173

88. Petcau A, Sargent MD, Chelack WS, Gerrard JM (1988) Response of human bone marrow progenitor cells to X-rays *in vitro*. International Journal of Radiation Biology 54(4):593-600

89. Kyoizimi S, McCune JM, Namikawa R (1994) Direct evaluation of radiation damage in human hematopoietic progenital cells *in vivo*. Radiation Research 137(1):76-83

90. Zherbin EA, Kolesnikova AI, Konoplyannikov AG, et al. (1979) Radiation injury to the bone-marrow granulopoiesis progenitor cells (CFU-K) from exposure to gamma and neutron radiations. In: Abstracts of the 7th USSR Conference on Recovery and Compensatory Processes After Exposure to Radiation. Leningrad, 1979. Leningrad, pp. 65-66 (Russian)

91. Zherbin EA, Kolesnikova AI, Konoplyannikov AG, Khoptynskaya SK (1978) Radiosensitivity of the human bone-marrow cells forming fibroblast colonies in single-layer cultures. Meditsinskaya Radiologiya 23(7):48-51 (Russian)

92. Khoptynskaya SK, Kolesnikova AI, Konoplyannikov AG (1979) Some radiobiological characteristics of the human bone-marrow CFU-F. Radiatsiya i Organizm 3:46-50 (Russian)

93. Kolesnikova AI, Konoplyannikov AG, Khoptynskaya SK, et al. (1980) Radiosensitivity of stromal progenitor cells (CFU-F) in the bone marrow of the sarcoma patients. Meditsinskaya Radiologiya 25(10):48-54 (Russian)

94. Chigeta CH, Tanaka K, Oguma N, et al. (1988) Radiation sensitivity of human bone marrow fibroblast colony-forming unit (CFU-F) to various radiation sources. Journal of Radiation Research 29(3):182-188

95. Diatloff-Zito C, Deschavanne P, Loria E, et al. (1981) Comparison between the radiosensitivity of human, mouse, and chicken fibroblast-like cells using short-term endpoints. International Journal of Radiation Biology 39(4):419-430

96. Knax J, Greenberg BR, Anderson RW, Rosenblatt RA (1983) Studies of *T*-lymphocytes in preleukemic disorder and nonlymphocytic leukemia: *In vitro* radiosensitivity, mitogenic responsiveness, colony formation and enumeration of lymphocyte subpopulations. Blood 61(3):449-455

97. Lewis PD, Corr JB, Arlett CF, Harcourt SA (1979) Increased sensitivity to γ-irradiation of skin fibroblast in Friedreich's ataxia. Lancet 2:474-475

98. Chamberlain S, Lewis PD (1982) Studies of cellular hypersensitivity to ionizing radiation in Friedreich's ataxia. Journal of Neurology, Neurosurgery, and Psychiatry 45(12):1136-1138

99. Arlett CF, Cole J, Green MHL (1989) Radiosensitive individuals in the population. In: Low dose radiation: Biological bases of risk assessment. London, pp. 240-252

100. Cox R, Hasking GP, Wilson J (1978) Ataxia telangiectasia. Evaluation of radiosensitivity in cultured skin fibroblasts as a diagnostic test. Archives of Disease in Childhood 53(2):386-390

101. Astakhova VS, Panchenko LM (1991) Changes of the biorhythm of the stromal stem cell activity in the human bone marrow as a result of the Chernobyl disaster. In: Abstracts of the Ukraine Conference on Health Aftereffects of the Chernobyl Disaster. Kiev, 1991. Kiev: USSR Ministry of Health, pp. 12-13 (Russian)

102. Bech-Hansen NN, Blattner WA, Sell BM, et al. (1981) Transmision of *in vitro* radioresistance in a cancer-prone family. Lancet 1:1335-1337

103. Lewis PD (1987) Variation in individual sensitivity to ionizing radiation. In: Jones RR, Southwood R (eds) Radiation and health. The biological effects of low-level exposure to ionizing radiation. Chichester; New York; Brisbane; Toronto; Singapore: John Wiley and Sons, pp. 167-177

104. Seshadri R, Matthews C, Morley AA (1985) Radiation sensitivity of human malignant lymphocytes. Acta Radiologica Oncology 24(5):411-414

Task IV

Summary

E. E. Kovalev, principal investigator
O. A. Smirnova, senior researcher

CHAPTER 7

Summary

This report provides a new approach to radiation risk assessment based on the concept of individual variability of mammalian radiosensitivity. A family of mathematical models was constructed to calculate the dynamics of the principal critical systems of an organism exposed to radiation. Knowledge of the dynamics enables prediction of the mortality of populations that are nonhomogeneous to radiosensitivity. The concepts forming the basis of the models were used to analyze radiobiological data obtained in experiments with various mammalian species and in clinical observations of irradiated individuals. Particular attention was given to data collected on those who had been involved in eliminating the aftereffects of the Chernobyl catastrophe. The introduction formulates the problem and provides a brief review of the literature that served as the base for our research.

7.1. Mathematical Model of the Blood-Forming System

Chapter 1 describes mathematical modeling of the effects of acute and chronic irradiation on hematopoiesis, one of the principal critical systems. The introduction in chapter 1 briefly reviews existing mathematical models and formulates the goals that motivated the construction of our new models of hematopoiesis. Section 1.2 describes a universal approach to modeling hematopoiesis dynamics in nonirradiated and irradiated mammals. Sections 1.3-1.6 examine the four principal hematopoietic lines—thrombocytopoiesis, lymphopoiesis, erythropoiesis, and granulocytopoiesis. Section 1.7 provides the principal conclusions.

The blood-forming system was regarded as a complex of four subsystems: thrombocytopoiesis, lymphopoiesis, erythropoiesis, and granulocytopoiesis. Each subsystem includes the entire set of cells, from stem cells (in the microenvironment predetermining the differentiation of a pluripotent cell toward the respective hematopoietic line) to mature functional blood cells of this particular line.

The models of individual hematopoietic lines include the principal stages of development of hematopoietic cells and the specific features of the lines: the variable average ploidy of megakaryocytes and the existence of a bone marrow depot of granulocytes. The models are based on the chalone theory of hematopoiesis regulation. According to this theory, certain tissue-specific substances, chalones, are the material carriers of the feedback in cell division control. Chalones are the product of the vital activity and the decay of cells of some self-renewing systems of the mammalian organism, including thrombocytopoiesis, lymphopoiesis, erythropoiesis, and granulocytopoiesis.

The models of the individual lines considered three types of cell: (1) bone marrow precursor cells (from stem cells in the respective microenvironment to morphologically identifiable dividing cells), (2) nondividing maturing bone marrow cells, and (3) mature blood cells. The granulocytopoiesis model considered one more cell type: tissue granulocytes. Based on experimental data, pools of radiosensitive cells were divided into three groups, according to their responses to radiation. The first group included cells undamaged by radiation. The second group included cells damaged by radiation and dying within 1-2 days (mitotic death). Heavily damaged cells that died at interphase made up the third group. The concentration dynamics of all these cells is described by nonlinear differential equations.

Separation of cells into groups according to the extent of their damage and consideration for their dynamics makes it possible to collect more detailed information concerning the damage and recovery of pools of these cells than other approaches. Our approach made it possible to describe the contribution of radiation-damaged cells to the chalone control of hematopoiesis. It is important that both the dose rate of chronic radiation and the dose of acute radiation enter the models as variable parameters and that the constant coefficients are terms commonly adopted in radiobiology and hematology. In particular, some coefficients are expressed through conventional radiobiological quantities characterizing the radiosensitivity of hematopoietic cells.

In the absence of radiation, the models describe the dynamics of hematopoietic lines in nonirradiated mammals. In these conditions, the models were reduced to systems of three nonlinear differential equations. The systems were investigated by methods of qualitative theory of differential equations and oscillation theory. Estimated were the stability and type of stability of singular points, which have specific biological interpretations. For each model system, being in the first (trivial) singular point is equivalent to a complete depletion of the respective hematopoietic line. The coordinates of the second singular point, when it is stable, correspond to normal concentrations of cells of a hematopoietic line. A bifurcation analysis and computer studies of the models revealed one more particular solution: a stable limit cycle. It arises when the second singular point is unstable. Stable oscillations of concentrations of circulating blood cells and of their precursors in the bone marrow correspond to this particular solution. This modeling result has analogs in actual life. For instance, oscillatory hematopoiesis dynamics was observed in grey collies.

Computer studies showed that when the second singular point is stable, the recovery processes in the thrombocytopoietic, lymphopoietic, erythropoietic, and granulocytopoietic systems can be either aperiodic or oscillatory. These modeling results also agree with experimental data.

The models were used to simulate hematopoiesis dynamics in laboratory mice and rats exposed to acute and chronic radiation. The values of most independent coefficients of the equations in the dimensionless form were determined from experimental hematological and radiobiological data. Only a few parameters that could not be measured experimentally were chosen in the course of a computer-assisted study of the models.

Concentration dynamics for mature blood cells and their bone marrow precursors was studied as a function of dose of acute irradiation. A comparative analysis of the kinetics of the hematopoietic lines was made, and interpretation of the results was suggested. It was established that the models provided a qualitative and quantitative description of postirradiation injury and recovery of thrombocytopoiesis, lymphopoiesis, erythropoiesis, and granulocytopoiesis in small laboratory animals (mice and rats).

When modeling the effect of chronic irradiation on hematopoiesis, the dose rate was varied from low to high levels. Calculations showed that the models can describe the experimentally observed ability of the hematopoietic system to adapt itself to prolonged exposure to radiation at low and moderate dose rates. Actually, in mammals exposed to chronic radiation at low and moderate dose rates, the models simulate the ability of hematopoiesis to recover homeostasis, i.e., the dynamic equilibrium. An equilibrium state is characterized by new (other from normal) stationary concentrations of functional cells in the blood and their precursors in the bone marrow. For the erythroid and thrombocytic lines, these values decrease as radiation dose rate increases. For the lymphoid and granulocytic lines, the same rule applies at moderate dose rates. With chronic irradiation at low dose rates, the stationary concentrations of precursor cells of these two systems in the bone marrow and of granulocytes in the blood exceed the normal level. These predictions of the model, which were also corroborated by experimental data, can be regarded as effects of radiation hormesis.

When dose rates of chronic irradiation exceed certain critical values, the models reproduce an irreversible depletion of the system considered. It shows that the critical dose rate depends on the coefficient that is a measure of radiosensitivity of bone marrow precursors capable of dividing in a particular hematopoietic line and on two kinetic parameters specifying the proliferative potential of these cells. For the thrombocytopoietic, lymphopoietic, erythropoietic, and granulocytopoietic systems of mice, the critical dose rates are 2.4 Gy/day, 1.4 Gy/day, 1.53 Gy/day, and 5.1 Gy/day, respectively. There is quantitative agreement between data from actual and model experiments on the dynamics of the above-indicated systems in mice exposed to chronic radiation at dose rates close to the critical values found. Therefore, formulas

for calculating critical dose rates derived from the models can be used to calculate levels of chronic radiation that may be harmful to various mammalian species.

Comparison of modeling results and respective experimental data revealed qualitative and quantitative agreement in a broad range of doses of acute exposure and dose rates of continuous exposure. The models can be used to quantitatively predict hematopoiesis dynamics in small laboratory animals under different radiation conditions. With appropriate substitution of the numerical values of the coefficients, the models can also be used to study the effects of radiation on large mammals, including man.

7.2. Mathematical Model of the Small Intestine Epithelium System

Chapter 2 deals with modeling the effects of ionizing radiation on the small intestine epithelium system, the second principal critical system of an organism. The introduction (section 2.1) states the purpose for constructing new models of the small intestine epithelium system. The next three sections present three models describing the dynamics of the small intestine epithelium system in nonirradiated mammals and in those exposed to chronic and acute radiation. The final section summarizes the chapter.

The first model is based on the chalone theory of regulation of renewal of the small intestine epithelium, which consists of crypts and villi. Basic (cylindrical) cells of the crypt-villus system were considered. These cells were divided into three groups according to current views on their degrees of differentiation. Group 1 includes precursor cells, from the stem cell to the dividing maturing crypt cell. Nondividing maturing crypt cells and functional villus cells make up group 2 and group 3, respectively. The dynamics of the crypt-villus system is described by a system of nonlinear differential equations for concentrations of these cells. It should be noted that the model reflects the principal stages of differentiation of cylindrical cells of the intestinal epithelium and also considers the functioning peculiarities of the small intestine epithelium system that relate to motion of cells over the crypt and villus in the course of division and maturation. Each coefficient of the model has a generally accepted gastroenterological meaning, and most of the coefficients are determined experimentally.

The system of nonlinear differential equations obtained was analyzed by methods of qualitative theory of differential equations, oscillation theory, and numerically on a computer. The extent and character of stability of singular points were evaluated. The first singular point (trivial) corresponds to complete depletion of the small intestine epithelium system. The coordinates of the second singular point, when it is stable, are equivalent to normal concen-

trations of the above-mentioned cell types of the crypt-villus system. The system of nonlinear differential equations has one more particular solution, a stable limit cycle, if the second singular point is unstable. Computer calculations have shown that when the second singular point is stable, the recovery processes in the small intestine epithelium system have the form of damped oscillations.

Based on the model of the dynamics of the small intestine epithelium system in nonirradiated mammals, we constructed a mathematical model of optimal complexity that describes the dynamics of the intestinal epithelium system during chronic irradiation. The model includes four differential equations for concentrations of radioresistant villus cells and their precursors in the crypt incapable of dividing, as well as for concentrations of radiation-damaged and undamaged crypt precursor cells that are capable of dividing and are sensitive to radiation. The fact that the model considers the dynamics of radiation-damaged cells of the small intestine epithelium system makes it possible to study in more detail the damage and recovery processes in this system under radiation and to describe the contribution of these cells to the chalone regulation of renewal in the small intestine epithelium system. The key parameters of the equations are radiation dose rate and a quantity characterizing the radiosensitivity of crypt precursor cells capable of dividing. Studies have shown that the model provides qualitative and quantitative description of two possible regimes of the dynamics of the small intestine epithelium system during chronic irradiation of mice and rats: (1) total injury of the small intestine epithelium at dose rates exceeding a certain critical value, and (2) setting up a new homeostasis in the small intestine epithelium system when the dose rates are lower. The new stable equilibrium is characterized by stationary concentrations of villus functional cells and crypt precursor cells. These concentrations decrease as the dose rate of chronic radiation increases. As with the thrombocytopoietic, lymphopoietic, erythropoietic, and granulopoietic systems, the critical dose rate for the small intestine epithelium system depends only on the radiosensitivity of precursor cells capable of dividing and on the proliferation potential of these cells. Recovery of homeostasis in the crypt-villus system is achieved through intensified mitotic activity of crypt cells in compensation for those crypt cells that have been killed by chronic radiation. This prediction of the model is supported experimentally.

Chapter 2 also describes a model of the dynamics of the small intestine epithelium system in mammals after acute irradiation, a simplified version of the preceding model. The dose of acute radiation and the quantity specifying radiosensitivity of crypt precursor cells capable of dividing enter as parameters into formulas setting the initial conditions. Computer studies of the model have shown that it qualitatively and quantitatively reproduces depletion of the crypt-villus system in mammals (mice) at high radiation doses and also simulates the damage and recovery processes in this system after doses that are not as high.

The models thus reproduce a broad range of experimental data characterizing the dynamics of the small intestine epithelium in nonirradiated and irradiated mammals. This demonstrates that the models do account for the principal cause-effect relationships governing the function of the crypt-villus system under normal conditions and under radiation. As in the model of hematopoiesis, we performed a bifurcation analysis of the system of equations describing the dynamics of the small intestine epithelium system in nonirradiated mammals and found specific features of its behavior. We also found the values of constant coefficients and quantitatively compared the modeling results with experimental data. The agreement obtained suggests that the models can be used to simulate and predict the dynamics of the intestinal epithelium in mammals exposed to acute and chronic radiation at broad ranges of doses and dose rates.

7.3. Mathematical Model of Mortality for a Homogeneous Mammalian Population

Chapter 3 describes investigations of mortality dynamics in irradiated homogeneous mammalian populations by methods of mathematical modeling. Section 3.1 lists the objectives of the model study. Section 3.2 describes a model of radiation-induced mortality of a homogeneous mammalian population. Sections 3.3 and 3.4 describe how the model was used to study the pattern of mortality of mice exposed to acute and chronic radiation in the range of doses and dose rates responsible for the intestinal form of radiation injury and the bone marrow syndrome. Conclusions are summarized in section 3.5.

The principal cause of radiation-induced death in mammals is known to be failure of one of the organism's vital systems, which manifests itself in the disruption of cellular kinetics and in a decrease in the number of functional cells of the particular system below the level required for survival. For each of the studied dose and dose rate intervals there seems to be a specific critical system whose damage determines the mechanism of radiation sickness and eventual death of the mammals. This radiobiological concept of a critical system forms the basis of our model. Also used in the model was the stochastic approach proposed by Sacher, who modeled a homogeneous population in which every individual had the same average values for all physiological variables and their fluctuation parameters. Sacher described this population by a random variable that served as a generalized index of physiological state, and when this variable reached or exceeded a particular critical level, he regarded the result as death.

Based on the radiobiological concept of the critical system, we chose the deviation of the concentration of critical system functional cells from the normal level as an index of physiological state, and we assumed that reaching or exceeding a threshold value by this deviation is a death analog. In this way

a model was created that relates statistical biometric functions (mortality rate, probability density, and life span probability) to dynamics of critical system functional cell concentration and to statistical characteristics of this physiological index in the mammalian species in question.

The model was used to simulate mortality in CBA mice exposed to acute and chronic radiation when the small intestine epithelium and bone marrow hematopoiesis (thrombocytopoiesis) are the critical systems. The dynamics of concentration of functional elements of these systems—villus cells and platelets—was calculated by the thrombocytopoiesis and small intestine epithelium system models described in chapters 1 and 2. There is qualitative and quantitative agreement of modeling results and experimental data on mortality dynamics and average life shortening in CBA mice exposed to a wide variety of dose rates of chronic radiation and doses of acute radiation.

A major difference and advantage of the model described, as compared to models of other authors, is that identification of the model's coefficients does not require data on mortality dynamics of irradiated mammalian populations. Only data on the population's mortality in the absence of radiation and some limited number of experimental or clinical observations of behavior of the respective critical system under acute or chronic irradiation are needed. Therefore, the model developed can be used to predict life shortening of large mammals and humans under various radiation conditions, including chronic irradiation with low dose rates whose duration is commensurate with life span.

7.4. Mathematical Model of Mortality for a Nonhomogeneous Mammalian Population

Chapter 4 deals with modeling the mortality dynamics of an irradiated mammalian population with nonuniform individual response to radiation. Section 4.1 states the goals of this model study. The next section presents a generalized mathematical model of radiation-induced mortality of a nonhomogeneous population. A mathematical interpretation of this model for cases of normal and log-normal distribution of individuals in the radiosensitivity index of the critical system cells is given in the next section. Two subsequent sections examine the mortality patterns of mice exposed to radiation that induces either the intestinal or the bone marrow syndrome. Section 4.6 provides the principal conclusions of the chapter.

The model of radiation-induced mortality of a nonhomogeneous population is based on the assumption of nonuniform individual radiosensitivity of critical system cells. Accordingly, the distribution of individuals in the radiosensitivity index is described by a continuous function. An important component of the mortality model is an adequate approximation of the continuous function by a discrete function. This transition from a continuous distribution to a

discrete one is equivalent to the representation of the initial nonhomogeneous population as a set of a finite number of homogeneous subpopulations. The radiosensitivity index of the critical system cells in individuals of each homogeneous subpopulation and also the number of these individuals are uniquely determined by the initial continuous distribution. Other important components of the model are the formulas used to express the biometric functions describing the mortality dynamics of the nonhomogeneous population through the biometric functions defining the mortality dynamics of the constituent homogeneous subpopulations. To calculate the radiation-induced mortality dynamics of the subpopulations, use was made of the mathematical model of mortality dynamics for the homogeneous population and the mathematical models of critical systems (see chapters 1-3), which formed parts of the model of radiation-induced mortality for the nonhomogeneous mammalian population. The resulting structure of the model reflects the actually existing levels of manifestation of adverse radiation effects in mammals. The first level is that of a critical system, whose radiation injury is largely determined by the radiosensitivity of the constituent cells. The second level is that of the whole organism. Here, the probable outcome of irradiation depends mainly on the extent of radiation injury of the respective critical system, i.e., on the individual cell radiosensitivity of the system. The third level is that of the population, which includes animals with differing individual radiosensitivity of the critical system cells. It follows, then, that the elaborated model of mortality is actually a mathematical description of cause-effect relationships set up in the course of radiation injury of mammals.

This model was used to study the effect of radiation on the mortality of nonhomogeneous populations of mice. We made use of the two most popular distribution types in biology—normal (Gaussian) and log-normal—to describe the distribution of individuals of a nonhomogeneous population in the radiosensitivity index of the critical system precursor cells. In model experiments, we studied the dynamics of radiation-induced mortality of the nonhomogeneous population as a function of both the type of animal distribution in the radiosensitivity index and the magnitude of the variance (the most important parameter of the distribution). We simulated (1) exposures to very high doses at pulsed or continuous dose rates and (2) prolonged exposures at low dose rates whose duration is commensurate with the maximum life span of intact animals. In the former case, the critical system was represented by the small intestine epithelium system, and in the latter case, by bone marrow thrombocytopoiesis.

The studies performed initially revealed a direct correlation between the variability of survival of some animals of the nonhomogeneous population and the variability of individual radiosensitivity of the respective critical system precursor cells. It was shown that when exposed to high radiation doses at pulsed or at continuous dose rates, the probability to die from the intestinal syndrome increases with radiosensitivity of the intestinal epithelium system precursor cells. In turn, for an animal exposed to prolonged radiation at a low dose rate, the probability to survive to a certain age increases with decreasing

radiosensitivity of the bone marrow precursor cells of the thrombocytopoietic system. These results of modeling seem to confirm once more that the adopted concept of a critical system is indeed valid.

Modeling results also support our hypothesis that the reason for the more pronounced radiobiological effects in the Chernobyl catastrophe zone than could be expected is the variability of individual radiosensitivity in a mammalian population. For instance, the model shows that consideration for the normal and log-normal distributions of individuals in the radiosensitivity index of the critical system precursor cells results in reproducing higher rates of radiation-induced mortality and lower survival than could have been predicted from the averaged radiosensitivity indices alone. Differences in prediction are more pronounced with greater scatter in individual radiosensitivity indices of the respective critical system precursor cells in a nonhomogeneous population. These differences are greatest when the specimen distribution in the nonhomogeneous population is log-normal with a high variance.

The model studies suggest that the levels of doses and dose rates of acute and chronic exposures that present a certain danger for nonhomogeneous mammalian populations decrease as the scatter of values of the individual radiosensitivity index for the critical system precursor cells in these populations increases. For animals having hyperradiosensitive precursor cells, even low-level radiation can have fatal consequences. These model results have considerable theoretical and practical importance since they outline new pathways in the development of methods of radiation risk assessment.

7.5. Variability of the Radiosensitivity of Mammals: Experimental Data

Chapter 5 summarizes and analyzes experimental radiobiological data on species-specific and individual radiosensitivity of mammals. Section 5.1 touches on the history of this topic. Sections 5.2 and 5.3 examine the role of critical systems and the constituent cells in forming the species-specific and individual radiosensitivity in mammals. Section 5.4 presents our conclusions.

Two concepts were used in developing the mathematical model to describe the dynamics of radiation-induced mortality in nonhomogeneous mammalian populations. The first is a radiobiological concept of a critical system. The second concept suggests variability of individual radiosensitivity in nonhomogeneous populations, which manifests itself at the organism's level and at the levels of critical systems and constituent cells. It was the purpose of this chapter to illustrate the validity of these concepts by the example of experimental data on species-specific radiosensitivity. Experimental data on radiation-induced mortality and on radiosensitivity of the critical systems and their

cells were compared for various mammalian species. A direct correlation was established between the species radiosensitivity manifested at the population mortality level and the species radiosensitivity at the level of critical systems and cells involved.

The experimental data collected in this chapter also demonstrate that animals of the same species have differing radiosensitivities at both the level of population mortality and the level of critical systems and their cells, thereby proving convincingly that the basic concepts of our mathematical model of radiation-induced mortality of mammals are correct.

7.6. Variability of the Radiosensitivity of Mammals: Clinical Data

Chapter 6 summarizes and analyzes clinical data on the variability of individual radiosensitivity in humans. Section 6.1 gives a brief historical review of this problem. Sections 6.2 and 6.3 describe the variability of human radiosensitivity that manifests itself both at the population level and at the level of critical systems and their cells. Section 6.4 presents our conclusions.

Some of the clinical data on the effects of radiation on man were collected in the course of examination of several groups of patients that had undergone medical treatment with ionizing radiation. The patients of each group had the same type of health problem and received the same radiation treatment. Analysis of the data showed a broad variability of radiosensitivity both at the organism's level and at the level of the corresponding critical system (e.g., the central nervous system when the head is irradiated). It should be noted that the percentage of individuals with increased radiosensitivity is rather similar among different groups of patients: 10% to 20%, of which 7% to 10% are hyperradiosensitive. The number of radioresistant patients varies from 14% to 20%.

Also summarized are clinical data on persons directly involved in the elimination of the Chernobyl catastrophe aftereffects (cleanup crew). These data are particularly valuable because they characterize the response to low radiation doses (0.002-0.68 Gy) of large groups (cohorts) of healthy people. Each cohort included persons of approximately the same age performing similar jobs for more or less similar lengths of time. So the total radiation dose for most individuals in a cohort was roughly the same. Moreover, the contributions of all other nonradiation factors were also similar.

Analysis of the whole body of collected clinical data reveals considerable individual variability of radiosensitivity in all the cohorts examined: adverse health effects were found only in some of the cleanup crew and were related

to a deficiency or a disease of a particular organ, tissue, or vital system (e.g., immunological, gastrointestinal, or central nervous systems).

Grouping the data according to total doses (low and moderate) revealed that there were hyperradiosensitive and radioresistant individuals in the studied cohorts. For instance, in cohorts of the cleanup crew whose total dose was not high (below 0.2 Gy), the percentage of persons who developed a chronic disease after 1986 (the year of the Chernobyl disaster) ranges from 4% to 25% (table 6.2). At higher total doses (0.2-0.68 Gy), the percentage of persons that remained practically healthy for 5 years after the disaster was 8% (table 6.2). These results are consistent with foregoing estimates of the percentages of radiosensitive and radioresistant individuals.

The data presented in this chapter, which show the variability of radiosensitivity of two critical systems of the human organism—bone marrow lymphopoiesis and granulocytopoiesis—are unique because they are the results of a "pure" experiment. To select personnel to work under conditions of exposure to radiation, 50 healthy men had to be subjected to a single dose of irradiation at the same dose (not a high dose). The radiosensitivity of the lymphopoietic and granulocytopoietic systems was estimated from the minimal (compared to the initial) level of leukocyte concentration in the blood. Less than a third of these men had enhanced radiosensitivity of the above systems. This result is of the same order as those cited above.

Variability of radiosensitivity of the human organism and its critical systems is directly related to variability of radiosensitivity of precursor cells of these systems. For example, in healthy persons, differences in sensitivity to γ radiation can be fourfold for granulocyte-macrophage CFUs, 2.5-fold for fibroblast CFUs, and 1.4-fold for erythroid CFUs (table 6.4).

Of particular importance are experimental data demonstrating asymmetric distribution of individuals with radiosensitive skin fibroblasts (the skin can also be a critical system in certain irradiation conditions). This asymmetry is a result of a greater representation of individuals whose skin fibroblasts are highly radiosensitive. Moreover, the same experiments established a direct correlation between radiosensitivity of skin fibroblasts and of the human organism as a whole. These findings are of great significance when choosing the type of distribution to describe a nonhomogeneous (in radiosensitivity) human population because they suggest that a human population is probably characterized by a log-normal distribution.

Thus, the analysis of clinical data on irradiated persons presented in chapter 6 supports the validity of the principal concepts forming the basis of the model of radiation-induced mortality of mammals and indicates that these concepts must be considered in modeling the radiation effects on human populations.

Quite significant is the finding that 10% to 20% of individuals have enhanced radiosensitivity. It relates to the above-mentioned conclusion, drawn from the study of the model of mortality of a nonhomogeneous population, that even very low irradiation can have fatal consequences for individuals who have hyperradiosensitive critical system precursor cells.

This modeling result suggests that a new strategy of radiation protection must be adopted for the population in areas with an elevated radiation background: identification of and priority for hyperradiosensitive individuals when applying the whole set of preventive and protective measures, including moving them to noncontaminated places of residence.

By analogy with epidemiologic terminology, the subpopulation of hyperradiosensitive individuals can be called the group of radiation risk. The task of singling out this group among the population is not trivial. For example, some authors proposed that radiosensitivity be predicted according to indices showing the organism reactivity under normal conditions and when exposed to nonradiation factors. This technique appears promising and warrants further experimental study. In our opinion, however, this technique is more suitable for persons that are expected to be exposed to radiation and less suitable for populations residing in contaminated areas. The fact is that the response of an organism that experiences chronic irradiation at low or moderate dose rates has already been altered, and additional exposure to adverse nonradiation factors can lead to adverse reactions.

We propose a safe, simple, and inexpensive technique for identifying the radiation risk group among the populations of areas with an elevated radiation background. The technique is based on the modeling results presented in this report. In the range of dose rates typical of most contaminated areas, the critical system of the human organism is the bone marrow blood-forming system. Consequently, individuals whose bone marrow blood-forming precursor cells show hyperradiosensitivity should be considered the radiation risk group. Taking samples of bone marrow cells is not a harmless procedure. Direct determination of radiosensitivity of bone marrow blood-forming precursor cells is labor-consuming and cannot be the routine method to identify persons with elevated radiosensitivity, but it can be done in extraordinary cases. There exists, however, a method of radiosensitivity assessment for these cells from indirect data. As already noted, chronic irradiation with low and moderate dose rates brings about new concentrations of blood cells that differ from normal thrombocytes, lymphocytes, erythrocytes, and granulocytes. As shown by model calculations and experiments, radiation hormesis effects can occur in the lymphopoietic and granulocytopoietic systems. As a consequence of continuous irradiation in certain ranges of low dose rates, the new stationary concentrations of bone marrow precursor cells in these systems and even of functional cells (granulocytes) may exceed the normal level. Additional studies of the erythropoiesis model have shown that under certain conditions this model can also reproduce the effects of radiation hormesis: setting up of higher-than-normal stationary concentrations of bone marrow precursor cells

in this system as a result of prolonged irradiation at low dose rates. This prediction of the model is consistent with results of some experiments on animals larger than mice. Therefore, concentrations of lymphocytes, granulocytes, and erythrocytes in the blood of mammals exposed to radiation at low dose rates cannot serve as an adequate characteristic of radiosensitivity of early precursor cells of these systems. At the same time, analysis of the thrombocytopoiesis model has revealed the following picture. New stationary concentrations of bone marrow precursor cells of this system and of thrombocytes in the blood of mammals exposed to prolonged irradiation at any dose rate are always below the normal level. Furthermore, at a constant dose rate, the new stationary concentration of thrombocytes decreases as the radiosensitivity of thrombocyte precursor cells capable of dividing in the bone marrow increases. In many cases of the bone marrow syndrome, it is the failure of the thrombocytopoietic system that is responsible for the death of mammals—the level of thrombocyte concentration in the blood can thus serve as a reliable indicator of bone marrow precursor cell radiosensitivity. Therefore, it can be expected that in a radiation-contaminated area with a nearly uniform radiation background, individuals with enhanced radiosensitivity will have lower thrombocyte concentrations in the blood than the average for the population of the area. Routine blood sampling to determine the thrombocyte concentration and subsequent simple calculations to find the average thrombocyte concentration for a homogeneous cohort of persons are sufficient to identify hyperradiosensitive individuals in each cohort[1].

Thus, even the qualitative result of the study of the mortality model developed by us makes it possible to give quite specific recommendations for the radiation protection of populations in areas with elevated radiation backgrounds.

7.7. Conclusions

The principal result of the research described in this report is a new approach to modeling the dynamics of radiation-induced mortality in mammals and the practical use of this approach in a family of mathematical models. The latter would enable prediction of the effects of a broad range of radiation exposures on the principal critical systems (hematopoietic and intestinal) and the organism as a whole, as well as on mammalian populations that are nonhomogeneous in radiosensitivity. The constructed models are specifically for small laboratory animals (mice and rats). The choice was dictated by the availability and sufficiency of experimental data required to specify and test the model.

[1]This is just a general idea of the proposed method for identifying individuals belonging to the radiation risk group. Clearly, practical application of this method must be preceded by working out, on the basis of available clinical data, some optimal criteria for grouping individuals in cohorts and by elaborating mathematical programs for statistical processing of the results.

The analysis of clinical data on irradiated individuals in this report has demonstrated that the principal concepts of the developed model of mortality are also applicable to human populations. The models described can serve as the basis for building a mathematical model of radiation-induced mortality for man. The need for such a model and the promise it offers are obvious. But so are the difficulties to be encountered in the efforts to solve this problem. The difficulties are primarily related to the heterogeneity, ambiguity (in the dosimetric sense), and obvious shortage of clinical data necessary for specifying and testing the models of the critical systems. In addition, an adequate description of radiation effects on large groups of people may require reconstruction of a complex model of an entire population that would include children, elderly people, and men and women of different ages. The family of mathematical models presented in this report would then become only a part of a global model of radiation-induced mortality.

DISTRIBUTION LIST

DEPARTMENT OF DEFENSE

ARMED FORCES RADIOBIOLOGY RESEARCH INSTITUTE
ATTN: PUBLICATIONS BRANCH
ATTN: LIBRARY

ARMY/AIR FORCE JOINT MEDICAL LIBRARY
ATTN: DASG-AAFJML

ASSISTANT TO THE SECRETARY OF DEFENSE
ATTN: AE
ATTN: HA(IA)

DEFENSE NUCLEAR AGENCY
ATTN: TITL
ATTN: DDIR
ATTN: RAEM
ATTN: MID

DEFENSE TECHNICAL INFORMATION CENTER
ATTN: ACQUISITION
ATTN: ADMINISTRATOR

FIELD COMMAND DEFENSE NUCLEAR AGENCY
ATTN: FCIEO

INTERSERVICE NUCLEAR WEAPONS SCHOOL
ATTN: DIRECTOR

LAWRENCE LIVERMORE NATIONAL LABORATORY
ATTN: LIBRARY

UNDER SECRETARY OF DEFENSE (ACQUISITION)
ATTN: OUSD(A)/R&E

UNIFORMED SERVICES UNIVERSITY OF THE HEALTH SCIENCES
ATTN: LIBRARY

DEPARTMENT OF THE ARMY

HARRY DIAMOND LABORATORIES
ATTN: SLCSM-SE

OFFICE OF THE SURGEON GENERAL
ATTN: MEDDH-N

U.S. ARMY AEROMEDICAL RESEARCH LABORATORY
ATTN: SCIENCE SUPPORT CENTER

U.S. ARMY CHEMICAL RESEARCH, DEVELOPMENT, & ENGINEERING CENTER
ATTN: SMCCR-RST

U.S. ARMY INSTITUTE OF SURGICAL RESEARCH
ATTN: COMMANDER

U.S. ARMY MEDICAL DEPARTMENT CENTER AND SCHOOL
ATTN: MCCS-FCM

U.S. ARMY MEDICAL RESEARCH AND MATERIEL COMMAND
ATTN: COMMANDER

U.S. ARMY MEDICAL RESEARCH INSTITUTE OF CHEMICAL DEFENSE
ATTN: MCMR-UV-R

U.S. ARMY NUCLEAR AND CHEMICAL AGENCY
ATTN: MONA-NU

U.S. ARMY RESEARCH INSTITUTE OF ENVIRONMENTAL MEDICINE
ATTN: DIRECTOR OF RESEARCH

U.S. ARMY RESEARCH LABORATORY
ATTN: DIRECTOR

WALTER REED ARMY INSTITUTE OF RESEARCH
ATTN: DIVISION OF EXPERIMENTAL THERAPEUTICS

DEPARTMENT OF THE NAVY

BUREAU OF MEDICINE & SURGERY
ATTN: CHIEF

NAVAL AEROSPACE MEDICAL RESEARCH LABORATORY
ATTN: COMMANDING OFFICER

NAVAL MEDICAL RESEARCH AND DEVELOPMENT COMMAND
ATTN: CODE 42

NAVAL MEDICAL RESEARCH INSTITUTE
ATTN: LIBRARY

NAVAL RESEARCH LABORATORY
ATTN: LIBRARY

OFFICE OF NAVAL RESEARCH
ATTN: BIOLOGICAL & BIOMEDICAL S&T

DEPARTMENT OF THE AIR FORCE

BROOKS AIR FORCE BASE
ATTN: AL/OEBZ
ATTN: OEHL/RZ
ATTN: USAFSAM/RZB

OFFICE OF AEROSPACE STUDIES
ATTN: OAS/XRS

OFFICE OF THE SURGEON GENERAL
ATTN: HQ AFMOA/SGPT
ATTN: HQ USAF/SGES

U.S. AIR FORCE ACADEMY
ATTN: HQ USAFA/DFBL

U.S. AIR FORCE OFFICE OF SCIENTIFIC RESEARCH
ATTN: DIRECTOR OF CHEMISTRY & LIFE SCIENCES

OTHER FEDERAL GOVERNMENT

ARGONNE NATIONAL LABORATORY
ATTN: ACQUISITIONS

BROOKHAVEN NATIONAL LABORATORY
ATTN: RESEARCH LIBRARY, REPORTS SECTION

CENTER FOR DEVICES AND RADIOLOGICAL HEALTH
ATTN: DIRECTOR

GOVERNMENT PRINTING OFFICE
ATTN: DEPOSITORY ADMINISTRATION BRANCH
ATTN: CONSIGNED BRANCH

LIBRARY OF CONGRESS
ATTN: UNIT X

LOS ALAMOS NATIONAL LABORATORY
ATTN: REPORT LIBRARY

NATIONAL AERONAUTICS AND SPACE ADMINISTRATION
ATTN: RADLAB

NATIONAL AERONAUTICS AND SPACE ADMINISTRATION
GODDARD SPACE FLIGHT CENTER
ATTN: LIBRARY

NATIONAL CANCER INSTITUTE
ATTN: RADIATION RESEARCH PROGRAM

NATIONAL DEFENSE UNIVERSITY
ATTN: LIBRARY

NATIONAL INSTITUTE OF STANDARDS AND TECHNOLOGY
ATTN: IONIZING RADIATION DIVISION

U.S. DEPARTMENT OF ENERGY
ATTN: LIBRARY

U.S. FOOD AND DRUG ADMINISTRATION
ATTN: WINCHESTER ENGINEERING AND ANALYTICAL CENTER

U.S. NUCLEAR REGULATORY COMMISSION
ATTN: LIBRARY

RESEARCH AND OTHER ORGANIZATIONS

AUSTRALIAN DEFENCE FORCE
ATTN: SURGEON GENERAL

AUTRE, INC.
ATTN: PRESIDENT

BERGISCHE UNIVERSITÄT
ATTN: LIBRARY

BRITISH LIBRARY
ATTN: ACQUISITIONS UNIT

CENTRE DE RECHERCHES DU SERVICE DE SANTE DES ARMEES
ATTN: DIRECTOR

FEDERAL ARMED FORCES DEFENSE SCIENCE AGENCY FOR NBC PROTECTION
ATTN: LIBRARY

INHALATION TOXICOLOGY RESEARCH INSTITUTE
ATTN: LIBRARY

INSTITUTE OF RADIOBIOLOGY, ARMED FORCES MEDICAL ACADEMY
ATTN: DIRECTOR

INTERNATIONAL CENTRE FOR THEORETICAL PHYSICS
ATTN: LIBRARY

KAMAN SCIENCES CORPORATION
ATTN: DASIAC

OAK RIDGE ASSOCIATED UNIVERSITIES
ATTN: MEDICAL LIBRARY

RESEARCH CENTER OF SPACECRAFT RADIATION SAFETY
ATTN: DIRECTOR

RUTGERS UNIVERSITY
ATTN: LIBRARY OF SCIENCE AND MEDICINE

UNIVERSITY OF CALIFORNIA
ATTN: DIRECTOR, INSTITUTE OF TOXICOLOGY & ENVIRONMENTAL HEALTH
ATTN: LIBRARY, LAWRENCE BERKELEY LABORATORY

UNIVERSITY OF CINCINNATI
ATTN: UNIVERSITY HOSPITAL, RADIOISOTOPE LABORATORY

UNIVERSITY OF OXFORD
ATTN: LIBRARY

UNIVERSITY OF TENNESSEE
ATTN: DIRECTOR, DEPARTMENT OF MATHEMATICS

UNIVERSITY OF ULM
ATTN: DIRECTOR, INSTITUTE OF SOCIAL AND OCCUPATIONAL HEALTH

XAVIER UNIVERSITY OF LOUISIANA
ATTN: COLLEGE OF PHARMACY

REPORT DOCUMENTATION PAGE

Form Approved
OMB No. 0704-0188

1. AGENCY USE ONLY *(Leave blank)*	2. REPORT DATE	3. REPORT TYPE AND DATES COVERED
	June 1996	Contract

4. TITLE AND SUBTITLE

Estimation of Radiation Risk Based on the Concept of Individual Variability of Radiosensitivity

5. FUNDING NUMBERS

NWED QAXM

6. AUTHOR(S)

Kovalev, E.E., and Smirnova, O.A.

7. PERFORMING ORGANIZATION NAME(S) AND ADDRESS(ES)

Armed Forces Radiobiology Research Institute
8901 Wisconsin Avenue
Bethesda, MD 20889-5603

8. PERFORMING ORGANIZATION REPORT NUMBER

CR 96-1

9. SPONSORING/MONITORING AGENCY NAME(S) AND ADDRESS(ES)

Uniformed Services University of the Health Sciences
4301 Jones Bridge Road
Bethesda, MD 20814-4799

10. SPONSORING/MONITORING AGENCY REPORT NUMBER

11. SUPPLEMENTARY NOTES

12a. DISTRIBUTION/AVAILABILITY STATEMENT

Approved for public release; distribution unlimited.

12b. DISTRIBUTION CODE

13. ABSTRACT *(Maximum 200 words)*

This report was prepared for the Defense Nuclear Agency under contract number DNA001-93-C-0152. A description and analysis of mathematical models developed for two critical systems, the hematopoietic and intestinal systems, are presented. The models, based on modern theories of regulation of the hematopoietic and intestinal epithelium systems, describe the dynamics of these systems in nonirradiated mammals and in mammals exposed to acute and chronic radiation. The first model uses the radiosensitivity indices of hematopoietic cells as its principal parameters. The key parameter of the second model is the radiosensitivity index of precursors of principal crypt cells. The variable parameters of the models are represented by the dose of acute radiation and the dose rate of chronic radiation. These models can be used for quantitative prediction of the effects of acute and chronic radiation on the hematopoietic and intestinal systems of mammals.

14. SUBJECT TERMS	15. NUMBER OF PAGES
	203
	16. PRICE CODE

17. SECURITY CLASSIFICATION OF REPORT	18. SECURITY CLASSIFICATION OF THIS PAGE	19. SECURITY CLASSIFICATION OF ABSTRACT	20. LIMITATION OF ABSTRACT
UNCLASSIFIED	UNCLASSIFIED	UNCLASSIFIED	UL